Empirical and Theoretical Approaches for Assessing the Local Radiocarbon Marine Reservoir Effect



Eduardo Queiroz Alves

St Cross College

University of Oxford

A thesis submitted for the degree of

Doctor of Philosophy

Hilary 2019

I dedicate this work to the employees of the National Museum of Brazil, which was engulfed and largely destroyed by fire on 2 September 2018. Access to this important collection, and the professionalism and helpfulness of the museum staff, have greatly benefited this research. I hope that the completed project here presented will help to stimulate further work in areas of importance to the museum, and I therefore offer it in contribution to its eventual reconstruction and lasting legacy.

“Eventually man, too, found his way back to the sea. Standing on its shores, he must have looked out upon it with wonder and curiosity, compounded with an unconscious recognition of his lineage. He could not physically re-enter the ocean as the seals and whales had done. But over the centuries, with all the skill and ingenuity and reasoning powers of his mind, he has sought to explore and investigate even its most remote parts, so that he might re-enter it mentally and imaginatively.”
- Rachel Carson, The Sea Around Us (1951).

Abstract

The radiocarbon activity of a reservoir is a function of both intra- and inter-reservoir phenomena. In general, any process removing ^{14}C from a reservoir (or equivalently introducing pre-aged carbon) without its replenishment by a counteracting process will cause a reservoir effect. First defined in 1986, the ^{14}C marine reservoir effect (MRE) still puzzles researchers worldwide. Its quantification is paramount for the application of the radiocarbon dating tool in marine environments, bearing important consequences for the chronology of coastal archaeological sites. Unfortunately, a significant lack of MRE data has hindered chronometric studies in regions such as the coast of Brazil, where thousands of prehistoric shell mounds remain poorly investigated.

The geographic and temporal fluctuations of the MRE have led me to employ a two-pronged approach, using known-age and archaeological samples, in an effort to understand this variability for the Brazilian coast. In this kind of study, the importance of contextualization cannot be overstated and, therefore, my methodology has involved a range of accessory techniques (e.g., anthracology, stable isotopes and X-ray diffraction analyses) to ensure the suitability of samples for MRE quantification and thus to enhance the accuracy of the results. The pre-bomb local components of the MRE - i.e., $\triangle$R values - are mostly within the range from -100 to 100 ^{14}C yr, but record the influence of phenomena such as upwelling and limestone dissolution at specific locations on the coast. The archaeological $\triangle$R value of -102 $\pm$ 74 ^{14}C yr, in turn, was derived from the Late Holocene shell mound Sambaqui da Cabeçuda, a massive coastal site in Southern Brazil, where the archaeological evidence suggests a funerary function. The highly negative $\triangle$R value is likely caused by the input of recently formed carbon species in the system and I discuss different Bayesian models for the calculation of this offset, as well as a series of complications for MRE studies in Brazilian shell mounds.

In order to disentangle the complex relationships between archaeology and the environment, I have used stable isotopes of N and C together with Bayesian analysis to assess the diet of 5 humans from Cabeçuda. The quantification of the high proportion of marine diet (up to 80%) allowed me to calibrate bone ^{14}C ages with an appropriate mixed curve. Despite various obstacles, the current practice of using $\triangle$R and a global calibration curve remains the best available approach for marine calibration. Nonetheless, by acknowledging that discussion of other possibilities is paramount for the progress of radiocarbon research, I present a method for the

achievement of local marine calibration curves. The advantages and limitations of this method are discussed at the end of the thesis. Overall, this research uses interdisciplinary techniques to tackle questions of archaeological and environmental significance and provides useful methodological insights for future studies.

Contents

Preface **xii**

Acknowledgements **xiii**

1 Scientific Background **1**

1.1 Radioisotopic Dating 2
1.2 Radiocarbon Dating 3
1.2.1 An Overview of the Experimental Methods 6
1.2.2 Carbon Isotopic Fractionation 9
1.2.3 Conventional Radiocarbon Age (CRA) 11
1.2.4 The Need for Calibration 12
1.2.5 Terrestrial Calibration 17
1.3 The Atmospheric and Marine Carbon Reservoirs 20
1.3.1 Marine Dissolved Inorganic Carbon and ^{14}C 22
1.4 Reservoir Effects 24
1.4.1 The Marine Reservoir Effect (MRE) 25
1.4.2 A Quantitative Description of the MRE 30
1.4.3 Hard Water and Freshwater Effects 31
1.4.4 Marine Calibration 33
1.5 Accounting for Common Issues in ^{14}C Dating 36
1.5.1 Recrystallization 38
1.5.2 The Old Wood Effect 39
1.6 Stable Isotopes Analyses ($\delta^{13}C$, $\delta^{15}N$, $\delta^{18}O$) 41
1.6.1 $\delta^{13}C$ and $\delta^{18}O$ in Aquatic Carbonates 41
1.6.2 $\delta^{13}C$ and $\delta^{15}N$ Correlation with Diet 43

2 Environmental Context **46**
2.1 The Brazilian Coastal Environment 46
2.2 The Oceanography of the Brazilian Coast 48
2.2.1 The Guanabara Bay 51
2.2.2 The Laguna Lagoonal System 53

3 Archaeological Context **55**
3.1 Shell Mounds 56
3.2 Sambaqui 58
3.2.1 Sambaqui de Cabeçuda 60

4 Methodology **64**
4.1 ^{14}C-AMS 64
4.1.1 ORAU 67
4.1.2 LAC-UFF 70
4.1.3 Quality Control 73
4.2 Stable Isotopes (δ^{13}C, δ^{15}N and δ^{18}O) Analyses 74
4.3 X-Ray Diffraction and Anthracology 75

5 The MRE Along the Brazilian Coastline **77**
5.1 Previous Studies 78
5.2 Pre-Bomb Samples 81
5.2.1 Sample Selection 81
5.2.2 Calculation of the $\triangle$R Values 84
5.2.3 Results and Discussion 87
5.3 Paired Archaeological Samples 111
5.3.1 Sample Selection 111
5.3.2 Calculation of the $\triangle$R Values 113
5.3.3 Results and Discussion 114
5.4 Conclusions 125

6 Implications for the Chronology of Cabeçuda **128**
6.1 Previous Studies 129
6.2 The Cabeçuda Burials 130
6.3 Analyses 131
6.4 The Diet of Sambaqui Populations 133
6.4.1 Modelling Human Diet at Cabeçuda 136

6.5 The Calibration of Cabeçuda ^{14}C Ages 140
6.6 Conclusions 143

7 A Theoretical Approach to Assess the MRE 144
7.1 Motivation 145
7.2 Methodology 146
7.3 Results and Discussion 148
7.4 Conclusions 159

8 Conclusions and Perspectives 161
8.1 Future Perspectives 164

Appendices 166

A Science at Sea: European and American Voyages of Scientific Exploration 167
A.1 Expeditions of Exploration and Discovery 168

B X-Ray Diffractograms 171

C OxCal Code 175
C.1 Independent $\triangle$R 175
C.2 Common $\triangle$R (Different Phases) 176
C.3 Single Phase $\triangle$R 178
C.4 Single Phase R 179
C.5 Burials Multiplot 180
C.6 Burials Phase Model 181

D Species habitat 182

Bibliography 184

List of Figures

1.1 Simplified illustration of radiocarbon production, oxidation, absorption, and distribution throughout the Earth's reservoirs. 5
1.2 Radiocarbon decay. 6
1.3 Anthropogenic perturbations to the atmospheric carbon reservoir. 16
1.4 Sections of the most recent ^{14}C atmospheric calibration curves. 19
1.5 Diagram depicting the global carbon cycle. 20
1.6 The air-sea gas exchange. 23
1.7 Simplified depiction of the global overturning or thermohaline circulation. . 27
1.8 Reservoir age recostruction for the Atlantic, Pacific and Indian oceans averaged by latitude. 29
1.9 The MRE worldwide 31
1.10 Processes influencing the MRE. 33
1.11 Marine13 and the MRE offsets. 34
1.12 The influence of the MRE correction on marine calibration. 35
1.13 Impact of contamination on measured radiocarbon ages (adapted from Gillespie (1984)) 38
1.14 Preservation of wood anatomical features after combustion. 40
1.15 $\delta^{13}C$ variation due to environment change. 42
1.16 Stable carbon and nitrogen values for terrestrial and marine ecosystems. . 45

2.1 Zonation of part of the Brazilian littoral. 48
2.2 South Atlantic circulation and the Cabo Frio upwelling system. 49
2.3 The Guanabara Bay. 53
2.4 The Laguna Lagoonal System. 54

3.1 The location of Cabeçuda at Santa Catarina state, Southern Brazil. 61
3.2 The Cabeçuda archaeological site. 62

4.1 Carbonate line and graphitization rig at the ORAU. 68

4.2 The 2 MV HVEE acceletator at the ORAU. 69
4.3 Carbonate line and graphitization tube at the LAC-UFF. 71
4.4 The SSAMS system used at the LAC-UFF. 73
4.5 Anthracology methodology. 76

5.1 Sample selection at museums. 82
5.2 Distribution of the studied marine samples on the Brazilian coast. 82
5.3 Some of the shells used in this research. 84
5.4 Flowchart for ΔR calculation using the known-age approach 85
5.5 Illustration of the ΔR and uncertainty calculation for known-age samples employed in Reimer and Reimer (2016). 86
5.6 Ambiguous collecting localities. 87
5.7 Stable isotopes (δ^{18}O and δ^{13}C) results for the known-age samples. 92
5.8 Relationship between δ^{18}O and ΔR for known-age marine samples. 95
5.9 Variation of δ^{13}C and ΔR with the proportion of marine water in a mixture. 96
5.10 Relationship between δ^{13}C and ΔR for known-age samples from different environments. 97
5.11 Boxplot for ΔR according to environment. 99
5.12 Histogram for the ΔR results according to environment. 100
5.13 Histogram for the ΔR results (undetermined environment). 101
5.14 Temporal evolution of the pre-bomb ΔR values. 102
5.15 ΔR values versus latitude. 104
5.16 Prebomb ΔR values on the Brazilian coast. 106
5.17 Prebomb ΔR values within the Guanabara Bay. 108
5.18 Modelled and experimental MRE on the Brazilian coast. 110
5.19 Flowchart for ΔR calculation using the paired sample approach . . . 113
5.20 XRD diffractogram for sample 180304. 116
5.21 Stable isotopes results for the archaeological shells. 118
5.22 Individual ΔR values obtained for each Cabeçuda burial studied. 120
5.23 Common ΔR value obtained for all the Cabeçuda burials studied. 120
5.24 Modelled radiocarbon dates for the Cabeçuda shellmound considering a common ΔR for the different burials. 121
5.25 Single R value obtained considering a single phase for the Cabeçuda burials. 122
5.26 Single ΔR value obtained considering a single phase for the Cabeçuda burials. Burials 1 and 5 were excluded from this analysis. 123

5.27 Modelled ΔR time series for latitude = $28.75°$S and longitude = $45°$W. Data from Butzin et al. (2017). 125

6.1 Cabeçuda burials studied in this research. 132
6.2 Some of the bone fragments analysed in this research. 134
6.3 Diet model output for 5 Cabeçuda inhumations. 139
6.4 The calibrated ^{14}C ages of the Cabeçuda burials. 142
6.5 Boundaries of a phase model for the Cabeçuda bones. 143

7.1 Flowchart illustrating the methodology employed for the curves construction. 148
7.2 MRA plotted against latitude. Data from Butzin et al. (2017). 149
7.3 MRA (0 cal BP, 0 – 100 m depth) derived from the model described in Butzin et al. (2017) plotted together with experimental MRA data (pre-bomb samples from depths shallower than 75 m) from the marine reservoir database (Reimer and Reimer, 2001). 150
7.4 Comparison of LOCal13 and Marine13 for Kiritimati (Grothe et al., 2016) and Solomon Islands (Burr et al. 2015) 151
7.5 Local calibration curves for a tropical (latitude = $1.25°$N; longitude = 0) and a polar (latitude = $68.75°$S; longitude = $45°$W) region plotted together with the global curve Marine13. 152
7.6 Comparison of LOCal13 and Marine13 for the calibration of hypothetical radiocarbon ages (5, 8, 15 and 30 kBP) from a location near the South Pole. 153
7.7 Comparison of calibrated ages for hypothetical radiocarbon ages with Marine13 and available ΔR vs LOCal13 curve for latitude = $36.25°$N and longitude $75°$W. 155
7.8 Comparison of calibrated ages for hypothetical radiocarbon ages with Marine13 and available ΔR vs the LOCal13 curve for latitude = $1.25°$S and longitude = $45°$E. 156
7.9 MRA plotted against latitude. The figure shows the average over the longitudes available in the model output for 15ka cal BP. 157
7.10 The three scenarios output by Butzin et al. (2017) for low latitudes and high latitude regions 158

A.1 The route of HMS Challenger. 170

List of Tables

1.1 Typical δ^{13}C values for various materials (Stuiver and Polach, 1977; Aitken, 1990). 11
1.2 Influence of contamination on the measured radiocarbon age. 37

4.1 Quantity of material necessary to yield $\sim$1 mg of carbon for ^{14}C-AMS analysis, taking into account losses during treatments. Table from Tuniz et al. (1998). Values may vary according to laboratory and treatment employed. 66

5.1 Summary of previous known-age MRE studies on the Brazilian coast. 80
5.2 Summary of previous archaeological MRE studies on the Brazilian coast. 81
5.3 Results for the known-age samples of marine origin measured for this research. 88
5.4 Results for the known-age samples of freshwater origin measured for this research. 89
5.5 Results for the known-age samples of estuarine origin measured for this research. 89
5.6 Results for the known-age samples of unknown origin measured for this research. 90
5.7 Anthracological and isotopic results, including ^{14}C-AMS, for archaeological samples from the shellmound Sambaqui da Cabeçuda. . . . 117

6.1 Previous radiocarbon measurements for the Cabeçuda shellmound. 129
6.2 Results for the bone samples analysed in the present study. 133

D.1 Habitat preferences for some of the mollusc species analysed in this research. 183

Preface

In 2009, Professor Kita Macario introduced me to the ^{14}C-AMS technique and, later, to the ^{14}C Marine Reservoir Effect (MRE). The idea of proposing this topic for a DPhil project arose from our early discussions at the Brazilian ^{14}C facility back in 2014. Our reasoning derived from the fact that the scarcity of MRE data brings uncertainties to the reliability of radiocarbon dates obtained from marine material in Brazil, which has been challenging researchers for many decades. In a country with such an extensive coastline and a massive number of coastal archaeological sites lacking a proper chronology, the quantification of the MRE was a natural step for developing a more scientific approach in the local archaeology. As expected, this has proven to be an arduous task in many ways.

This research was part of an ambitious project that aims to map the MRE on the coast of Brazil following a two-pronged approach (i.e., the use of known-age pre-bomb and archaeological material). Exhaustive searches in large natural history collections worldwide and the lack of documentation for many of the (few) specimens I have found were only the first challenge I had to face when pursuing this research. Infrastructure and bureaucratic matters have further complicated this project and, throughout, I have encountered all sorts of funding and technical setbacks involving the Radiocarbon Laboratory of the Universidade Federal Fluminense. It was only with the help and support of the people thanked in the acknowledgements that difficulties have slowly been overcome during the course of this research, thereby enabling the completed thesis to unlock a bounty of useful information for researchers working on the coast of Brazil to build upon. The results of this research show that much was yet to be discovered after the pioneer study of Eastoe et al. (2002). Given the diversity entailed by the Brazilian coastal zone, I argue that there is still much more to be done.

Acknowledgements

I am deeply indebted to several people for their feedback, encouragement and support during the last few years. First and foremost, I must thank my supervisors for their guidance throughout this research. I am honoured for the opportunity to work with Professor Christopher Bronk Ramsey and I am grateful for the several productive discussions we have had in the last few years. I also had the privilege of working with Professor Kita Macario, who had an enormous influence on my career and created all the opportunities for me to bring this project to fruition. Thanks are also due to the staff and fellow students at the Research Laboratory for Archaeology and the History of Art (RLAHA), especially Kathryn Mears, David Chivall, Angela Bowles, Philip Leach and Joe Graystone for their endless patience in providing laboratory training. I cannot leave RLAHA without acknowledging the extensive support I have received from Diane Baker and Barbara Morris, who endured my constant presence at their office. I must recognise the assistance of the students and staff of the Radiocarbon Laboratory of the Universidade Federal Fluminense, in Brazil. Special thanks to Fabiana Oliveira and Marcelo Muniz for their practical support with sample processing. Thanks also to those at the Australian National University ^{14}C laboratory, especially Stewart Fallon, for prioritising the measurement of my samples. For this research, I have had the chance of working with Professor Rita Scheel-Ybert whose efforts have been contributing to a more scientific approach in Brazilian archaeology. She is undoubtedly a great source of inspiration for my future career. I would also like to extend my sincere thanks to Dr. Martin Butzin, who gave me valuable advice for the last part of this thesis. This research also benefited from very useful discussions with Dr. Rick Schulting and Dr. André Carlo Colonese. Special thanks to Adam Baldinger, Andreia Salvador, Anita Eschner, Christine Zorn, Luiz Ricardo Simone, Rosa Souza, Maria Pivel, and Tom Schiote for devoting their time to helping me find very specific specimens in large natural history collections.

The completion of this research would not have been possible without the support of my friends. I am especially grateful to Konrad Braun, Rafael Wong, Takao Sasaki, Gabriela Veras, Fernando Pardo Urrutia, Ingrid Chanca, Katy Sparrow, Stephanie Ward, Wesley Correia, Adir Fonseca and Lorena Becerra-Valdivia. Special thanks are owed to my good friend Dr. Jacob Seifert whose passion for science was always a source of inspiration for me. I am extremely grateful to Dr. Peter Lynan for proof-reading this thesis and for all the support and encouragement I have received from him. Thanks should also go to Dr. Renan Pereira Cardoso with whom I have had many fruitful scientific discussions. A heartfelt thank you to Katerina Douka who encouraged me to apply for this program and always made herself available for whatever help I needed. Finally, I am grateful to Professor Tom Higham for hiring me as a temporary part time laboratory technician at the RLAHA. This has helped provide financial support in the final stages of my work.

I am grateful to the Brazilian Council for Scientific and Technological Development (CNPq) for funding this research. I also would like to express my appreciation for the financial support I have received from the School of Archaeology and the University of Oxford as a whole, which enabled me to pursue this project.

I owe everything to my parents, Celi and Joaquim, and my siblings Emerson, Cintia and Cristian. I will never be able to express my full love and gratitude.

Chapter 1

Scientific Background

Introduction

Research on cosmogenic radiation interactions in the atmosphere (Korff, 1939; Montgomery and Montgomery, 1939; Bethe et al., 1940; Clarke and Korff, 1941; Korff and Clarke, 1942; Korff and Hamermesh, 1946) led Libby (1946) to postulate that living carbonaceous matter contains the three naturally occurring carbon isotopes: ^{12}C, ^{13}C, and ^{14}C. Soon thereafter, this was proved to be true (Anderson et al., 1947), leading to the development of the ^{14}C dating method (Arnold and Libby, 1949; Libby et al., 1949), which is the main technique used in this work. In this chapter, I begin with a brief description of the ^{14}C dating tool, which leads to a discussion on ^{14}C reservoir effects. Common issues (e.g., post-depositional effects) and the accessory techniques used to avoid them are briefly discussed and stable isotopes analyses (δ^{13}C, δ^{15}N, δ^{18}O) are presented alongside their applications. Overall, this chapter summarizes the foundations of the scientific tools used in this research, providing the background knowledge necessary to understand the rest of this thesis.

1.1 Radioisotopic Dating

The underlying basis of radioisotopic or radionuclide dating methods is the radioactive decay of the relevant isotope. This mechanism is a statistical process governed by quantum mechanics laws. For a large number of nuclides N, the quantity dN of nuclides that decay in a time interval dt is proportional to N:

$$\mathrm{d}N = -\lambda N \mathrm{d}t, \tag{1.1}$$

where λ represents the probability per unit time for an atom disintegration, being distinct for each nuclide. Equation 1.1 is a first order differential equation that can be solved to give:

$$t = \frac{-1}{\lambda} \ln\left(\frac{N}{N_0}\right) \tag{1.2}$$

where N_0 and N are the initial and final number of radioactive nuclides, respectively, and t is the time elapsed. Hence, one can determine the age of a sample by measuring its isotopic concentration or, alternatively, defining the *activity* of a sample as its decay rate:

$$A(t) = -\frac{\mathrm{d}N}{\mathrm{d}t} \tag{1.3}$$

one can write Equation 1.2 as follows:

$$t = \frac{-1}{\lambda} \ln\left(\frac{A}{A_0}\right) \tag{1.4}$$

Therefore, the activity of a sample can also be used to calculate its age, which is done in the so-called conventional dating method. The *half-life* $t_{\frac{1}{2}}$ of a sample is defined as the time required for the number of radioactive nuclides in the sample to decay to half of its initial value. The *mean-life* τ, in turn, is defined as the average

life-time of a radionuclide before decay. Those two quantities are related by:

$$\tau = \frac{1}{\lambda} = \frac{t_{1/2}}{\ln 2} \tag{1.5}$$

which can be used to rewrite Equation 1.2:

$$t = -\tau \ln \left(\frac{N}{N_0} \right) \tag{1.6}$$

and Equation 1.4:

$$t = -\tau \ln \left(\frac{A}{A_0} \right) \tag{1.7}$$

These equations would hold for any decay chain where one would only be able to measure the parent isotope level. For instance, they find a practical application in radiocarbon (^{14}C) dating, which is employed in a number of different fields due to its useful time frame and the universal presence of radiocarbon within the biosphere. Indeed, disciplines such as archaeology and the geosciences were profoundly influenced by the development of the radiocarbon dating tool by Arnold and Libby (1949) and Libby et al. (1949).

1.2 Radiocarbon Dating

Radiocarbon is produced by a wide range of processes such as nuclear transformations (Vorobyov et al., 1972; Rose and Jones, 1984; Price, 1989) and nuclear reactions induced by different factors (Zito et al., 1980; Lal, 1988). In 1946, Libby noticed that cosmic radiation produces a considerable amount of ^{14}C in the upper layers of the atmosphere. Soon thereafter, experiments confirmed the existence of cosmogenic radiocarbon (Anderson et al., 1947), which proved to be the most relevant source of ^{14}C on Earth (Lingenfelter, 1963; Lal and Peters, 1967).

High energy nucleons are the major component of the galactic cosmic radiation. These particles travel, essentially from outside the solar system, and reach Earth initiating spallation reactions through interactions with atmospheric nuclei (Gosse and Phillips, 2001; Muzikar et al., 2003). Among the multiple particles released in these reactions are the so-called fast secondary neutrons, which are energetic particles that promote further cascades of nuclear reactions. As energy is lost due to successive inelastic and elastic collisions, fast neutrons eventually slow down to thermal energies. Thermal neutrons then move in a Brownian fashion until they are absorbed by atmospheric nuclei to form cosmogenic nuclides (Gosse and Phillips, 2001). Radiocarbon is by far the most important of these nuclides (Libby, 1946; Gosse and Phillips, 2001), mainly produced by the reaction between thermal neutrons and nitrogen nuclei:

$$^{14}_{7}\mathrm{N} + n \longrightarrow {}^{14}_{6}\mathrm{C} + p \tag{1.8}$$

The global average ^{14}C production rate is estimated to be approximately 2 atoms cm^{-2} s^{-1} (Castagnoli and Lal, 1980).[1] Upon formation, ^{14}C is a hot atom that either rapidly oxidises or loses energy and interacts by thermal reaction (Damon et al., 1978; Pandow et al., 1960). The main product of this primary reaction is a $^{14}\mathrm{CO}$ molecule that undergoes further oxidation by interaction with hydroxyl radicals to produce $^{14}\mathrm{CO_2}$ (Pandow et al., 1960):

$$^{14}\mathrm{C} + \mathrm{O_2} \longrightarrow {}^{14}\mathrm{CO} + \mathrm{O} \tag{1.9}$$

$$^{14}\mathrm{CO} + \mathrm{OH} \longrightarrow {}^{14}\mathrm{CO_2} + \mathrm{H} \tag{1.10}$$

[1] In a more recent paper, Masarik and Beer (1999) found this rate to be 2.02 atoms cm^{-2} s^{-1}.

Since these heavy carbon dioxide molecules present the same chemical properties as ordinary CO_2, they are metabolically assimilated by primary producers, reaching higher trophic levels via the food chain (Figure 1.1).

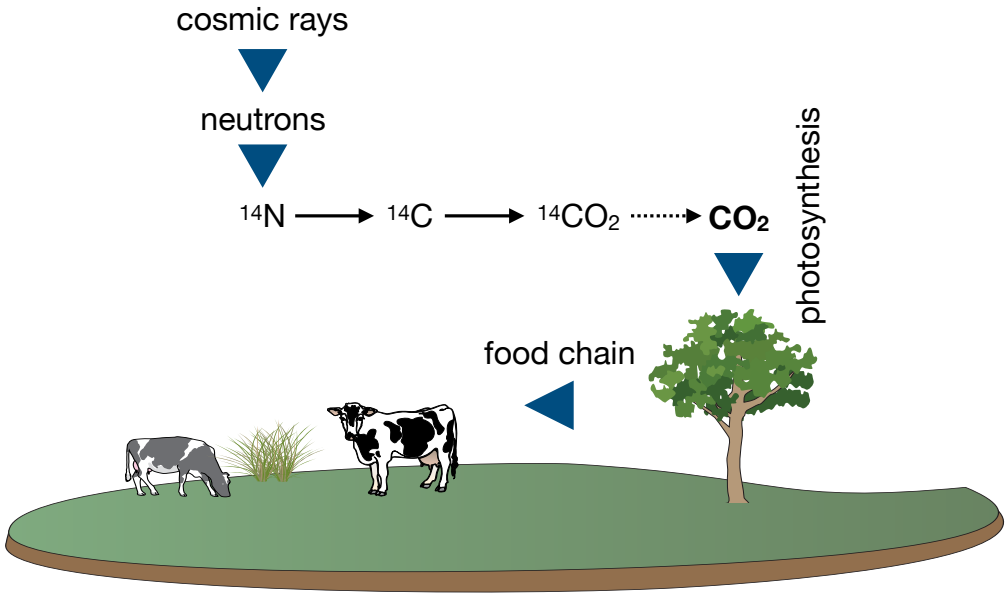


Figure 1.1. Simplified illustration of radiocarbon production, oxidation, absorption, and distribution throughout the Earth's reservoirs. Adapted from Aitken (1990). Some graphic elements are courtesy of the Integration and Application Network, University of Maryland Center for Environmental Science (http://ian.umces.edu/symbols/).

The radiocarbon dating method relies on the principle that the three carbon isotopes (^{12}C, ^{13}C and ^{14}C) are present in different concentrations in living carbonaceous matter (as first showed by Anderson et al., 1947) and, when the carbon exchange between a sample and its surrounding environment ceases (i.e., upon final formation or death), radioactive decay becomes the dominant process, decreasing the ^{14}C content in the material at a known rate (Figure 1.2). Radioactive decay of ^{14}C to the stable nuclide ^{14}N occurs via β^- decay:

$$^{14}\mathrm{C} \longrightarrow {}^{14}\mathrm{N} + e^- + \overline{\nu}_\mathrm{e} \tag{1.11}$$

where e^- is an electron and $\overline{\nu}_e$ is an electron antineutrino. Provided that radiocarbon $t_{\frac{1}{2}}$, N and N_0 are known,[2] one can determine the time elapsed since cessation of carbon exchange using Equation 1.6. In other words, one can *radiocarbon date* the sample.

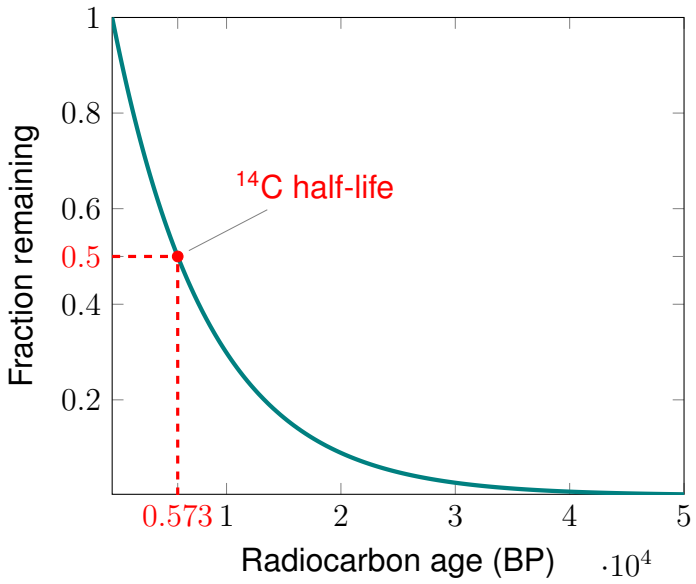


Figure 1.2. Radiocarbon decays to ^{14}N via β^- decay (Equation 1.11). Its convenient half-life (5,730 years) turns ^{14}C into a powerful clock for all sorts of processes happening in the Late Quaternary. After 10 half-lives, the quantity of residual radiocarbon is very low and the limit of the technique is reached.

1.2.1 An Overview of the Experimental Methods

There are different methods of determining the isotopic composition of a given sample (Fifield, 1999; Povinec et al., 2009; Zare, 2012). From beta particles detection to the direct counting of atoms, different techniques were developed one after another or even simultaneously over the course of time, with the later ones presenting advantages in sensitivity and precision.

[2] In practice, the ratio of the number of ^{14}C atoms (N) to that of total carbon is what is actually measured and one can define this quantity as the radiocarbon concentration (C) of the sample.

The conventional method (composed by the generally called *beta-counting techniques*) is based on activity measurements using either gas or liquid scintillation counters. This group of methods emerged when Geiger and Müller (1929) developed the first gas counter, which was able to count pulses generated from the ionization of a gas by the emission of beta-particles from the sample inside its chamber. Following this invention, Libby (1934) developed a screen-wall Geiger-Müller detector for the study of soft beta-emitters and, in order to analyse large carbon samples, he attached the solid material on his detector wall. Nevertheless, poor sensitivity and high backgrounds imposed obstacles to the measurements (Povinec et al., 2009). The replacement of the Libby counter by proportional gas counters allowed better precision in carbonaceous material measurements by incorporating gas samples, taking into account the low energy of the ^{14}C beta-electrons (Povinec et al., 2009).

Almost concurrently with the development of gas counters, Reynolds et al. (1950) started working on liquid scintillation instruments. In this approach, the sample is converted to an organic solvent – often benzene for carbon samples due to a number of advantages described in detail in Povinec et al. (2009) and references therein. In liquid scintillation techniques, an organic material with the capacity of emitting light absorbs radiation and emits photons proportionally to the number of received particles. These photons are then counted with the aid of a photomultiplier.

The methods listed above share limitations. The quantity of material needed is relatively large (several grams of carbon), which makes it impracticable to apply such methods for dating rare archaeological material or to other sciences requiring submilligram samples. Furthermore, the measurement time necessary for achieving a reasonable statistical precision is very long, this problem being worse for old samples whose activity is already very reduced. In the case of ^{14}C ($t_{1/2}$ = 5,730

years), it would be necessary to measure the activity of a sample of 1 g for 12 h to count 10,000 events and thus achieve 1% precision. For this reason, beta-counting methods cannot be applied to radionuclides of long half-life. In order to overcome these limitations, a new method had to be developed.

During the initial years of ^{14}C research, the idea that it may be possible to count atoms by mass spectrometry was a common suggestion (Olsson, 1970; Povinec et al., 2009). However, even though a conventional mass spectrometer has the required energy to separate carbon isotopes (^{14}C accounts for 0.0000000001% of atmospheric CO_2), ^{14}C ions would be masked by relatively intense fluxes of isobars (e.g., ^{14}N, ^{13}CH, $^{12}CH_2$, ^{12}CD and $^{7}Li_2$) and by background from the stable isotopes ^{12}C and ^{13}C (Fifield, 1999). It was only in the late 1970s that the coupling of particle accelerators, developed for nuclear physics research, with mass spectrometers allowed the detection of ions with energies in the order of MeV (Muller, 1977). This ultra-sensitive means of counting individual atoms, named *Accelerator Mass Spectrometry (AMS)*, basically consists of the ionization of the atoms extracted from the sample, followed by acceleration to high energies, break up of molecules and discrimination of isotopes according to momentum, charge and energy. Soon after the articulation of the technique by Muller (1977), Nelson et al. (1977) and Bennett et al. (1977) simultaneously reported the first observations made by AMS of ^{14}C in natural materials. To summarize the significance of this innovative analytical technique on radiocarbon measurements, Fifield (1999) observes that employing AMS, the radiocarbon age of a sample less than 10,000 years old could be determined to a precision of 0.5% in a few minutes using a mg or less of carbon.[3] Tuniz et al. (1998) point out that the revolution brought about by AMS immediately embraced long-lived radioactive nuclides, emphasizing that the method is applicable to many isotopes (e.g., ^{10}Be, ^{26}Al, ^{36}Cl and ^{129}I). Thus, traditional radiocarbon dating is no

[3]Nowadays this precision is higher even for samples older than 10 ka.

longer the dominant application and a revision made by Fifield (1999) covers the utilization of AMS in diverse research fields such as global climate change via studies of ocean circulation, atmospheric processes and past climate.

More recently, carbon isotopic measurements have been performed by means of infrared absorption (Galli et al., 2011; Zare, 2012; Galli et al., 2013, 2016). In this method, the sample is converted to CO_2 and the carbon isotopes can be distinguished because of differences in the infrared spectra (each isotope absorbs infrared light in slightly different frequencies). This optical method should be much simpler and less costly than AMS and Galli et al. (2013) present a comparison between both methods for the measurement of radiocarbon concentrations.

1.2.2 Carbon Isotopic Fractionation

Differences in mass between carbon isotopes are known to alter thermodynamic properties – responsible for governing the uptake of carbon in chemical and physical processes – of molecules such as CO_2. As a result, variation in atomic mass leads to isotopic differences between the source and product of a chemical or physical transformation, a phenomenon known as *isotopic fractionation*. In fact, early observations conducted by Craig (1953) revealed that biological systems often present carbon isotopic ratios that differ from their supplier reservoir. Indeed, lighter isotopes usually undergo faster reaction kinetics, resulting in products that are enriched in the lighter isotope.

Isotopic fractionation poses an obstacle to radiocarbon dating.[4] As the method relies upon measuring carbon isotopes concentrations, any processes affecting isotopic ratios must be considered. Fortunately, isotopic fractionation can be corrected making use of the fact that relative depletion in ^{14}C is twice that of ^{13}C

[4] The ^{14}C activity of terrestrial plants is lower than the atmospheric one by 3 or 4%, corresponding to an apparent age excess of 240–320 years (Aitken, 1990).

(Craig, 1954). Therefore, it is possible to use the time-independent stable isotope ratio (^{13}C/^{12}C) to determine the relevant corrections for the ratio ^{14}C/^{12}C:[5]

$$(^{14}C/^{12}C)_{\text{initial}} = (^{14}C/^{12}C)_{\text{final}} \left[\frac{(^{13}C/^{12}C)_{\text{initial}}}{(^{13}C/^{12}C)_{\text{final}}} \right]^2 \tag{1.12}$$

When measuring the ratio ^{14}C/^{13}C, Equation 1.12 becomes:

$$(^{14}C/^{13}C)_{\text{initial}} = (^{14}C/^{13}C)_{\text{final}} \frac{(^{13}C/^{12}C)_{\text{initial}}}{(^{13}C/^{12}C)_{\text{final}}} \tag{1.13}$$

Isotopic fractionation is commonly expressed using the δ notation. The sample stable isotope ratio is compared to that of the Pee Dee Belemnite (PDB)[6] ($\mathrm{CaCO_3}$ from the fossil of *Belemnitella americа* (d'Orbigny, 1840) collected from the Peedee Formation of South Carolina, USA) international standard (Coplen, 1994) through the relation:

$$\delta^{13}\mathrm{C}(‰) = \left[\frac{(^{13}C/^{12}C)_{\mathrm{s}}}{(^{13}C/^{12}C)_{\mathrm{PDB}}} - 1 \right] \times 1000 \tag{1.14}$$

where δ^{13}C is the deviation (enrichment or depletion) of the ^{13}C/^{12}C ratio of the sample relative to the standard (Craig, 1957; Keith et al., 1964). Table 1.1 summarises typical δ^{13}C values for important archaeological materials.

By convention, the radiocarbon concentration of a sample, regardless of its environment, is normalized to δ^{13}C = -25‰, the mean isotopic value for terrestrial wood (Stuiver and Polach, 1977). Thus, the fractionation-corrected ^{14}C concentration of a sample ($\mathrm{C_{[-25]}}$) can be derived from its measured ^{14}C concentration (C) and its δ^{13}C value by:

$$\frac{C_{[-25]}}{C} = \left[\frac{1 + (-25/1000)}{1 + (\delta^{13}\mathrm{C}/1000)} \right]^2 \tag{1.15}$$

[5] Although Equation 1.12 is internationally accepted, Stuiver and Robinson (1974) advise the use of an exponent of 1.9 instead of 2.

[6] Currently exhausted and replaced by the Vienna Pee Dee Belemnite (VPDB) standard.

Table 1.1: Typical δ^{13}C values for various materials (Stuiver and Polach, 1977; Aitken, 1990).

Material	δ^{13}C (‰)
NBS Oxalic acid I	-19 $\pm$ 1
Bone collagen, wood cellulose	-20 $\pm$ 2
Wood, charcoal, peat	-25 $\pm$ 3
Freshwater plants	-16 $\pm$ 2
Arid zone grasses, sedges, papyrus	-13 $\pm$ 2
Marine plants	-12 $\pm$ 2
Grains, seeds, maize, millet	-10 $\pm$ 2
Bone apatite	-10 $\pm$ 2
Atmospheric $\mathrm{CO_2}$	-9 $\pm$ 2
Non-marine carbonates	-5 $\pm$ 5
Marine carbonate	0 $\pm$ 3

1.2.3 Conventional Radiocarbon Age (CRA)

The outcome of a ^{14}C measurement is commonly reported as a *conventional radiocarbon age (CRA)*, given in radiocarbon years before present (^{14}C yr BP) (Stuiver and Suess, 1966). This value is not an age in the usual sense of the word, but rather a function of the radiocarbon concentrations in the sample and in a standard material from 1950,[7] both corrected for isotopic fractionation:

$$CRA = -8{,}033 \ln \left(\frac{C_{[-25]}}{C_{1950[-25]}} \right) \tag{1.16}$$

where the ratio in the logarithm is defined as the *fraction modern carbon* $\mathrm{F_m}$. Equation 1.16 derives from Equation 1.6 and convention dictates that the so-called *Libby's half-life* (5,568 years) should be used in the calculation (Stuiver and Polach, 1977).[8] Stuiver and Polach (1977) present a complete discussion on the calculation of radiocarbon ages but, to summarize, the use of Equation 1.16 involves the following conventions and assumptions:

[7] This represents the atmospheric radiocarbon concentration at that year.

[8] Despite the availability of the more precise value of 5,730 $\pm$ 40 years, this agreement was established in order to simplify comparisons with radiocarbon dates obtained before 1962 (Godwin, 1962).

1. The use of Libby's half-life (5,568 years) for ^{14}C.

2. The assumption that the atmospheric levels of ^{14}C were kept constant in the past.

3. The use of oxalic acid (directly or indirectly) as a standard.[9]

4. Normalization of isotopic concentrations to $\delta^{13}C$ = -25‰ relative to the PDB standard.

5. 1950 is the present, with all radiocarbon ages being given in years before 1950.

Knowledge of the initial carbon isotopic concentration of a sample is essential to quantify any depletion. The use of a CRA for chronological purposes is based on the premise that the carbon isotopic concentration of the reservoir where the sample was formed has been constant (Stuiver and Suess, 1966). If this was indeed the case, then it would not be necessary to go any further than the result obtained by the application of, for instance, Equation 1.6 (provided the correct ^{14}C half-life is used). However, the atmospheric radiocarbon concentration varies in a non-linear fashion over time, and thus the second postulate is not a reasonable assumption. Fortunately, this can be corrected by the process of calibration of radiocarbon ages.

1.2.4 The Need for Calibration

Conventional radiocarbon ages cannot be used in calendrical time-scale interpretations or for comparisons with dates obtained by other dating methods (de Vries, 1958; Stuiver and Suess, 1966; Blockley and Housley, 2009). Although radiocarbon dating is now consolidated as a valid and powerful technique, the correction of

[9] In Equation 1.16, C_{1950} is equal to $0.95C_{OX[-19]}$, where C_{OX} is the radiocarbon concentration of the oxalic acid standard normalized to -19‰ relative to the PDB standard.

underlying assumptions is a step that must be taken towards reaching a calendar date. The following paragraphs present some of the reasons for variations in ^{14}C concentration in Earth's reservoirs, illustrating the necessity of calibration.

The geomagnetic field influences the flux of cosmic rays into the atmosphere. In fact, a charged particle experiences the effects of Earth's magnetic field long before it reaches the terrestrial atmosphere. This has the effect of creating a latitude dependence of the production rate of cosmogenic nuclides (Gosse and Phillips, 2001; Muzikar et al., 2003). Indeed, the geomagnetic field works as a shield, deflecting low energy charged particles (Muzikar et al., 2003) and, as a result, changing the cut-off energies of the cosmic radiation (Lal and Jull, 2001; Masuda et al., 2009). This deflection is governed by the magnetic term of the Lorentz force, being strongest at low latitudes, where the velocity of incoming particles is mostly perpendicular to the magnetic field lines (Muzikar et al., 2003). Therefore, ^{14}C production rates are enhanced at high latitudes, where geomagnetic deflection is minimal. Temporal changes in the Earth's magnetic field also lead to variations in radiocarbon production rates (e.g., Voelker et al., 2000).

Radiocarbon production rates are also affected by altitude. There is a peak of fast neutron production at approximately 15 km above Earth's surface (Gosse and Phillips, 2001). At this height, the density of target nuclei and the number and energy of the cosmic radiation are the highest (Muzikar et al., 2003). Consequently, collisions between thermal neutrons and nitrogen atoms are more likely, enabling a maximum in ^{14}C production.

The interplanetary magnetic field also affects charged particles travelling through our solar system. This field permeates the interplanetary space and helps to inhibit primary cosmic radiation from penetrating Earth's atmosphere, playing an important role in the production of cosmogenic nuclides (Korff and Mendell, 1980; Stuiver et al., 1997; Gosse and Phillips, 2001; Muzikar et al., 2003). Stuiver (1961) noticed

that the modulation of the interplanetary magnetic field by solar winds results in variations in ^{14}C production. Indeed, sunspots[10] have been recorded for centuries and their abundance is inversely correlated with the rates of ^{14}C formation (Masuda et al., 2009). Fluctuations in solar activity occur in different time scales and, at the minimum of the 11-year Schwabe cycles[11], ^{14}C production rates reach 1.15 times the normal rate (Masarik and Beer, 1999). The same inverse proportional relation between cosmic rays intensity and solar activity is shown in the radiocarbon record for long-term modulation of the solar magnetic activity (e.g., 210 year De Vries cycles and 2,300 year Hallstatt cycles) (Tobias et al., 2004; Clilverd et al., 2003, 2004).

Regional differences in radiocarbon concentration caused by the latitude dependence of ^{14}C production rates are attenuated by the rapid mixing of the atmosphere. Nevertheless, offsets in the atmospheric ^{14}C concentration between the two hemispheres (as divided by the thermal equator) do persist (McCormac et al., 2002; Hogg et al., 2011, 2013). Lerman et al. (1970) observed the so-called *interhemispheric offset* through ^{14}C measurements in contemporaneous wood from the Southern and Northern Hemispheres. They found that Southern samples appear to be older by approximately 30 ^{14}C yr. More recently, other studies were performed to confirm this offset (e.g., Vogel et al., 1993; McCormac et al., 1998; Stuiver and Braziunas, 1998) and it is now known that its magnitude varies temporally (McCormac et al., 2002; Hogg et al., 2011; Rodgers et al., 2011). It is widely accepted that the interhemispheric offset is a result of the larger oceanic area of the Southern Hemisphere, which increases the air-sea interface and, consequently, the CO_2 exchange fluxes between the atmosphere of the Southern Hemisphere and radio-

[10] These features have proven to be a useful index for solar activity (Masuda et al., 2009) due to their magnetic field being higher than the average field displayed by the sun (Korff and Mendell, 1980; Tobias et al., 2004).

[11] These are caused by changes in the amplitude of the solar magnetic activity.

carbon depleted surface waters in the upwelling zone of the circumpolar region (Levin et al., 1987; McCormac et al., 2002; Hogg et al., 2011, 2013).

Volcanic eruptions also play a role in the atmospheric radiocarbon concentration as they release ^{14}C-depleted $\mathrm{CO_2}$. Plants near volcanic sites absorb a proportion of this $\mathrm{CO_2}$, lowering their radiocarbon content (Sulerzhitzky, 1971; Bruns et al., 1980). The influence of volcanos is particularly relevant for samples younger than 10,000 years and may lead to apparent ages of up to 1,600 years (Sulerzhitzky, 1971; Bruns et al., 1980). Nevertheless, the effect of volcanic eruptions on the radiocarbon budget is generally thought to be very local, being considered negligible on a global scale.

Modern economies, especially those of industrialized countries, are highly dependent upon fossil fuels and the burning of materials such as coal, oil and natural gas provides energy for several industrial and domestic activities. Many of these processes release ^{14}C-free $\mathrm{CO_2}$ into the atmosphere, disturbing the atmospheric carbon signal as first reported by Suess (1955). He observed a dilution in the atmospheric ^{14}C concentration, and associated changes in the stable isotopes content, through measurements of the carbon isotopic ratio in modern tree rings, which is termed the industrial, fossil fuel or, more commonly, the *Suess effect*. Consistently, other reservoirs are also affected to different extents.

From the industrial revolution onwards, combustion of fossil fuels has been occurring on a large scale. Attempts to quantify the Suess effect through the analysis of tree rings from the last two centuries revealed that wood from 1950 AD exhibits lower ^{14}C concentration than wood grown in 1850 AD (Suess, 1955; Stuiver and Quay, 1981; Tans et al., 1979) (Figure 1.3a). The carbon isotopic record also shows geographic variations in the Suess effect, with increased magnitudes registered in more polluted and highly populated areas (Jong and Mook, 1982; Levin et al., 1989). Furthermore, there is a seasonal pattern, as fossil fuel $\mathrm{CO_2}$ emissions

intensify over the winter due to domestic heating, when the vertical mixing of the atmosphere is already reduced (Levin and Hesshaimer, 2000).

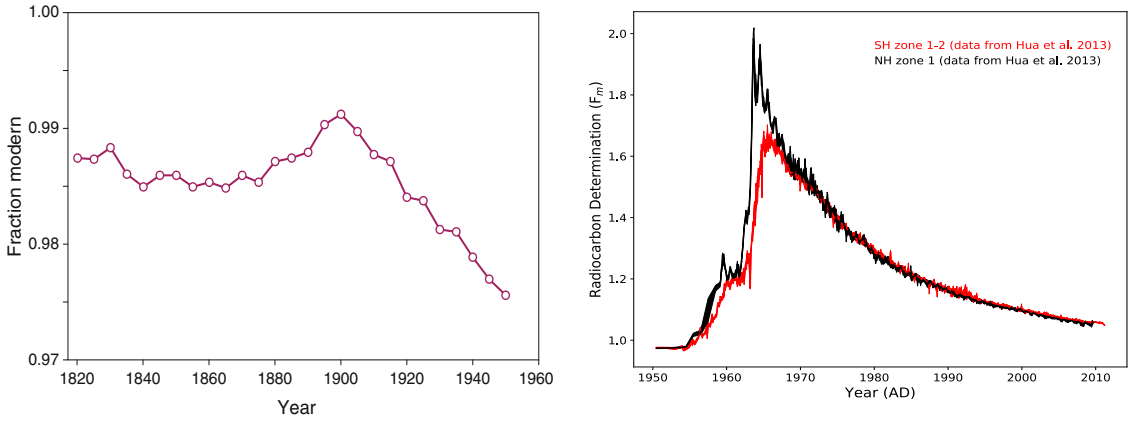


Figure 1.3. Anthropogenic perturbations to the atmospheric carbon reservoir. a: The dilution of atmospheric radiocarbon due to the Suess Effect. Fraction modern values were defined as 1.00 for the preindustrial atmosphere, specifically based on wood from 1890. Source: Schuur et al. (2016). b: The ^{14}C bomb peak curves for the period 1950-2010 AD. SH = Southern Hemisphere and NH = Northern Hemisphere. Data from Hua et al. (2013), where the definitions of the different zones can be found.

Another important anthropogenic perturbation in the global carbon budget is a consequence of nuclear weapons testing in the 1950s and early 1960s, when several nations performed tests involving nuclear explosions in the atmosphere. When detonated, a nuclear bomb produces neutrons that eventually form what is called artificial, anthropogenic or bomb radiocarbon.[12] For the global carbon budget, the outcome of the tests was the production of 630 x 10^{26} or more atoms of ^{14}C (Hesshaimer et al., 1994). This large quantity of radiocarbon caused a significant disequilibrium between the different reservoirs, doubling the atmospheric ^{14}C concentration in the Northern Hemisphere, where the great majority of explosions took place (Levin and Hesshaimer, 2000). This ^{14}C concentration maximum in the Northern Hemisphere was reached in 1963 and in the same year nuclear tests were prohibited by the Test Ban Treaty (Rakowski et al., 2005). In the South-

[12]The formation of bomb-produced ^{14}C occurs in the same manner as the natural one (Equation 1.8).

ern Hemisphere the peak was lower and occurred later due to the time it took for the influence of the tests performed in the Northern Hemisphere to reach the Southern Hemisphere (Figure 1.3b). Moreover, wind patterns prevent a complete inter-hemispheric mixing of the atmosphere (Hua et al., 2013). Since the ban of the tests, the bomb peak has been decreasing due to carbon exchange between the reservoirs and the counteracting Suess effect (Broecker et al., 1985b; Hesshaimer et al., 1994; Levin and Hesshaimer, 2000; Rakowski et al., 2005; Hua et al., 2013). It is also important to mention the useful tracer properties of the bomb pulse, which allow the study of carbon fluxes within the global carbon cycle (Levin and Hesshaimer, 2000; Hua et al., 2013).

Due to the reasons discussed above, the efficiency of the ^{14}C dating technique is partially dependent on highly refined calibration data. These data are used to account for variations in the ^{14}C concentration of reservoirs and convert radiocarbon ages to calendar years using notations such as cal BP (Before Present, where 1950 AD is the present), cal CE (Common Era), cal BCE (Before Common Era), cal BC (Before Christ), and cal AD (Anno Domini). Calibration is performed in an empirical way, using radiocarbon ages measured for known-age samples. Following this procedure, a calibration curve of ^{14}C age versus calendar date is constructed (Pearson and Stuiver, 1993; Stuiver et al., 1998a,b; Reimer et al., 2004, 2009, 2013).

1.2.5 Terrestrial Calibration

Terrestrial (or atmospheric) calibration is achieved by means of curves containing the ^{14}C data of known-age samples, mostly wood dated by dendrochronology (e.g., Pearson and Stuiver, 1993; Stuiver et al., 1998a,b; Reimer et al., 2004, 2009, 2013). Radiocarbon measurements are performed in the annual growth rings of certain tree species (e.g., sequoias and oaks) and the correspondent calendar

years are obtained from the counting of these rings.[13] In this way, the tree-ring approach yields accurate and high resolution data, being defined as the heart of the calibration process for the period 0-12.4 cal kyr (Blockley and Housley, 2009). Nevertheless, one of the most challenging tasks in the construction of calibration curves is the selection of suitable samples. Beyond the limits of dendrochronology applicability, ^{14}C data obtained from materials formed in other reservoirs are incorporated to the atmospheric curves. These comprise a variety of samples such as foraminifera from varved sediments (e.g., Hughen et al., 2006) and Th-U dated corals (e.g., Bard et al., 1998; Fairbanks et al., 2005) and speleothems (e.g., Southon et al., 2012). The ^{14}C ages of these samples must be treated to yield equivalent terrestrial ages, in a process much less straightforward than the tree-rings approach. Furthermore, Bronk Ramsey et al. (2015) point out that the known-ages of these records are subjected to, e.g., deposition models and measurement errors that would increase the uncertainty of the dataset.

Multiple calibration curves have been published and are continuously updated (e.g., Klein et al., 1982; Stuiver et al., 1986; Stuiver and Braziunas, 1993; Stuiver et al., 1998a; Reimer et al., 2004, 2009; Hogg et al., 2013; Reimer et al., 2013). The most recent atmospheric calibration curves are IntCal13 (Reimer et al., 2013) for the Northern Hemisphere, and SHCal13 (Hogg et al., 2013) for the Southern Hemisphere.[14] The vertical axis of these curves is the radiocarbon age in ^{14}C years BP while the horizontal axis represents the absolute calendar years in cal BC, cal AD, or cal BP implying pre-1950 (Figure 1.4).

[13] The wood deposited in such structures does not exchange carbon with the surroundings and thus is a reliable representation of the atmospheric ^{14}C concentration in their specific years of formation.

[14] The use of different calibration curves for the Southern and Northern Hemispheres accounts for the interhemispheric offset discussed in subsection 1.2.4.

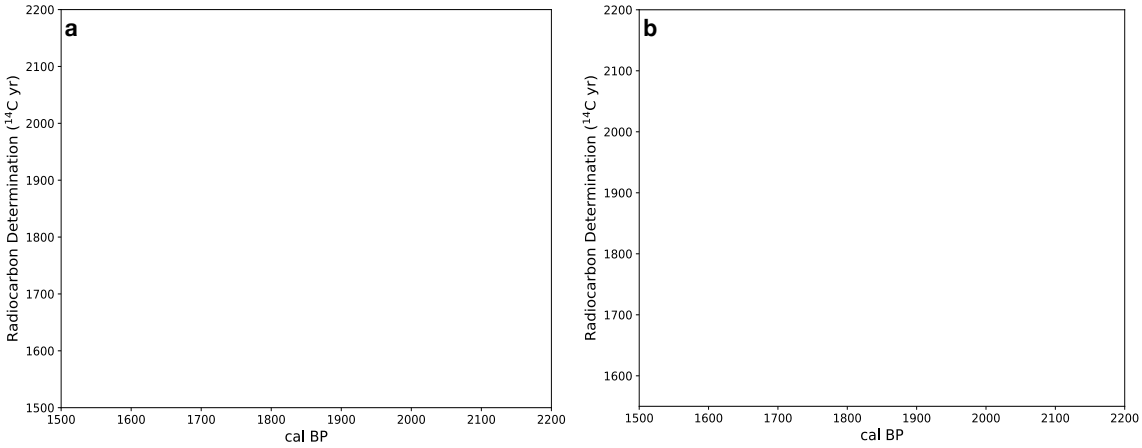


Figure 1.4. Sections of the most recent ^{14}C atmospheric calibration curves. a: IntCal13 (Reimer et al., 2013) is used for the Northern Hemisphere. b: SHCal13 (Hogg et al., 2013) represents the Southern Hemisphere.

Calibration is performed through the interpolation of the probability distribution for the ^{14}C age of the sample and its associated error with the calibration curve.[15] Due to the non-linear fashion of the curves, there may be multiple interception points (Pearson, 1987), resulting in non-Gaussian distributions for the calibrated age in the horizontal axis. Depending on the slope of the curve in the point of interception, calibrated age intervals can be quite large, which means that a ^{14}C age intercepting a curve plateau will yield a less precise estimate for the calendar date. However, using Bayesian analysis, it is possible to generate a time interval with the probability distribution for the calibrated age (Dehling and van der Plicht, 1993). Radiocarbon ages are generally calibrated through software containing a database with the experimental points that form the calibration curves, such as CALIB (Stuiver and Reimer, 1993) and OxCal (Bronk Ramsey, 1995, 2001, 2009; Bronk Ramsey et al., 2015).

[15]The overall uncertainty for the calibrated ^{14}C age is derived from the uncertainties in the measurement and in the calibration curve itself.

1.3 The Atmospheric and Marine Carbon Reservoirs

Every year, approximately 150 gigatons (Gt) of carbon are exchanged between the different compartments of the Earth system. The set of chemical and physical processes involved in this exchange is called the *global carbon cycle* and the total amount of carbon in the three active reservoirs of atmosphere, biosphere and sea is known as the *exchangeable system* (Craig, 1957). This biogeochemical cycle allows carbon to be recycled and reused throughout the reservoirs (Figure 1.5). Indeed, by the mass conservation principle, there are no losses and any shift in carbon content that takes place in a reservoir affects the amount of carbon in the others.[16]

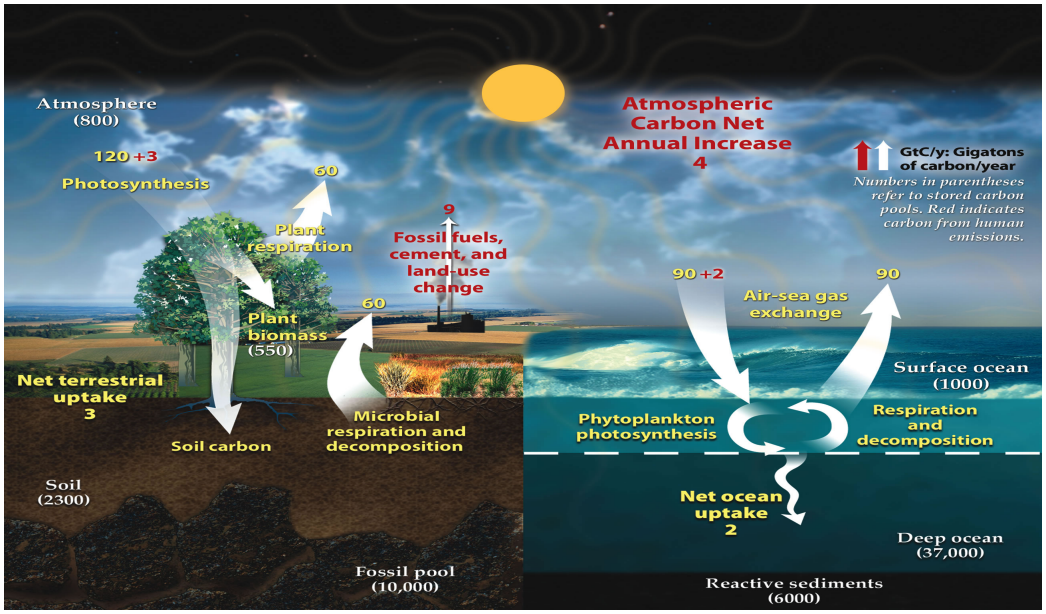


Figure 1.5. Diagram showing the global carbon cycle. Yellow numbers are natural fluxes and red numbers are human contributions in gigatons of carbon per year. Source: Nasa Earth Observatory webpage.

The size of the atmospheric carbon reservoir has been accurately known since 1958 when Charles Keeling started measuring CO_2 at the Mauna Loa observatory

[16]This can be illustrated by the current ocean acidification issue (e.g., Doney et al., 2009). Activities such as deforestation and the burning of fossil fuels are increasing the CO_2 input to the atmosphere, whereas there is no matching increase in potential sinks for this CO_2, which pushes the global carbon cycle out of equilibrium.

in Hawaii (Post et al., 1990). Since then, it is also known that the amount of CO_2 in the atmosphere has grown exponentially as a result of human activity (see subsection 1.2.4). Fossil fuel burning (5.6 - 6.0 Gt C yr^{-1}), decomposition of organic residues (35 - 65 Gt C yr^{-1}) and plant respiration (40 - 60 Gt C yr^{-1}) are among the main sources of CO_2 being added to the atmosphere (Bolin and Fung, 1992). Oceanic respiration also plays a significant role (55 - 76 Gt C yr^{-1}) (del Giorgio and Duarte, 2002). Yet, there is a consensus that the Earth's atmosphere is the reservoir containing the smallest amount of carbon. This, combined with its homogeneity, turns the atmosphere into the reservoir most sensitive to perturbations in the carbon cycle (Cook et al., 2009).

The ocean holds significantly more carbon than the atmosphere.[17] The amount of carbon stored in a reservoir is influenced by turnover rates, as some reservoirs do not cycle carbon quickly.[18] Carbon atoms reside only 4 to 8 years in the terrestrial biosphere due to rapid exchange with the surrounding atmosphere (Gaudinski et al., 2000). Exchange between the upper layers of the ocean and the overlying atmosphere is also relatively fast, with carbon being cycled much more quickly than in the deep ocean. This has the effect of establishing a dependence of marine carbon residence times on depth.[19] Indeed, carbon atoms can stay in the deep ocean for thousands of years (e.g., Sigman and Boyle, 2000) before returning to the atmospheric reservoir through upwelling followed by exchange at the ocean surface. Residence times in the deep ocean vary due to ocean geography and circulation,

[17] Atmosphere-ocean CO_2 exchange fluxes amount to approximately 90 Gt C yr^{-1} in each direction (see review in Falkowski et al., 2000) and, since the Industrial Revolution, a net flux of 0.8–2.4 Gt C yr^{-1} into the oceans (Bolin and Fung, 1992, and references therein).

[18] Cook et al. (2009) discuss the concepts of dynamic and sedimentary compartments in the global carbon cycle. Indeed, carbon turnover rates for geological processes are often thousands or millions of years, whereas the plant fixation of carbon via photosynthesis, for instance, involves time scales of one year or less.

[19] I follow Craig (1957) and define the residence time of a nuclide as the time during which this element remains in a reservoir before being transferred to another. Nevertheless, multiple definitions for this term are encountered in the literature (Sierra et al., 2017, and references therein).

whereas the surface residence times are influenced by the deep ocean regime and the air-sea gas exchange.

1.3.1 Marine Dissolved Inorganic Carbon and ^{14}C

The air-sea exchange of $\mathrm{CO_2}$ is responsible for the oceanic uptake of atmospheric ^{14}C (Figure 1.6). This process occurs at the air-sea interface, where differences between the $\mathrm{CO_2}$ partial pressures of the reservoirs determine the direction of the flux:[20]

$$F = \mathrm{k_g}(p\mathrm{CO_2^{at}} - p\mathrm{CO_2^{sea}}) = \mathrm{k_g}\Delta p\mathrm{CO_2} \tag{1.17}$$

where $\mathrm{k_g}$ is a gas exchange coefficient based on a complex set of physical processes such as turbulent mixing and surface waves (Merlivat and Memery, 1983; Siegenthaler and Sarmiento, 1993; Jahne and Haussecker, 1998). Temperature affects $\mathrm{pCO_2^{sea}}$ by changing the solubility of $\mathrm{CO_2}$ in seawater. Indeed, due to the higher solubility of $\mathrm{CO_2}$ in cold waters, high latitude regions tend to act as sinks of $\mathrm{CO_2}$.[21] In these areas, enhanced primary production also contributes to the removal of $\mathrm{CO_2}$ from surface waters, which lowers $\mathrm{pCO_2^{sea}}$ and increases the oceanic uptake of atmospheric $\mathrm{CO_2}$ (McElroy, 1983; Siegenthaler and Sarmiento, 1993; Sarmiento et al., 1998; Sigman and Boyle, 2000; Herndl and Reinthaler, 2013).[22] Conversely, in the tropics, warm waters exhibit low $\mathrm{CO_2}$ solubility and high $\mathrm{pCO_2^{sea}}$, which leads to $\mathrm{CO_2}$ evasion. These regions act as sources of $\mathrm{CO_2}$ to the atmo-

[20] In fact, given that $\mathrm{CO_2}$ is well mixed in the lower atmosphere, the flux direction depends mostly on the $\mathrm{CO_2}$ partial pressure at the ocean surface, which is constantly being reset due to the interaction between different water masses (Sigman and Boyle, 2000; Williams and Follows, 2011).

[21] This phenomenon, known as the *solubility pump*, is driven by thermohaline circulation and ocean ventilation (Taylor, 1992; Raven and Falkowski, 1999).

[22] Photosynthetic organisms remove $\mathrm{CO_2}$ from surface waters and, upon their death, this carbon is transferred to the deep ocean. This accounts for the export of 11 - 16 Gt of organic carbon per year. Without this mechanism, known as the *biological pump*, little $\mathrm{CO_2}$ could be transferred from the atmosphere to the ocean (Post et al., 1990; Falkowski et al., 2000, and references therein).

sphere (Williams and Follows, 2011).[23] Sigman and Boyle (2000) discusses a more complex control, exerted by the ocean chemical composition, on pCO_2^{sea}.

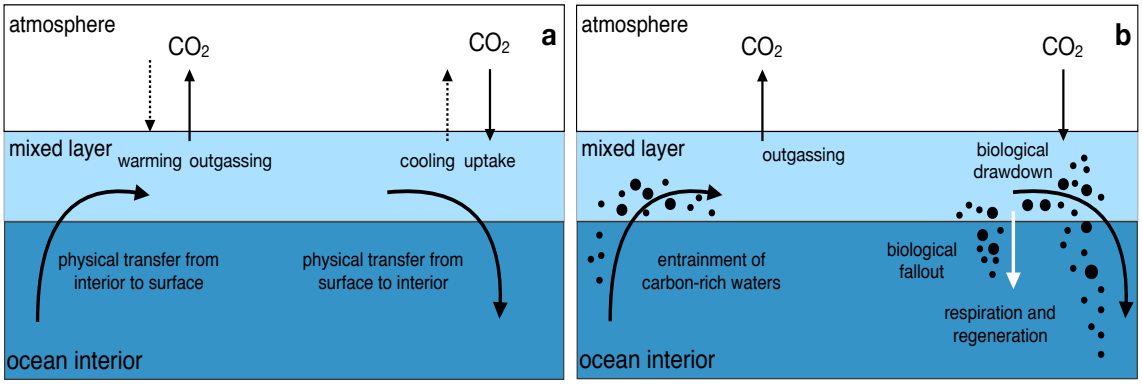


Figure 1.6. a: The effect of temperature on the marine uptake of CO_2. b: Organic matter is transported to the ocean interior. The return of these carbon-rich waters to the mixed layer leads to CO_2 outgassing. Source: Modified from Williams and Follows (2011).

To summarize, the air-sea CO_2 exchange is a heterogeneous process over the globe (Takahashi et al., 2002, 2009), meaning that the uptake of atmospheric ^{14}C by the marine reservoir varies both temporally and geographically. After CO_2 dissolution in the water, it dissociates forming what is collectively known as *Dissolved Inorganic Carbon (DIC)*:

$$CO_2 + H_2O \rightleftharpoons H_2CO_3 \rightleftharpoons H^+ + HCO_3^- \rightleftharpoons 2H^+ + CO_3^{2-} \tag{1.18}$$

DIC constitutes the pool of inorganic carbon in the oceans and consists of three carbonate species: the sum of the aqueous form of CO_2 and carbonic acid (H_2CO_3), bicarbonate ions (HCO_3^-) and carbonate ions (CO_3^{2-}) (Mills and Urey, 1940; Mook et al., 1974; Siegenthaler and Sarmiento, 1993; Zeebe and Wolf-Gladrow, 2001). Oceanic DIC holds 40 times more carbon than organic carbon forms and 90% of DIC is bicarbonate ions (Williams and Follows, 2011). This thesis is based on

[23] The upwelling of carbon-rich waters can lead to CO_2 evasion to the atmosphere. On the other hand, upwelling enhances primary production by supplying nutrients to the photic zone, which could lead to CO_2 uptake from the atmosphere. The role of upwelling systems in the air-sea CO_2 fluxes still seems to be a subject of debate (Hales et al., 2005; Friederich et al., 2008; Williams and Follows, 2011).

isotopic measurements in the shells of organisms that sample DIC from the seawater.[24]

1.4 Reservoir Effects

Various compartments in the global carbon cycle exhibit ^{14}C activities that differ from those in the atmospheric reservoir. In some cases (e.g., the terrestrial biosphere), rapid exchange with the atmosphere ensures that the disparity can be corrected by simply accounting for isotopic fractionation effects. Nevertheless, for some reservoirs, this offset is the result of complex mechanisms in the biogeochemical cycles, responsible for the exchange of carbon between different compartments of the Earth system. Indeed, the processes governing the transfer of carbon between reservoirs happen at different time scales, leading to distinct residence times and affecting the availability of carbon isotopic species in different environments. The situation is further complicated by intra-reservoir variability due to slow mixing rates. As a consequence, the isotopic composition of materials formed by carbon sourced from reservoirs other than the atmosphere (e.g., speleothems and all sorts of aquatic material) present the so-called *reservoir effects*. This term was first used by Stuiver and Polach (1977) to introduce adjustments necessary for the radiocarbon ages of such materials. Corrections are needed if one wants to derive the coeval atmospheric signal or compare radiocarbon ages from different reservoirs, and a solid knowledge of the factors affecting the transport and residence times of carbon in different reservoirs is needed for the evaluation of such corrections. Radiocarbon offsets between the atmosphere and other reservoirs can also arise when the reservoir being considered receives carbon input from

[24] In large scale, this mechanism significantly reduces the DIC concentration at the surface ocean by delivering it to the deep layers. The phenomenon is known as the *carbonate pump* and has a competing effect on pCO_2^{sea} (Volk and Hoffert, 1985).

sources that differ from the atmosphere in ^{14}C activity. This is the case for *hard water and freshwater reservoir effects*, for instance. The main object of study of this research is perhaps the most well studied reservoir effect, the one that takes place in marine environments: the *Marine Reservoir Effect (MRE)*.

1.4.1 The Marine Reservoir Effect (MRE)

Marine samples yielding inconsistent ^{14}C results have been reported since the initial years of radiocarbon research. The measurement of stable carbon isotopes showed that marine carbonates preferentially incorporate the heavy isotope ^{13}C and thus present a 2.5% enrichment in ^{13}C when compared to terrestrial materials (Nier and Gulbransen, 1939). Since isotopic fractionation is mass dependent, it follows that marine carbonates should be enriched in ^{14}C by about 5% when compared to terrestrial material. Due to the large errors involved in the measurements, this hypothesis was supported by results published in the first radiocarbon assay (Libby et al., 1949). Soon thereafter, modern sea shells were shown to be enriched in ^{14}C by about 8% when compared to terrestrial material (Anderson and Libby, 1951) and, despite the higher enrichment factor, this also corroborated the idea of marine samples presenting higher ^{14}C activity. The scenario started to change when archaeological shells measured by Kulp et al. (1952) appeared to be too old, which was attributed to the influence of upwelling. However, Blau et al. (1953) presented radiocarbon measurements of shells, from locations showing different oceanographic settings, that seemed to be in agreement with similar measurements of terrestrial material. Finally, Craig (1954) stated that higher precision methods did not show the predicted enrichment and concluded that this effect was a product of the slow transfer of ^{14}C across the air-sea interface, acknowledging that the effect should be greater in the deep ocean due to slow mixing rates.

The lower ^{14}C content of the ocean relative to the atmosphere is termed the Marine Reservoir Effect (MRE).

A practical implication of the MRE is that marine materials yield overestimated ^{14}C ages. The anomalies can reach thousands of years and the radiocarbon ages obtained from these samples are termed *apparent ages* (Mangerud, 1972). Early investigations on the subject discussed the offsets in association with the ocean dynamics, especially in upwelling regions (Craig, 1957; Berger et al., 1966; Taylor and Berger, 1967). Mangerud (1972) stated, in the first complete analysis of the topic, that carbon exchange between reservoirs, together with the internal carbon circulation in the ocean, causes the MRE. Moreover, the author concluded that ocean circulation is the dominant factor controlling ocean ^{14}C activity. Later, Bard (1988) discussed the effects of wind speed and climate-related parameters on the radiocarbon activity of surface waters. Since CO_2 is incorporated at the air-sea interface, waters removed from the surface undergo ^{14}C decay without replenishment. Considering that residence times are of the order of thousands of years in the deep ocean, these water masses can "age" significantly depending on how much time they spend at depth. Nevertheless, the MRE is not absent in surface waters. Indeed, these water masses contain both old carbon, from their interaction with the deep layers, and newly acquired carbon from the atmosphere. The surface ocean radiocarbon activity is enriched when compared to isolated deep waters but depleted relative to the atmosphere and terrestrial biosphere (Ascough et al., 2004).

The overturning or thermohaline circulation (Broecker, 1991; Talley et al., 2011; Talley, 2013) is an example of a global mechanism involving the vertical movement of water in the ocean (Figure 1.7). Cooling and/or salinification of wind-driven surface currents en route to the polar regions causes water to become denser and sink in a process known as downwelling. The water, isolated from the point of

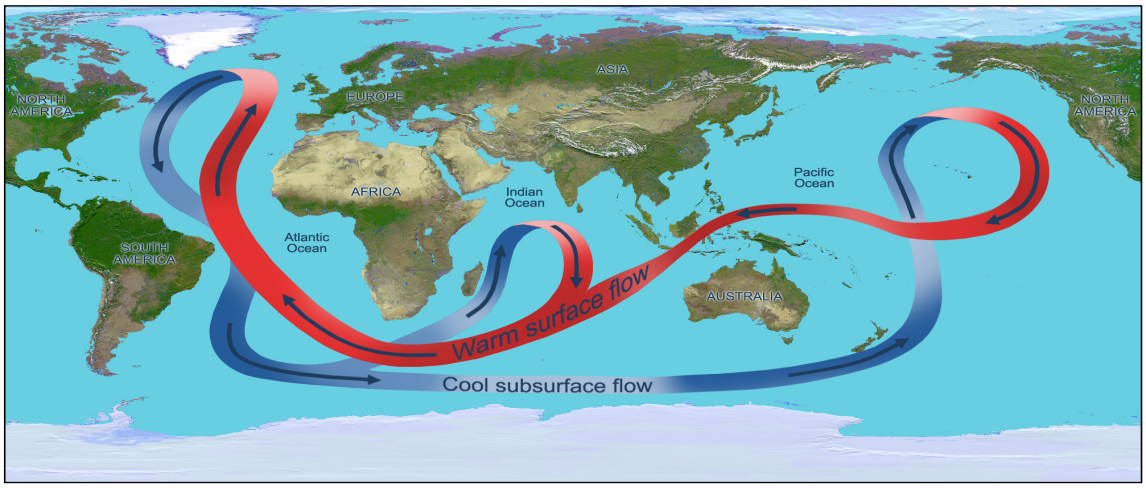


Figure 1.7. Simplified depiction of the global overturning or thermohaline circulation. See Talley et al. (2011) for a discussion on the limitations of this diagram. Source: USA National Ocean Service.

^{14}C atmospheric input, undergoes ^{14}C decay during its slow journey at intermediate and deep ocean layers (> 100 m approx.). In certain upwelling regions of the ocean, this ^{14}C depleted water is eventually brought back to the surface. At high latitudes, the major oceans show high reservoir ages due to the upwelling of radiocarbon depleted waters and sea ice reducing the air-sea CO_2 exchange (Figure 1.8). Nevertheless, it is interesting to note that this is not the case for the North Atlantic Ocean. Indeed, deep water formation inhibits upwelling in this part of the Atlantic, which also receives low latitude waters relatively enriched in radiocarbon (see Figure 1.7).

Due to the importance of the oceanic carbon cycle for climate, the MRE finds application in many different fields. In archaeology, the study of the MRE reflects the importance of the radiocarbon dating tool in this field. Indeed, much of the available MRE data were obtained by archaeologists or other scientists working in archaeology-related departments all over the world (e.g., Little, 1993; Ulm, 2002; Ervynck, 2014; Facorellis and Vardala-Theodorou, 2015). For the ocean sciences, the quantification of the MRE is important for the understanding of factors such as

ocean circulation modes, residence times and upwelling strength. For instance, any phenomenon influencing the patterns and rates of ocean ventilation will affect the oceanic radiocarbon distribution as demonstrated by extreme variations in ocean circulation during the last deglaciation, causing changes in the air-sea exchange and reservoir ages (e.g., Bard, 1988; Bard et al., 1989; Broecker and Barker, 2007; Stuiver et al., 1991). Alves et al. (2018) provide more examples for the applications of the MRE.

The multidisciplinary character of MRE research and its power to approach relevant questions such as the ones related to the Earth's climate system are evident. On a more methodological note, the quantification of the MRE is important for the construction of radiocarbon calibration curves (see Hogg et al., 2013; Reimer et al., 2013, for details on the construction of the most recent curves). More generally, regarding research involving ^{14}C in the ocean, as mentioned in subsection 1.2.4, the relatively high signal of bomb-produced radiocarbon in the upper oceanic layers can be used to track ocean circulation in the main ocean basins (e.g., in the World Ocean Circulation Experiment (WOCE) (McNichol et al., 2000)).

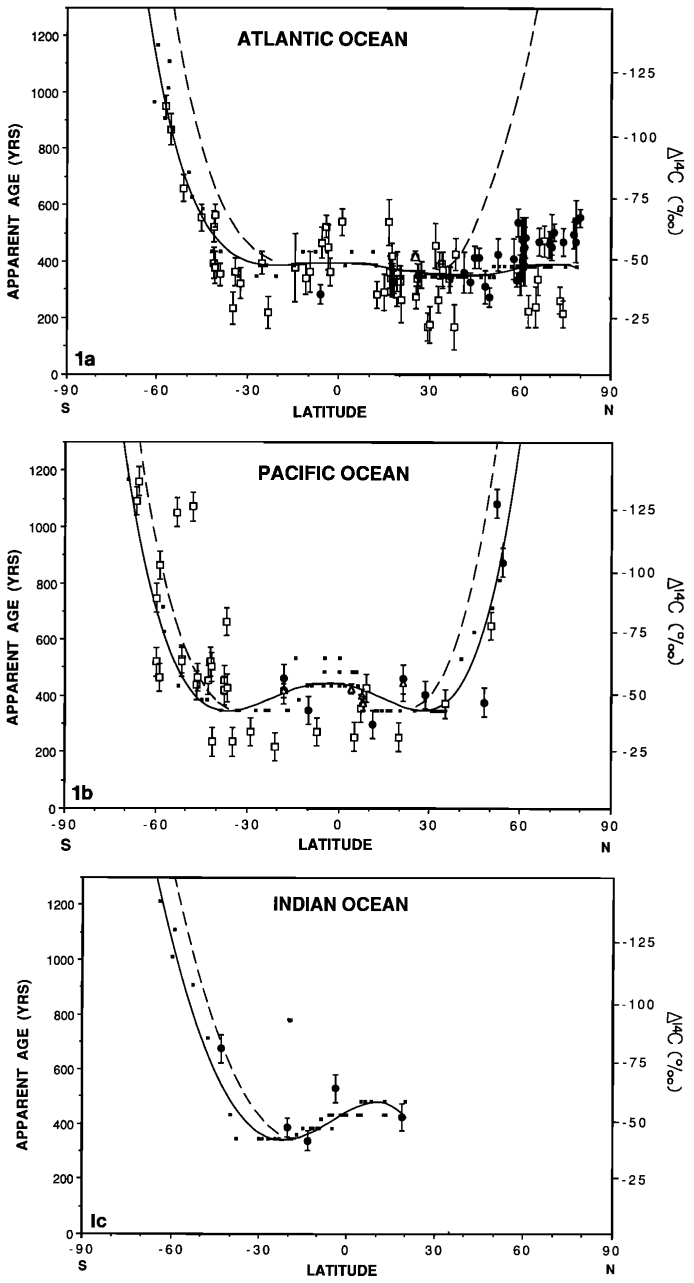


Figure 1.8. Reservoir age recostruction for the Atlantic, Pacific and Indian oceans. The plots show mollusc measurements (closed circles), coral measurements (open triangles), sea water measurements (open squares) and pre-bomb $\Delta^{14}C$ reconstructions from Broecker et al. (1985a). The solid lines are least-squares polynomials fitted to the data and the dashed curves represend a hypothetical profile for the last glacial maximum. Source: Bard (1988).

1.4.2 A Quantitative Description of the MRE

In subsection 1.4.1, I presented qualitative statements about the MRE. Yet, the concept of ^{14}C offsets between the atmosphere and the ocean can be translated into a more mathematical language. Stuiver et al. (1986), in a seminal paper on marine calibration and the MRE, introduced the idea of a *reservoir age R(t)*:

$$R(t) = {}^{14}C_{\mathrm{mar}} - {}^{14}C_{\mathrm{atm}} \tag{1.19}$$

where $^{14}\mathrm{C}_{\mathrm{mar}}$ is the radiocarbon age of a marine sample and $^{14}\mathrm{C}_{\mathrm{atm}}$ is its atmospheric radiocarbon age determined independently for a given time t.[25] Because of the factors discussed in subsection 1.4.1, the ocean is considered to be the most heterogeneous ^{14}C reservoir (Cook et al., 2009) and, in order to account for this heterogeneity, Stuiver et al. (1986) and Stuiver and Braziunas (1993) adopted the concept of a ΔR value:[26]

$$\Delta R = R_{\mathrm{measured}} - R_{\mathrm{expected}} \tag{1.20}$$

where $\mathrm{R}_{\mathrm{measured}}$ represents the regional reservoir age and $\mathrm{R}_{\mathrm{expected}}$ represents the modelled global marine reservoir age. The latter is the difference between the atmospheric and marine calibration curves for any point in time. Although Stuiver et al. (1986) considered ΔR values to be time-independent in first approximation, the literature presents data supporting the temporal variability of these offsets (e.g., Austin et al., 1995; Kennett et al., 1997; Soares and Dias, 2006; Ortlieb et al., 2011). Published R and ΔR values for the modern ocean surface are com-

[25] The term "reservoir age" can be misleading. As an example, shifts in the atmospheric ^{14}C content would not affect the deep ocean isotopic signal but would still change its reservoir age.

[26] $\Delta\mathrm{R}_{\mathrm{a}}$ is the atmospheric equivalent of ΔR (Stuiver and Braziunas, 1993). Nevertheless, the only significant ^{14}C intrareservoir discrepancy in the atmosphere is the interhemispheric variation discussed in subsection 1.2.4.

piled in the *Marine Reservoir Database* (http://calib.qub.ac.uk/marine/) (Reimer and Reimer, 2001).

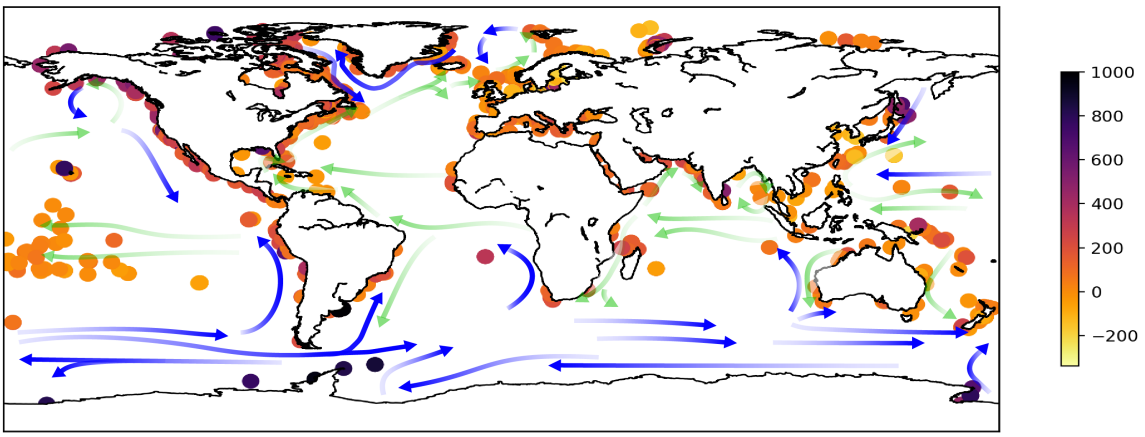


Figure 1.9. ΔR values (in ^{14}C yr) plotted on a colour scale alongside warm (green) and cold (blue) ocean currents. Data from The Marine Reservoir Database, which also holds the references for each value. Source: Alves et al. (2018).

In coastal regions, the factors discussed in subsection 1.4.3 can be the dominant control on the MRE. Nevertheless, Figure 1.9 shows large ΔR values in the Southern Ocean and in zones of coastal upwelling in the Pacific. The former is notably ^{14}C-depleted due to the upwelling of old water and the melting of ice, changing water properties (see, e.g., Berkman and Forman, 1996; Hall et al., 2010; Sikes et al., 2008, 2016, and references therein). The latter are well known upwelling systems that show as darker points on the west coasts of the United States and South America (see, e.g., Huyer, 1983; Strub et al., 1998, respectively).

1.4.3 Hard Water and Freshwater Effects

Reservoir offsets for estuaries, lakes, and peatlands must be considered on an individual basis. Freshwater and hard water effects are not MREs *per se* but both can significantly impact the MRE in estuarine regions. Indeed, riverine discharge introduces exogenous carbon to estuaries, altering their ^{14}C signal. The addition

of ^{14}C-depleted carbon into the sea enhances the MRE magnitude while the incorporation of recent terrestrial material has the opposite effect. The degree of this influence depends on the amount of exogenous material being introduced to the marine environment, as well as on the carbon signal being carried by this material. Organisms from estuaries, including aquatic plants, exhibit a particular radiocarbon content which is neither marine nor atmospheric.

While assessing radiocarbon ages of material from the British Isles, Godwin (1951) found unexpected offsets. Some samples exhibited large discrepancies from the expected age, with material from deep lake muds yielding ages that were too young. This led the author to hypothesize that the input of more recent organic material by moving water could be responsible for such offsets. This supports the idea of a freshwater effect, which is essentially caused by the incorporation of recently formed carbon species in freshwater reservoirs. Indeed, these reservoirs are shallower and less stratified than the ocean, which leads to enhanced mixing and exchange with the atmosphere. Moreover, the decomposition of organic detritus carrying a terrestrial ^{14}C signal can also impact the ^{14}C activity of freshwater systems. For samples that yielded ages that were too old, the author argued that this would be a result of the introduction of old carbon, such as bicarbonate derived from ancient limestones, into the lake. Indeed, hard water effects are caused by groundwater dissolution of depleted or ^{14}C-devoid underlying bedrock. Alternatively, the mineralization of ancient dissolved organic carbon (DOC) (e.g., derived from peat) is also likely to increase the radiocarbon ages of DIC in freshwater systems (Olsson, 1983, 1996). Following Godwin (1951), Deevey et al. (1954) performed subsequent investigations on hard water effects in a lake in New York and advised care with radiocarbon analyses in lakes located in highly calcareous regions due to the probability of finding offsets up to 2,000 yr from the true ages. Figure 1.10 summarizes the processes affecting the magnitude of the MRE.

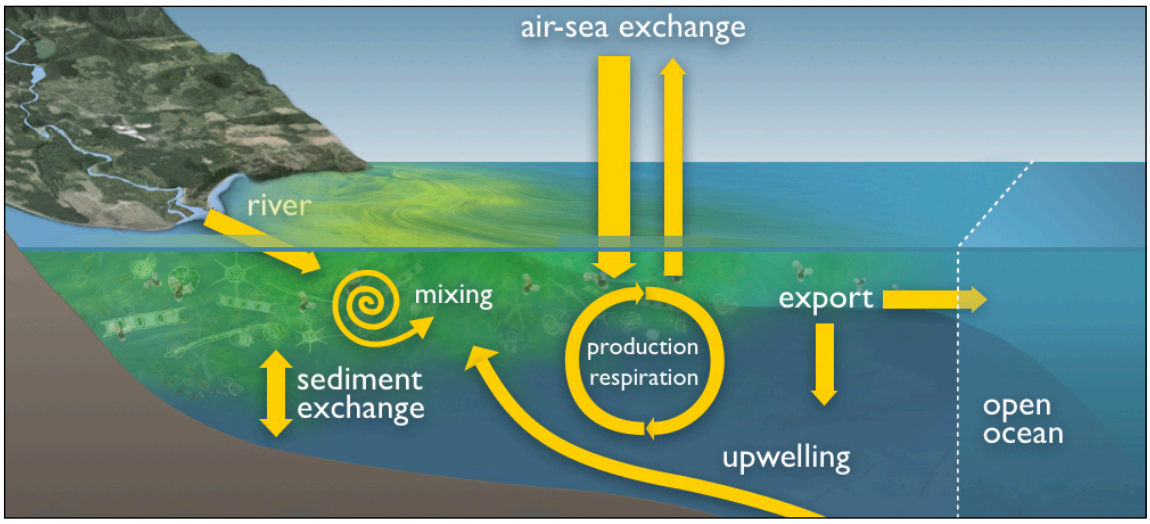


Figure 1.10. Summary of the processes discussed in subsection 1.4.1 and subsection 1.4.3. These phenomena cause different levels of ^{14}C depletion in the ocean, leading to inherent geographical variability of the MRE (Gordon and Harkness, 1992). Source: USA National Oceanic and Atmospheric Administration (NOAA).

1.4.4 Marine Calibration

Because the ocean and the atmosphere are linked by CO_2 exchange (subsection 1.3.1), variations in the atmospheric ^{14}C content are reflected in the oceanic reservoir. Marine calibration is, however, more complex and involves more steps than the terrestrial calibration discussed in subsection 1.2.5. Due to the delayed and smoothed oceanic response to short-term variations in the atmosphere, the use of atmospheric curves such as the IntCal13 and SHCal13 data sets, presented in subsection 1.2.5, is not possible (see Stuiver et al., 1986). Moreover, the MRE imposes an additional obstacle for the use of such curves. For these reasons, the radiocarbon community has been working on internationally accepted marine calibration curves (e.g., Stuiver et al., 1986; Stuiver and Braziunas, 1993; Hughen et al., 2004; Reimer et al., 2009, 2013). The lack of continuous and highly resolved records in the ocean hinders the construction of empirical marine calibration data sets (Stuiver and Braziunas, 1993). Therefore, marine curves are created based on an ocean-atmosphere box diffusion model that estimates the oceanic response to

atmospheric ^{14}C fluctuations (Oeschger et al., 1975; Stuiver and Braziunas, 1993). The construction of Marine13, the most recent version of a marine ^{14}C calibration curve, is based on the ^{14}C measurements of marine material and on modelled data from IntCal13. Critically, the Holocene part of Marine13 is purely modelled, with no experimental data incorporated. This curve can be used for the period starting from 1950 AD and going back 50,000 years (Figure 1.11a).

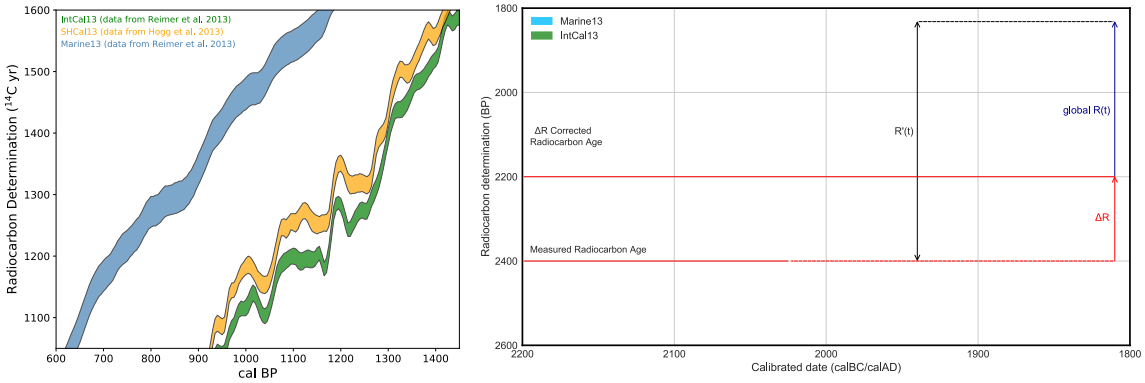


Figure 1.11. a: Section of the marine ^{14}C calibration curve Marine13 together with the previously shown atmospheric curves. Note how short-term ^{14}C variations are smoothed or absent in the marine curve (see Stuiver et al., 1986). b: A summary of the offsets involved in the MRE. Source: Alves et al. (2018).

The global difference in ^{14}C age between the atmosphere and the modelled surface ocean (represented by Marine13) is known as $\mathrm{R_g}$ or global R.[27] Although this offset is incorporated in Marine13, regional effects are not accounted for by a global curve and, therefore, ΔR values are used in the process of marine calibration (Stuiver and Braziunas, 1993). These regional offsets are subtracted from the measured radiocarbon ages, bringing them to a worldwide context that is suitable for calibration with a global curve. Since the marine and atmospheric calibration curves follow the same long-term trend, R values (Equation 1.19) can also be used in the calibration process. However, by subtracting R from the measured ^{14}C age and then calibrating the result with an atmospheric curve, one is considering radiocarbon fluctuations that are not realistic for the marine environment (Stuiver and

[27]The value of this offset is 405 $\pm$ 22 ^{14}C yr (Hughen et al., 2004).

Braziunas, 1993).[28] A simple example can demonstrate the effects of the MRE correction on the calibration of marine ^{14}C ages. The offsets involved in the MRE are summarized in Figure 1.11b. Figure 1.12 shows the calibration of a marine ^{14}C age of 1,000 ± 30 ^{14}C yr under the following conditions:

1. **Calibration with a $\mathrm{R_g}$ correction and an atmospheric curve:** the value of 400 ^{14}C yr is subtracted from the measured age and calibration is then performed with the atmospheric curve IntCal13 with an uncertainty of 40 ^{14}C yr (blue) and without uncertainty (black).

2. **The MRE is corrected through the application of different $\triangle$R values:** $\triangle$R values of -100 $\pm$ 40 ^{14}C yr (pink), 0 ^{14}C yr (red), and +100 $\pm$ 40 ^{14}C yr (green) were subtracted from the measured age prior calibration with Marine13.

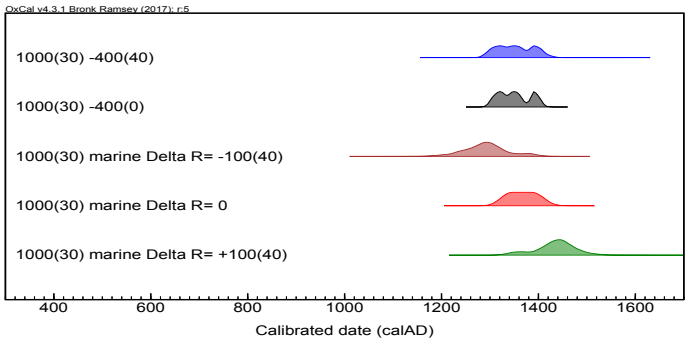


Figure 1.12. The effect of different MRE corrections in marine calibration. The different conditions are described in the main text. Source: Alves et al. (2018).

The first procedure results in a probability distribution for the calibrated age that reflects the ^{14}C fluctuations present in the atmospheric curve but absent in the marine curve. Alternatively, by employing the second procedure, it is possible to shift the calibrated age range to younger or older values relative to the uncorrected calibration. As argued by Cook et al. (2015), although the use of a $\triangle$R value

[28] For reservoirs in ^{14}C equilibrium with the overlying atmosphere, such as shallow lakes, this may be the most accurate approach.

and its uncertainty to correct a marine radiocarbon age is likely to cause a loss in precision, the probability distribution for the calibrated age will be a more accurate reflection of the true age.[29] Finally, the calibration of partially marine ^{14}C ages depends on the proportion of marine-derived carbon in the sample and is usually performed with mixed terrestrial/atmospheric calibration curves (see e.g., Beavan and Sparks, 1998; Arneborg et al., 1999; Beavan-Athfield et al., 2001; Naito et al., 2010; Commendador, 2014; Ervynck, 2014; Cook et al., 2015).[30]

1.5 Accounting for Common Issues in ^{14}C Dating

A sample is considered to be contaminated whenever, after deposition, processes other than radioactive decay change its carbon isotopic ratio; any carbon that was not initially part of the sample matrix is defined as a contaminant (Gillespie, 1984; Taylor, 1987). Contamination is classified by Hedges (1992) in two main categories: field and laboratory originated, with the former being subdivided into mechanical, chemical, and microbiological and the latter being essentially the incorporation of modern carbon during laboratory sample handling. Explanations and examples of each of these classifications can be found in Hedges (1992).

Generally, contamination effects on the measured isotopic ratios are conditional on factors such as the type of contaminant, the degree of contamination and the relative age between sample and contaminant (Taylor, 1987). Nevertheless, one can use the values of $\mathrm{F_m}$ [modern contamination ($\mathrm{F_m}$ = 1); 'dead' contamination ($\mathrm{F_m}$ = 0)] to evaluate the impact of foreign carbon on the measured radiocarbon age of a given sample (Table 1.2 and Figure 1.13). Comparing the fraction modern carbon value of the sample ($\mathrm{F^s_m}$) with that of the contaminant ($\mathrm{F^c_m}$), it follows that if

[29] In extreme cases, the MRE correction can either cause or avoid the interception of plateaus in the calibration curve.

[30] For human bones, for instance, stable isotope analyses can provide an estimation of the percentage marine diet and establish to what extent the sample is marine (see Figure 6.3).

$F_m^s < F_m^c$, the contaminant increases F_m^s, making the sample look younger (modern contamination). On the other hand, if $F_m^s > F_m^c$, then the contaminant reduces F_m^s, making the sample appear to be older (old contamination).

Table 1.2: Influence of contamination on the measured radiocarbon age.

Modern Carbon (F_m = 1)		Real Age (yr BP)	Dead Carbon (F_m = 0)	
5%	1%		1%	5%
47	49	50	131	462
95	99	100	181	612
474	494	500	581	912
946	989	1,000	1,081	1,412
4,660	4,931	5,000	5,081	5,412
9,064	9,804	10,000	10,081	10,412
23,768	35,555	50,000	50,081	50,412

The quantitative effects of modern and old contamination on the measured radiocarbon age of a sample are rather distinct. Minute amounts of modern carbon cause large apparent ages in old samples due to their low radiocarbon concentration, an effect that aggravates with increasing age of sample. On the other hand, the addition of 1% of dead carbon increases the sample age by about 80 years, irrespective of age (Aitken, 1990).

Isolating the pristine sample has been a challenge since the early developments of the radiocarbon dating technique (Libby, 1954). Since then, with the objective of enhancing the accuracy and precision of results, radiocarbon laboratories around the world have been improving their methods to remove contamination for an ever-expanding variety of sample materials (e.g., Brown et al., 1988; Aitken, 1990; Klinken and Mook, 1990; Van Klinken et al., 1994; Douka et al., 2010).

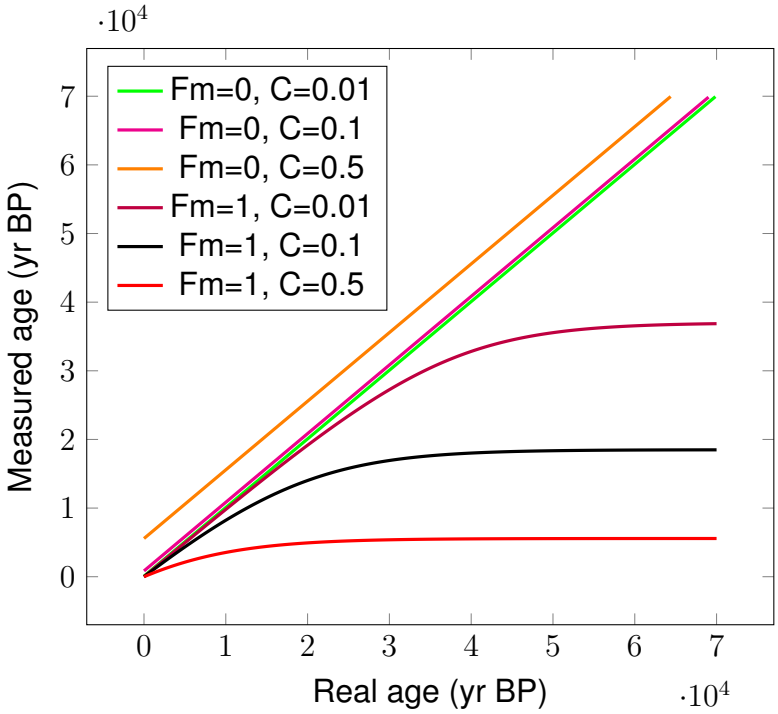


Figure 1.13. Impact of contamination on measured radiocarbon ages (adapted from Gillespie (1984)). The value of C expresses the fraction of contamination. Fm = 0 represents old contamination, whereas Fm = 1 represents modern contamination. The disproportionally large effect of very small amounts of modern contamination on the measured ages of very old samples is remarkable.

1.5.1 Recrystallization

Shell diagenesis may lead to carbonate dissolution, accompanied by *recrystallization* and the substitution of the original crystal structure, possibly affecting even the most interior layers of a sample (Taylor, 1987). Such reactions, known as neomorphisms, take place in the presence of water via mechanisms of dissolution and precipitation (Tucker and Wright, 1990), showing their strong dependence upon the deposition enviromental conditions (Douka et al., 2010, and references therein). The less soluble/more stable $\mathrm{CaCO_3}$ polimorph low-magnesium calcite (LMC, 0-4% $\mathrm{MgCO_3}$) is preferentially crystallized after the dissolution of the metastable polimorphs high-magnesium calcite (HMC, >4% $\mathrm{MgCO_3}$) and aragonite (Reid and Macintyre, 1998, and references therein). Nevertheless, although unusual, isomin-

eralogic diagenetic changes (aragonite to aragonite recrystallization) are also possible (see e.g., Enmar et al., 2000; Webb et al., 2007).

Aragonite is the principal mineral component of shell carbonates in most species (Taylor, 1987; Douka et al., 2010). Therefore, the presence of calcite in such shells is an indicator of contamination by recrystallization. Although the secondary phase may be contemporary with the original shell carbonate or even derived from its dissolution-recrystallization process, in which cases it would not represent a contaminant for the radiocarbon dating of the material, there is always the possibility of material of younger/older age in the immediate environment influencing the isotopic composition of the secondary phase (Taylor, 1987; Douka et al., 2010). A powdery or "chalky" appearance can be associated with recrystallization in regions where the rate of aragonite dissolution is higher than that of calcite precipitation (Aitken, 1990; McGregor and Gagan, 2003) and procedures such as staining methods (e.g., Feigl, 1958; Friedman, 1959) and X-ray diffraction (see e.g., Als-Nielsen and McMorrow, 2011) can be used to detect secondary calcite (e.g., Chappell and Polach, 1972; Sepulcre et al., 2009; Douka et al., 2010).

1.5.2 The Old Wood Effect

Radiocarbon dating determines the time elapsed since the cessation of carbon exchanges between sample and environment. Therefore, the association of this event with the context to be dated must be careful (see Waterbolk, 1971). In archaeology, charcoal remains collected from hearths are often radiocarbon dated to establish a chronology for ceremonial and domestic activities. Although this approach assumes that the burning happened immediately or shortly after wood formation, this is not always the case and ages may be largely overestimated if charcoal is derived from the heartwood of long-lived species (e.g., oak) or if the

death of the tree significantly pre-dates its use as fuel.[31] In both cases, this inbuilt age is a product of the so-called *old-wood effect* and leads to uncertainties of up to hundreds of years (McFadgen, 1982; Schiffer, 1986; Gavin, 2001). Since the old wood effect does not affect structures such as bark, twigs and seeds, the ^{14}C dating of these materials is usually preferred (e.g., Albero et al., 1986; Anderson, 1991; Erlandson et al., 1996; Facorellis, 1998; Rieth et al., 2011; Wilmshurst et al., 2011; Deforce et al., 2013). One way of identifying short-lived plant species or structures in the charcoal assemblage is the use of anthracological analyses (e.g., Vernet, 1999; Ludemann et al., 2004; Emery-Barbier and Thiébault, 2005; Byrne et al., 2013; Moskal-del Hoyo, 2013; Euba et al., 2016). Indeed, by comparing the wood anatomic features preserved in charcoal (Figure 1.14) with a reference collection and the specialized literature (e.g., Metcalfe and Chalk, 1950), it is possible to taxonomically classify charcoal fragments and thus avoid the old wood effect.

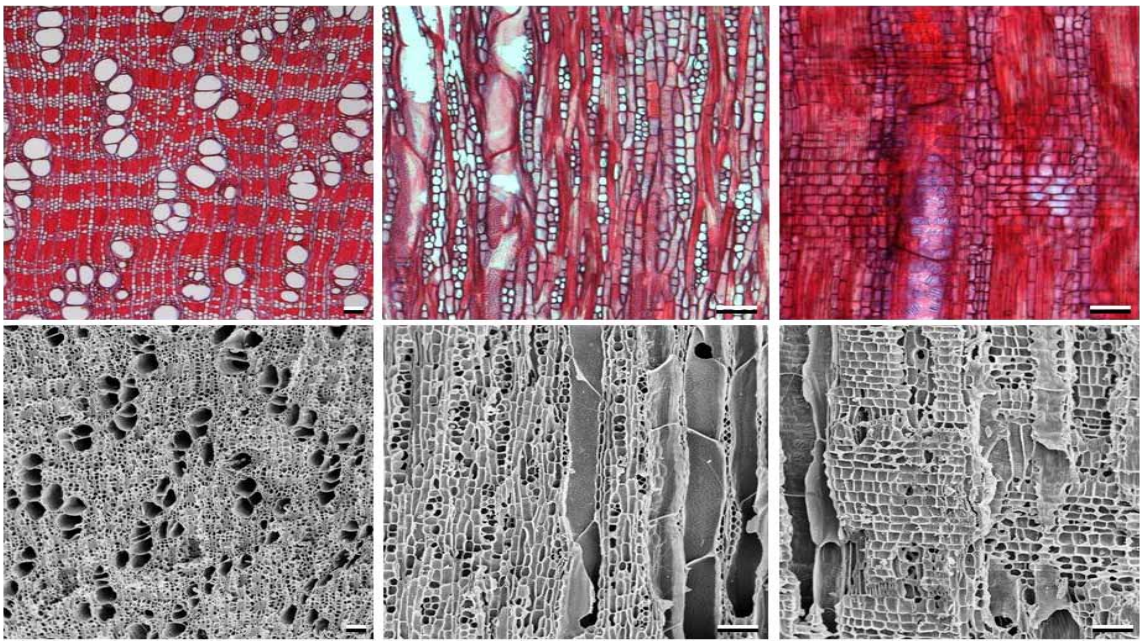


Figure 1.14. Photomicrographs of wood cross sections of *Pouteria torta* (Sapotaceae) before (above) and after (below) combustion. Structures preserved after combustion can be useful for taxonomic identification. Scale = 100 μm. Source: Gonçalves (2010).

[31] In this case, the time passed between these two events has been defined as *storage age* (McFadgen, 1982).

1.6 Stable Isotopes Analyses (δ^{13}C, δ^{15}N, δ^{18}O)

As discussed in subsection 1.2.2, the behaviour of atoms and molecules in chemical and physical processes depends upon their mass. By measuring the isotopic composition of the sources and products of a given reaction, one is able to quantify the isotopic fractionation involved in the mechanism, which provides clues for the study of a wide range of processes in biological systems. In this context, the measurement of stable (i.e., non-radioactive) isotope ratios allows for the identification of sources and sheds light on the mechanisms involved in the incorporation of atoms and molecules by living organisms. Below I briefly discuss the applications of δ^{13}C, δ^{15}N and δ^{18}O values[32] that are relevant for this work. For different elements or more applications see e.g. Hoefs (1997) and Fry (2006).

1.6.1 δ^{13}C and δ^{18}O in Aquatic Carbonates

Marine animals that deposit calcium carbonate in equilibrium with seawater record the isotopic composition of their environment. In this way, isotopic species in aquatic carbonates provide clues about environmental conditions during shell formation (e.g., Surge et al., 2003; Chauvaud et al., 2005; Gillikin et al., 2005; Goewert et al., 2007; Harding et al., 2010). For instance, carbonate δ^{13}C and δ^{18}O values are correlated with water salinity (e.g., Keith et al., 1964; McConnaughey and Gillikin, 2008; Leng and Lewis, 2016, and references therein), meaning that marine and freshwater calcifying organisms present distinct carbon and oxygen isotopic signatures that resemble those of DIC at the environment where they were formed.[33] Isotopic species in estuarine molluscs, in turn, reflect a mix of fluvial and oceanic DIC (Mook and Vogel, 1968; Gillikin et al., 2006).

[32] δ^{15}N and δ^{18}O are defined similarly to δ^{13}C (Equation 1.14), with different standards (AIR and VSMOW, respectively).

[33] In fact, although aquatic molluscs build their shells primarily from ambient DIC, the fractionation of carbon isotopes may be a complex function of metabolic and DIC carbon contributions (see e.g.,

Despite the variability that can be considerably high in aquatic systems, freshwater organisms present lower δ^{13}C values than their marine counterparts (Figure 1.15). Indeed, riverine δ^{13}C values can be depleted by 5-10‰ relative to ocean water DIC (which is close to isotopic equilibrium with atmospheric CO_2) due to the influence of processes such as the input of land-derived carbon in freshwater systems (Keith et al., 1964; Culleton et al., 2006; McConnaughey and Gillikin, 2008). In the case of oxygen, seawater is enriched in ^{18}O when compared to continental waters and δ^{18}O values vary according to salinity due to processes such as fractionation effects during precipitation (Epstein and Mayeda, 1953; Dansgaard, 1964; Araguas-Araguas et al., 2000; Bar-Yosef Mayer et al., 2012).[34] For surface marine waters, δ^{18}O values increase not only with salinity but also with temperature.[35]

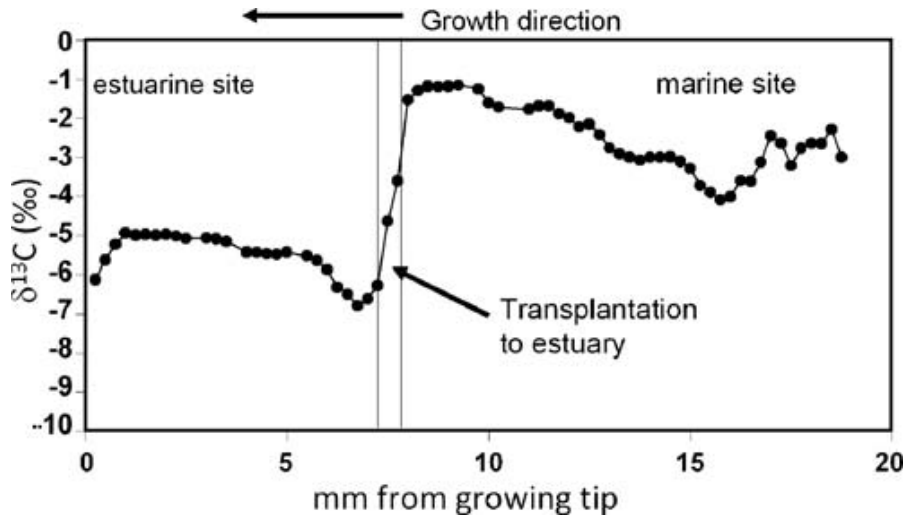


Figure 1.15. δ^{13}C change due to the transplantation of a mussel from a marine site (salinity$\sim$35) to an estuarine site (salinity$\sim$20). Sampling may smooth the isotopic transition. Source: McConnaughey and Gillikin (2008). Data: Gillikin et al. (2006).

Gillikin et al., 2006; McConnaughey et al., 1997; McConnaughey and Gillikin, 2008, and references therein)

[34] There is also a latitude and altitude dependence on the δ^{18}O values of continental waters (e.g., Epstein and Mayeda, 1953).

[35] In marine molluscs living where seawater salinity is relatively constant, temperature exerts the major control on δ^{18}O. For estuarine molluscs, salinity is the controlling factor (Leng and Lewis, 2016).

The fractionation of oxygen isotopes during the precipitation of carbonate shells by marine organisms has been shown to be temperature dependent (e.g., Urey, 1947, 1948; McCrea, 1950; Urey et al., 1951), reflecting the thermodynamic isotopic equilibrium between the ambient seawater and the shell. Carbonate δ^{18}O values decrease by about 0.24‰ for each $1^{\circ}\mathrm{C}$ increase in temperature (Craig, 1965).[36] This phenomenon allows for the development of a paleothermometer based on the correlation of carbonate δ^{18}O values and water temperature (e.g., Epstein et al., 1951; Urey et al., 1951; Epstein et al., 1953; Craig, 1965; Shackleton, 1974; Grossman and Ku, 1986; Chauvaud et al., 2005). Nevertheless, the determination of temperature based on the oxygen isotopes thermometer should be careful since the degree of oxygen isotopic fractionation between calcite and water differs from that between aragonite and water (see Grossman and Ku, 1986, and references therein). Moreover, stable isotopes values in biogenic carbonates depend on the context, temperature and salinity variations, and physiological effects that may further complicate possible interpretations (see e.g., Tanaka et al., 1986; Romanek and Grossman, 1989; Wefer and Berger, 1991; Kim and O'Neil, 1997; Dettman et al., 1999; Owen et al., 2002; Schwalb, 2003; Lorrain et al., 2004; Burman and Schmitz, 2005; Gillikin et al., 2006, 2007; McConnaughey and Gillikin, 2008, and references therein).

1.6.2 δ^{13}C and δ^{15}N Correlation with Diet

Photosynthesis (Equation 1.21) is a relatively well-understood biological mechanism in which the isotopic fractionation of carbon occurs. Plants tend to discriminate against heavy isotopes (^{13}C and ^{14}C), preferentially assimilating ^{12}C, which has the effect of depleting plant tissues in ^{13}C and ^{14}C relative to atmospheric

[36] At $25^{\circ}\mathrm{C}$ the ^{18}O/^{16}O ratio is 2.85% higher in the shell than in the water while at $7^{\circ}\mathrm{C}$ the difference increases to 3.27% (Clayton, 1961).

CO_2 (Craig, 1953; O'Leary, 1988). This discrimination is mainly a reflection of metabolism and environment, varying among the Calvin cycle (C3), the Hatch-Slack pathway (C4), and the Crassulacean Acid Metabolism (CAM) photosynthetic groups (see e.g., Calvin and Benson, 1948; Hatch and Slack, 1970; Smith and Epstein, 1971; O'Leary, 1981, 1988).

$$6CO_2 \; + \; 12H_2O \xrightarrow{\text{light + chlorophyll}} C_6H_{12}O_6 \; + \; 6O_2 \; + \; 6H_2O \qquad (1.21)$$

The carbon isotopic composition of these groups of plants is transferred to their consumers via the food chain. It has been shown that, despite further isotopic fractionation throughout the food chain, the carbon isotopic concentration in the tissues of herbivores and carnivores reflects that of their diet (see e.g., De Niro and Epstein, 1978). Therefore, stable carbon isotope measurements can be used for diet analyses and allow for the quantification of the relative contribution of different food classes from the same (e.g., C3 vs C4 plants) or distinct (e.g., marine vs terrestrial species) environments (e.g., Van de Merwe, 1982; Chisholm et al., 1982; Schwarcz et al., 1985; Walker and DeNiro, 1986; Ambrose, 1986).

Similar to what happens with carbon, stable isotopes of nitrogen are passed along food webs and can provide diet information (e.g., DeNiro and Epstein, 1981; Schoeninger et al., 1983). While consumers present δ^{13}C values that are similar to their diet, there is a +2-6‰ ^{15}N enrichment for each increase in trophic level (e.g., DeNiro and Epstein, 1981; Minagawa and Wada, 1984; Schoeninger and DeNiro, 1984) (Figure 1.16). It follows that measurements of δ^{15}N values allow for the differentiation between herbivores and carnivores or between marine and terrestrial food webs (e.g., Schoeninger et al., 1983; Schoeninger and DeNiro, 1984; Walker

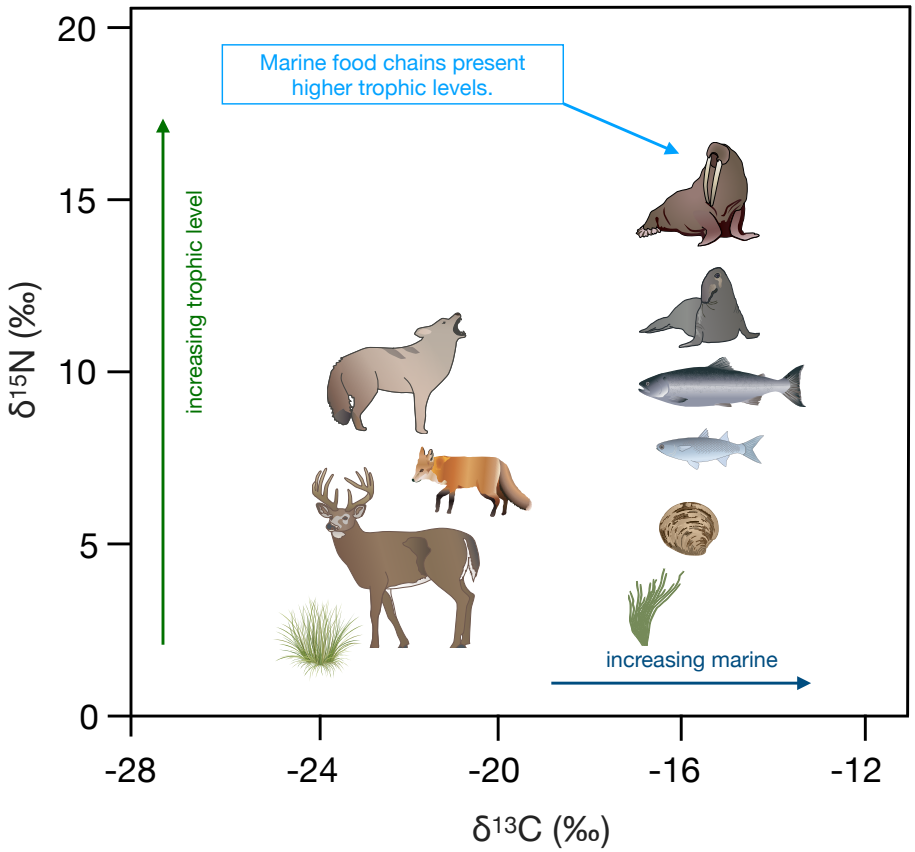


Figure 1.16. Stable carbon and nitrogen values for terrestrial and marine ecosystems. Values are relative to flesh. Source: Modified from Schulting (1998).

and DeNiro, 1986).[37] Nevertheless, there are environmental and physiological factors influencing nitrogen isotope ratios which limit diet interpretations based on these values (see e.g., Hedges and Reynard, 2007).

For the reconstruction of paleodiets based on δ^{13}C and δ^{15}N analyses, bone collagen is considered to be the most reliable material due to the preservation of its original isotopic composition (Ambrose, 1986, 1991, and references therein).[38] A complete discussion of the use of stable isotopes for prehistoric diet reconstruction can be found in Lee-Thorp (2008).

[37] Marine food chains are longer than terrestrial ones, presenting higher δ^{15}N values. Freshwater food chains also contain more trophic levels than terrestrial ones and can be distinguished from the marine food webs by their δ^{13}C values (Dufour et al., 1999; Eriksson, 2013).

[38] Collagen is formed from protein sources in the diet and thus its isotopic values mostly reflect those of dietary protein (Krueger and Sullivan, 1984).

Chapter 2

Environmental Context

Introduction

Environments can be characterized by their unique and intricate network of physical, chemical and biological systems. In this work, by using a variety of isotope and accessory techniques, I address the connections between some of these systems and establish a geographic and chronological framework for their variations on the coast of Brazil. In the next sections I briefly describe the climate and vegetation of the Brazilian littoral, which is important for the interpretation of the archaeological data that is presented later in this thesis. In this chapter, I also present a brief description of some of the major oceanographic features of the Southwestern Atlantic Ocean, which are important for the discussion of the MRE data generated in this study.

2.1 The Brazilian Coastal Environment

This section presents a summary of the Brazilian coastal environment; the information given here has been obtained from Prous (1991), Prates et al. (2010) and

IBGE (2011), where details can be found. The Brazilian coastal zone is about 10,800 km long, extending from the mouth of the Oiapoque river (04°52'45"N) to the mouth of the Chuí river (33°45'10"S).[1] This significant latitudinal range encompasses regions with different environmental parameters, explaining the diversity of ecosystems on the Brazilian coast.

Subtropical and equatorial climate, with alternate dry and wet seasons, prevails in most of the country. The littoral is relatively homogeneous, mostly consisting of a narrow coastal zone separated from a plateau by escarpments that are more than 1,000 m high. The geology is diverse, with a significant presence of calcareous rocks on the Northeast coast. The coastal zone is dominated by extensive sandy beaches with occasional rocky outcrops and the landscape shows an alternation of beaches and coves.[2] On the coast, rivers present a few kilometres of extension and the Atlantic Forest dominates.[3] Generally, herbivores in this environment are small animals and plants, with some exceptions (e.g., avocado and peanuts), tend to present low nutritional values, which suggests that aquatic animals were the most important source of protein for ancient populations. Since the coast represents a transition zone between the marine and terrestrial environments, it is a rich and diverse region where ancient human groups obtained a variety of resources for their industries and/or subsistence. Figure 2.1 shows the zonation of the Brazilian coast from São Paulo to Santa Catarina.

Throughout the Holocene, the scenario described above changed, more due to sea-level fluctuations than to variations in temperature or humidity. Sea-level rise (80 m in the last 15,000 years) was responsible for the submersion and loss of the sites and vestiges left by the oldest populations. Moreover, an additional challenge

[1] These dimensions place Brazil among the countries with the longest coastlines in the world.

[2] The landscape can also be characterized by the presence of muddy beaches, *restingas*, coastal lagoons, estuaries, mangroves and coral reefs.

[3] Today the Atlantic Forest coverage has been reduced to about 7% of its original area but this biome is still one of the richest areas for endemic species in the world.

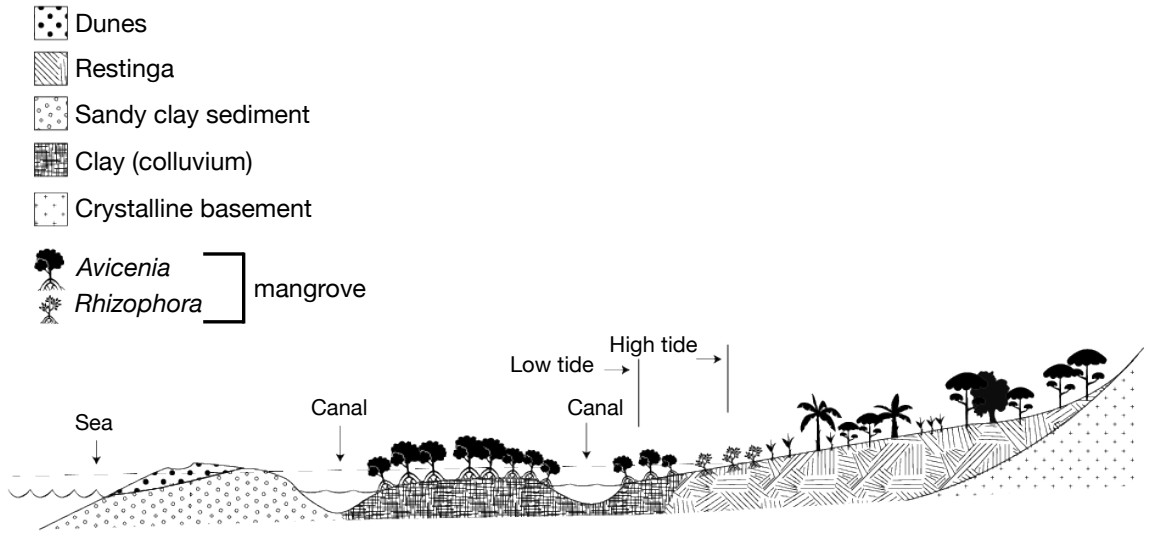


Figure 2.1. Zonation of the Brazilian littoral from São Paulo to Santa Catarina. Source: Modified from Prous (1991).

for archaeologists working in this region is that the environmental conditions are not ideal for the preservation of archaeological remains. Due to the fact that the Brazilian territory is situated in a tropical and humid zone, the preservation of archaeological vestiges is relatively poor, with the acidic soil being responsible for the degradation of material such as bones. Moreover, since the humid and warm soil presents enhanced biochemical activity, organic materials such as wood are rapidly degraded.

2.2 The Oceanography of the Brazilian Coast

In the South Atlantic Ocean, the surface circulation pattern (Figure 2.2a) is characterized by a large anticyclonic subtropical gyre whose western boundary current is the *Brazil Current (BC)*. Out of this South Atlantic Gyre (SAG), in the west side of the South Atlantic basin, there is a significant equatorward flow of water known as the *Malvinas or Falkland Current (MC)*. Together with tides, freshwater discharge, and high speed winds, the BC and the MC significantly influence the oceanic cir-

culation over the Southwestern Atlantic Shelf (e.g., Peterson and Stramma, 1991; Matano et al., 2010; Talley et al., 2011).

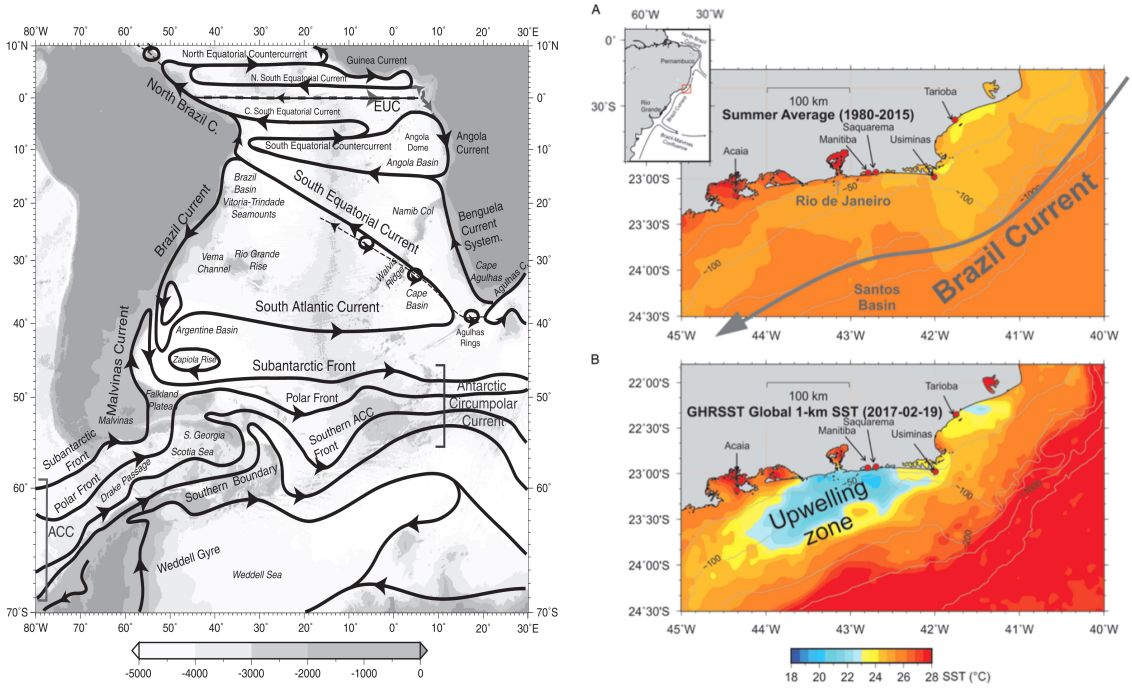


Figure 2.2. a: The South Atlantic Ocean surface circulation patterns. Source: Talley et al. (2011). b: The Cabo Frio upwelling system on the coast of Rio de Janeiro, southeast Brazil. (A) Summer average temperature of superficial waters from 1980 to 2015 and (B) values for February 19, 2017. The sea surface temperature data (SST) was obtained from the yearly averaged monthly Pathfinder Version 5.2 dataset (obtained from NOAA ERDDAP portal). Source: Macario et al. (2018).

The South South Equatorial Current (South SEC) flows westward as the northern boundary of the SAG and, on the South American coast at around 10-15°S, it bifurcates to form the northward flowing North Brazil Current (NBC) and the southward flowing BC (volume transport of 25-40 Sv) (e.g., Peterson and Stramma, 1991; Piola and Matano, 2001; Lumpkin and Garzoli, 2011; Talley et al., 2011, and references therein). The former takes over most of the South SEC water and further incorporates much of the freshwater discharge from the Amazon river (Talley et al., 2011). The latter flows along the continental margin of South America, becoming deeper and more intense at higher southern latitudes (Peterson and Stramma, 1991, and references therein). The upper portion of the BC is composed

of subtropical warm (θ> 20°C), salty (S > 36 PSU), nutrient-depleted and relatively oligothrophic waters (Olson et al., 1988; Bisbal, 1995; Piola and Matano, 2001; Chiessi et al., 2007; Lumpkin and Garzoli, 2011). The MC (volume transport of 40-70 Sv), on the other hand, starts as a narrow branch of the Subantarctic Front (SAF) of the Antarctic Circumpolar Current (ACC) and enters the South Atlantic Ocean via the Drake Passage (e.g., Olson et al., 1988; Peterson, 1992; Spadone and Provost, 2009; Talley et al., 2011). It flows north along the eastern boundary of the continental shelf of Argentina and is composed of cold (θ <15 °C), fresh (S < 34.2 PSU) and nutrient-rich subantarctic waters (Olson et al., 1988; Piola and Matano, 2001; Chiessi et al., 2007; Matano et al., 2010; Lumpkin and Garzoli, 2011). The BC and the MC collide at 36-38°S, near the mouth of the La Plata river, creating the Brazil/Malvinas Confluence (BMC), a thermohaline front with strong lateral temperature gradients and mesoscale activity (e.g., Gordon, 1981; Cheney et al., 1983; Gordon and Greengrove, 1986; Gordon, 1989; Garzoli and Garrafo, 1989; Garzoli and Giulivi, 1994).[4] The currents then flow away from the shore in a southward direction.[5] For the present study, it is important to consider that BC water is considerably enriched in ^{14}C when compared to the MC water (Broecker et al., 1960). Another relevant aspect of the BC and MC is that they may flow closer or further from the coast, depending on the season (Emilsson, 1961).

Another important oceanic feature of the Brazilian coast is a seasonal[6] upwelling system that occurs in the Brazilian southeast continental shelf, in the vicinity of the city of Cabo Frio (23°S, 42°W) (Ikeda et al., 1974; Valentin, 2001, and ref-

[4]This region is one of the most energetic and dynamic areas of the global ocean (Chelton et al., 1990; Willson and Rees, 2000).

[5]The location where this occurs varies seasonally, possibly due to wind variations and/or changes in the SEC or ACC, affecting the respective currents (e.g., Olson et al., 1988; Garzoli and Garrafo, 1989).

[6]The phenomenon occurs predominantly during the austral Spring and Summer (Castelao and Barth, 2006).

erences therein) (Figure 2.2b).[7] In this region, the prevailing northeasterly winds present a significant component parallel to the coast, which leads to the Ekman effect displacing surface waters offshore and developing the coastal upwelling of subsurface waters (Emilsson, 1961; Ikeda et al., 1974; Rodrigues and Lorenzzetti, 2001).[8] During Winter, winds blowing from the southwest become more intense and frequent, favouring the opposite phenomenon (downwelling) (Castelao and Barth, 2006). The Cabo Frio upwelling system can be considered an anomaly when compared to the more common and intense systems on the eastern side of the Atlantic and Pacific basins (e.g., Peru, California, Benguela) (Valentin, 2001). Nevertheless, the phenomenon is relevant for the economy of the region since the upwelling of cold and nutrient-rich waters promotes the growth of fish populations (Matsuura, 1996).

2.2.1 The Guanabara Bay

The majority of the estuarine samples analysed in this research were collected in the Guanabara Bay. This is an estuarine bay located on the Southeastern Brazilian coast, in the state of Rio de Janeiro (22°40' – 23°00' S; 43°00 – 43°18' W). It presents an area of approximately 384 km^2, being the second largest bay in Brazil, and communicates with the South Atlantic Ocean through a narrow channel. When not indicated otherwise, the information presented below was extracted from Kjerfve et al. (1997).

Most of the bay's area consists of relatively shallow regions (depth < 10 m). There are 45 rivers and stream channels flowing into the Guanabara Bay, but the

[7] The name "Cabo Frio" derives from *Capo Frigido*, meaning Cold Cape. The term appeared in charts of Portuguese navigators in the 15th century in reference to the cold upwelled waters in the region (Valentin, 2001).

[8] Although this is a coastal upwelling system associated with the local wind regime, a change of coastal direction from north-south to east-west also favours upwelling in this location (Valentin, 2001).

contribution of freshwater accounts for only 17% of its volume and saline waters (S between 25 and 34 PSU) predominate (see Costa Santos et al., 2015). The low amplitude of the tides combined with a low riverine input hinders the complete stratification of the water column and is responsible for elevated water residence times.[9] The circulation patterns are complex, involving tides, winds and geomorphology changes.

Based on the spatial variability of geomorphological and oceanographic characteristics, some studies (e.g., Mayr et al., 1989; JICA, 1994; Cotovicz Junior, 2016) described the Guanabara Bay as divided into five different compartments (Figure 2.3b). The first of those is located in the more external region and therefore presents high exchange rates with the South Atlantic ocean waters. The second compartment is located in the west part of the bay and has limited exchange with the open ocean. Compartment three consists of a transition region with intermediate characteristics. The fourth compartment, in the northwest part of the bay, is the one receiving more freshwater discharge.[10] Finally, the fifth compartment is the most isolated one with the longest residence times.

Amador (1997) discusses in detail how sea level fluctuations significantly affected the Guanabara Bay. To summarize, between 20,000 and 18,000 years BP, the relatively low sea level (approximately 130 m below the current level) made the Guanabara Bay resemble a river with all its islands emerged. Between 10,000 and 8,000 years BP, the sea level was between 40 and 50 m below the current value, which was reached for the first time at about 7,000 years BP. Amador (1997) presents the complete scenario of how the bay changed due to sea level variations and how aspects such as vegetation and climate changed accordingly.

[9] 50% of the water is renewed in 11.4 days, but this value varies spatially across the bay.
[10] In fact, this region receives about 50% of the fluvial discharge.

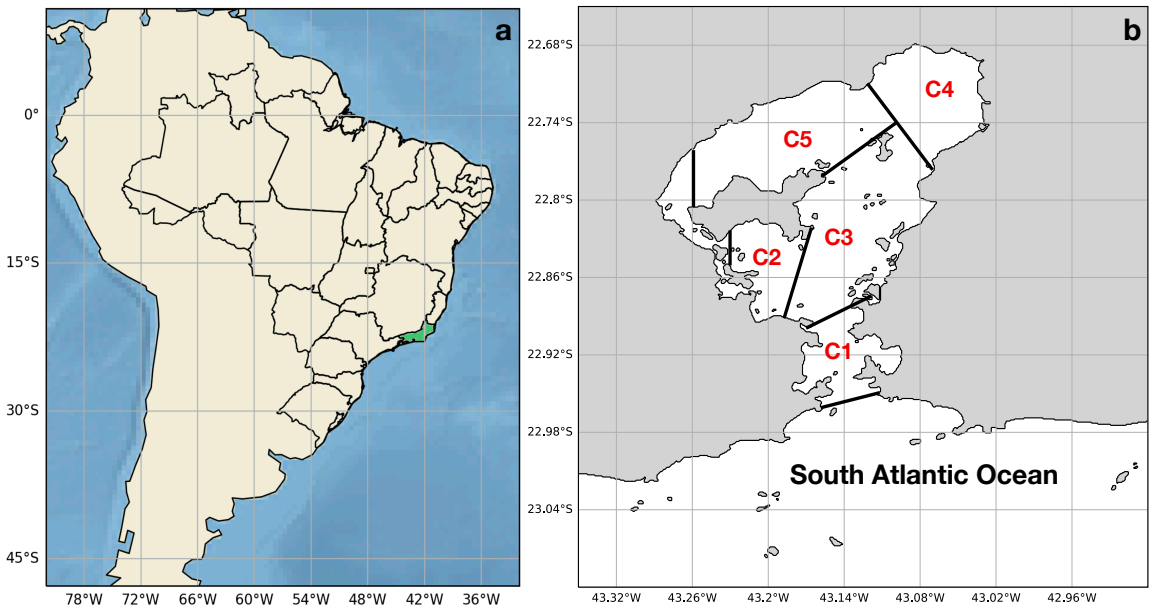


Figure 2.3. a: Rio de Janeiro state in southeast Brazil. b: The division of the Guanabara Bay according to its geomorphological and oceanographic characteristics. Source: Modified from Cotovicz Junior (2016).

2.2.2 The Laguna Lagoonal System

As mentioned in chapter 3, Cabeçuda is located between two lagoons (Santo Antônio dos Anjos and Imaruí lagoons, see fig. 3.1). Together with the Mirim lagoon, they form the Laguna Lagoonal System that covers an area of 180 km^2 (Figure 2.4). These lagoons are connected by narrow channels and receive a significant amount of their inflow from the two main rivers in the region: the Tubarão and the D'Una rivers. The former discharges in the Santo Antônio dos Anjos lagoon while the Mirim and Imaruí lagoons receive freshwater from the latter (Fonseca and Netto, 2006). Kjerfve (1994) classifies this system as a choked lagoon, connected to the sea by a single entrance channel that contributes to the greater salinity of the Santo Antônio dos Anjos lagoon when compared to the other two. In fact, the north portion of this estuary presents salinity < 0.5 during the entire year, while the middle estuary has a salinity of 0.5 - 5, mostly influenced by rainfall patterns (Barletta et al., 2017, and references therein). The mean depth of the system is

approximately 2 m, meaning that wind can significantly influence circulation. Much of the tidal influence is filtered out by the narrow channel that connects the ocean and the Santo Antônio dos Anjos lagoon (Fonseca and Netto, 2006).

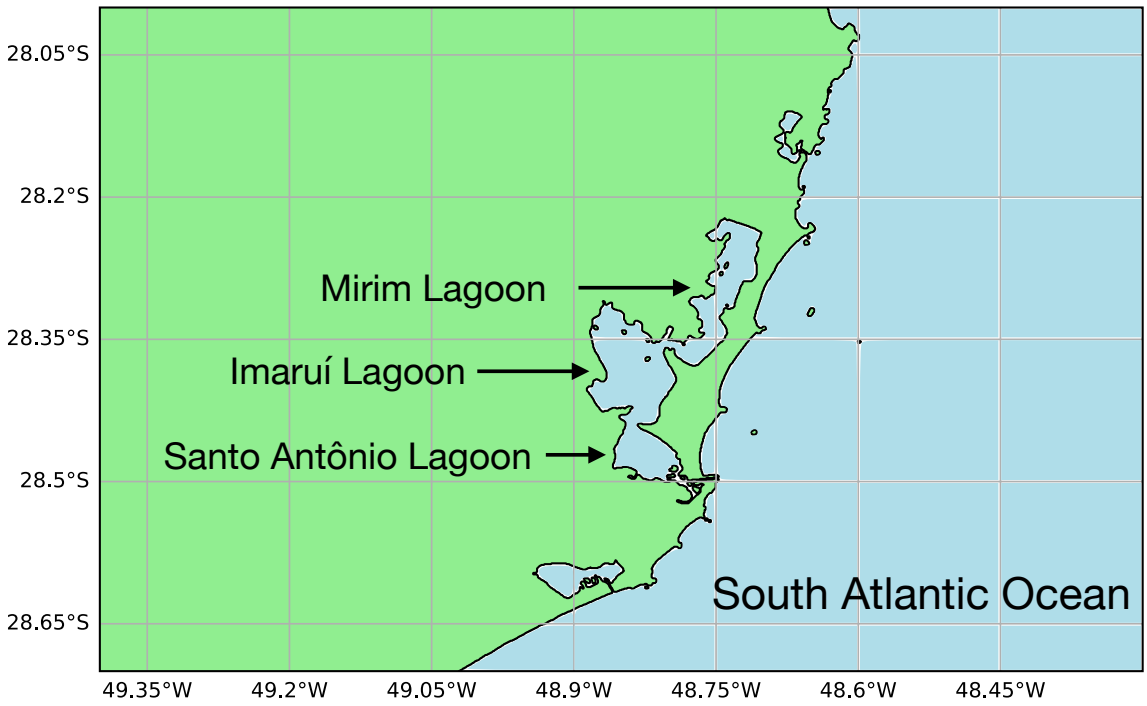


Figure 2.4. The Laguna Lagoonal System at Southern Brazil. The main characteristics of this estuary are discussed in the main text.

For the discussion presented in this study, it is important to understand how the environmental conditions evolved in this system during the Holocene. There is evidence that, during the early Holocene, due to a sea-level higher than that of the present day (Angulo et al., 1999, 2006), the system was submerged. This happened due to post-glacial sea-level rise and led to the formation of a bay presenting direct oceanic circulation. At about 6 ka cal BP, due to the formation of a sand barrier, this paleobay changed to its present configuration of coastal lagoon. More details about the temporal evolution of the Laguna Lagoonal System can be found in e.g., Giannini et al. (2010) and Fornari et al. (2012).

Chapter 3

Archaeological Context

Introduction

Prehistoric shell mounds can be useful for the quantification of the MRE and, at the same time, knowledge about the MRE allows for the establishment of robust chronologies for these sites. This creates a loop in which the archaeological setting has a dual role: it is part of both the method and the application. Therefore, it is paramount to address these sites from both archaeological and scientific perspectives and, as Stein (1992) points out, it is important to investigate their origin and diagenesis in order to overcome biases caused by post-depositional alterations. Thus, in order to use the archaeological record to make cultural and environmental interpretations, it is imperative to control the context, understanding formation and transformation processes over time and space (Ceci, 1984).

The presence of marine and terrestrial material in close stratigraphic association at coastal archaeological sites along the Brazilian shoreline makes it possible to derive marine reservoir corrections for the region. In order to yield meaningful MRE quantifications, stratigraphic pairing must be a reliable indicator for contemporaneity. Therefore, the validity of such an approach depends on a careful analysis

of the stratigraphy of these sites, which is intrinsically associated with the cultural practices of the societies responsible for their construction. This chapter introduces the archaeological context in which this research was performed.

3.1 Shell Mounds

"Shell middens" or "shell mounds" are shell-matrix sites, i.e. archaeological sites whose structure is characterized by the prominent presence of shell derived from aquatic fauna, often found near water settings in coastal or inland regions (e.g., Stein, 1992; Bailey et al., 2013; Woodman, 2013).[1] In these sites, the archaeological context is greatly affected by the remarkable concentration of shell. Indeed, shell mounds present distinctive chemical and physical properties such as (1) enhanced porosity, permeability and alkalinity; (2) low density of artifacts; (3) complex discontinuous strata; (4) high probability of saturation by water bodies; (5) high archaeological visibility; and (6) rapid rates of accumulation (Bailey and Parkington, 1988; Stein, 1992, and references therein).

Although the relative contribution of shellfish as a food resource has been the subject of debate since the initial years of shell mound research (e.g., Parmalee and Klippel, 1974; Bailey, 1975; Erlandson, 1988), the sheer abundance of mollusk remains usually evokes the assumption that edible taxa were consumed by prehistoric people and the interpretation of all shell mounds as food debris deposits (Claassen, 1991). This oversimplified perception overlooks the possibility of the deliberate and systemic uses of shell as fish bait (Larson, 1980; Riser, 1987; Claassen, 2013) and construction or artifact material (Onat, 1985; Ceci, 1984; Lima et al., 1986, and references therein). Moreover, by ignoring symbolic meanings for the shell (e.g., Hamell, 1992; Saunders, 1999), the normative thinking de-

[1] More accurate and specific typologies based on formation processes and functions have been proposed (see e.g., McManamon, 1984; Waselkov, 1987; Widmer, 1989).

fined by Claassen (1991) also neglects its use in activities such as ritual practices (Roksandic et al., 2014). Shell mound functionality encompasses a number of classifications (e.g., living platforms, sacred mounds, cemeteries, and landscape markers) (Bailey, 1978; Meehan, 1982; Claassen, 1991, and references therein) and although formation processes are related to the site function, overall, shell mounds were built through the cultural deposition of biological remains (Roksandic et al., 2014).[2] As such, this type of site represents an abundant source of archaeological and palaeoenvironmental information and holds clues for understanding the past use of natural resources, subsistence practices and environmental changes.

Materials commonly found deposited in shell mounds (e.g., shell, bone and charcoal from variable taxa) can be used in a variety of analyses (e.g., species frequency, growth increment analysis, chemical and physical composition analyses) (e.g., Bailey and Parkington, 1988; Rollins et al., 1990; Claassen, 1991; Stein, 1992; Álvarez et al., 2011; Burchell et al., 2014, and references therein). Nevertheless, it is paramount to acknowledge that these elements were culturally selected and, thus, a distinction between availability and cultural preference is essential for palaeoenvironmental reconstructions and the study of activities happening at the site (Rollins et al., 1990). Moreover, unlocking the wealth of information offered by shell mounds can be challenging due to complex stratigraphies hampering precise excavations and preventing the fine chronological resolution expected from these fast accumulating sites (Stein, 1992; Roksandic et al., 2014; Bailey and Parkington, 1988).

[2]Considering post-depositional effects, shell mound stratigraphy may not be purely cultural (Stein, 1992).

3.2 Sambaqui

Sambaqui (*Tamba* = shell, *ki* = heap)[3] is a word of Tupi[4] etymology used to designate a specific type of shell mound found in Brazilian coastal and inland areas, near large bodies of water (e.g., Prous, 1991; Bruhns, 1994; DeBlasis et al., 1998; Gaspar, 1998, 2000; Lima, 2000; Prous, 2006; DeBlasis et al., 2007; Gaspar et al., 2008; Fish et al., 2013; Villagran, 2013; Figuti and Plens, 2014; Gaspar et al., 2014). These shell mounds are abundant, with more than 1,000 sites recorded, and present an astonishing coverage of almost the entire 8,000 km long Brazilian coast (Gaspar, 1998; Lima et al., 2004; Gaspar et al., 2008). Most of the sambaquis have been dated to between 5,000 and 3,000 yr BP, with the oldest one dated to approximately 8,000 yr BP (Lima et al., 2002, 2004), but there may be older sites submerged due to sea level changes (Prous, 1991; Bailey et al., 2013). As expected, this complex sociocultural system exhibits geographic and temporal variability (Villagran, 2013, and references therein). In some regions, the sites present thousands of cubic metres of volume and reach over 70 m in height, with the largest ones estimated to contain approximately 2.5 billion shellfish (Gaspar, 2000; DeBlasis et al., 2007). These majestic dimensions make sambaquis among the biggest shell mounds in the world, for which they can be categorized as *megamiddens*[5] (Ceci, 1984; Braje et al., 2014). Currently, sambaquis are perceived by researchers to be the result of organised social activity aiming, among other things, to construct landscape features which served as important spatial references above the surrounding coastal plains for their builders (DeBlasis et al., 1998; Gaspar, 1998, 2000).

[3]There are other interpretations of the term. For instance, Rauth (1962) proposes "house of the dead" as an alternative translation.

[4]Language spoken by horticulturalist indigenous groups that occupied a significant part of the Brazilian coast when the European colonization started (Emperaire and Laming-Emperaire, 1956; Prous, 1991; Gaspar, 1998, 2000; Lima, 2000).

[5]This term was coined in the 1970s and refers to large coastal shell mounds such as those in Maine, California and Japan and on the West coast of South Africa (Braje et al., 2014).

The prehistoric groups who built coastal sambaquis are depicted as fishers, gatherers and hunters that occupied and harvested the rich marine, estuarine and terrestrial environments of the Brazilian littoral (Prous, 1991; Gaspar, 2000; Lima, 2000; Prous, 2006; Gaspar et al., 2008; Wagner et al., 2011; Fish et al., 2013; Roksandic et al., 2014). By strategically placing their sites in areas of environmental intersection (e.g., nearby rivers, mangroves, lagoons and forests), sambaqui builders were able to harvest a bounty of resources and remain sedentary, as further evidenced by the lack of hiatus in the stratigraphy of many sites (Gaspar, 2000). The sambaquis functioned as living spaces where daily activities were held, cemeteries where extremely elaborate funerary rituals took place, or both (DeBlasis et al., 1998; Gaspar, 2004; DeBlasis et al., 2007; Klokler, 2008, 2012; Gaspar et al., 2014; Klokler, 2014a; Villagran and Giannini, 2014, and references therein). The ritual paraphernalia included adornments made of bone, shell and animal teeth, commonly found deposited in the burials, and certainly elements that did not preserve (Prous, 1991; Bruhns, 1994; Gaspar, 2000, 2004; Gaspar et al., 2008; Klokler, 2008; Fish et al., 2013; Gaspar et al., 2014; Klokler, 2014a; Okumura and Eggers, 2014). There is evidence that the sambaqui people established exchange relations with ceramists that were expanding to the littoral, such as the Tupi Guarani people. This interaction with a technologically superior culture could have led to the destructuration and collapse of the Sambaqui society (Gaspar, 2000; Lima, 2000; Gaspar et al., 2008; Villagran, 2013).

Human and faunal bones, fish otoliths, charcoal, lithic and bone artifacts and animal teeth are examples of materials that can be found deposited in sambaquis (DeBlasis et al., 1998; Gaspar, 1998; Lima, 2000; Gonzalez and Amenomori, 2003; Gaspar et al., 2008; Klokler, 2008; Gaspar et al., 2014; Villagran and Giannini, 2014). It is important to bear in mind that these materials were culturally selected and do not represent the totality of the regional fauna and flora. Moreover, they

represent only a small fraction of a broad range of materials that in many cases do not preserve well. Nevertheless, the presence of diverse elements in sambaquis testifies to the intricate set of activities that happened at the sites and, as is the case for other types of shell mound, these vestiges offer numerous possibilities for the investigation of both cultural activities and the palaeoenvironment. Although sambaquis have been the object of intensive multidisciplinary research (e.g., Scheel-Ybert, 1999, 2000, 2001; Scheel-Ybert et al., 2003; Scheel-Ybert and Dias, 2007; Scheel-Ybert et al., 2009; Scheel-Ybert, 2013; Storto, 1999; Oliveira and Horn Filho, 2001; Okumura et al., 2006; Nadal De Masi, 2009; Giannini et al., 2010; Wesolowski et al., 2010; Bastos et al., 2011; Lessa, 2011; Villagran et al., 2011; Boyadjian and Eggers, 2014; Colonese et al., 2014; Scheel-Ybert, 2014; Villagran and Giannini, 2014; Bastos et al., 2015, and references therein), the absence of sampling strategies and appropriate radiocarbon age calibration hinders an accurate overview of Brazilian prehistory (Gaspar, 2000). In this thesis, I have employed carbon isotope measurements and accessory techniques to develop archaeological and environmental interpretations for one of the largest Brazilian sambaquis.

3.2.1 Sambaqui de Cabeçuda

Cabeçuda was a sambaqui of gigantic proportions, situated on the Southern Brazilian coast, in the state of Santa Catarina, between the Santo Antônio dos Anjos and the Imaruí lagoons (UTM 22J 712601-6852170 SAD69), in a region of great sambaqui density (Rodrigues-Carvalho and de Souza, 1998; Kneip, 2004; Klokler, 2014b) (Figure 3.1). The site is partly located on a paleodune of red/brown sandy-clayey sediment and on a rocky basement containing pink granite (Guerra, 1950). In its original size, this site is estimated to have been 22 m in height, 400 m in diameter and 53,000 m^3 in volume (Rohr, 1961; Mendonça de Souza, 1995;

Klokler, 2014b). Currently, due to urban expansion and severe exploitation for lime production,[6] less than 25% of the original site area is preserved (Scheel-Ybert, 2011, 2012; Klokler, 2014b, and references therein) (Figure 3.2). Cabeçuda was the first sambaqui of large dimensions to be systematically investigated and its abundance and diversity of archaeological remains places it in a special position in Brazilian archaeology (Scheel-Ybert, 2011; Rodrigues-Carvalho et al., 2011; Klokler, 2014b). Indeed, despite anthropic intervention, this remains a key site for the reconstruction of the paleoenvironment and the understanding of the social dynamics of sambaqui builders in Brazil.

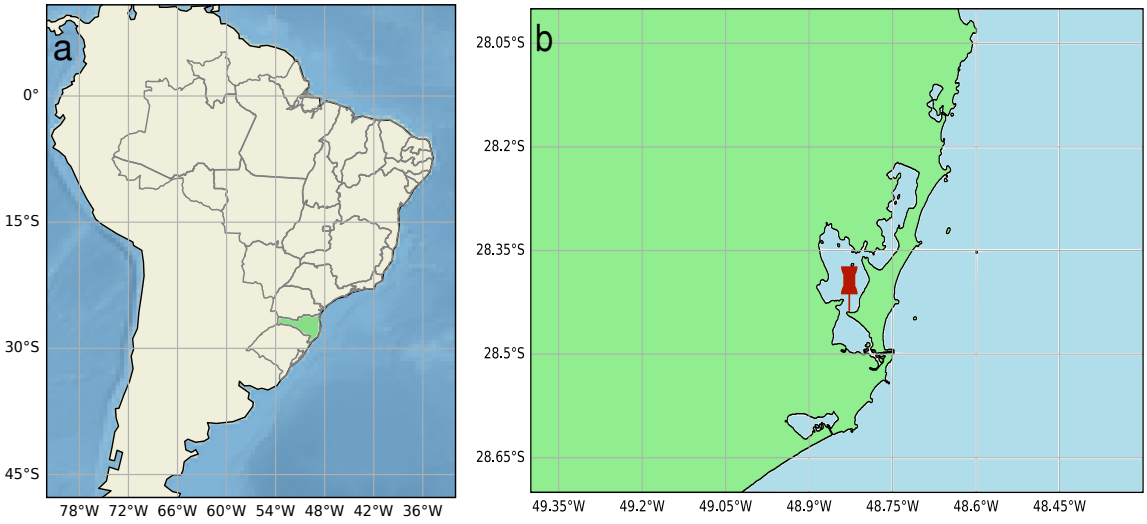


Figure 3.1. a: Santa Catarina state in Southern Brazil. b: The location of Cabeçuda in Laguna, Santa Catarina.

Cabeçuda was first dug in 1950 (Castro Faria, 1952, 1955; Faria, 1959). The excavation covered an area of 140 m^2 at the still intact central portion of the site and reached a depth of 8.5 m in some locations (Scheel-Ybert, 2011). The presence of burials throughout the excavation profile, with the highest densities at 2-3 m and 6-8 m depth, suggests a mortuary function for this sambaqui (Scheel-Ybert, 2011; Klokler, 2014b). Nevertheless, the presence of lithic cooking structures led to the interpretation of the site as a place of habitation (Castro Faria, 1955). The

[6] These activities started in 1928 and went on until the 1960s (Scheel-Ybert, 2012).

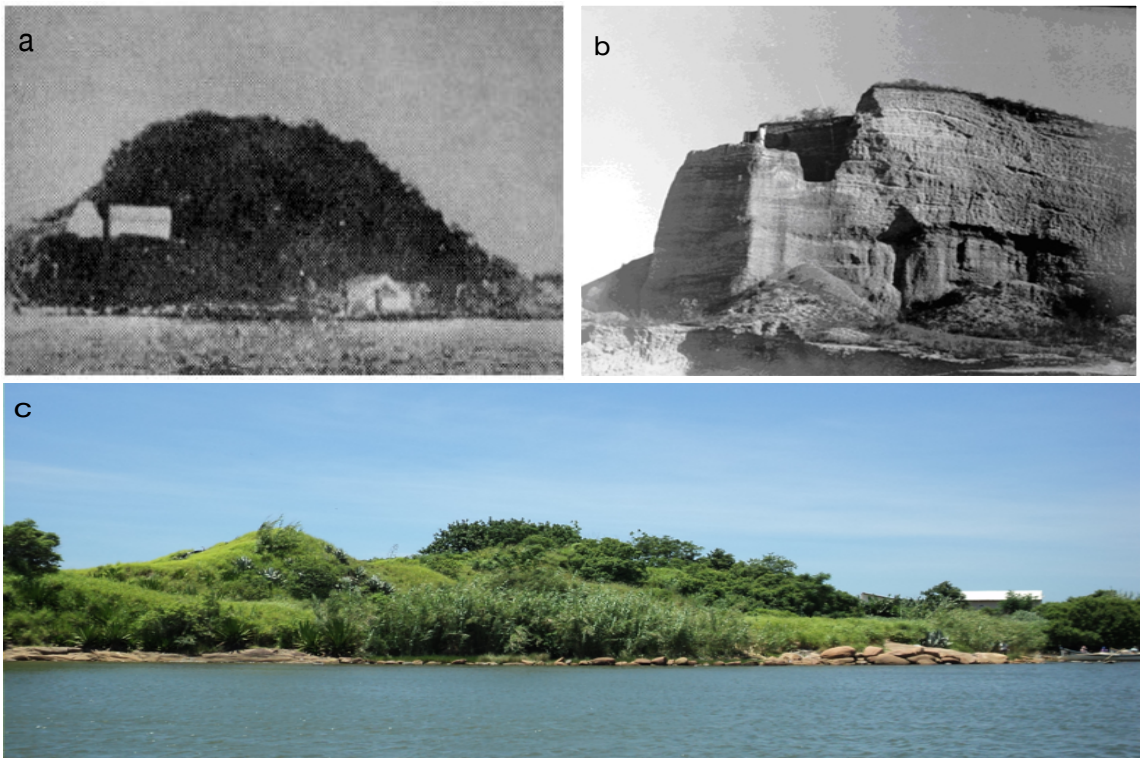


Figure 3.2. a and b: Cabeçuda at the time of the first excavation (1950). c: Cabeçuda at the time of the second excavation (2010) (Photos: Castro Faria, L. and Scheel-Ybert, R.).

burials were associated with food and hearth remains as well as bone, shell and lithic artifacts produced for different purposes (Faria, 1959; Rodrigues-Carvalho and de Souza, 1998; Klokler, 2014b). The stratigraphy was described as layers of shell intercalated with sediment rich in fish, bird, and mammal bones, charcoal and blocks of granite and diabase. Tools such as fish hooks and harpoons were also recovered from the site (Castro Faria, 1952, 1955; Faria, 1959). Overall, this first excavation yielded one of the largest collections of coastal archaeological remains in Brazil and this material has been the subject of intensive research since then (e.g., Mello e Alvim and Seyferth, 1971a,b; Neves, 1982; Ferigolo, 1987; Mello e Alvim and Gomes, 1989; Mello e Alvim and Mendonça de Souza, 1990; Mendonça de Souza, 1995; Rodrigues, 1997; Lessa and Medeiros, 2001; Teixeira, 2004; Salles et al., 2005; Okumura, 2007; Weska, 2010). Notably, the astonishing

number of shell adornments associated with the funerary context (> 16,000)[7] provides evidence to support the symbolic meaning of this material for the builders of Cabeçuda (Klokler, 2014b).

A second digging was performed in 2010 (Scheel-Ybert, 2011, 2012). This was a surface excavation aiming to identify areas of funerary activity and thus test the hypothesis that Cabeçuda was a cemetery. Moreover, this second intervention allowed the contextualization of more than 200 skeletons recovered in 1950 (Scheel-Ybert, 2011). In locus 1, where the excavation was performed, the stratigraphy was defined as complex, presenting an alternation of light coloured shellfish-rich layers and dark organic layers. In the former, fish bones and charcoal are found scattered and there is no evidence of in-situ combustion. In the latter, compact sandy sediments predominate over shellfish remains, hearths and burials are present, and fish bones, charcoal, and lithic artifacts are abundant. These layers are less thick and covered by the shellfish layers. During this excavation, a total of 25 burials were exhumed, some of which were newborns[8] associated with shell adornments and ochre. High concentrations of fish bones were found under funerary hearths, suggesting the presence of offerings, while hearths and charcoal associated with the burials may indicate the importance of fire in the funerary ritual (Scheel-Ybert, 2011). Evidence of the site as a living place was not found and the monumentality of the sambaqui is associated with the funerary ritual, which characterizes Cabeçuda as a cemetery (Rodrigues-Carvalho et al., 2011; Scheel-Ybert, 2011, 2012). Indeed, Klokler (2016a) analysed material from both excavations and states that the characterization of the site as a cemetery is confirmed by the lack of unequivocal evidence of its use as habitation. Samples used in the present study were recovered in the 2010 excavation.

[7]Shell beads were associated with the majority of burials but were more numerous in child inhumations (Castro Faria, 1952).

[8]This is exceptional since skeletons of children under 10 are extremely scarce, if not totally absent, in Brazilian sambaquis (R. Scheel-Ybert, personal communication).

Chapter 4

Methodology

Introduction

In this chapter, I describe the experiments performed in this study. Sample preparation and measurement for the ^{14}C-AMS and Isotopic Ratio Mass Spectrometry (IRMS) techniques are discussed. I present the different protocols routinely run by the Oxford Radiocarbon Unit (ORAU), the ^{14}C Laboratory of the Universidade Federal Fluminense (LAC-UFF), the ^{14}C Laboratory of the Australia National University (ANU ^{14}C Laboratory) and the Stable Isotope Facility of the University of California, Davis (SIF UCDavis). Methods for the accessory techniques of X-Ray diffraction and anthracology, used to increase the accuracy of my interpretations, are also briefly discussed. The calculation of the MRE offsets is presented in the next chapter.

4.1 ^{14}C-AMS

The AMS technique has reduced sample size requirements for radiocarbon dating analysis (see Aitken, 1990; Tuniz et al., 1998, and references therein), which

had the effect of increasing the influence of contamination issues (see e.g., Vogel et al., 1987; Donahue et al., 1990; Bronk Ramsey et al., 2004). Even though a complete decontamination is inherently impossible (Gillespie, 1984), in order to achieve high precision and accuracy in the measured radiocarbon age, exogenous carbon must be removed from the original sample structure (Gillespie, 1984; Taylor, 1987; Aitken, 1990; Hedges, 1992). This is done by means of meticulous treatments that depend on the carbon-containing compounds of the sample and on its post-depositional context. Although sample preparation protocols vary among distinct laboratories (e.g., Aerts-Bijma et al., 1997; Hua et al., 2001; Hajdas et al., 2004; Passariello and Rubino, 2016; Molnár et al., 2013), they are often divided into the following two major categories, performed in this order:

1. **Physical Pre-Treatment:** This sequence of steps is often the first treatment that samples must go through. Protocols for this process comprise any procedure intended to remove visible contaminants[1] without the use of chemical reagents. Hence, tools such as magnifiers, blades, scrapers and tweezers are commonly employed and, depending on the sample conditions, washes with MilliQ water or even an ultrasonic bath may be necessary. The physical pre-treatment is also meant to reduce sample size, separating the mass required for the next step (Table 4.1) and increasing the contact surface[2] for the subsequent use of reagents.

2. **Chemical Pre-Treatment:** These procedures are performed through the use of chemicals selected according to the material being treated. The aim is to isolate the pristine sample, removing any contaminants that persist after the physical pre-treatment. Most radiocarbon laboratories adopt the same chemicals for similar materials, but factors such as molarity, reaction time,

[1] These can be surface and/or intrusive non-sample material such as small stones and fine rootlets.

[2] This can be done by using a mortar and pestle to crush the samples.

and temperature can vary and depend on the conditions of each individual sample.[3]

Table 4.1: Quantity of material necessary to yield ∼1 mg of carbon for ^{14}C-AMS analysis, taking into account losses during treatments. Table from Tuniz et al. (1998). Values may vary according to laboratory and treatment employed.

Material	Minimum (mg)	Optimum (mg)
Wood	1	5
Bone	500	2000
Charcoal	1	3
Shell, carbonates	5	10
Textiles	2	5
Sediment organics	200	1000

Laboratory equipment used to process samples must be rigorously cleaned in order to minimize sample cross-contamination[4] or the contamination introduced from the laboratory environment.[5] Most of the samples used in the present study were radiocarbon dated at the Oxford Radiocarbon Accelerator Unit (ORAU) and at the Radiocarbon Laboratory of the Universidade Federal Fluminense (LAC-UFF). Protocols for the main steps of carbonate, charcoal and bone sample processing adopted in both laboratories are described in the following subsections and can be found in greater detail in Brock et al. (2010) and Macario et al. (2015), respectively.[6] A few samples were prepared at LAC-UFF and measured at the ANU ^{14}C Laboratory.

[3]For heterogeneous materials such as peat, the same sample mass may yield different amounts of carbon.

[4]This would be the contamination of one sample by another.

[5]These decontamination stages follow distinct protocols for different materials (e.g., glassware and stainless steel tools) and laboratories.

[6]Some AMS systems present gas ion sources and, therefore, graphitization is not always a necessary step for ^{14}C-AMS measurements.

4.1.1 ORAU

– **Carbonates Pretreatment:** Mollusc shell is mostly composed of calcium carbonate, with minor amounts of organic components. At the ORAU, shell treatment started with the removal of the outer surface,[7] using fine aluminium oxide (Al_2O_3) powder (29 μm diameter) abrasion. A small piece ($\sim$20 mg) of the last growth band of the shell was then left overnight in Fiegl's solution to check for recrystallization (Friedman, 1959). Next, these samples were crushed with a mortar and pestle and placed in the longer arm of a 2-armed Pyrex® reaction vessel with 1 mL of phosphoric acid (H_3PO_4) (85%) in the shorter arm. These vessels were attached to rigs and pumped down (<10^{-1} mbar) in a vacuum line consisting of stainless steel pieces separated by valves and connected to a mechanical pump (Figure 4.1a). After that, they were sealed, removed from the line, and sample CO_2 was released by acid hydrolysis with H_3PO_4. The reaction vessels were left overnight in a water bath at 50 °C for the reaction to complete. The rigs were then re-attached to the vacuum line and water was removed through the use of a methanol ($MeOH$) cryogenic trap (-65 °C). Finally, sample CO_2 was transferred to glass ampoules, which were sealed with the help of a small torch.

– **Bone Pretreatment:** Bone can be considered as a composite of collagen and bioapatite, the former being relatively resistant to diagenesis (Collins et al., 2002). Bone samples were subjected to two different treatments at the ORAU. Samples coded AF underwent an acid-base-acid (ABA) treatment with 0.5M hydrochloric acid (HCl) ($\sim$4 rinses for over 18 h), 0.1M sodium hydroxide ($NaOH$) (30 min) and 0.5M HCl (1 h). Rinses with MilliQ water were performed between each step. The ABA treatment was followed by the gelatinization of collagen using pH 3 solution at 75 °C for 20 h (Longin, 1971) and ultrafiltration (Brown et al., 1988). Details

[7] This part of the shell is more prone to post-depositional carbon exchange with the environment. See e.g., Aitken (1990); also Douka et al. (2010) and subsection 1.5.1.

about these steps can be found in Brock et al. (2010). Samples coded AG underwent the AF treatment without the ultrafiltration step in order to increase the collagen yield. Nevertheless, since this parameter is an indicator of the bone suitability for dating (and indeed of its preservation state), the AG pretreatment is only recommended in some special cases (see Brock et al., 2010).[8] In both cases (AF and AG), the collagen samples were weighed into clean tin capsules.

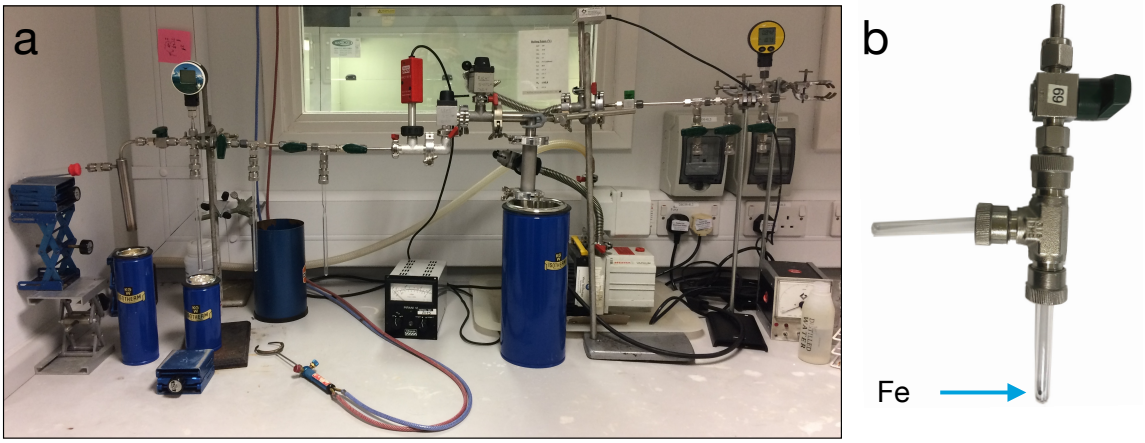


Figure 4.1. a: The carbonate line at the ORAU, used for the preparation of some of the shells involved in this research. b: Reaction rig for the graphitization of samples at the ORAU.

– **Graphitization:** The ampoules with purified carbonate CO_2 and the tins containing solid collagen were taken to a collection system where the latter were combusted in an elemental analyzer (e.g., a Carlo-ERBA NA 2000). Hydrogen gas was added to the sample CO_2 and the mixture was collected and transferred to a specially designed rig containing iron catalyst (Figure 4.1b) (Bronk Ramsey and Hedges, 1997). The rig valve was then closed and the reactor taken to the oven (6 h at $90\,^{\circ}C$). The reactions happening in this system are as follows:[9]

[8] Brock et al. (2010) discuss other analytical parameters for the dating suitability of bone, such as the collagen C:N atomic weight ratio (van Klinken, 1999).

[9] More details on the graphitization method used at the ORAU can be found in Dee and Bronk Ramsey (2000) and references therein.

$$CO_{2(g)} + 2H_{2(g)} \longrightarrow C_{(s)} + 2H_2O_{(g)} \tag{4.1}$$

$$CO_{2(g)} + H_{2(g)} \longleftrightarrow CO_{(g)} + H_2O_{(g)} \tag{4.2}$$

$$CO_{(g)} + CO_{(g)} \longleftrightarrow C_{(s)} + CO_{2(g)} \tag{4.3}$$

$$CO_{(g)} + H_{2(g)} \longleftrightarrow C_{(s)} + H_2O_{(g)} \tag{4.4}$$

$$CO_{(g)} + 3H_{2(g)} \longleftrightarrow CH_{4(g)} + H_2O_{(g)} \tag{4.5}$$

The final pressure in the reactors was measured to check for the completeness of the reaction. After that, the mixture of graphite and iron was finally pressed in an aluminium cathode and taken to the ion source of a 2 MV accelerator system, produced by High Voltage Engineering Europa (HVEE) (Figure 4.2), for measurement.



Figure 4.2. The 2 MV HVEE acceletator at the ORAU used to measure the samples of this work. Source: ORAU website and Phil Leach.

4.1.2 LAC-UFF

– **Carbonate Pretreatment:** At the LAC-UFF, carbonate pretreatment follows the standard protocols for the preparation of inorganic samples. The remains of organic tissues were removed manually with scalpels, and washing with MilliQ water was not necessary.[10] Although pre-bomb samples were not tested for recrystallization, this phenomenon would be very unlikely for such a young material, removed from the environment soon after deposition. In any case, for each shell, the last growth band was sampled ($\sim$40 mg) and etched overnight with HCl 0.5M at $90\,^{\circ}\mathrm{C}$ to remove the external layer ($\sim$50% of the sample).[11] After the chemical pre-treatment, vials containing the samples were sealed with rubber septa and evacuated (<10^{-3} mTorr) in a vacuum line similar to the one used at the ORAU (Figure 4.3a).[12] Finally, 1 mL of $\mathrm{H_3PO_4}$ (85%) was inserted into each vial with the help of a syringe. The samples were left to react overnight at room temperature and the acid hydrolysis of $\mathrm{CaCO_3}$ generated $\mathrm{CO_2}$.

– **Charcoal Pretreatment:** The incomplete combustion of plant tissue gives rise to charcoal. At the LAC-UFF, charcoal samples underwent an ABA treatment.[13] This consisted of a wash with HCl 1.0M (2 h at $90\,^{\circ}\mathrm{C}$), a wash with NaOH 1.0M (1 h at $90\,^{\circ}\mathrm{C}$) and a second wash with HCl 1.0M (2 h at $90\,^{\circ}\mathrm{C}$), performed in this order. In each step, the washes were repeated until the solution became clear and, after the final wash of each step, samples were rinsed with MilliQ water. The ABA treatment was carried out in order to remove contaminants such as carbonates and organic acids. The second acid step is necessary for the removal

[10] Pre-bomb material from museum collections is usually free from sediments or other remnants from the depositional environment.

[11] The efficacy of this step for recrystallized samples has been shown by Macario et al. (2017).

[12] The main difference between these vacuum systems is that the turbomolecular pump used at the LAC-UFF allows for a better vacuum.

[13] For charcoal expected to be significantly older than the samples analysed in this research ($\sim$ 25 ka or older) the ABOx-SC may be a better treatment (e.g., Wood et al., 2012).

of atmospheric CO_2 contamination that may be introduced during the base step (Goh and Molloy, 1972). After the chemical treatment, samples were dried and placed into previously prepared combustion tubes[14] that were later evacuated and taken to a muffle furnace (3 h at 900 °C). During this combustion step, the samples were converted to CO_2.

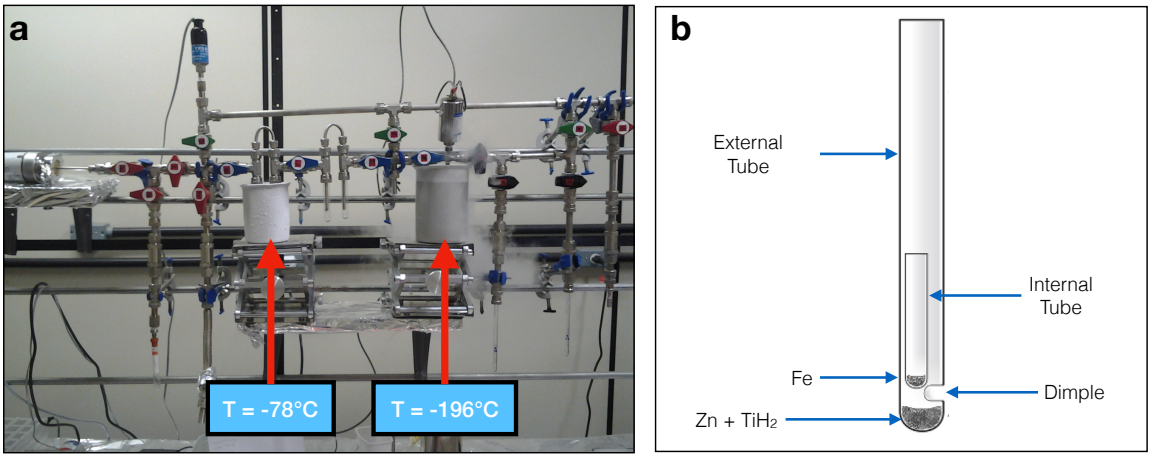


Figure 4.3. a: The carbonate line at the LAC-UFF, used for the preparation of some of the shells used for this research. b: Graphitization reaction tube. A pyrex tube (150 mm long, 9 mm O.D.) containing zinc and titanium hydride at the bottom. Sitting on a dimple in the outside tube (2 cm from the base) there is a pyrex tube (50 mm long, 6 mm O.D.) containing iron. Modified from Xu et al. (2007).

– **Graphitization:** For both charcoal and carbonate samples, the CO_2 obtained in the previous step was inserted into the vacuum line for purification. This process started with the use of a cryogenic trap of ethanol and dry ice (-78 °C) to freeze the water present in the sample. CO_2 was then frozen with liquid nitrogen (-196 °C) whilst other gases were discarded by pumping. Next, CO_2 was transferred to a previously prepared graphitization tube, which consists of a small tube containing iron (Fe) inside a larger tube containing zinc (Zn) and titanium hydride

[14]These tubes contain cupric oxide (CuO) to act as an oxidative agent and silver (Ag) to assist in the removal of the sulphur compounds released during the reaction.

(TiH_2) (Figure 4.3b). The graphitization tube was sealed with a torch and taken to the oven (7 h at 90 °C) for the following reactions to take place:[15]

$$TiH_2 \xrightarrow{440°C} 2H_2 + Ti \tag{4.6}$$

$$CO_2 + H_2 \longrightarrow CO + H_2O \tag{4.7}$$

$$CO_2 + Zn \longrightarrow CO + ZnO \tag{4.8}$$

$$CO + H_2 + Fe \xrightarrow{520°C} C_{graphite} + H_2O \tag{4.9}$$

$$2CO \longrightarrow C_{graphite} + CO_2 \tag{4.10}$$

$$Zn + H_2O \longrightarrow Zn + H_2 \tag{4.11}$$

The mixture of graphite and iron, formed inside the inner reaction tube, was pressed in small aluminium cathodes. At the LAC-UFF, samples are measured in a 250 kV Single Stage AMS (SSAMS) system produced by the National Electrostatics Corporation (NEC) (Figure 4.4). This compact accelerator, dedicated to the measurement of carbon isotopes, is the same system used at the ANU ^{14}C Laboratory (Fallon et al., 2010), where some of the samples (graphite) were sent for measurement.

[15]Other reactions within the sealed tube can also occur and, as expected, contamination and isotopic fractionation are likely to happen at this stage. For details of the zinc reduction method used at the LAC-UFF for the graphitization of carbon samples, see Xu et al. (2007).

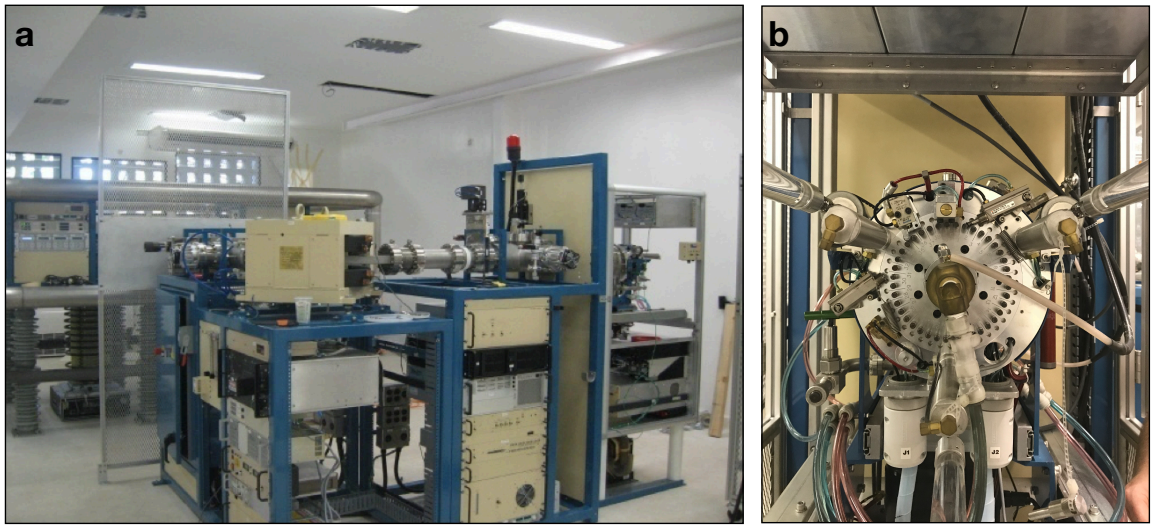


Figure 4.4. a: The 250 kV SSAMS system used at the LAC-UFF. The same machine is used at the ANU ^{14}C Laboratory. b: The ion source of the SSAMS showing the wheel where the cathodes are placed.

4.1.3 Quality Control

Foreign carbon is very likely to be systematically introduced to the sample by chemical processing, target production, and measurement (see Gillespie and Hedges, 1984; Aitken, 1990; Hedges, 1992; Tuniz et al., 1998; Mueller and Muzikar, 2002).[16] The influence of this inevitable laboratory contaminaton is such that it limits the oldest dates that can be measured in an AMS system (Hedges, 1992). To assess the contamination level introduced by each step, the preparation of batches of control samples (background and reference materials) is part of the routine of radiocarbon laboratories. Background samples, or blanks, consist of material old enough to be ^{14}C-free (e.g., coal, marble, graphite). As seen in Figure 1.13 and Table 1.2, even very small amounts of modern carbon would be noticeable in such samples. Therefore, by measuring blanks with similar mass and using the same procedures as the ones used for the actual samples, one can quantify the intro-

[16] Surfaces on labware or solid reagents can adsorb significant amounts of $^{14}CO_2$ from the atmosphere.

duction of modern carbon and correct for this contamination in the age calculation (see e.g., Beukens, 1990; Schleicher et al., 1998).[17] Because blanks would not be able to reveal the presence of old carbon contamination, the preparation of modern references is advised in order to account for this possibility.[18] References undergo the same preparation procedures as blanks and actual samples.

4.2 Stable Isotopes (δ^{13}C, δ^{15}N and δ^{18}O) Analyses

In the ORAU, some of the shells and all of the bone samples had their stable isotope concentrations determined (δ^{13}C for shells and δ^{13}C and δ^{15}N for bones).[19] This was done in a CF-IRMS system, which is composed by a combustion elemental analyzer (e.g., a Carlo-Erba NA 2000) and a gas source isotope ratio mass spectrometer (e.g., a Sercon 20/20). For bone samples, through the combustion of collagen, $\mathrm{N_2}$ and $\mathrm{CO_2}$ were liberated. After the removal of water via the use of a chemical trap, these two gases were separated in a GC column packed with Car-bosieve™ (Supelco G60/80 mesh; Bellefonte, Pennsylvania, USA) packing medium. During the process, helium was used as a carrier gas and $\mathrm{N_2}$ and $\mathrm{CO_2}$ were sequentially analyzed on the mass spectrometer for each sample. The same elemental analyzer, GC, and IRMS system were used for the $\mathrm{CO_2}$ derived from shells. The calculations of δ^{13}C and δ^{15}N were performed relative to the results of an alanine (for bone) or marble (for carbonates) standard and isotopic ratios are reported as delta per mil relative to the VPDB and AIR international standards for carbon and nitrogen respectively (Coplen, 1994). Details on this process can be found in Brock et al. (2010).

[17] Carrara marble (IAEA standard C1) and Waikato Kauri wood (IAEA-C4) can be used for carbonate and charcoal, respectively.

[18] Travertine (IAEA-C2) and Two Creeks wood (IAEA-C5) can be used for carbonate and charcoal, respectively. In the ORAU, fragments of pig rib (1545 AD) are used as reference for bone samples.

[19] This was done using an aliquot of the same sample used for ^{14}C-AMS analyses.

The δ^{13}C and δ^{18}O values of most of the carbonates used in this research were determined at the SIF UCDavis using a GasBench II system interfaced to a Delta V Plus IRMS (Thermo Scientific, Bremen, Germany). Approximately 0.3 mg of powdered sample[20] was placed into vials and loaded into an autosampler rack (at $70\,^{\circ}\mathrm{C}$). Next, the capped vials were flushed/filled with helium using a CTC PAL autosampler device. Several drops of $\mathrm{H_3PO_4}$ (103$\%$) were then manually injected into each vial with the aid of a syringe to release $\mathrm{CO_2}$. The vials were returned to the autosampler rack to equilibrate for 24 h at $30\,^{\circ}\mathrm{C}$. A ThermoFisherScientific GasBench II device connected to a ThermoFisherScientific Delta V Plus gas-isotope ratio mass spectrometer was used to analyse the sample $\mathrm{CO_2}$. Final adjustments were made in order to obtain the correct δ values for real samples and laboratory references. Details on the experimental method and calculations can be found at the SIF webpage.

4.3 X-Ray Diffraction and Anthracology

In order to check for recrystallization (see subsection 1.5.1), the archaeological shells used in this research had their crystalline structure characterized at the X-ray Diffraction Laboratory of the Universidade Federal Fluminense (LDRX-UFF). Samples[21] were crushed with a mortar and pestle, and the fine powder was analysed in a Bruker AXS D8 Advance (Cu Kα radiation, 40 kV, 40 mA) diffractometer. The machine was operated in a Bragg–Brentano θ/θ configuration with the diffraction patterns being collected in a flat geometry with steps of 0.02 degrees and accumulation time of 2.0 s per step using a PSD detector (Bruker AXS LynexEye model). Data were refined following the Rietveld method and using the GSAS-II software (Toby and Von Dreele, 2013).

[20] These were fragments of the same growth layer used for ^{14}C-AMS analyses.
[21] These were fragments of the same growth layer used for ^{14}C-AMS analyses.

Charcoal samples were subjected to anthracological investigations to avoid the old wood effect (see subsection 1.5.2). These analyses were performed at the Archaeology and Landscape Laboratory of the National Museum of Brazil - Universidade Federal do Rio de Janeiro (LAP-MN/UFRJ). Samples[22] were manually broken, exposing the three fundamental wood sections (transversal, tangential longitudinal, and tangential radial), and examined with a reflected light brightfield/darkfield microscope (Figure 4.5). Anatomical structures were then exhaustively compared to a well-identified reference collection (Antracoteca/Charcoal collection from the National Museum of Brazil, UFRJ), allowing taxonomic identification. Additionally, descriptions and photographs from the specialized literature (e.g., Record and Hess, 1943; Metcalfe and Chalk, 1950; Detienne and Jacquet, 1983; Mainieri and Chimelo, 1989) were consulted to support the identifications.

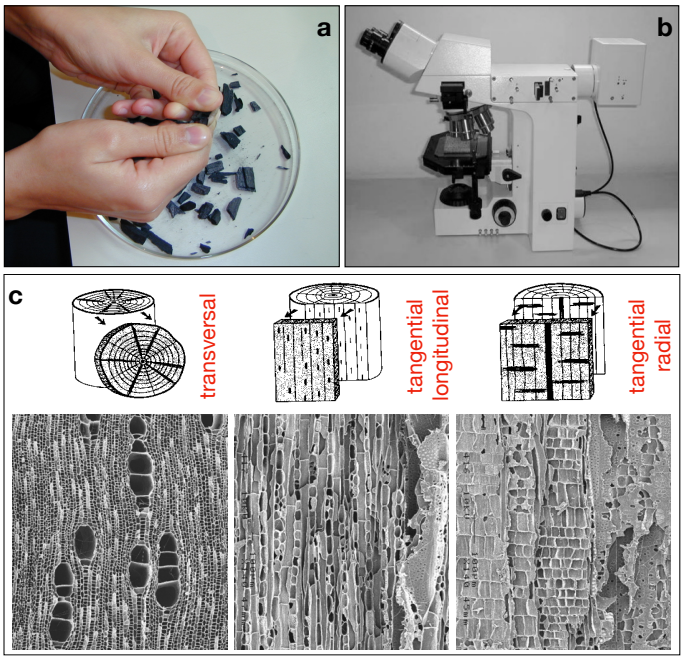


Figure 4.5. a: Charcoal fragments are manually broken. b: Wood anatomic features are investigated under a microscope. c: The three fundamental wood sections. Source: Scheel-Ybert, R.

[22]These were the same charcoal fragments used for ^{14}C-AMS analyses.

Chapter 5

The MRE Along the Brazilian Coastline

Introduction

This chapter begins with a brief presentation of what is currently known in terms of the MRE for the Brazilian coast. Next, the chapter is divided into two different sections, corresponding to the use of pre-bomb and archaeological samples for the derivation of $\triangle$R values.[1] While the pre-bomb approach is useful for studying the present day MRE, sambaqui material sheds light on the phenomenon in the Late Holocene. I describe my methodology (e.g., sample selection procedures and $\triangle$R calculation) and discuss the results of both approaches individually, considering the archaeological and environmental contexts presented in the previous chapters. I conclude with a thorough discussion of the temporal evolution and spatial patterns of the MRE on the western South Atlantic ocean.

[1] There are other possible approaches and a complete discussion, including their advantages and disadvantages, can be found in Ascough et al. (2005a).

5.1 Previous Studies

Much of the MRE research in Brazil has focused on the Southern and Southeastern parts of the coast. This may be due to a higher number of museums/zoological collections and/or archaeological sites in these regions, which makes it easier to obtain suitable material for this kind of study. In the next paragraphs, I present a short description of previous studies, summarizing their results (Table 5.1 and Table 5.2).[2] Details of the samples and methods used for the derivation of the offsets can be found in the publications cited.

In Brazil, the first MRE investigation was performed by Nadal De Masi (2001), who analysed eight pre-bomb shells to derive R values for the Santa Catarina coast. Excluding a sample that exhibited ^{14}C activity higher than modern ^{14}C signals, it was possible to determine an average R value of 460 $\pm$ 38 ^{14}C yr for the region. Next, Eastoe et al. (2002) published R values derived from known-age and archaeological samples. By combining their results with the ones obtained by Nadal De Masi (2001) for the same region, it was possible to derive a $\triangle R$ = 185 $\pm$ 30 ^{14}C yr. When combining the result of a Rio de Janeiro known-age shell with the results of two Santa Catarina shells presented by Nadal De Masi (2001), a $\triangle R$ = 105 $\pm$ 24 ^{14}C yr was obtained for the region encompassing the coasts of both states. Angulo et al. (2005) analysed six known-age shells from the states of Paraná and Santa Catarina to obtain an average value of $\triangle R$ = 33 $\pm$ 24 ^{14}C yr for the southern Brazilian coast. By using the data published by Nadal De Masi (2001) and Eastoe et al. (2002), the authors encountered an average $\triangle R$ of 8 $\pm$ 17 ^{14}C yr for the Southern and Southeastern Brazilian coasts.

In 2007, results for archaeological samples from the coast of Rio de Janeiro were inconclusive in attempting to identify possible influences from the Cabo Frio

[2] In Table 5.1 and Table 5.2, results from publications dealing with the R offset were converted to $\triangle R$.

upwelling system (Angulo et al., 2007). From the Usiminas shellmound, the authors derived R values between 358 $\pm$ 44 and 565 $\pm$ 44 ^{14}C yr, compatible with values found in other studies (Nadal De Masi, 2001; Eastoe et al., 2002; Angulo et al., 2005). Nevertheless, Macario et al. (2016) used data published by Angulo et al. (2007) to re-calculate a $\triangle$R = 67 $\pm$ 33 ^{14}C yr for the Usiminas shellmound. For the region of Cabo Frio, Alves et al. (2015b) found a $\triangle$R = 96 $\pm$ 48 ^{14}C yr using a pre-bomb shell. In the same paper, $\triangle$R values of 58 $\pm$ 53 ^{14}C yr, 28 $\pm$ 52 ^{14}C yr and 17 $\pm$ 56 ^{14}C yr were found for the coasts of Bahia, São Paulo and Rio Grande do Sul, respectively. By combining these values, the authors derived a correction of $\triangle$R = 50 $\pm$ 35 ^{14}C yr for the Brazilian coast. If previously published $\triangle$R values are included, this mean becomes 32 $\pm$ 44 ^{14}C yr.

Recently, more studies have been perfomed with archaeological samples from the coast of Rio de Janeiro. For the Sambaqui da Tarioba (22°31'37"S, 41°56'42"W), a value of $\triangle$R = -127 $\pm$ 67 ^{14}C yr was obtained (Macario et al., 2014, 2015). In the Saquarema region (22°55'12"S, 42°30'36"W), the Manitiba and Saquarema shellmounds yielded corrections of $\triangle$R = -82 $\pm$ 71 (Carvalho et al., 2015) and $\triangle$R = -140 $\pm$ 66 ^{14}C yr (Alves et al., 2015a), respectively. A recent study on the Usiminas shellmound obtained a $\triangle$R value of 67 $\pm$ 33 ^{14}C yr (Macario et al., 2016), confirming the positive values obtained by Macario et al. (2015). Finally, Macario et al. (2018) obtained a value of -80 $\pm$ 87 ^{14}C yr for $\triangle$R in the Acaiá shellmound (23.17°S, 44.37°W).

Table 5.1: Summary of previous known-age MRE studies on the Brazilian coast.

Laboratory Code	Species	Class	Collecting year	Locality	State	Region	$\delta^{13}C_{VPDB}$ (‰)	^{14}C Age ± 1σ (^{14}C yr)	$\triangle$R ± 1σ (^{14}C yr)*	Reference
LACUFF140127	*Tivela mactroides*	Bivalvia	1942	Santos	SP	Southeast	—	493 ± 25	30 ± 24	Alves et al. (2015)
LACUFF140126	*Olivancillaria auricularia*	Gastropoda	1947	Cabo Frio	RJ	Southeast	—	563 ± 17	96 ± 16	Alves et al. (2015)
LACUFF140128	*Anomalocardia brasiliana*	Bivalvia	1948	Ilha de Itaparica	BA	Northeast	—	527 ± 26	60 ± 26	Alves et al. (2015)
LACUFF140125	*Thais haemastoma*	Gastropoda	1949	São José do Norte	RS	South	—	486 ± 29	18 ± 30	Alves et al. (2015)
GX-29109	*Nassarius vibex*	Gastropoda	1933	Mar de Dentro, Ilha do Mel	PR	South	0.4	490 ± 40	34 ± 40	Angulo et al. (2005)
GX-29111	*Raeta plicatella*	Bivalvia	1940	Campeche	SC	South	-0.9	550 ± 40	90 ± 40	Angulo et al. (2005)
GX-29113	*Janthina janthina*	Gastropoda	1940	Ilha do Francês, Canasvieiras	SC	South	-1.3	500 ± 40	40 ± 40	Angulo et al. (2005)
GX-29114	*Pugilina morio*	Gastropoda	1940	Ilha do Mel	PR	South	-0.6	410 ± 40	-50 ± 40	Angulo et al. (2005)
GX-29112	Cirriped	Crustacea	1940	Ilha do Mel	PR	South	-1.3	460 ± 40	0 ± 40	Angulo et al. (2005)
GX-29110	*Callista maculata*	Bivalvia	1944	Ilha do Francês, Canasvieiras	SC	South	0.3	580 ± 40	116 ± 40	Angulo et al. (2005)
A-10038	*Amiantis purpurata*	Bivalvia	1939	Jurujuba, Niterói	RJ	Southeast	-0.1	670 ± 26	210 ± 26	Eastoe et al. (2002)
A-10037	*Iphigenia braziliana*	Bivalvia	1944	Fazenda Japuiba, Angra dos Reis	RJ	Southeast	0	404 ± 42	-60 ± 42	Eastoe et al. (2002)
CAMS-51904	*Tellina lineata*	Bivalvia	1942	Ponta das Canas	SC	South	—	690 ± 40	228 ± 40	Nadal de Masi (2001)
CAMS-52524	*Tellina lineata*	Bivalvia	1942	Ponta das Canas	SC	South	—	720 ± 40	258 ± 40	Nadal de Masi (2001)
CAMS-52523	*Tellina lineata*	Bivalvia	1942	Ponta das Canas	SC	South	—	510 ± 40	48 ± 40	Nadal de Masi (2001)
CAMS-48547	*Ventricolaria rigida*	Bivalvia	1942	Canasvieiras	SC	South	—	500 ± 40	38 ± 40	Nadal de Masi (2001)
CAMS-51903	*Tellina lineata*	Bivalvia	1942	Ponta das Canas	SC	South	—	450 ± 40	-12 ± 40	Nadal de Masi (2001)
CAMS-52772	*Tellina lineata*	Bivalvia	1942	Ponta das Canas	SC	South	—	450 ± 40	-12 ± 40	Nadal de Masi (2001)
CAMS-52773	*Tellina lineata*	Bivalvia	1942	Ponta das Canas	SC	South	—	390 ± 40	-72 ± 40	Nadal de Masi (2001)

*These values were re-calculated using the Marine13 calibration curve.

Table 5.2: Summary of previous archaeological MRE studies on the Brazilian coast.

Site	State	Region	$\triangle$R ± 1 σ (^{14}C yr)	Reference
Jabuticabeira	SC	South	-62 ± 73	Macario et al. in prep.
Tarioba	RJ	Southeast	-127 ± 60	Macario et al. (2014, 2015)
Manitiba	RJ	Southeast	-82 ± 71	Carvalho et al. (2015)
Saquarema	RJ	Southeast	-140 ± 66	Alves et al. (2015)
Usiminas	RJ	Southeast	67 ± 33	Macario et al. (2016)
Acaiá	RJ	Southeast	-80 ± 87	Macario et al. (2018)

5.2 Pre-Bomb Samples

The set of known-age pre-bomb samples used in this research was obtained from museum collections in Brazil, Europe, and the USA. It consists of the $\mathrm{CaCO_3}$ remains of marine organisms such as molluscs and sea urchins. Information about this material has not been modified and is presented exactly as given in the museum labels (Table 5.3, Table 5.4, Table 5.5 and Table 5.6). It is possible to note that samples collected during 19th century expeditions tend to present more detailed labels, with precise dates and places of collection. I chose to prioritise these samples due to the higher confidence I had in their collection information. Figure 5.2 shows the number of marine samples measured for this research and their geographic distribution on the coast.

5.2.1 Sample Selection

Further to the difficulties involved in choosing samples for radiocarbon dating (Gillespie, 1984; Taylor, 1987; Aitken, 1990; Hedges, 1992), there are several obstacles inherent in the selection of suitable samples for marine reservoir studies (Ascough et al., 2005a). Considering the use of known-age marine samples from



Figure 5.1. The collection of the Museum of Comparative Zoology of the University of Harvard. The way natural history collections are organized in most of the museums hinders the search for specimens that are relevant for MRE studies. The specimens are catalogued according to their species while the collection details are the most important information for MRE investigations.

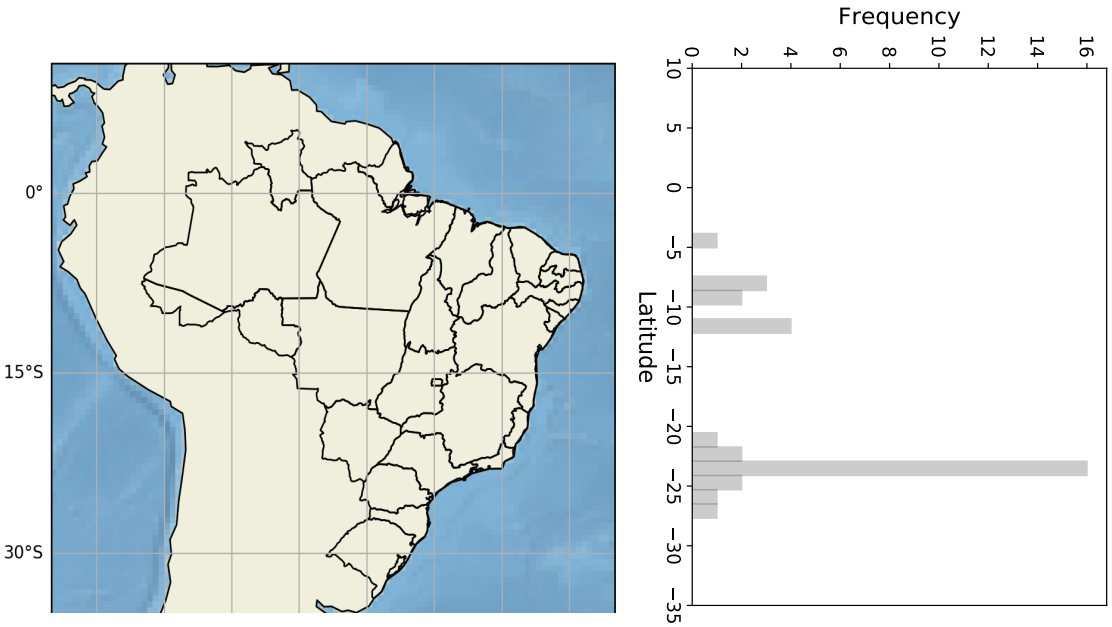


Figure 5.2. Distribution of the studied marine samples on the Brazilian coast. Most of the samples in the sample set are derived from the south and southeastern parts of the coast.

museum collections, the following criteria must be satisfied by the material (see e.g., O'Connor et al., 2010):

- **It must have been collected alive or shortly after the death date.** In order to derive a reservoir correction from the radiocarbon age of a marine sample, one needs to know the year of death of the organism. Therefore, provided that a given sample meets this requirement, its collection year marks its death and can be used in the calculations. Fading colours, round edges and the absence of periostracum[3] may indicate that, after the mollusc death, the shell was exposed for some time before collection. Articulating bivalves (see Figure 5.3) and the presence of soft tissue, on the other hand, corroborates live collection.

- **It must have been collected prior to 1950 AD**. This is to guarantee that the material is free from the ^{14}C bomb signal (subsection 1.2.4).

- **Ideally, it should be derived from a suspension feeder organism.** Ingestion of sediments by deposit feeders may reflect in the carbon isotopic concentration of their shells, leading to apparent ages. Thus, whenever possible, the use of suspension feeding bivalves should be prioritised (see Petchey et al., 2012, and references therein).

- **Its place and year of collection must be known.** The use of a calibration curve to infer the ^{14}C concentration of the coeval atmosphere (subsection 5.2.2) requires that the death/collection year is reported in the museum records. Labels must also contain information on the place of collection, since this is intrinsically necessary to ensure the usefulness of the geographic variable MRE corrections.

[3] This is a thin organic layer that covers the shell.

Moreover, it is preferable to use samples derived from sedentary organisms in order to guarantee that the MRE offsets are representative of a single location (Ascough et al., 2005a). It is not always possible to fulfill all these requirements and often the only samples available are not ideal, but still suitable.



Figure 5.3. Some of the shells used in this research. The labels show important information about the collection of the specimens and the presence of two valves corroborates the hypothesis of live collection. Scale in cm.

5.2.2 Calculation of the $\triangle$R Values

For a given time t, by inserting Equation 1.19 into Equation 1.20, we obtain:

$$\Delta \mathrm{R} = {}^{14}\mathrm{C}^{\mathrm{m}}_{\mathrm{mar}} - {}^{14}\mathrm{C}^{\mathrm{m}}_{\mathrm{atm}} - {}^{14}\mathrm{C}^{\mathrm{exp}}_{\mathrm{mar}} + {}^{14}\mathrm{C}^{\mathrm{exp}}_{\mathrm{atm}} \tag{5.1}$$

Considering that the terms $^{14}C^{m}_{atm}$ and $^{14}C^{exp}_{atm}$ should cancel out, we are left with:

$$\Delta R = {}^{14}C^{m}_{mar} - {}^{14}C^{exp}_{mar} \tag{5.2}$$

where $^{14}C^{m}_{mar}$ is the radiocarbon age measured for a marine sample and $^{14}C^{exp}_{mar}$ is the expected age obtained from the interpolation between the known-age (AD) of the sample and Marine13.[4] Therefore, following the known-age approach, the collecting (death) year of the sample was interpolated to Marine13 to generate a marine ^{14}C age ($^{14}C^{exp}_{mar}$). This modelled age was then subtracted from the measured age ($^{14}C^{m}_{mar}$) in order to yield ΔR (Figure 5.4).

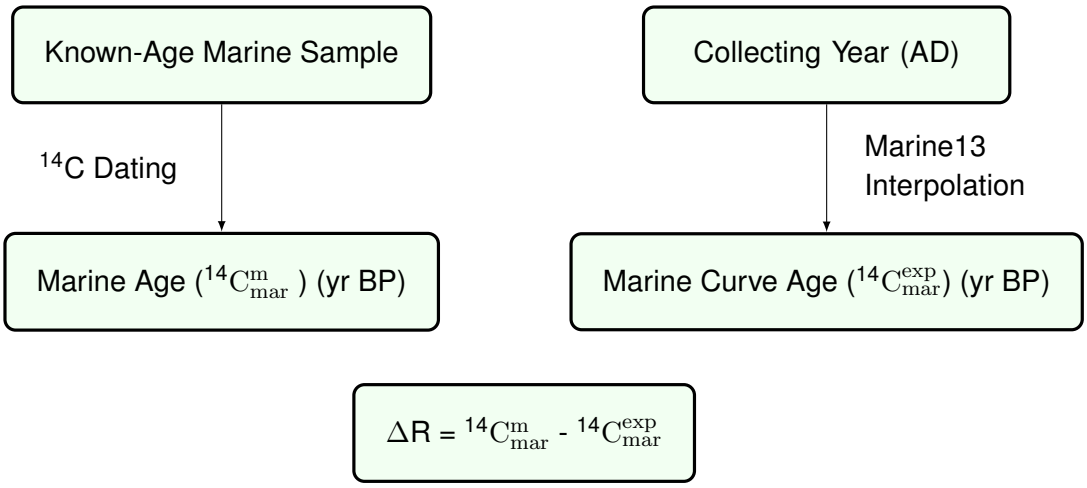


Figure 5.4. Flowchart illustrating the steps to be taken towards the determination of ΔR offsets using the known-age approach.

In this thesis, I have employed the *deltar* application (Reimer and Reimer, 2016) for the calculation of ΔR values from known-age samples. Effectively, this application uses the Marine13 calibration curve to determine the modelled ^{14}C age at the known-collection year of the sample, a process called *reverse-calibration*. After that, this modelled age is subtracted from the measured ^{14}C age for the marine sample to yield the ΔR value (Figure 5.5).

[4] Stuiver et al. (1986) writes Equation 5.2 as ΔR = P - Q, where P is the ^{14}C age measured for a marine sample and Q is the modelled global marine age.

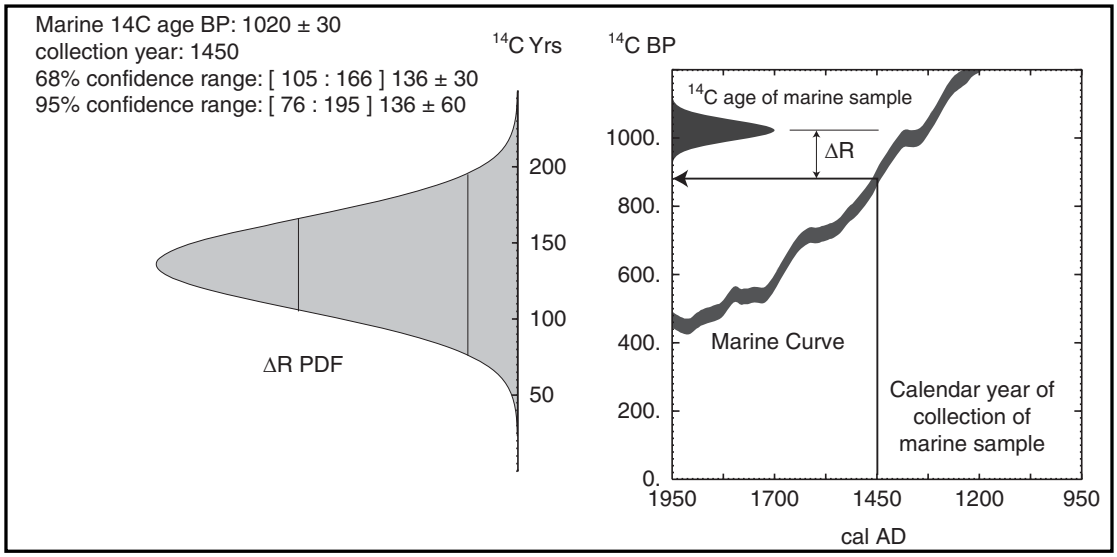


Figure 5.5. Illustration of the ΔR and uncertainty calculation for known-age samples. Source: Reimer and Reimer (2016). The different steps are described in the main text.

For the known-age approach, the ΔR uncertainty was taken as the uncertainty of the marine ^{14}C measurement (Reimer and Reimer, 2016). Usually, when ΔR values are averaged, the standard deviation is given as the unweighted scatter of the data:

$$\sigma_{\mathrm{mean}} = \frac{\sigma_u}{\sqrt{n}} \tag{5.3}$$

where n is the number of values being averaged and σ_{u} is the unweighted standard deviation of the set of ΔR values. Nevertheless, the error associated with measurement precision:

$$\sigma_\mu = \sqrt{\frac{1}{\sum_i \frac{1}{\sigma_{\mathrm{i}}^2}}} \tag{5.4}$$

is used when its value is larger than the one obtained by the use of Equation 5.3 (Stuiver et al., 1986).

5.2.3 Results and Discussion

(a) Stable Isotopes and Environment Identification

Although all the samples analysed for this research have well established collecting places, the resolution of this geographic information varies among the sample set. In some cases, the name of an entire state is reported as the collection locality, while in others the exact geographic coordinates are given. For convenience and to facilitate discussion, the results are grouped by sample environment in Table 5.3 (marine), Table 5.4 (freshwater) and Table 5.5 (estuary). This distinction was made based on the samples' collection localities (as registered in the museum records) and is further corroborated by their stable isotope values, as discussed in the next paragraphs. An additional group (Table 5.6) comprises samples with ambiguous collection places where more than one environmental setting is present (e.g., open ocean, lagoons, rivers and estuaries), which makes it difficult to be completely sure of their origin (see Figure 5.6).

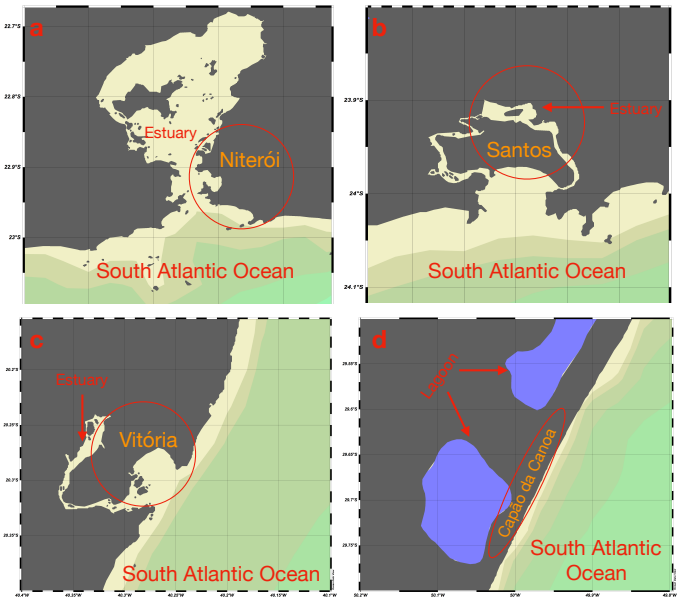


Figure 5.6. Examples of inconclusive collecting environments in the sample set. From the information available in the labels it was not possible to know whether the samples came from open ocean or estuarine settings. a: Niterói (RJ), b: Santos (SP), c: Vitória (ES) and d: Capão da Canoa (RS).

Table 5.3: Results for the known-age samples of marine origin measured for this research. The collection localities (as registered in the museums records) are oceanic regions, which leaves little or no-doubt that these organisms were collected from marine settings.

Museum	Museum Code	LACUFF/ORAU	Expedition	Collecting Year	Genus and species	Class	Reference	Verbatim Locality	State	Region	$\delta^{13}C_{VPDB} \pm 1\sigma$ (‰)	$\delta^{18}O_{VPDB} \pm 1\sigma$ (‰)	^{14}C Age $\pm 1\sigma$ (^{14}C yr BP)	$\Delta R \pm 1\sigma$ (^{14}C yr)
Museum of Comparative Zoology - Harvard University	73235	180115	Thayer Expedition	1865	*Iphigenia brasiliana*	Bivalvia	(Lamarck, 1818)	Pernambuco	PE	Northeast	0.9 ± 0.10	-0.99 ± 0.20	484 ± 32	4 ± 32
Museum of Comparative Zoology - Harvard University	143463	180117	Thayer Expedition	1865	*Pteria colymbus*	Bivalvia	(Röding, 1798)	Alagoas, Maceio	AL	Northeast	2.48 ± 0.10	-0.47 ± 0.20	453 ± 33	-28 ± 34
Museum of Comparative Zoology - Harvard University	73189	180122	Thayer Expedition	1865	*Pitar circinata*	Bivalvia	(Born, 1778)	Masseio, AL	AL	Northeast	0.88 ± 0.10	-1.34 ± 0.20	596 ± 32	116 ± 32
Museum of Comparative Zoology - Harvard University	194378	180131	—	1971	*Mulinia quadeloupensis*	Bivalvia	Récluz, 1852.	Aracaju, SE	SE	Northeast	0.08 ± 0.10	-0.45 ± 0.20	930 ± 29	462 ± 30
Museum of Comparative Zoology - Harvard University	192714	180132	—	1949	*Mactra alata*	Bivalvia	Spengler, 1802	Aracaju, SE	SE	Northeast	1.17 ± 0.10	-0.28 ± 0.20	512 ± 29	44 ± 30
Museum of Comparative Zoology - Harvard University	89721	180256*	Thayer Expedition	1865	*Divaricella quadrisulcata*	Bivalvia	(d'Orbigny, 1845)	Pernambuco	PE	Northeast	-0.11 ± 0.10	-1.02 ± 0.20	510 ± 30	30 ± 30
Museum of Comparative Zoology - Harvard University	161941†	180260*	Hassler Expedition	1872	*Laevicardium sybariticum*	Bivalvia	(Dall, 1886)	off Bahia	BA	Northeast	2.07 ± 0.10	-0.53 ± 0.20	455 ± 25	-26 ± 24
Museum of Comparative Zoology - Harvard University	145170	180269*	—	1937	*Anomalocardia brasiliana*	Bivalvia	(Gmelin, 1791)	Atalara Velha - Aracaju, SE	SE	Northeast	0.36 ± 0.10	-0.78 ± 0.20	500 ± 25	42 ± 24
Museum of Comparative Zoology - Harvard University	194203	180270*	—	1941	*Mactrela alata*	Bivalvia	Spengler, 1802	Boa Viagem, Recife, PE	PE	Northeast	0.59 ± 0.10	-0.35 ± 0.20	500 ± 20	38 ± 20
Natural History Museum London	NHMUK 1887.2.9.460-2	40,202	HMS Challenger	1873	*Nerita ascensionis*	Gastropoda	Gmelin, 1791	Fernando de Noronha, St Michael Rock	PE	Northeast	1.6 ± 0.30	—	411 ± 25	-66 ± 24
Museu de Zoologia da Universidade de São Paulo	21170	15P18A06; 33,089†	—	1933	*Anomalocardia brasiliana*	Bivalvia	(Gmelin, 1791)	Ilha do Mel, Saco do Miguel	PR	South	0.2 ± 0.30	—	428 ± 23	-28 ± 24
Museum of Comparative Zoology - Harvard University	194384	180271*	—	1940	*Anatina plicatella*	Bivalvia	Lamarck, 1818	Campeche, SC	SC	South	0.75 ± 0.10	-0.7 ± 0.20	490 ± 25	30 ± 24
Museu de Zoologia da Universidade de São Paulo	392	13P18A30; 32,148†	—	1898	*Oliva litterata*	Gastropoda	Lamarck, 1811	São Sebastião	SP	Southeast	3 ± 0.30	—	403 ± 25	-54 ± 24
Museu de Zoologia da Universidade de São Paulo	11306	15P18A01; 31,913†	—	1902	*Atrina seminuda*	Bivalvia	(Lamarck, 1819)	Iguapé	SP	Southeast	2.37 ± 0.30	—	445 ± 21	-8 ± 20
Museu de Zoologia da Universidade de São Paulo	311	15P18A02; 31,914†	—	1915	*Atrina seminuda*	Bivalvia	(Lamarck, 1819)	Ilha de São Sebastião	SP	Southeast	2.46 ± 0.30	—	530 ± 21	82 ± 15
Museu de Zoologia da Universidade de São Paulo	14298	15P18A03; 32,781†	—	1936	*Chione pubera*	Bivalvia	(Bory Saint-Vicent, 1827)	Ilha de São Sebastião	SP	Southeast	0.7 ± 0.30	—	439 ± 27	-20 ± 26
Museu de Zoologia da Universidade de São Paulo	49381	15P18A04; 31,917†	—	1937	*Thais haemastoma*	Gastropoda	(Linnaeus, 1767)	Itanhaém	SP	Southeast	2.09 ± 0.30	—	481 ± 21	22 ± 20
Museu de Zoologia da Universidade de São Paulo	24371	15P18A11; 32,782†	—	1905	*Neritina virginea*	Gastropoda	Linnaeus, 1758	Ilha Grande	RJ	Southeast	4.9 ± 0.30	—	420 ± 25	-30 ± 24
Museu de Zoologia da Universidade de São Paulo	24371	15P18A18; 32,788†	—	1905	*Neritina virginea*	Gastropoda	Linnaeus, 1758	Ilha Grande	RJ	Southeast	3.1 ± 0.30	—	396 ± 25	-54 ± 24
Museu de Zoologia da Universidade de São Paulo	24371	15P18A20; 32,789†	—	1905	*Neritina virginea*	Gastropoda	Linnaeus, 1758	Ilha Grande	RJ	Southeast	3.5 ± 0.30	—	383 ± 25	-66 ± 24
Museu de Zoologia da Universidade de São Paulo	14298	15P18A21; 32,152†	—	1936	*Chione pubera*	Bivalvia	(Bory Saint-Vicent, 1827)	Ilha de São Sebastião	SP	Southeast	1.5 ± 0.30	—	451 ± 21	-8 ± 20
Museu de Zoologia da Universidade de São Paulo	14210	15P18A27; 32,147†	—	1936	*Cerithium atratum*	Gastropoda	(Born, 1778)	Baia dos Castelhanos	SP	Southeast	2.6 ± 0.30	—	462 ± 24	4 ± 24
Museu de Zoologia da Universidade de São Paulo	14210	15P18A27; 32,326†	—	1936	*Cerithium atratum*	Gastropoda	(Born, 1778)	Baia dos Castelhanos	SP	Southeast	0.2 ± 0.30	—	821 ± 29	362 ± 30
Museu de Zoologia da Universidade de São Paulo	14210	15P18A28; 32,150†	—	1936	*Cerithium atratum*	Gastropoda	(Born, 1778)	Baia dos Castelhanos	SP	Southeast	3.8 ± 0.30	—	448 ± 28	-10 ± 28
Museu de Zoologia da Universidade de São Paulo	10666	15P18A31; 32,149†	—	1896	*Oliva litterata*	Gastropoda	Lamarck, 1811	São Sebastião	SP	Southeast	-0.5 ± 0.30	—	405 ± 28	-54 ± 28
Museum of Comparative Zoology - Harvard University	74183	180118	Thayer Expedition	1865	*Macoma constricta*	Bivalvia	(Bruguière, 1792)	Itabapuana, Campos, RJ	RJ	Southeast	-0.07 ± 0.10	-0.86 ± 0.20	405 ± 30	-76 ± 30
Museum of Comparative Zoology - Harvard University	74076	180121	Thayer Expedition	1865	*Lucina jamaicensis*	Bivalvia	Lamarck, 1801	Santa Ana Island	RJ	Southeast	0.73 ± 0.10	-0.85 ± 0.20	483 ± 29	2 ± 30
Museum of Comparative Zoology - Harvard University	193842	180130	—	1951	*Amiantis purpurata*	Bivalvia	(Lamarck, 1818)	Santos, SP	SP	Southeast	0.41 ± 0.10	-1.3 ± 0.20	532 ± 37	64 ± 38
Museum of Comparative Zoology - Harvard University	145166	180145	—	1939	*Tivela mactroides*	Bivalvia	(Born, 1778)	Recreio dos Bandeirantes, RJ	RJ	Southeast	1.85 ± 0.10	-0.12 ± 0.20	497 ± 43	38 ± 44
Museum of Comparative Zoology - Harvard University	153517	180146	—	1940	*Pincdata radiata*	Bivalvia	(Leach, 1814)	Praia de Copacabana, RJ	RJ	Southeast	2.18 ± 0.10	0.88 ± 0.20	483 ± 42	22 ± 42
Museum of Comparative Zoology - Harvard University	194208	180149	—	1872	*Mactra isabelliana*	Bivalvia	d'Orbigny, 1846	Cabo de Sao Thome, RJ	RJ	Southeast	0.98 ± 0.10	0.73 ± 0.20	804 ± 43	326 ± 44
Museum of Comparative Zoology - Harvard University	145111	180151	—	1939	*Divaricella quadrisulcata*	Bivalvia	(d'Orbigny, 1845)	Recreio dos Bandeirantes, DF, RJ	RJ	Southeast	-0.72 ± 0.10	-0.68 ± 0.20	391 ± 42	-68 ± 42
Museum of Comparative Zoology - Harvard University	226191	180267*	—	1939	*Donax hanleyanus*	Bivalvia	Philippi, 1847	Recreio dos Bandeirantes, DF, RJ	RJ	Southeast	1.29 ± 0.10	-0.4 ± 0.20	575 ± 25	116 ± 24

*These samples were measured at the ANU ^{14}C Laboratory.
†A chi-squared test was performed and the values reported are the weighted mean of the measurements.
‡Sample may have been collected at depth (verbatim depth “to 200 fms").

Table 5.4: Results for the known-age samples of freshwater origin measured for this research. The collection localities (as registered in the museums records) are rivers, which leaves little or no-doubt that these organisms were collected from freshwater settings.

Museum	Museum Code	LACUFF/ORAU†	Collecting Year	Genus and species	Class	Reference	Verbatim Locality	State	Region	$\delta^{13}C_{VPDB}$ ± 1σ (‰)	^{14}C Age ± 1σ (^{14}C yr BP)	$\triangle$R ± 1σ (^{14}C yr)
Museu de Zoologia da Universidade de São Paulo	5688	15P18A09; 33,087	1914	*Anodontites trapesialis*	Bivalvia	(Lamarck, 1819)	Itaqui, Rio Uruguai	RS	South	-6.1 ± 0.30	180 ± 25	-268 ± 24
Museu de Zoologia da Universidade de São Paulo	369	15P18A19; 32,787	1939	*Neritina zebra*	Gastropoda	Bruguière, 1792	Rio Paraguassú, Cachoeiras	BA	Northeast	-6.8 ± 0.30	300 ± 25	-160 ± 24
Museu de Zoologia da Universidade de São Paulo	369	15P18A17; 31,915	1939	*Neritina zebra*	Gastropoda	Bruguière, 1792	Rio Paraguassú, Cachoeiras	BA	Northeast	-6.96 ± 0.30	319 ± 20	-140 ± 20
Museu de Zoologia da Universidade de São Paulo	21485	15P18A14; 33,091	1912	*Tagelus plebeius*	Bivalvia	(Lightfoot, 1786)	Rio Paraíba, São João da Barra	RJ	Southeast	-1.3 ± 0.30	383 ± 23	-66 ± 24
Museu de Zoologia da Universidade de São Paulo	21486	15P18A15; 32,785	1911	*Tagelus plebeius*	Bivalvia	(Lightfoot, 1786)	Rio Paraíba (close to the sea)	RJ	Southeast	-3 ± 0.30	395 ± 25	-54 ± 24
Museu de Zoologia da Universidade de São Paulo	21486	15P18A08; 32,779	1911	*Tagelus plebeius*	Bivalvia	(Lightfoot, 1786)	Rio Paraíba (close to the sea)	RJ	Southeast	-3 ± 0.30	395 ± 26	-54 ± 26
Museu de Zoologia da Universidade de São Paulo	14577	15P18A05; 33,088	1938	*Anodontites trapesialis*	Bivalvia	(Lamarck, 1819)	Rio Miranda, Salobra	MT	Central-West	-8.2 ± 0.30	945 ± 28	486 ± 28
Museu de Zoologia da Universidade de São Paulo	21485	15P18A07; 33,090	912	*Tagelus plebeius*	Bivalvia	(Lightfoot, 1786)	Rio Paraíba, São João da Barra	RJ	Southeast	-2 ± 0.30	514 ± 25	66 ± 24
Museu de Zoologia da Universidade de São Paulo	369	15P18A24; 32,151	1939	*Neritina zebra*	Gastropoda	Bruguière, 1792	Rio Paraguassú, Cachoeiras	BA	Northeast	-7.9 ± 0.30	435 ± 26	-24 ± 26

†A chi-squared test was performed and the values reported are the weighted mean of the measurements.

Table 5.5: Results for the known-age samples of estuarine origin measured for this research. The collection localities (as registered in the museums records) are estuaries, which leaves little or no-doubt that these organisms were collected from estuarine settings.

Museum	Museum Code	LACUFF/ORAU	Expedition	Collecting Year	Genus and species	Class	Reference	Verbatim Locality	State	Region	$\delta^{13}C_{VPDB}$ ± 1σ (‰)	$\delta^{18}O_{VPDB}$ ± 1σ (‰)	^{14}C Age ± 1σ (^{14}C yr BP)	$\triangle$R ± 1σ (^{14}C yr)
Museu de Zoologia da Universidade de São Paulo	21460	15P18A10; 32,780†	—	1939	*Tagelus plebeius*	Bivalvia	(Lightfoot, 1786)	Ilha das Peças	PR	South	-5.4 ± 0.30	—	451 ± 33	-8 ± 34
Museu de Zoologia da Universidade de São Paulo	21460	15P18A16; 32,786†	—	1939	*Tagelus plebeius*	Bivalvia	(Lightfoot, 1786)	Ilha das Peças	PR	South	-6.1 ± 0.30	—	479 ± 25	20 ± 24
Museum of Comparative Zoology - Harvard University	245220	180157	—	1949	*Semele proficua*	Bivalvia	(Pulteney, 1799)	Ilha Pinheiro	RJ	Southeast	1.01 ± 0.10	-0.42 ± 0.20	453 ± 42	-16 ± 42
Museum of Comparative Zoology - Harvard University	145174	180154	—	1941	*Anomalocardia brasiliana*	Bivalvia	(Gmelin, 1791)	Praia Grossa, Ilha de Paquetá, RJ	RJ	Southeast	-3.5 ± 0.10	-1.72 ± 0.20	461 ± 42	0 ± 42
Museum of Comparative Zoology - Harvard University	245224	180155	—	1949	*Tellina angulosa*	Bivalvia	Gmelin, 1791	Ilha do Fundao, RJ	RJ	Southeast	0.55 ± 0.10	-1.12 ± 0.20	493 ± 42	24 ± 42
Museum of Comparative Zoology - Harvard University	124422	180266	—	1941	*Semele proficua*	Bivalvia	(Pulteney, 1799)	Praia Grossa, Ilha de Paquetá, RJ	RJ	Southeast	-0.83 ± 0.10	-2.44 ± 0.20	545 ± 15	84 ± 14
Museum of Comparative Zoology - Harvard University	195747	180148	—	1949	*Barnea (Anchomasa) truncata*	Bivalvia	(Say, 1822)	Parada Sahy, Sepetiba Bay, RJ	RJ	Southeast	0.83 ± 0.10	0.5 ± 0.20	587 ± 42	118 ± 42
Museum of Comparative Zoology - Harvard University	145021	180156	—	1941	*Dosinia concentrica*	Bivalvia	(Born, 1778)	Praia Grossa, Ilha de Paquetá, RJ	RJ	Southeast	-0.15 ± 0.10	-1.08 ± 0.20	585 ± 52	124 ± 52
Natural History Museum London	NHMUK 1860.5.2.13	33,437; 33,438†	HMS Rattlesnake	1847	*Pitaria (Macrocallista) maculata*	Bivalvia	(Linnaeus, 1758)	Botafogo Bay, Rio de Janeiro	RJ	Southeast	0.8 ± 0.30	—	533 ± 19	46 ± 18
Natural History Museum London	NHMUK 60.4.21.27	40,184	HMS Rattlesnake	1847	*atratum = C. caudatum*	Gastropoda	(Born, 1778)	muddy sand 3 fms Botafogo Bay, Rio de Janeiro	RJ	Southeast	3.3 ± 0.30	—	561 ± 27	74 ± 26

†A chi-squared test was performed and the values reported are the weighted mean of the measurements.

Table 5.6: Results for the known-age samples of unknown origin measured for this research. The collection localities (as registered in the museums records) leave doubts about the kind of environment where these shellfish were collected.

Museum	Museum Code	LACUFF/ORAU	Expedition	Collecting Year	Genus and species	Class	Reference	Verbatim Locality	State	Region	$\delta^{13}C_{VPDB} \pm 1\sigma$ (‰)	$\delta^{18}O_{VPDB} \pm 1\sigma$ (‰)	^{14}C Age $\pm 1\sigma$ (^{14}C yr BP)	$\Delta R \pm 1\sigma$ (^{14}C yr)
Museu de Zoologia da Universidade de São Paulo	1946	15P18A23; 32,153; 32,154[†]	—	1896	*Neritina virginea*	Gastropoda	Linnaeus, 1758	—	BA	Northeast	0.2 ± 0.30	—	377 ± 19	-82 ± 18
Museu de Zoologia da Universidade de São Paulo	1946	15P18A25; 31,918[†]	—	1896	*Neritina virginea*	Gastropoda	Linnaeus, 1758	—	BA	Northeast	0.37 ± 0.30	—	395 ± 23	-64 ± 24
Museu de Zoologia da Universidade de São Paulo	51194	15P18A12; 32,783[†]	—	1927	*Olivancillaria urceus*	Gastropoda	(Roding, 1798)	Guaratuba	PR	South	1.7 ± 0.30	—	396 ± 25	-56 ± 24
Museu de Zoologia da Universidade de São Paulo	1946	15P18A26; 32,155[†]	—	1896	*Neritina virginea*	Gastropoda	Linnaeus, 1758	—	BA	Northeast	1.7 ± 0.30	—	453 ± 25	-6 ± 24
Museu Oceanográfico "Eliézer de C. Rios"	MORG 5045	16P11A06	—	1950	*Stramonita haemastoma*	Gastropoda	(Linnaeus, 1767)	Armação C.	SC	South	—	—	360 ± 52	-108 ± 52
Museu Oceanográfico "Eliézer de C. Rios"	MORG 16407	16P11A05	—	1930	*Olivella formicacoisii*	Gastropoda	Klappenbach, 1962	Capão da Canoa, RS	RS	South	—	—	491 ± 66	38 ± 66
Museu Oceanográfico "Eliézer de C. Rios"	MORG 4162	16P11A08	—	1950	*Caputus incurvatus*	Gastropoda	Gmelin, 1791	Guarapari, ES	ES	Southeast	—	—	632 ± 52	164 ± 52
Museum für Naturkunde Berlin	ZMB/Moll. 250156	40,198	Die Preussiche Expedition nach Ostasien	1860	*Littorina columellaris*	Gastropoda	d'Orbigny, 1840	RJ	RJ	Southeast	1.9 ± 0.30	—	348 ± 23	-134 ± 24
Museum für Naturkunde Berlin	ZMB/Moll. 250155	40,203	—	1935	*Littorina scabra*	Gastropoda	(Linnaeus, 1758)	PE	PE	Northeast	-5.1 ± 0.30	—	321 ± 24	-136 ± 24
Museum für Naturkunde Berlin	ZMB/Moll. 250152	40,195	Die Preussiche Expedition nach Ostasien	1860	*Cerithium atratum*	Gastropoda	(Born, 1778)	RJ	RJ	Southeast	2.3 ± 0.30	—	483 ± 26	2 ± 26
Museum für Naturkunde Berlin	ZMB/Moll. 250153	40,196	Die Preussiche Expedition nach Ostasien	1860	*Tellina lineata*	Bivalvia	Turton, 1819	RJ	RJ	Southeast	3 ± 0.30	—	557 ± 25	76 ± 24
Museum für Naturkunde Berlin	ZMB/Moll. 250157	40,199	Die Preussiche Expedition nach Ostasien	1860	*Dosinia concentrica*	Bivalvia	(Born, 1778)	RJ	RJ	Southeast	1.8 ± 0.30	—	681 ± 29	200 ± 30
Museum of Comparative Zoology - Harvard University	193841	180125	—	1951	*Donax hanleyanus*	Bivalvia	Philippi, 1847	Santos, SP	SP	Southeast	1.12 ± 0.10	-0.59 ± 0.20	379 ± 28	-90 ± 28
Museum of Comparative Zoology - Harvard University	245214	180150	—	1949	*Diplodonta semiaspera*	Bivalvia	Philippi, 1836	Niteroi, RJ	RJ	Southeast	0.69 ± 0.10	-0.64 ± 0.20	413 ± 41	-56 ± 40
Museum of Comparative Zoology - Harvard University	73292	180116	Thayer Expedition	1865	*Tagelus gibbus*	Bivalvia	(Spengler, 1794)	Nova Almeida, ES	ES	Southeast	-8.36 ± 0.10	-4.33 ± 0.20	430 ± 31	-50 ± 30
Museum of Comparative Zoology - Harvard University	73012	180262	Thayer Expedition	1865	*Anomalocardia brasiliana*	Bivalvia	(Gmelin, 1791)	Victoria, ES	ES	Southeast	-1.86 ± 0.10	-2.34 ± 0.20	480 ± 25	0 ± 24
Museum of Comparative Zoology - Harvard University	73179	180120	Thayer Expedition	1865	*Venus (Chione) pectorina*	Bivalvia	Lamarck, 1818	N. of Cape Frio	RJ	Southeast	-0.9 ± 0.10	-1.42 ± 0.20	510 ± 31	30 ± 30
Museum of Comparative Zoology - Harvard University	203117	180126	—	1950	*Iphigenia brasiliana*	Bivalvia	(Lamarck, 1818)	near Recife, beach of Pina, PE	PE	Northeast	-3.64 ± 0.10	-1.6 ± 0.20	504 ± 36	36 ± 36
Museum of Comparative Zoology - Harvard University	245217	180147	—	1949	*Hiatella arctica*	Bivalvia	(Linnaeus, 1767)	Niteroi, RJ	RJ	Southeast	1.03 ± 0.10	0.07 ± 0.20	537 ± 45	68 ± 46
Museum of Comparative Zoology - Harvard University	245215	180152	—	1949	*Semele purpurascens*	Bivalvia	(Gmelin, 1791)	Niteroi, RJ	RJ	Southeast	1.04 ± 0.10	-1.61 ± 0.20	538 ± 50	70 ± 50
Museum of Comparative Zoology - Harvard University	73008	180257	Thayer Expedition	1865	*Anomalocardia brasiliana*	Bivalvia	(Gmelin, 1791)	Nova Almeida, ES	ES	Southeast	-1.73 ± 0.10	-2.44 ± 0.20	555 ± 20	74 ± 20
Museum of Comparative Zoology - Harvard University	349297	180258	Thayer Expedition	1865	*Anomalocardia brasiliana*	Bivalvia	(Gmelin, 1791)	Victoria, ES	ES	Southeast	-0.56 ± 0.10	-2.72 ± 0.20	625 ± 25	144 ± 24
Museum of Comparative Zoology - Harvard University	73013	180261	Thayer Expedition	1865	*Anomalocardia brasiliana*	Bivalvia	(Gmelin, 1791)	Pernambuco	PE	Northeast	-4.63 ± 0.10	-3.47 ± 0.20	570 ± 20	90 ± 20
Museum of Comparative Zoology - Harvard University	213386	180129	—	1950	*Divaricella quadrisulcata*	Bivalvia	(d'Orbigny, 1845)	Beach of Pina near Recife, PE	PE	Northeast	-1.32 ± 0.10	-1.19 ± 0.20	654 ± 28	186 ± 28
Natural History Museum London	NHMUK 1890.4.14.159	40,200	HMS Challenger	1873	*Cardium (Papyridea) bullatum*	Bivalvia	Locard, 1891	Bahia 7 - 20 fms	BA	Northeast	1.2 ± 0.30	—	455 ± 25	-22 ± 24
Natural History Museum London	NHMUK 59.10.12.1	40,188	HMS Herald	1852	*Anomalocardia brasiliana*	Bivalvia	(Gmelin, 1791)	Rio de Janeiro	RJ	Southeast	-1.5 ± 0.30	—	517 ± 26	32 ± 26
Natural History Museum London	NHMUK 1860.5.2.22	40,185	HMS Rattlesnake	1847	*Laevicardium (L.) serratum*	Bivalvia	(Linnaeus, 1758)	Rio de Janeiro	RJ	Southeast	1.1 ± 0.30	—	530 ± 25	42 ± 24
Naturhistorisches Museum Wien	NHV M2 / 32 / A / r / 10	40,189	Novara	1857	*Stramonita haemastoma*	Gastropoda	(Linnaeus, 1767)	RJ	RJ	Southeast	2 ± 0.30	—	468 ± 27	-14 ± 26
Naturhistorisches Museum Wien	NHV J10 / A21 / l / 6	40,190	Novara	1857	*Crypta marginalis*	Gastropoda	Broderip, 1834	RJ	RJ	Southeast	0.3 ± 0.30	—	510 ± 29	28 ± 30
Naturhistorisches Museum Wien	NHV R8 / 55 / l / 2B - 3A	40,191	Novara	1857	*Mytilus janeiroensis*	Bivalvia	Dunker & Zelebor, 1866	RJ	RJ	Southeast	1.7 ± 0.30	—	497 ± 29	14 ± 30
Naturhistorisches Museum Wien	NHV A33 / 52	40,192	Novara	1857	*Cerithium atratum*	Gastropoda	(Born, 1778)	RJ	RJ	Southeast	2.9 ± 0.30	—	515 ± 25	32 ± 24
Naturhistorisches Museum Wien	NHV J10 / A22 / l / 5	33,560; 34,490[†]	Corvette Saida	1887	*Nerita albicilla*	Gastropoda	Linnaeus, 1758	BA	BA	Northeast	1.25 ± 0.30	—	518 ± 22	36 ± 22
Statens Naturhistoriske Museum	ZMUC-ECH-722	15P18A13; 32,784[†]	—	1923	*Encope emarginata*	Echinoidea;	(Leske, 1778)	RJ	RJ	Southeast	1.3 ± 0.30	—	457 ± 25	6 ± 24

[†]A chi-squared test was performed and the values reported are the weighted mean of the measurements.

δ^{18}O entries have been omitted from the results tables in order to prioritise the measurement of samples that more closely meet the criteria listed in subsection 5.2.1. This information will in due course form part of further planned research on the subject. Previous MRE studies have employed δ^{18}O and δ^{13}C measurements for the purpose of establishing the ambient conditions of shell formation (e.g., Kennett et al., 1997; Culleton et al., 2006; Petchey et al., 2008; Ulm et al., 2009; Petchey and Clark, 2011; Petchey et al., 2013). In the case of this research, δ^{18}O and δ^{13}C values allow for a refinement of the historical evidence contained in the museum labels, thereby strengthening the hypotheses on shellfish environment. Indeed, aquatic molluscs tend to precipitate their carbonates in equilibrium with the surrounding water DIC. Therefore, neglecting the often small contributions of physiological effects (e.g., metabolic and kinetic), the isotopic composition of these shells primarily reflect that of environmental DIC (e.g., McConnaughey et al., 1997; Surge et al., 2001; McConnaughey and Gillikin, 2008; Hadden et al., 2018). Fluvial and marine DIC are isotopically distinct and while δ^{18}O values work as indicators of water temperature and salinity during biomineralization, δ^{13}C values can track water origin (see subsection 1.6.1). Results for the samples presenting both δ^{13}C and δ^{18}O values are shown in Figure 5.7. It is possible to see that marine bivalves cluster in the upper right corner of the graph (δ^{18}O > -2‰ and δ^{13}C > -1‰). Considering that shell δ^{13}C values are often slightly depleted relatively to the surrounding water DIC (McConnaughey and Gillikin, 2008) and oxygen fractionation depends on the carbonate crystalline structure, this is consistent with modelled δ^{13}C and δ^{18}O values for the South Atlantic Ocean, which are in the range 1 - 2‰ and -1.27 - 0.73‰, respectively (see Gruber et al., 1999; LeGrande and Schmidt,

2006; Tagliabue and Bopp, 2008).[5] The isotopic values presented here are also in agreement with those reported in the survey presented by Keith et al. (1964).

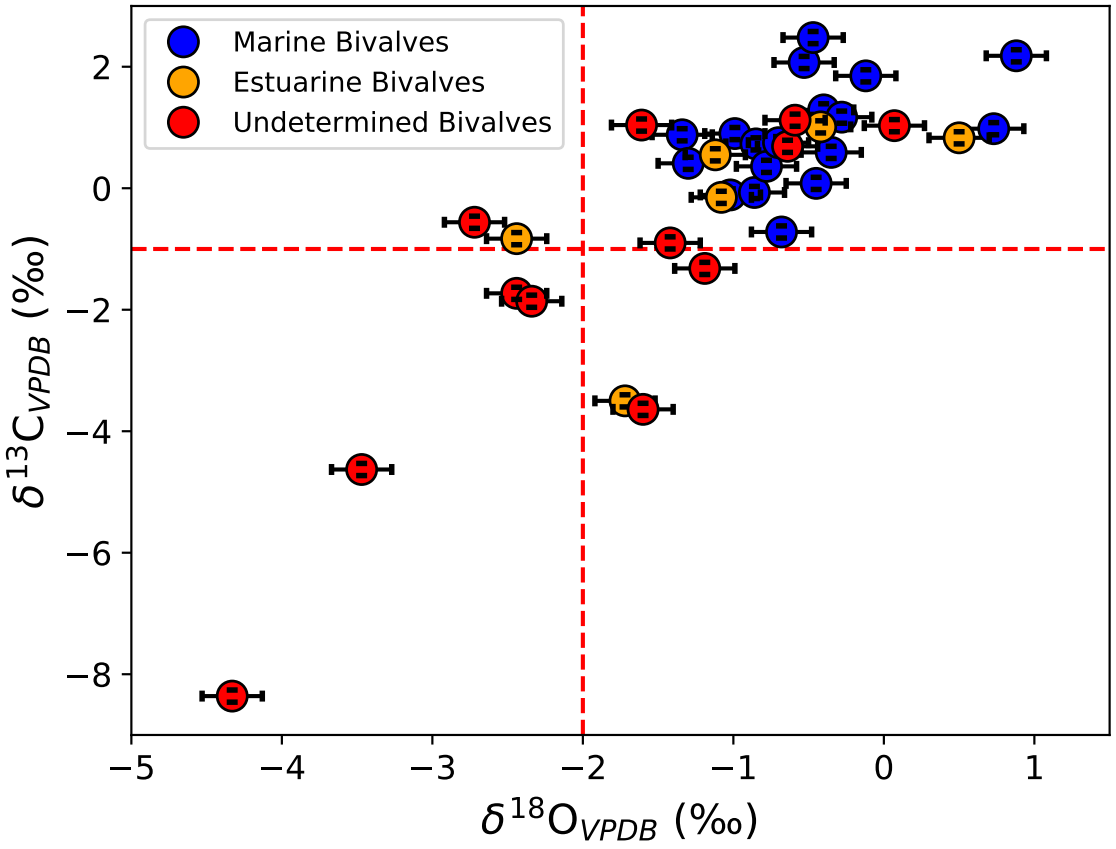


Figure 5.7. Stable isotopes (δ^{18}O and δ^{13}C) results for the known-age samples. Marine bivalves cluster in the upper right corner of the graph (δ^{18}O > -2‰ and δ^{13}C > -1‰).

Most of the marine samples in Figure 5.7 present positive δ^{13}C, the great majority of which are within the modelled range for the South Atlantic ocean. Considering that these models do not resolve coastal processes, samples presenting δ^{13}C > 2‰ could be explained by the enhanced primary production of the coast when compared to open ocean waters (Killingley and Berger, 1979; Krantz et al., 1987; Kirby et al., 1998; Gruber et al., 1999). As mentioned before, the uptake of ^{12}C is

[5]For δ^{18}O, the conversion between the VPDB and the VSMOW scales is controversial (e.g., Dettman et al., 1999; Chauvaud et al., 2005; Fenger et al., 2007; Lougheed et al., 2013, and references therein). Here I follow Lougheed et al. (2013) and subtract 0.27‰ from the measured value to convert from VSMOW to VPDB. See a discussion of this in Hut (1987).

favoured during photosynthetic activity, which results in enhanced ^{13}C availability for calcifying organisms. These samples present either enriched or only slightly depleted $\delta^{18}O$ values, which is a characteristic of carbonates formed in cold and nutrient rich waters (Culleton et al., 2006).

Since estuaries are transition zones between marine and freshwater environments, their isotopic signature will be a function of the relative mixing of these two water sources (Mook and Vogel, 1968; Gillikin et al., 2006). This indicates that variations in the contribution of fluvial and marine DIC led to the scattered estuarine values in Figure 5.7. Therefore, in Figure 5.7 it is possible to identify a group of estuarine samples whose isotopic signature matches that of marine samples (i.e., estuarine samples with a marine behaviour). Freshwater influence, on the other hand, typically causes the depletion of both $\delta^{18}O$ and $\delta^{13}C$ values (e.g., Gat, 1996; Keith et al., 1964; Culleton et al., 2006, and references therein).

The undetermined samples are dispersed in Figure 5.7, which indicates that they are of different origins. Nevertheless, the isotopic evidence gives an idea of the environmental system and thus allows for the identification of the most likely collection setting for these samples. The simultaneous dependence of shell $\delta^{18}O$ values on temperature, salinity and carbonate crystalline structure hinders the use of these values for environmental reconstructions (Grossman and Ku, 1986; Surge et al., 2003). Hence, $\delta^{13}C$ values are employed for environment identification in this thesis. The fact that all samples that are surely marine yielded $\delta^{13}C$ > -1 ‰ is the basis for choosing this value as the limit for the isotopic signature of marine settings. These samples are most likely derived from marine settings such as the open ocean or marine influenced estuaries and, from now on in this discussion, undetermined samples whose isotopic values fall within the marine range will be considered marine. The collection settings of samples analysed in previous studies were not possible to be identified and, therefore, the same reasoning

was employed to identify the environments of previous published data with stable isotopes information.

(b) The Relationship Between Stable Isotopes, Organism Class and the MRE

Figure 5.8 shows the relationship between the δ^{18}O and $\triangle$R values derived in this research. There is no correlation between these two variables in any of the environmental groups studied. The same is true for the relationship between δ^{13}C and $\triangle$R values (Figure 5.10). To understand why this is the case, it is important to recall that the study of the MRE in near-shore locations and estuaries is extremely complex due to the diversity of possible carbon sources. Most of the $\triangle$R results concentrate between -100 and 200 ^{14}C yr. As discussed in subsection 1.4.1, high positive $\triangle$R values are typically associated with the input of ^{14}C-depleted carbon sources in the environment (e.g., upwelling of deep waters, dissolution of limestone bedrock and peat material). Negative $\triangle$R values, on the other hand, are usually associated with the influence of terrestrial carbon sources presenting a higher radiocarbon activity than average marine waters (e.g., terrestrial plant material). Nevertheless, there are many other factors to be considered here. Below I discuss the overall behaviour of the different groups and later in this text I consider some outstanding individual cases.

Concerning the freshwater group in Figure 5.10, all of the samples are considerably depleted in ^{13}C when compared to the marine group (δ^{18}O data is not available for these samples). With the exception of two samples (MCZ14577 and MCZ21485), they present negative $\triangle$R values, meaning that their ^{14}C signal is closer to atmospheric than the marine one (Figure 5.11). This is expected in shallow and not stratified water bodies, where $\mathrm{CO_2}$ exchange with the atmosphere is

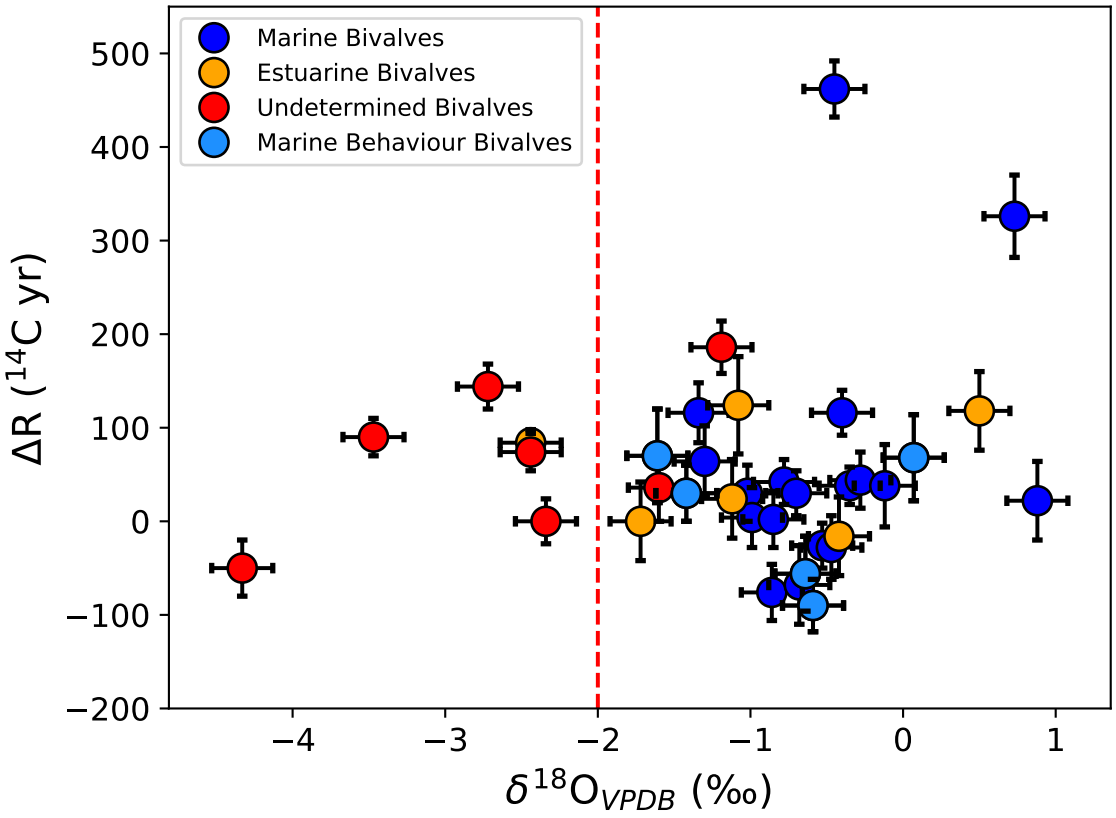


Figure 5.8. δ^{18}O and ΔR results for the known-age marine samples. There is no clear correlation between these two variables in any of the environmental groups studied.

enhanced comparatively to the ocean. Moreover, the breakdown of organic detritus carrying a terrestrial ^{14}C signal may also play a role.

Due to the complex mix of terrestrial and marine carbon that takes place in estuaries (Little, 1993; Olsen et al., 2017, and references therein), in this research estuarine samples present ΔR values slightly higher than the marine ones (Figure 5.11). This indicates that the estuaries considered in the present study are influenced by freshwater discharge and the ^{14}C content of the material being introduced by rivers into the estuaries is different from marine. However, some estuarine samples depleted in ^{13}C - a sign of freshwater influence - do not present ΔR values much different from the marine ones. More studies focusing on the ^{14}C content of the exogenous carbon brought to these basins are needed for the

interpretation of these results. Indeed, the use of stable isotopes and radiocarbon (expressed as ΔR) as indicators of the source of water in a given system needs to be carefully performed. Apparent inconsistencies regarding the marine and freshwater contributions to the system, i.e., positive ΔR associated with negative δ^{13}C or negative ΔR associated with positive δ^{13}C, can be explained by the carbon isotopic signal of each source. Figure 5.9 shows an example for 1865 AD, considering a pure freshwater signal that yields a ΔR = -300 ^{14}C yr (Fm_w = 0.978) and a δ^{13}C = -10‰ and a marine δ^{13}C value of 5‰. By varying the Fm values of the marine component (Fm_m), it is possible to estimate the Fm value of mixtures of different proportions and thus calculate how ΔR changes for each of these mixtures. The δ^{13}C signal of the mixture does not respond to variation in the ^{14}C content of the marine contribution. High, positive or negative, δ^{13}C values do reflect the main origin of the carbon present in a system but intermediate values can be difficult to interpret. The dashed red line in the graph shows a δ^{13}C signal that would be mostly marine. Corresponding ΔR values of the mixture depend on the purely marine ΔR. In this context, the ^{14}C signal has the potential to provide a fine adjustment.

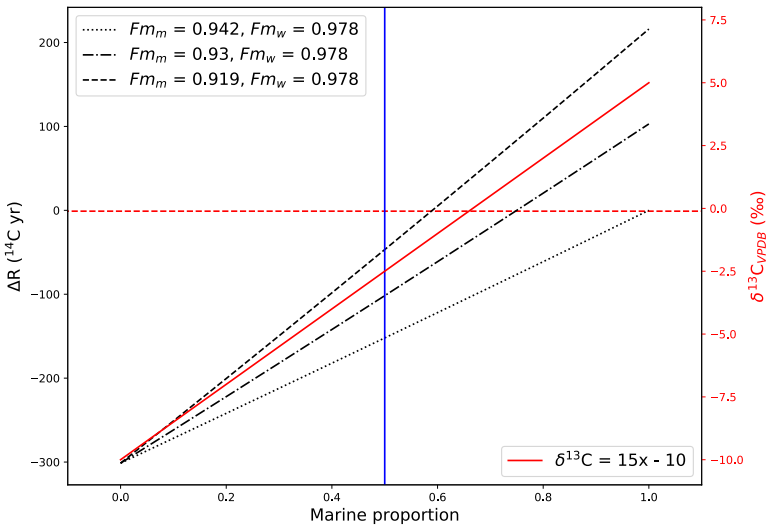


Figure 5.9. Variation of δ^{13}C and ΔR with the proportion of marine water in a mixture. The example refers to 1865 AD.

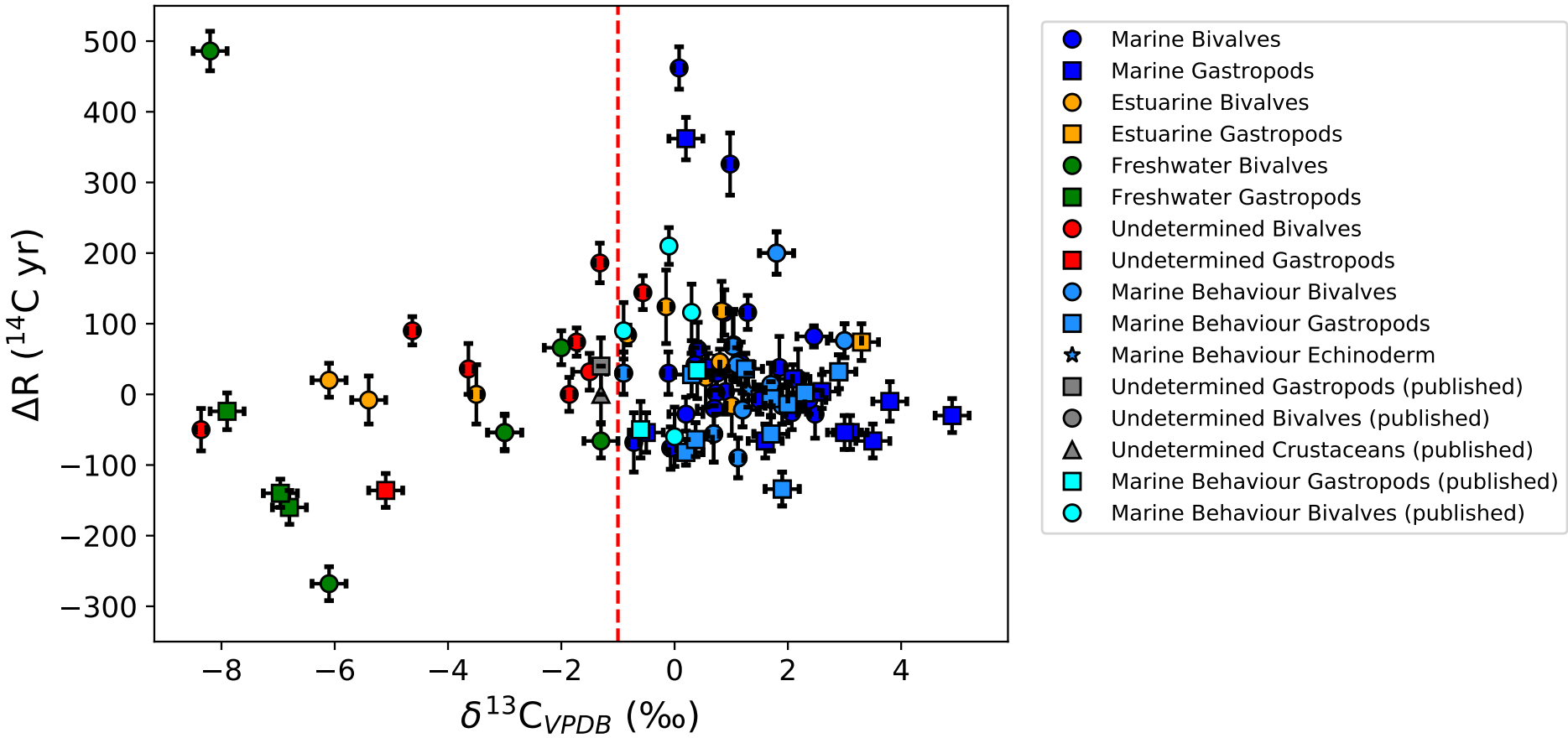


Figure 5.10. δ^{13}C and ΔR results for known-age samples from different environments. There is no clear correlation between these two variables in any of the environmental groups studied.

Even though the unrestricted circulation in open ocean regions attenuates possible effects of continental input, several marine samples present negative $\triangle$R values. This suggests a freshwater influence introducing a significant amount of terrestrial carbon to the mollusc habitat. However, the stable isotopic signature of most of these samples is enriched or only slightly depleted, which is not expected for organisms uptaking large amounts of terrestrial carbon. Although there is the chance of photosynthesis influencing the δ^{13}C values of the water, the possibility of physiological effects affecting the isotopic composition of these shells cannot be ruled out. Indeed, in the marine group, the majority of negative $\triangle$R values are presented by gastropods. Moreover most of the samples presenting δ^{13}C values greater than 2.5‰ are gastropods. Figure 5.11 shows that the median of the marine $\triangle$R values is close to 0, as expected for fully marine samples. Nevertheless, it is important to point that $\triangle$R values close to zero are expected to present stable isotopes results within the limits of the South Atlantic ocean values, but this is not always the case, meaning that some coastal, physiological or indeed both effects may be playing a role in the isotopic composition of these organisms. From Figure 5.11 it is also possible to notice that $\triangle$R values for the group presenting a marine behaviour are in agreement with the marine group values, corroborating the classification of the former.

Species-dependent variations in shell ^{14}C content are still a subject of debate within the radiocarbon community. While some studies found no significant difference among distinct species (e.g., Harkness, 1983; Ascough et al., 2005b), others suggest the opposite (e.g., Ingram and Southon, 1996; Forman and Polyak, 1997). Nevertheless, the radiocarbon community acknowledges that, since deposit feeders can ingest carbon from various sources (e.g., decaying terrestrial organic matter or sediment), care should be taken when analysing the ^{14}C signature of these animals in areas of limestone geology or high input of terrestrial sourced carbon.

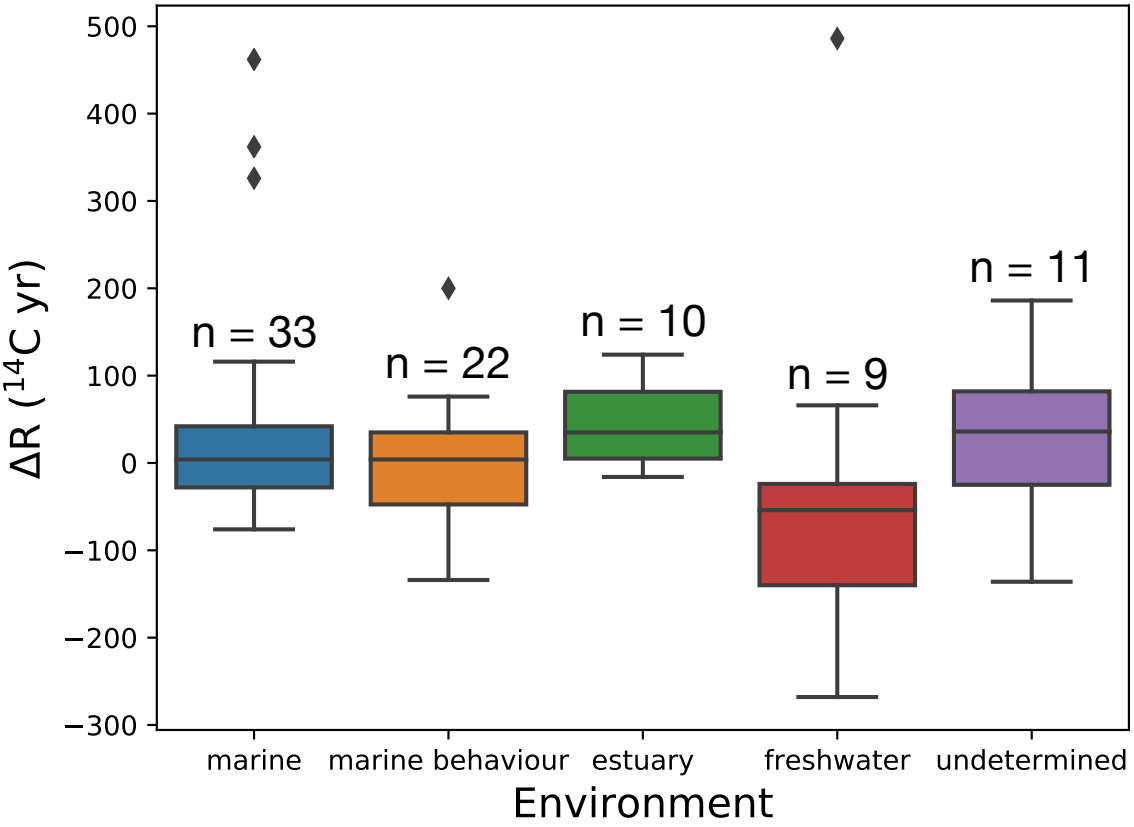


Figure 5.11. Boxplot for the ΔR results. Whiskers show maximum and minimum, black line shows median.

This ingested carbon becomes part of the metabolic carbon pool of the animal, which can contribute to shell carbonate in variable proportions (McConnaughey and Gillikin, 2008). Therefore, the use of filter feeder bivalves that feed primarily on suspended phytoplankton is recommended for MRE studies (see e.g., discussion in Petchey et al., 2012). Nevertheless, even in this case, habitats and feeding mechanisms should also be considered since some bivalves can modify their feeding habits according to environmental or physiological factors (Petchey et al., 2013, and references therein). Therefore, the fact that most of the samples measured in this study are bivalve shells does not guarantee the absence of metabolic effects.

Despite the low number of measurements for some of the groups, a good way of analysing the variability of the ΔR values obtained is to plot a histogram of the data. Figure 5.12 shows the spread of the ΔR values according to environ-

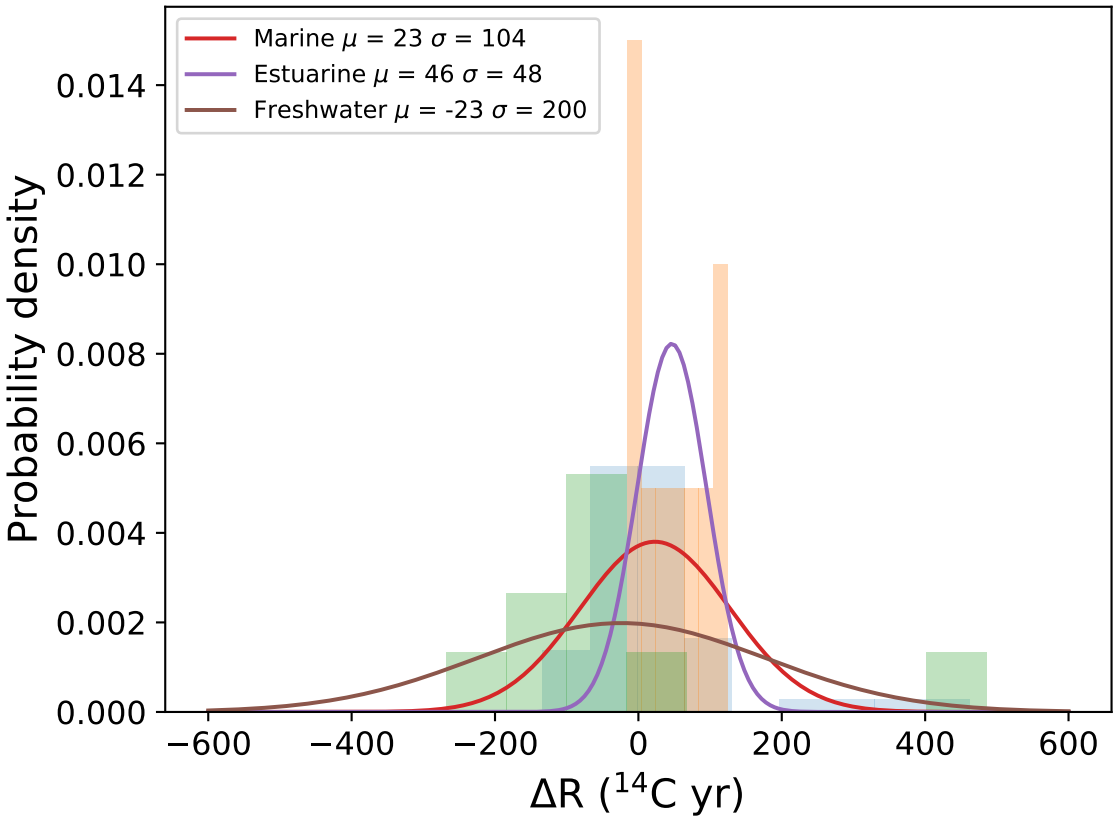


Figure 5.12. Histogram for the ΔR results according to environment. The histograms are for the marine (blue), freshwater (green) and estuarine (orange) groups. The freshwater group outliers are due to the presence of limestone in central Brazil, where some of these samples were collected.

ment. With the exception of the estuarine distribution (σ = 48 ^{14}C yr), Figure 5.12 shows distributions that are considerably widespread. The freshwater and marine results show some excursions possibly related to very local effects. These will be discussed in the next section. For the undetermined group, the ΔR distribution is relatively widespread, possibly reflecting different collection settings for these samples (Figure 5.13). Nevertheless, the mean is close to the marine group mean ΔR, suggesting that most of the undetermined samples may actually be of marine origin. In any case, given the extreme geographic variability of the MRE, it is difficult to be sure about this.

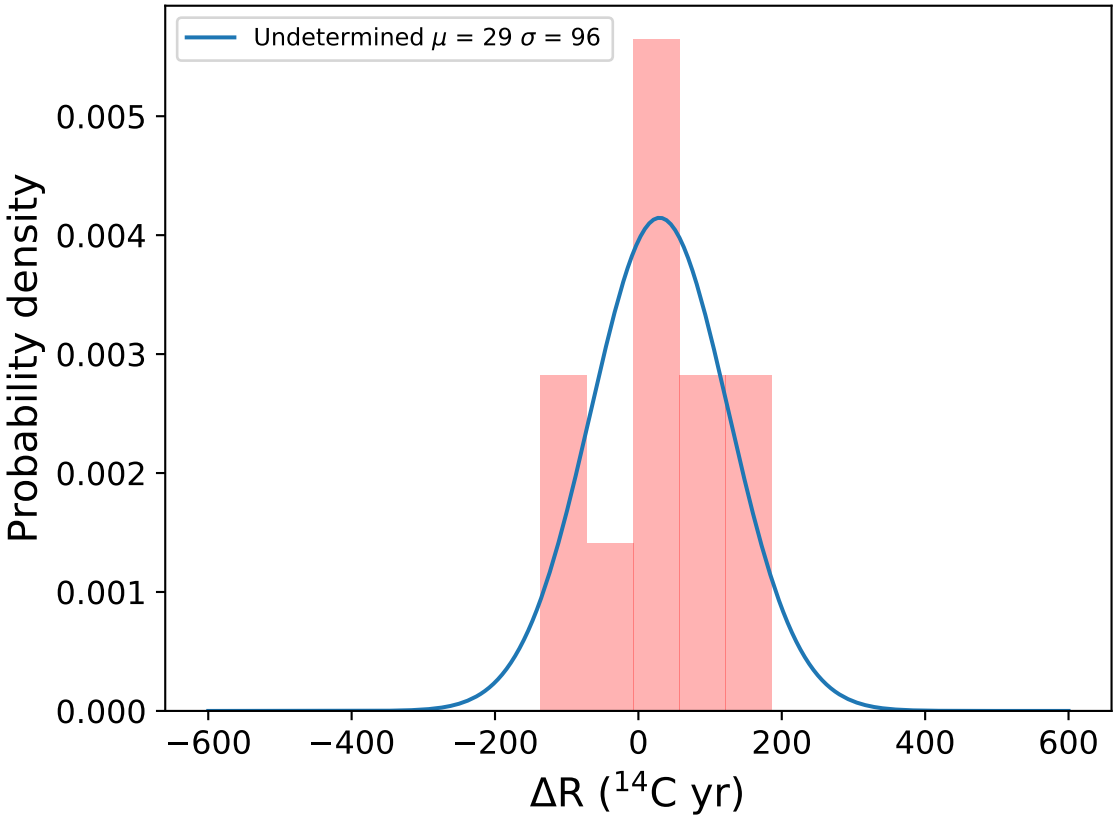


Figure 5.13. Histogram for the ΔR results (undetermined environment).

(c) Temporal and Geographic Variability in the MRE: Mapping ΔR Values on the Brazilian Coastline

Figure 5.14 shows the ΔR values derived in this research versus calendar year. Following previous graphs, Figure 5.14 shows that there is no significant temporal variation over the Brazilian coast in the considered timescale for the marine samples analysed (Spearman correlation r = 0.11; Pearson correlation r = 0.017). This indicates that either the local hydrology or ocean circulation regime does not change significantly in this time scale or the sample set is too limited to show these variations.

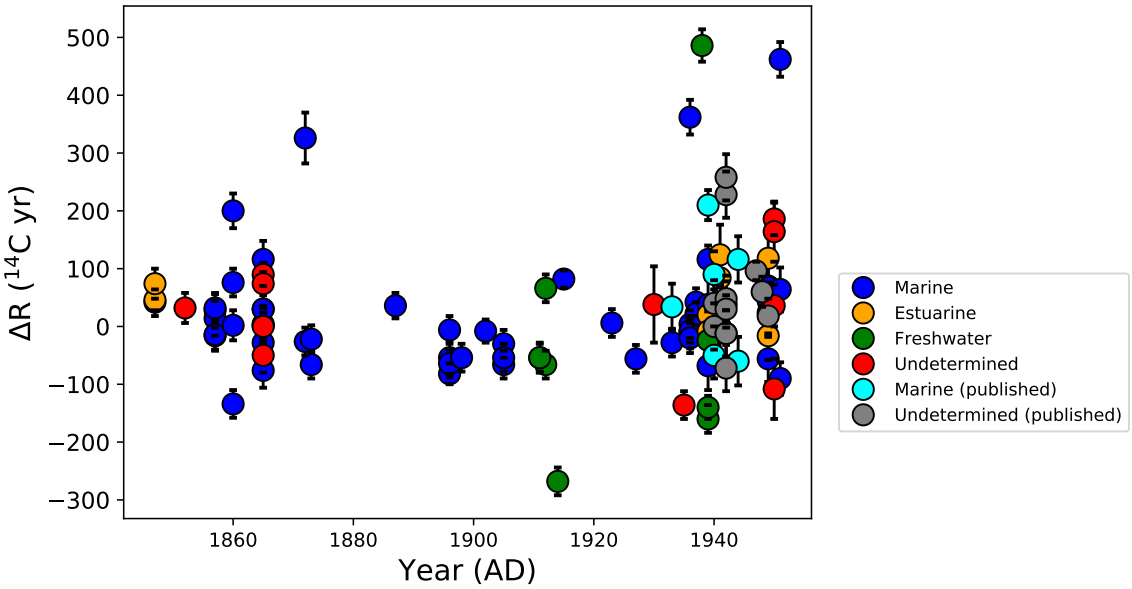


Figure 5.14. Temporal evolution of the pre-bomb ΔR results. There is no significant temporal variation over the Brazilian coast in the considered timescale for the marine samples analysed.

The Brazilian coast encompasses a large latitudinal range and, therefore, it is important to check for a possible latitudinal dependence of the marine ΔR values derived in this research. Figure 5.15 shows that the data presented in this thesis concentrates mostly on the southeastern and northeastern parts of the coast, with a considerable gap in between. The ΔR values are mostly between -100 and 100 ^{14}C yr, with some excursions to significantly higher values in both regions. A very helpful way of showing the geographic variable ΔR values is plotting these data on a map alongside a color scale. Therefore, following Alves et al. (2018), I present a map for ΔR on the coast of Brazil (Figure 5.16) and discuss the values observed. As discussed in subsection 1.4.2, ΔR expresses the deviation of the MRE at local settings from the global ocean. As such, the values are inherently spatially variable and regional factors play an important role in their magnitude. The collection setting of the samples, discussed in the previous paragraphs, are key to

interpret the obtained values for $\triangle$R since the influence of carbon from different sources will affect the offset.

In Figure 5.16 three samples yielding considerably large $\triangle$R values stand out. One of these samples was collected in Cabo de São Tomé, on the coast of Rio de Janeiro state, north of the Cabo Frio upwelling system discussed in section 2.2. It presents a $\triangle$R value of 326 $\pm$ 44 ^{14}C yr, compatible with the intensified MRE (expressed as large and positive $\triangle$R values) typical of upwelling regions (e.g., Ingram and Southon, 1996; Southon et al., 2002; Culleton et al., 2006). This is further corroborated by the positive δ^{18}O value displayed by this same sample (Figure 5.8). Given that shell δ^{18}O works as a proxy for water temperature, Figure 5.8 indicates low temperatures possibly associated with the upwelling of subsurface cold waters. Its positive δ^{13}C value, on the other hand, may be associated with high productivity in the region. Although the MRE in this region may be influenced by the advection of waters upwelled in Cabo Frio, there has been evidence of an eddy-induced upwelling system off Cabo de São Tomé (Calado et al., 2010) and it is not possible to discard the hypothesis of this local upwelling intesifying the regional MRE.

Another sample from the southeastern coast of Brazil displays a distinctively large $\triangle$R value of 362 $\pm$ 30 ^{14}C yr. It was collected from an island on the coast of São Paulo, south of the Cabo Frio upwelling system. There is no δ^{18}O data available for this sample but its positive δ^{13}C value may indicate high productivity, characteristic of upwelling regions. Although it is a gastropod mollusc that could be displaying a vital effect associated with its isotopic content, upwelling in the São Sebastião Island is likely the cause of the elevated MRE (Castelao and Barth, 2006). Other places presenting $\triangle$R values close to 100 ^{14}C yr include regions on the coast of São Paulo and Rio de Janeiro, all within the area of upwelling influence presented by Castelao and Barth (2006). The seasonal nature of the phenomenon

can explain why some samples collected near Cabo Frio do not show the high values predicted.

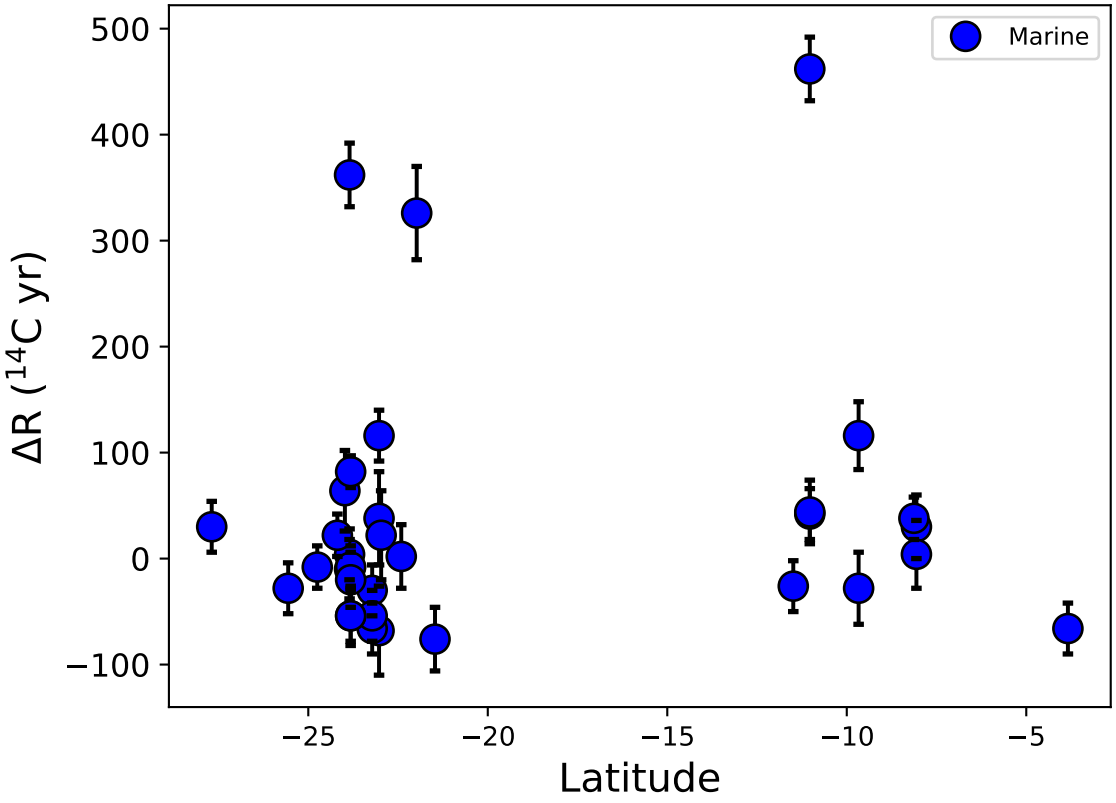


Figure 5.15. ΔR values versus latitude. Most of the samples used in this research are from the southern part of the coast.

The sample showing the highest ΔR value in this research was collected in Aracaju, on the coast of Sergipe, Northeast Brazil. It is a bivalve whose stable isotopic signal does not necessarily indicate upwelling. Moreover, upwelling has not been reported on this part of the coast and can therefore be discarded as the possible cause for the elevated ΔR in this region. Following the discussion in subsection 1.4.3, the ΔR value of 462 ± 30 ^{14}C yr displayed by this organism could result from the presence of limestone in the geology of this locality (see e.g., Dye, 1994; Gómez et al., 2008). The same may be true for the samples collected in the Alagoas state, also presenting high positive ΔR values. In fact, since the

presence of peat and calcareous bedrock in the Sergipe basin has been reported for the region (Walter, 2000, and references therein), these high $\triangle$R values on the northeast coast of Brazil could also be used to identify the collection setting of some of the undetermined samples. Sample 213386, collected on the Beach of Pina, Pernambuco, may indeed be a marine sample affected by hard waters resulting from the local geology. The organisms in this region may be uptaking old dissolved carbonate locally introduced in their habitats by rivers and groundwater (subsection 1.4.3). The variability displayed by the MRE in this region may be a result of variations in the input of these dissolved geological carbonates in the sea.

It is also possible to identify the presence of phenomena affecting the stable isotopes signatures of the organisms without influencing $\triangle$R (i.e., ^{14}C) values accordingly. This is exemplified by several marine samples presenting negative $\triangle$R values and can be noticed from the overall lack of correlation in Figure 5.10 and Figure 5.8. One possible explanation could be an enhanced air-sea $\mathrm{CO_2}$ exchange and the absence of mixing with old waters, but further investigation in the individual locations would be required. In any case, the relative abundance of carbon isotopes means that the same amount of freshwater influence can drastically change the radiocarbon signal without significantly altering δ^{13}C (Figure 5.9).[6] Overall the results for oceanic regions on the coast of Brazil (Figure 5.16) show a relatively uniform MRE with $\triangle$R within -100 and 100 ^{14}C yr and some spots showing excursions from this range. Based on the limited results of this research, it is possible to identify two regions that would require special care when one radiocarbon dates marine material. The first one is the vincinity of Cabo Frio due to the well-known upwelling effect happening in the region and the second one is the northeast coast of the country, where elevated $\triangle$R values may be a result of peat or limestone influence.

[6] Here it is possible to make an analogy with contamination. See section 1.5 and Figure 1.13.

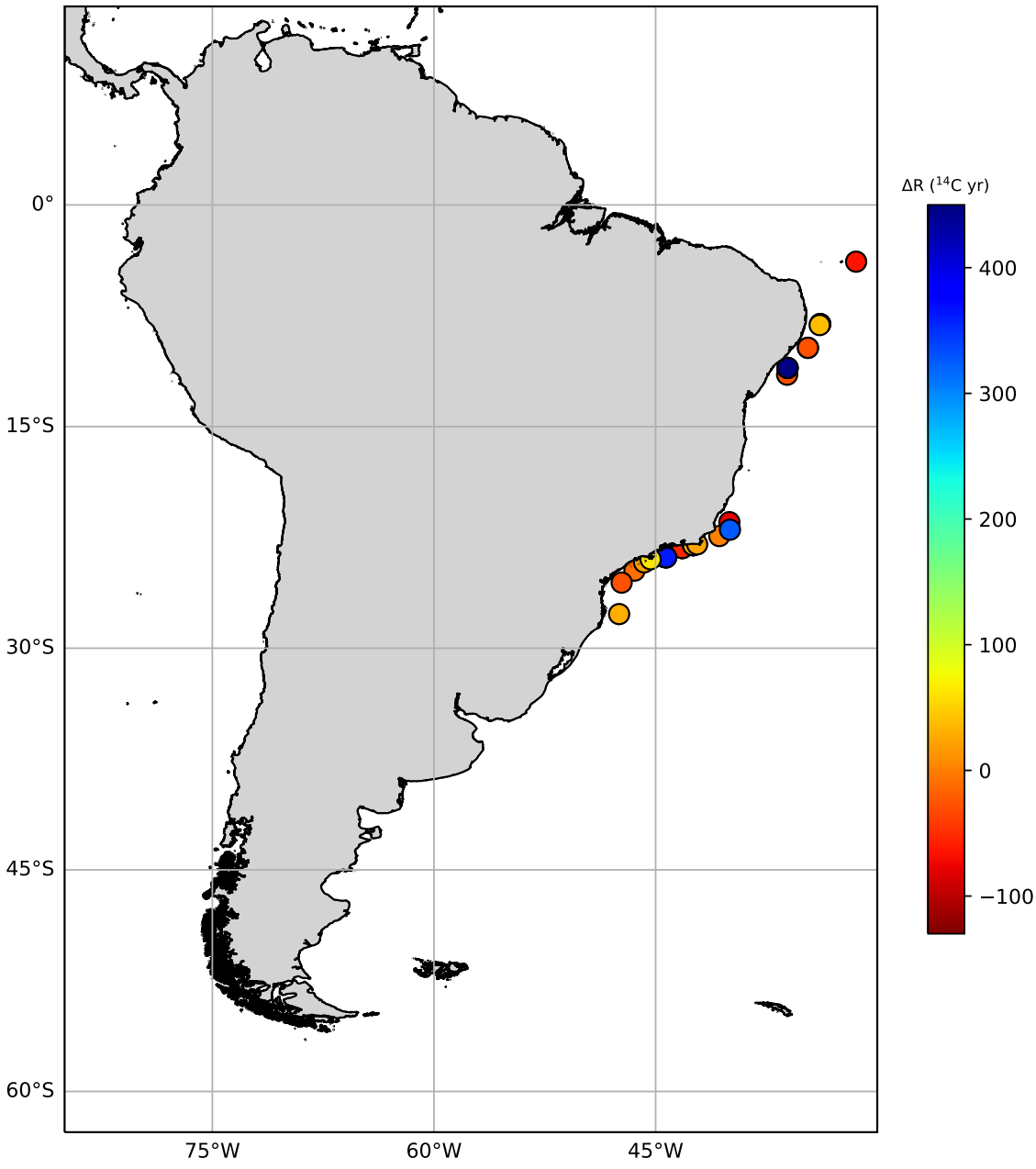


Figure 5.16. Prebomb ΔR values on the Brazilian coast.

Concerning the estuaries, the $\triangle$R values in the Paranaguá Bay tend to be lower than those in the Guanabara and Sepetiba bays. Its stable isotopes signal is also more depleted, reflecting its lower salinity (i.e., higher freshwater input). In estuarine contexts, temporal variations in $\triangle$R tend to be amplified due to fluctuations in factors such as rainfall and ocean circulation (Little, 1993; Ulm, 2002). This high variability is present in the dataset, which shows $\triangle$R in the Guanabara Bay varying from 0 $\pm$ 42 to 124 $\pm$ 52 ^{14}C yr in a single year (samples 145174, 124422 and 145021). These values were derived from three bivalves collected at the Paquetá island, close to the compartment four of the Guanabara Bay (Figure 2.3b). These shells exhibit both δ^{18}O and δ^{13}C depleted values, characteristic of compartment four which is heavily affected by freshwater input (subsection 2.2.1). Nevertheless, their positive $\triangle$R values are more characteristic of marine settings. The same happens in the Paranaguá Bay, where the shell presenting a more depleted δ^{13}C value shows a higher $\triangle$R.

The fact that the stable isotope and the radiocarbon signals in these estuarine shells are affected in different ways needs further investigation. Again, the final radiocarbon signal in the estuary (expressed as $\triangle$R) will be a function of the marine and freshwater ^{14}C contents and the relative contribution (i.e., the mixing ratio) of both water sources (Figure 5.9). The three estuaries investigated in this research (Paranaguá Bay, Sepetiba Bay and Guanabara Bay) seem to be unaffected by hard water effects. High positive $\triangle$R values for the Sepetiba and Guanabara Bay may indicate the invasion of these estuaries by water that upwelled around Cabo Frio, a phenomenon reported by Kjerfve et al. (1997). Most of the estuarine samples in this work comes from the Guanabara Bay (see subsection 2.2.1) and their locations are precisely defined within the estuary. Therefore, I present the distribution of $\triangle$R values in this estuary (Figure 5.17). As expected, lower offsets are found in the

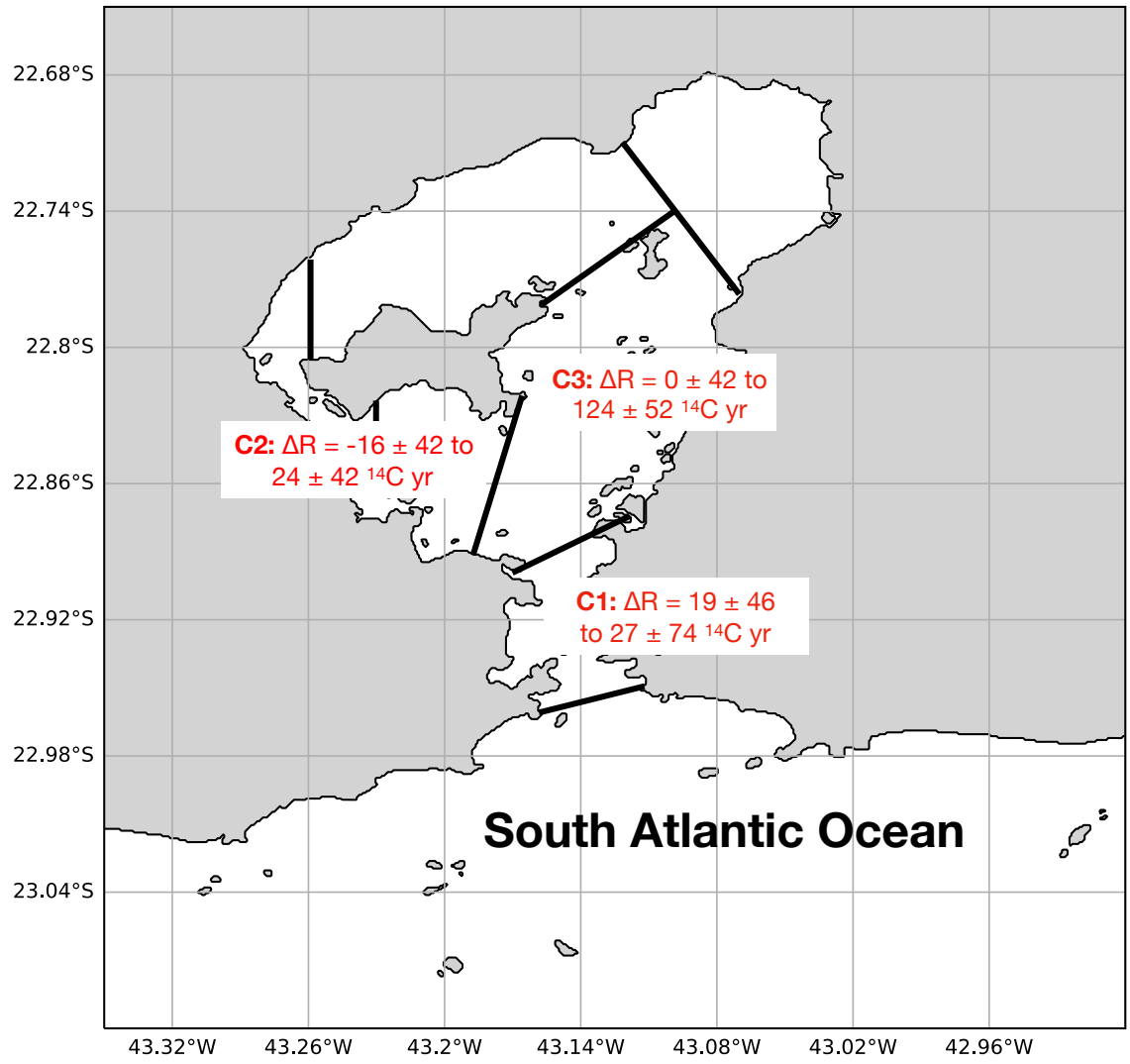


Figure 5.17. Prebomb ΔR values within the Guanabara Bay. Lower offsets indicate higher freshwater influence and subsection 2.2.1 explains the compartment classification system.

inner parts of the bay (C2 and C3), where oceanic influence may be reduced and freshwater input is higher (see subsection 2.2.1).

The freshwater samples present consistent negative ΔR values resulting from the input of newly formed carbon species. Some of these results are extremely low (e.g., -268 ± 24 ^{14}C yr for sample 5688), characteristic of a reservoir in close equilibrium with the atmosphere. Nevertheless, sample 14577, collected from the Miranda River, Mato Grosso do Sul state, inland Brazil, presents the highest ΔR

value of the entire sample set (486 $\pm$ 28 ^{14}C yr). This high value can be explained by the hinterland geology of the Serra da Bodoquena region, which presents some various karst features (Sallun Filho and Karmann, 2007, and references therein). Indeed, this value is in agreement with the high value derived in this work for Aracaju, Northeast Brazil.

Finally, Figure 5.18 aims to compare the measured and the predicted MRE on the Brazilian coast. It shows the marine reservoir ages (R) modelled by Butzin et al. (2017) and the values calculated in this research. For the derivation of the R values, I have simply calculated the difference between the SHCal13 dataset and the sample ^{14}C age in a specific year. The modelled values, on the other hand, are the closest ones available in the model output for the Brazilian coast. Although the model fails to resolve the MRE in regions of upwelling and hard waters, in more open ocean settings such as the Fernando de Noronha island, it shows good agreement with experimental data.

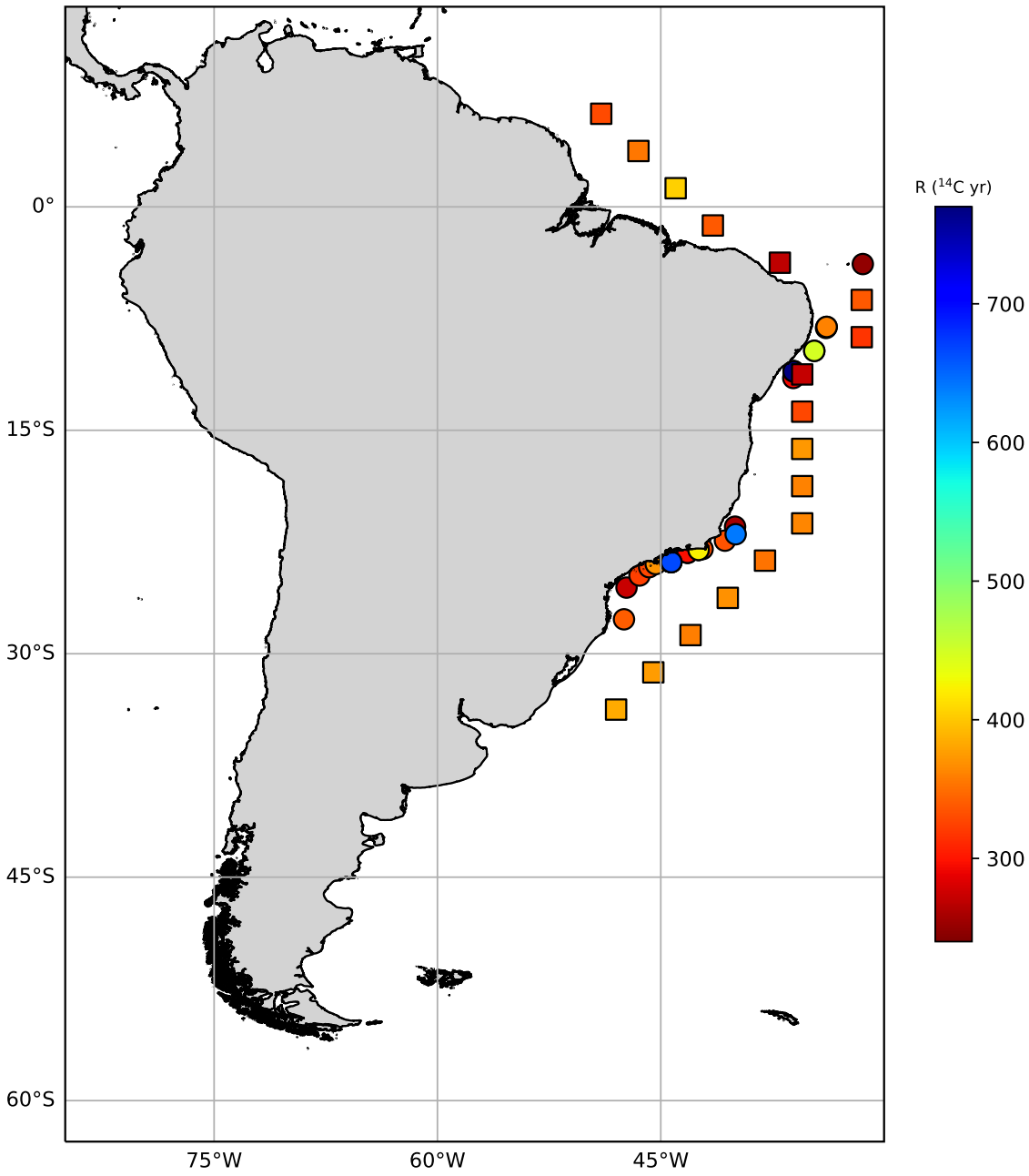


Figure 5.18. Modelled (squares) and experimental (circles) marine reservoir ages on the Brazilian coast. Modelled data is from Butzin et al. (2017).

5.3 Paired Archaeological Samples

By analysing both pre-bomb and archaeological samples, it is possible to investigate the temporal evolution of the MRE. In this work, pairs of archaeological charcoal and shell were used for the quantification of the phenomenon. Since these samples were collected from the Sambaqui da Cabeçuda (subsection 3.2.1), the results obtained by the use of this material shed light on the Late Holocene MRE on the coast of Santa Catarina, Southern Brazil. Moreover, given the influence of the MRE on the chronology of archaeological sites, the data obtained from these samples are useful for the establishment of a reliable chronology for Cabeçuda (chapter 6). Table 5.7 presents the samples analysed in the research, all of which were recovered in 2010 during a very well-documented excavation (Scheel-Ybert, 2011, 2012).

5.3.1 Sample Selection

In this approach, the contemporaneity of the samples is a fundamental requirement for the derivation of $\triangle$R values. Therefore, the charcoal and shell specimens used in this research are pairs of coeval samples, retrieved from the same archaeological context. Ascough et al. (2005a) defined the criteria to be used for sample selection using this approach, such as:

- **Disturbed contexts should be avoided:** The reworking of stratigraphic layers may lead to the mixing of material of different ages, compromising the assumption of coeval samples.
- **Deposits with abundant dateable material should be prioritised:** If a deposit contains a relatively large amount of dateable material, the likelihood of a single sample being affected by, e.g., post-depositional movement, is reduced.

- **Short deposition layers should be prioritised:** The shorter the deposition period of an archaeological layer, the narrower the possible age range of material within that layer. This increases the possibility of the samples being coeval.

- **Sample effects should be considered:** Similarly to the pre-bomb approach, feeding habits must be considered for mollusc shells. In the case of charcoal, the possibility of old-wood effect (subsection 1.5.2) should be taken into account.

- **If possible, the use of same species should be prioritised:** This increases the comparability of ^{14}C ages and, consequently, of the MRE offsets derived from them.

Moreover, Ascough et al. (2005a) argue that factors such as the input of freshwater and/or geological carbonate may represent contamination. Indeed, in these cases, the offsets obtained are not a result of the MRE *per se*. Nevertheless, for the purpose of correcting ^{14}C ages from the local contexts, which is the main reason for quantifying ΔR, these values are extremely important.

The individual pairs of charcoal and shell used for this research were associated with different burials in the archaeological site. In sambaquis, the presence of charcoal can be explained by the use of fire during the funerary ritual, while layers of shell and fish bone were deposited above the inhumations, possibly as the remnants of a funerary feast (Gaspar, 2000). Therefore, wood was burned at the same time molluscs were being eaten, which indicates the contemporaneity of the samples. As Ascough et al. (2005a) point out, the presence of individual dumps of material (e.g., articulated fish and/or small mammal bones) may correspond to activities over a period of days and, together with the absence of root penetration, this is evidence for the stability and lack of reworking within strata.

This is the case for Cabeçuda, where material such as mammal bones, shells, articulated bird skeletons and entire fish skeletons has been found associated with the funerary context (Klokler, 2016a).[7] Archaeological layers in Cabeçuda were indeed found undisturbed during the excavation, which minimises the possibility of post-depositional movements (e.g., bioturbation) and further corroborates the hypothesis of contemporaneity for the material.

5.3.2 Calculation of the $\triangle$R Values

According to Equation 5.2, both the measured and the modelled marine ^{14}C activity (or equivalently, ^{14}C age) are necessary for the calculation of $\triangle$R. Given that in the paired sample approach the organism death year is unknown, one can radiocarbon date a contemporaneous terrestrial sample to obtain the ^{14}C age of the coeval atmosphere. Via the interpolation of Marine13 and IntCal13, a modelled marine ^{14}C age can be derived from the atmospheric ^{14}C age.

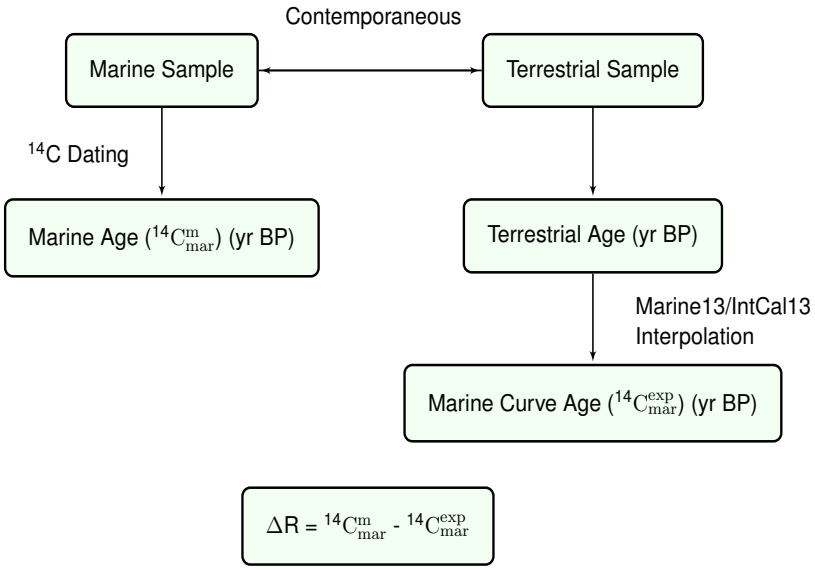


Figure 5.19. Flowchart illustrating the steps to be taken towards the determination of $\triangle$R offsets using the paired sample approach.

[7] Klokler (2014a) states that accumulations of shells usually mark burials in Cabeçuda.

In order to ensure sample contemporaneity and take into account the overall variability in $\triangle$R, Russell et al. (2011) proposes a multipair approach. Following their method, several marine and atmospheric samples are selected for the $\triangle$R calculation and every possible pairing is used. In this thesis, for the calculation of $\triangle$R values I have used the OxCal v4.2.3 calibration software, which has been shown to yield results equivalent to those obtained by the use of the multipair approach (Macario et al., 2015). OxCal employs Bayesian statistics for the calibration and modelling of radiocarbon ages and therefore takes into consideration prior information and assumptions (Bronk Ramsey, 2009). Charcoal ages were calibrated with the SHCal13 curve and shell ages were calibrated with the Marine13 curve. By including the atmospheric and marine ages of each group of samples in the same phase[8] and leaving $\triangle$R undetermined (within the interval from -500 to 500 ^{14}C years), it is possible to evaluate the magnitude of the offset that would result in coeval samples (Bronk Ramsey, 2013). The software outputs a probability distribution for $\triangle$R.

5.3.3 Results and Discussion

Table 5.7 presents the results of the anthracological and isotopic analyses of the archaeological samples collected at Cabeçuda. A large set of charcoal samples was analysed and structures such as barks and twigs were selected to avoid the old-wood effect. In the absence of those, charcoal pieces derived from families that are not usually composed of long lived species were selected. It was possible to identify fragments of Myrtaceae and Sapotaceae. They represent sandbank vegetation (e.g., the restinga ecosystem in Brazil) and comprise species that bear edible fruits during all seasons (Scheel-Ybert, 2001). Sapotaceae presents a pantropical distribution, with approximately 200 species that occur in Brazil. They are lactes-

[8] A phase is a group of events without internal order.

cent bushes or trees, many of which are fructiferous (e.g., Pouteria spp.) and quality wood species (e.g., Manilkara spp.). Myrtaceae presents pantropical and subtropical distribution. The family includes nearly 130 genera and 4,000 species, representing one of the largest families in the Brazilian flora (23 genera and approximately 1,000 species). Species of Myrtaceae include fructiferous trees such as guava (*Psidium guajava*), pitanga (*Eugenia uniflora*) and jaboticaba (*Myrsiaria cauliflora*). More charcoal samples are available for each burial and should be radiocarbon dated in due course.

Molluscs such as *Anomalocardia brasiliana*, *Ostrea sp.*, *Crassostrea sp*, *Lucina pectinata*, *Brachidontes sp*, *Tagelus plebeius*, *Thais haemastoma*, *Olivella sp*, *Olivancillaria sp* and *Megalobulimus sp* are commonly found in Cabeçuda, sometimes as artifacts presenting anthropic marks. The archaeological shells obtained for the present study were subjected to malacological analyses of their structures with the support of specialized literature (e.g., de Souza et al., 2011), and were compared to a reference collection. Shells of the suspension-feeder bivalve *Anomalocardia brasiliana* (Gmelin, 1791) were selected. This organism tolerates large variations in salinity and is geographically widespread (Abbott, 1974; Leonel et al., 1983; Monti et al., 1991; Rios, 1994; Rodrigues et al., 2013), typically inhabiting environments protected from the wave action, such as mangroves, estuaries, muddy beaches, and intertidal zones (Boehs and Magalhães, 2004; de Souza et al., 2011). This means that these shells were most probably collected from the lagoons adjacent to Cabeçuda. Indeed, Colonese et al. (2017) report the present day existence of this mollusc in the sandy sediments of the eastern portion of the Santo Antônio Lagoon.

Figure 5.20 shows the XRD results for sample 180279. The red vertical lines represent the spectral patterns (i.e., the diffraction peaks) for standard samples of pure aragonite. For instance, some peaks can be diagnostic of the presence of

calcite and aragonite minerals such as the characteristic peaks at 29.4° 2θ and 33° 2θ, respectively. By looking at these peaks in the spectrum, it is possible to conclude that calcite is not present. Although the results show the presence of an amorphous phase that may contain organic carbon, this would not be converted to CO_2 during the acid hydrolysis of the sample and thus does not constitute contamination. Indeed, the XRD results point to a crystalline structure that is primarily aragonite, which means that aragonite to calcite recrystallization is not an issue for the archaeological shells used in this study. In any case, the etching procedure performed for the shells has been shown to be a valid method to eliminate any possible secondary calcite (e.g., Macario et al., 2017). The spectra for the remaining samples can be found in the appendices.

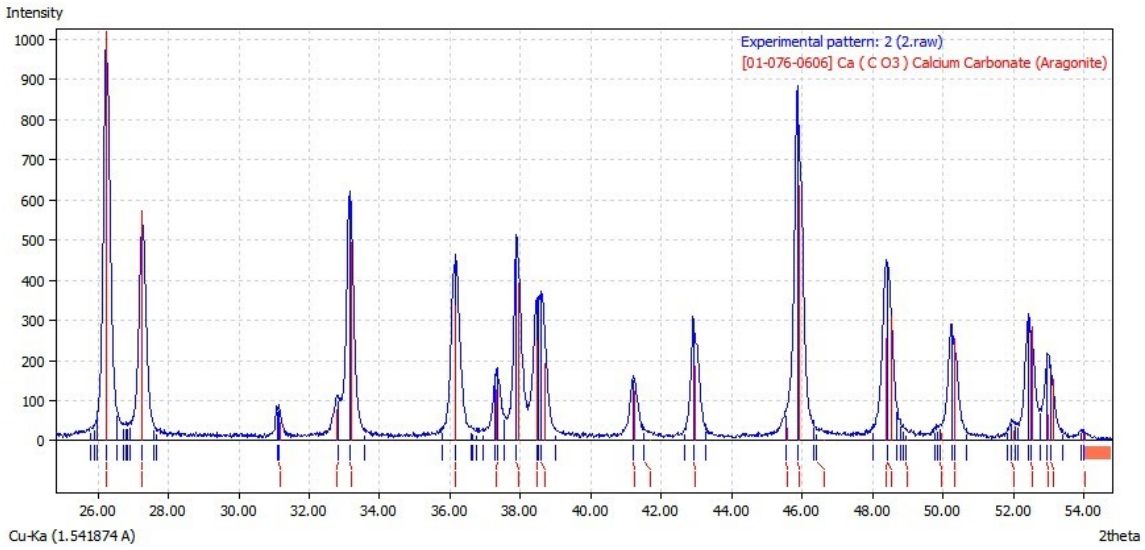


Figure 5.20. XRD diffractogram for sample 180304 showing the absence of aragonite to calcite recrystallization.

The δ^{13}C and δ^{18}O values for the Cabeçuda shells are in the range 0.96 - 1.81‰ and -1.35 - -0.31‰, respectively. These values are broadly consistent with the modelled present day values for the South Atlantic ocean and the variables show no correlation in the set of samples analysed in the present study (Figure 5.21a). The negative δ^{18}O signal points to the influence of freshwater carried by the re-

Table 5.7: Anthracological and isotopic results, including ^{14}C-AMS, for archaeological samples from the shellmound Sambaqui da Cabeçuda. The uncertainties for the δ^{13}C and δ^{18}O values are 0.10 and 0.20‰, respectively.

Site	LAC-UFF Code	Material	Species/Family	Burial	^{14}C Age ± 1σ (^{14}C yr BP)	$\delta^{13}C_{VPDB}$ (‰)	$\delta^{18}O_{VPDB}$ (‰)
Cabeçuda	180303*	Shell	*Anomalocardia brasiliana*	1	3725 ± 30	1.44	-0.78
Cabeçuda	180304*	Shell	*Anomalocardia brasiliana*	1	3750 ± 35	1.07	-1.10
Cabeçuda	180305*	Shell	*Anomalocardia brasiliana*	1	3705 ± 35	1.76	-0.77
Cabeçuda	180306*	Shell	*Anomalocardia brasiliana*	3	3740 ± 35	1.07	-1.34
Cabeçuda	180307*	Shell	*Anomalocardia brasiliana*	3	3735 ± 30	1.26	-1.35
Cabeçuda	180308*	Shell	*Anomalocardia brasiliana*	3	3735 ± 30	1.79	-0.83
Cabeçuda	180309*	Shell	*Anomalocardia brasiliana*	5	3795 ± 35	1.37	-0.99
Cabeçuda	180310*	Shell	*Anomalocardia brasiliana*	5	3835 ± 30	1.46	-1.08
Cabeçuda	180268*	Shell	*Anomalocardia brasiliana*	5	3675 ± 25	1.04	-0.85
Cabeçuda	180311*	Shell	*Anomalocardia brasiliana*	6	4035 ± 40	1.62	-0.31
Cabeçuda	180312*	Shell	*Anomalocardia brasiliana*	6	3805 ± 35	1.25	-1.12
Cabeçuda	180286	Shell	*Anomalocardia brasiliana*	6	3847 ± 41	0.96	-1.05
Cabeçuda	180272*	Shell	*Anomalocardia brasiliana*	7	3995 ± 35	1.79	-1.11
Cabeçuda	180313*	Shell	*Anomalocardia brasiliana*	7	3935 ± 35	1.50	-0.70
Cabeçuda	180314*	Shell	*Anomalocardia brasiliana*	7	3985 ± 30	1.54	-1.34
Cabeçuda	180315	Shell	*Anomalocardia brasiliana*	13	4085 ± 35	1.76	-0.76
Cabeçuda	180316	Shell	*Anomalocardia brasiliana*	13	3925 ± 35	1.41	-1.02
Cabeçuda	180317	Shell	*Anomalocardia brasiliana*	13	4060 ± 30	1.81	-0.96
Cabeçuda	180200	Charcoal	Sapotaceae	1	3868 ± 50	—	—
Cabeçuda	180201	Charcoal	Bark (undetermined)	3	3859 ± 50	—	—
Cabeçuda	180202	Charcoal	Myrtaceae	5	4229 ± 54	—	—
Cabeçuda	180203	Charcoal	Nut	6	3647 ± 52	—	—
Cabeçuda	180253*	Charcoal	Twig (undetermined)	7	3760 ± 35	—	—
Cabeçuda	180204	Charcoal	Bark (undetermined)	13	3865 ± 50	—	—

*These samples were measured at the ANU ^{14}C Laboratory.

gional rivers. In this context, the positive δ^{13}C values could be a result of enhanced primary production in the productive environment of the coastal lagoons. By looking at Figure 5.21b, it is possible to see that the δ^{18}O values remain broadly constant. The δ^{13}C values, on the other hand, seem to decrease with time (Figure 5.21c). This may be due to a lower marine influence in this period, possibly related to sea-level variations. Nevertheless, given that seasonality can alter these signals and cause significant intrashell variability, it is not possible to interpret these temporal changes without knowing the seasons associated with these values. Moreover, it is important to notice that in Figure 5.21 the radiocarbon ages are not calibrated.

Following variations of the method outlined in subsection 5.3.2, highly negative $\triangle$R values were obtained for Cabeçuda. First, considering that the burials can be from different time periods but the samples associated with a single burial are coeval, I assume an independent $\triangle$R value for each burial (phase) (see Macario

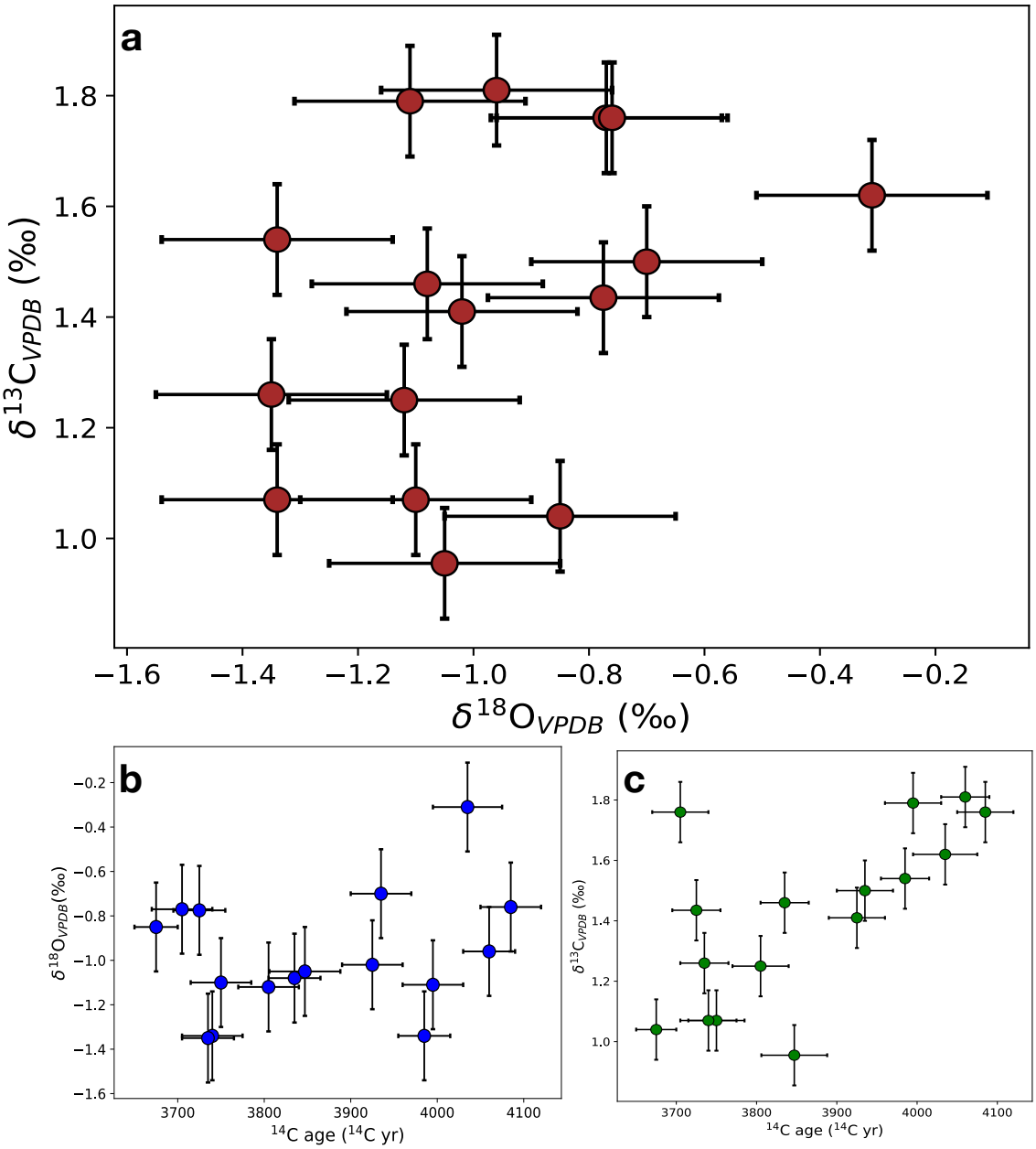


Figure 5.21. a: Stable isotopes (δ^{18}O and δ^{13}C) results for the archaeological shells. b: δ^{18}O and c: δ^{13}C results versus time for the archaeological shells.

et al., 2015). This yields ΔR values that range from -392 $\pm$ 100 ^{14}C yr to -21 $\pm$ 215 ^{14}C yr (Figure 5.22). This method would be ideal for assessing ΔR temporal variations. Nevertheless, a drawback of this approach is that any outlier can lead to inaccurate results for the ΔR. Moreover, more charcoal samples need to be measured in order to improve the statistics of this model. Another possible approach

is to follow the same premisses of the first model but assuming a $\triangle$R value that is roughly time-independent during the occupational period of the site, similar to the method employed by Macario et al. (2016). This approach yielded a $\triangle$R of -330 $\pm$ 110 ^{14}C yr (Figure 5.23a). By having a closer look at this model (Figure 5.24a), it is possible to note that burial 5 is problematic, with the charcoal (sample 180202) being older than the shells. A possible reason for this inconsistency is the remobilization of the charcoal fragment, meaning that it would not be associated with the burial. This means that more charcoal samples derived from this burial need to be measured for this research. Burial 7 presents the same issue (sample 180253). A third approach would be to consider all samples as part of the same occupation (a single phase for all samples), which enhances the statistics of the model (Macario et al., 2015). By employing this model, a $\triangle$R value of -334 $\pm$ 78 ^{14}C yr was derived for the set of samples (Figure 5.23b). This approach assumes that all samples are coeval but an outlier model shows that sample 180202 is remarkably older and sample 180203 is slightly younger (Figure 5.24b).

If the charcoal dates were reliable, the highly negative $\triangle$R results obtained in the present study would indicate that aquatic samples from the Laguna Lagoonal System could be accurately calibrated by the use of the SHCal13 atmospheric curve and the R offset (instead of Marine13 and $\triangle$R). I have employed a single phase model for the derivation of a R value, similar to the one used by Milheira et al. (2017) for the study of the earthen mounds in Southern Brazil, for the whole set of samples and obtained the value of R = -74 $\pm$ 76 ^{14}C yr (Figure 5.25). A negative value for R means an enhanced ^{14}C activity in the water in comparison to the overlying atmosphere, which does not make sense in this context. Even though the uncertainty of R encompasses R = 0, more samples need to be measured for the achievement of better statistics. A drawback of this approach is that marine

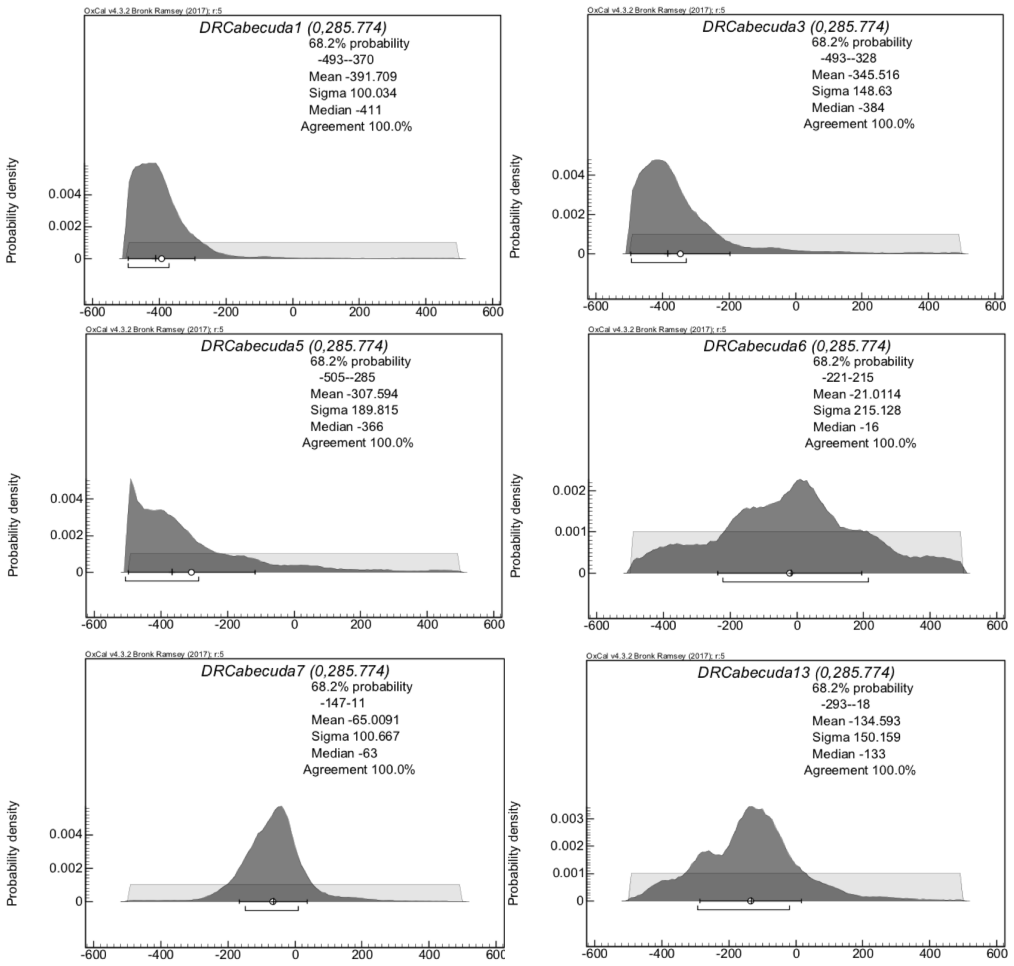


Figure 5.22. Individual ΔR values obtained for each Cabeçuda burial studied.

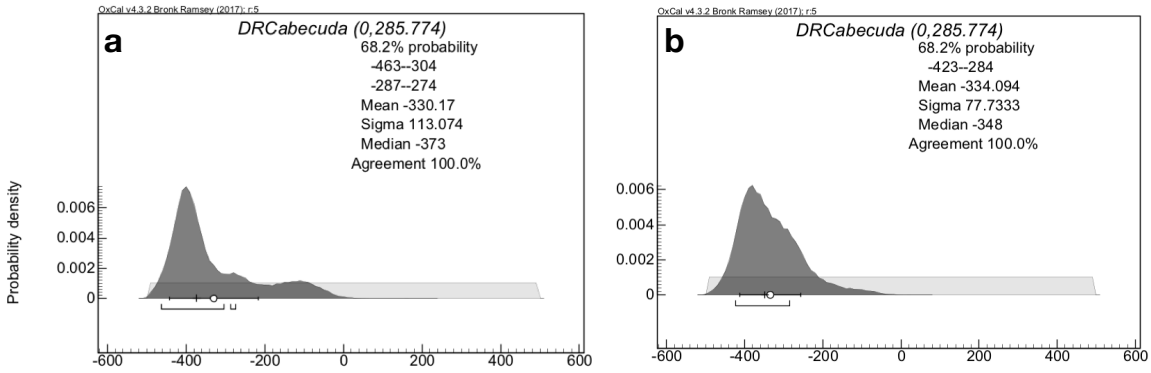


Figure 5.23. A common ΔR value obtained for all the Cabeçuda burials studied using a model with a: different phases and b: a single phase for the Cabeçuda burials.

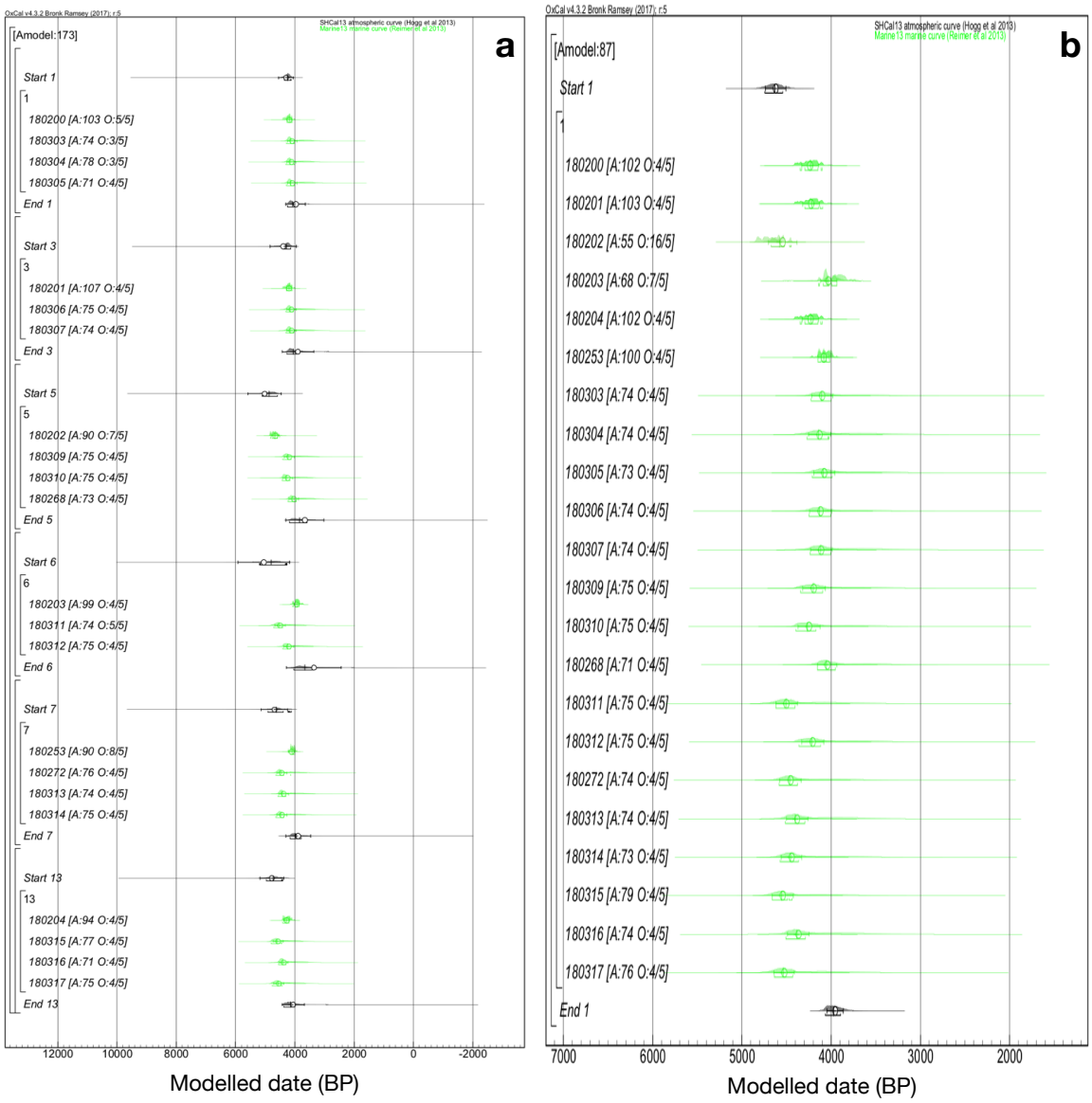


Figure 5.24. Modelled radiocarbon dates for the Cabeçuda shellmound considering a common ΔR for the burials using a: different phases and b: a single phase for the burials. Probability distributions for shell and charcoal samples. Boundaries for each phase are also shown. Lines indicate the 1σ range, and dots mark the mean values of each distribution.

^{14}C ages calibrated with atmospheric curves yield calibrated age distributions that present the oscillations characteristic of the atmospheric reservoir.

The ΔR values derived above are extremely negative and some probability distributions in Figure 5.22 are truncated even within the -500 to 500 ^{14}C yr range used in the model. It is important to acknowledge the possibility of samples as-

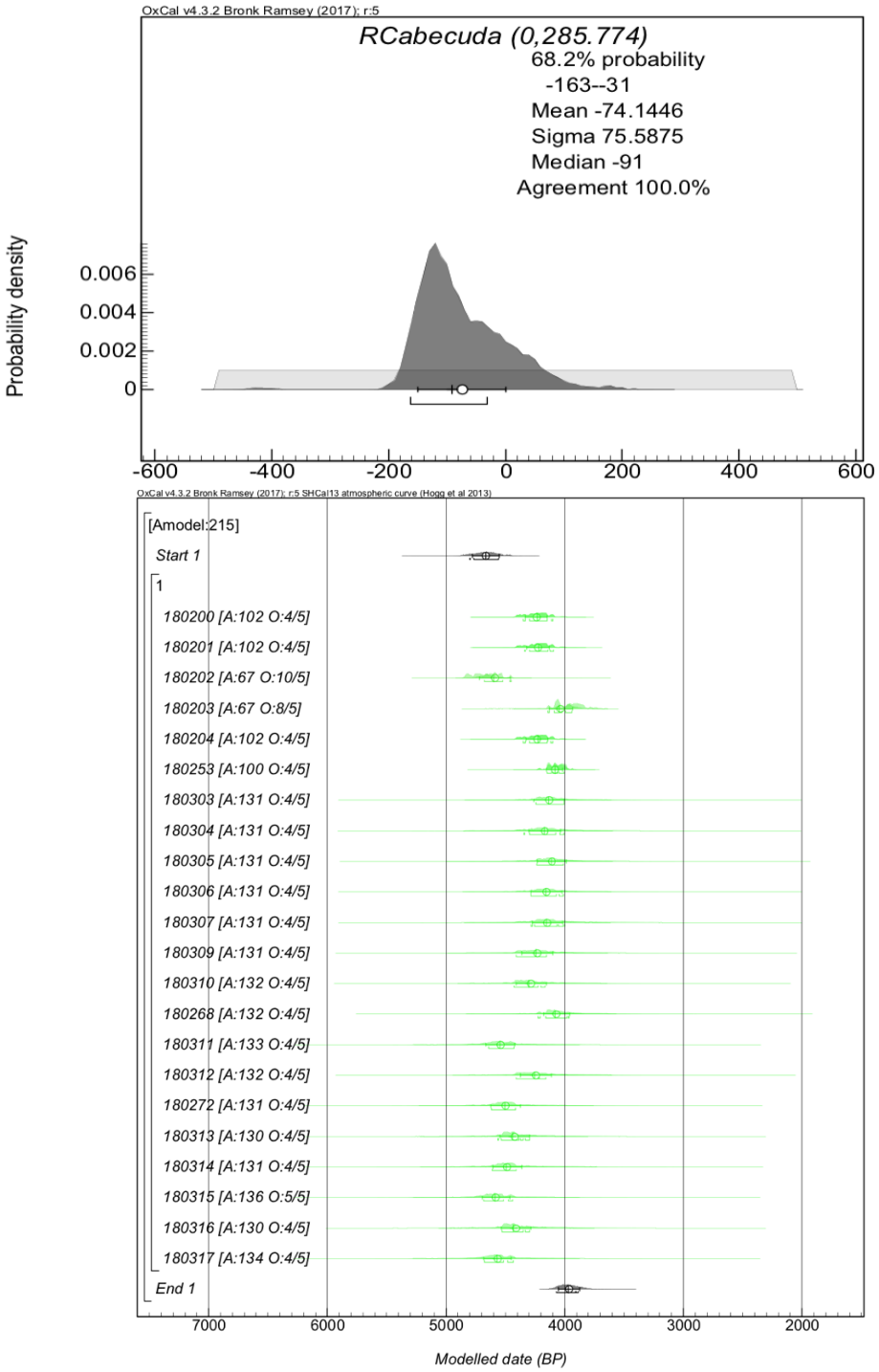


Figure 5.25. Single R value obtained considering a single phase for the Cabeçuda burials (top). Modelled radiocarbon dates for the Cabeçuda shellmound considering a common R value and a single phase for the burials. Probability distributions for shell and charcoal samples. Boundaries for each phase are also shown. Lines indicate the 1-σ range, and dots mark the mean values of each distribution (bottom).

sociated with burials 1 and 5 being unsuitable for MRE determinations (i.e., not coeval). Taking this into consideration and excluding these burials from the second model presented here, a ΔR of -102 $\pm$ 74 ^{14}C yr is obtained (Figure 5.26). I consider this to be the most reliable of all the approaches so far presented. Despite the low chances, charcoal samples derived from burials 1 and 5 are the only ones that could possibly be affected by the old-wood effect. Therefore, given that the shells do not present recrystallization, by excluding burials 1 and 5 from the ΔR determination I have also eliminated the chances of an old-wood effect affecting the result. I argue that the ΔR value of -102 $\pm$ 74 ^{14}C yr is therefore the one to be used for Cabeçuda until more samples are measured for the improvement of the statistics.

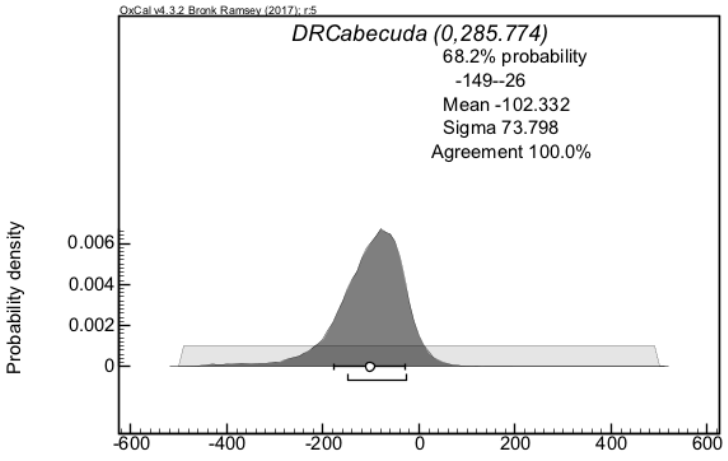


Figure 5.26. Single ΔR value obtained considering a single phase for the Cabeçuda burials. Burials 1 and 5 were excluded from this analysis.

These results are in disagreement with the present day ΔR value derived in the present study for a nearby region (Capão da Canoa; ΔR = 38 $\pm$ 66 ^{14}C yr) and are much higher in magnitude than some negative values derived for the Santa Catarina coast in previous studies (Table 5.1). Nevertheless, the ΔR value of -62 $\pm$ 73 ^{14}C yr obtained for the nearby Sambaqui de Jabuticabeira, also located near the margins of a lagoon, corroborates the result of this thesis. To understand this

discrepancy, it is important to consider the environmental setting of the Laguna Lagoonal System, where Cabeçuda is situated (see subsection 2.2.2). Although the higher sea-level during the late Holocene submerged this estuary, the coastal lagoon was already present at about 6 ka cal BP. The narrow channel connecting this system with the open ocean, already present during the occupation of Cabeçuda, is a significant obstacle for the intrusion of oceanic water in the estuary. This potentializes the effect of terrestrial carbon input by major rivers in this reservoir. Moreover, the shallow depths of the lagoons suggest that these are well-mixed reservoirs in isotopic equilibrium with atmospheric CO_2. Nevertheless, the low MRE quantified for the Laguna Lagoonal System in the present study disagrees with the findings of Colonese et al. (2017), who analysed stable isotopes of carbon and oxygen in archaeological samples from Cabeçuda. The authors report a strong marine influence in the system at 3 ka cal BP when compared to the present day conditions. The reason for this disagreement may be related to the temporal variation of the MRE or to the discrepancy between the stable isotopes and radiocarbon signals that happens, for instance, in the case of some known-age samples of the present study (Figure 5.9). The analyses of samples from different archaeological layers at Cabeçuda would allow for the assessment of the MRE temporal variation but, unfortunately, this was not possible due to the poor preservation of the site. Figure 5.27 shows the temporal variation of ΔR obtained from the MRE model presented by Butzin et al. (2017) for an open ocean region near Laguna (latitude = $28.75°$S and longitude = $45°$W) (see chapter 7). This is a purely marine signal and, considering that the model gives ΔR values that are positive but low in magnitude around 4 ka cal BP, the highly negative ΔR obtained in the present study for a region much closer to the coast is a conceivable result (see Figure 5.9).

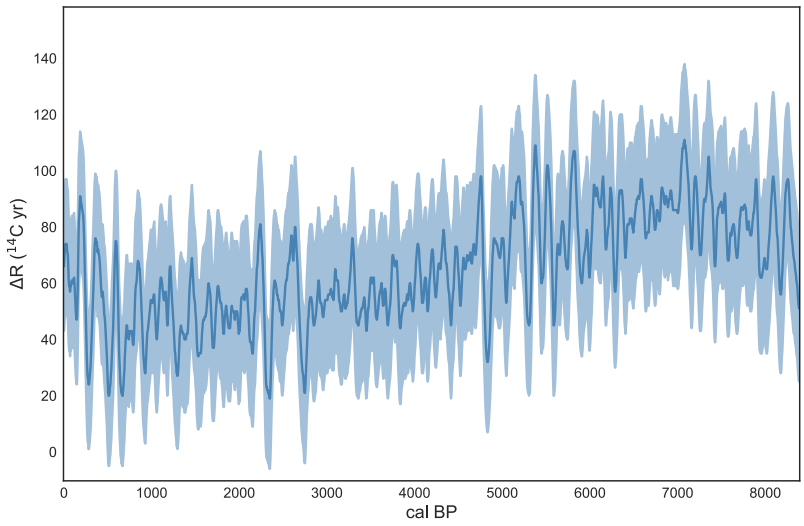


Figure 5.27. Modelled $\triangle$R time series for latitude = $28.75°$S and longitude = $45°$W. Data from Butzin et al. (2017).

5.4 Conclusions

Approximately 100 mollusc shells have been analysed in this research, which allowed for the mapping of the MRE along the Brazilian coastline. These organisms were mostly sampled in coastal waters, which are composed of a mixture of shelf waters (such as the BC and MC discussed in section 2.2) and freshwater outflow from the continent, masking the pattern of lower $\triangle$R values otherwise expected on the Southern coast of the country (Broecker et al., 1960). Through the approach of combining radiocarbon and stable isotopes of carbon and oxygen analyses, it was possible to more precisely identify the environmental settings where the shells were collected. Indeed, stable isotopes analyses have proven useful to the study of the environmental settings, but inconsistencies with the radiocarbon signal do occur. Therefore, based on the data presented here, I argue that the radiocarbon signal itself can be used as a "fine adjustment" for this information. The $\triangle$R values tend to be relatively low along the coast and we do not see the pattern of lower values in estuaries when compared to coastal samples (observed for instance by Ingram and Southon (1996) on the coast of California). Moreover, my results shed

light on very local phenomena occurring at specific locations along the shoreline. The data points to a rather large area of upwelling influence on the southeastern coast of Brazil, which is in contrast with archaeological MRE data for the region (Macario et al., 2018). More research is needed in order to evaluate whether this is caused by geographic or temporal MRE variation. Besides upwelling in Southeastern Brazil, possible limestone influence on the Northeast part of the coast contributes to the overall disagreement between MRE and stable isotopes experimental and modelled data for the western South Atlantic Ocean. There is scope for further investigation of both phenomena and any possible seasonal variations. Seasonal studies would also allow for the quantification of variations in the relative contribution of shelf waters and freshwater discharge along the coast.

The MRE associated with the shellmound Sambaqui da Cabeçuda was investigated through the analyses of archaeological samples of shell and charcoal. I have employed variations of a Bayesian model for the calculation of the $\triangle$R offset and obtained highly negative values. Considering that the assumption of temporally coeval samples must be satisfied, the elimination of any effects affecting this premise is paramount. Therefore, besides evidence from the archaeological context, I have used anthracology and XRD analyses to ensure contemporaneity. I have derived a $\triangle$R value of -102 $\pm$ 74 ^{14}C yr by excluding samples associated with burials 1 and 5 and consider this to be the most accurate estimate for the MRE at Cabeçuda. This negative $\triangle$R can be explained by the environmental conditions of the lagoonal system where the site is located (i.e., a shallow reservoir connected to the ocean by a narrow channel and receiving the discharge of local rivers). Nevertheless, the result disagrees with the findings of Colonese et al. (2017) who report a strong marine influence at the Laguna sytem at 3 ka cal BP. This could be due to the temporal variation of the MRE but, in any case, the measurement of more charcoal samples in the future will improve the accuracy of the model. Since the Brazilian

sambaquis are often found near coastal lagoons due to the productivity of these environments, negative $\triangle$R values are not uncommon (Macario et al., 2018) and the same approach may suit other settlements.

Chapter 6

Implications for the Chronology of Cabeçuda

Introduction

This chapter discusses the implications of the MRE quantification for the chronology of Cabeçuda, based on a suite of new δ^{13}C, δ^{15}N and ^{14}C-AMS results for five skeletons derived from different burials at the site. Previous radiocarbon measurements are extremely limited for Cabeçuda and lack a robust contextualization. In this chapter I briefly outline these results and move on to describe the burials I have analysed in this research. Next, I present the outcome of the analyses performed on this material and discuss them together with the results obtained from the charcoal/shell pairs associated with the burials (section 5.3). I discuss the diet of the prehistoric people buried in Cabeçuda and the implications of a highly negative $\triangle$R value for the calibration of samples at this site. Overall, this chapter presents my contribution to a better understanding of the chronology of the Brazilian shell mounds and the subsistence of their builders.

6.1 Previous Studies

There are a few radiocarbon dates available for Sambaqui da Cabeçuda (Table 6.1). Nevertheless, the contexts of many of these samples are not appropriately documented and, in some cases, there is conflicting information about the samples themselves (e.g., Scheel-Ybert, 2012; Klokler, 2014b). This adds uncertainty to the accuracy of the information presented in Table 6.1. Therefore, I opted not to use the available data for my analyses in the present study.

Table 6.1: Previous radiocarbon measurements for the Cabeçuda shellmound. Source: Scheel-Ybert (2012).

^{14}C age ± 1σ (^{14}C yr BP)	Material	Museum code	Lab. code
1800 ± 40	human bone	MN/UFRJ, 1749	Beta 297833
1990 ± 30	human bone	MN/UFRJ, 1750	Beta 297832
2030 ± 30	human bone	MN/UFRJ, 1682	Beta 297831
2290 ± 30	human bone	MN/UFRJ, 1798	Beta 297834
3640 ± 50	*Anomalocardia brasiliana* shell	2010 excavation (25-30 cm)	Beta 280005
4020 ± 50	*Anomalocardia brasiliana* shell	Locus 3, South Profile, surface	Beta 280007
3870 ± 40	human bone	Locus 1, profile 1, Burial 6	Beta 280009
4180 ± 60	*Anomalocardia brasiliana* shell	Locus 1, NW profile, Base - (22J 0712537 / 6852169)	Beta 280006
4180 ± 60	*Anomalocardia brasiliana* shell	Locus 3, South profile, Base - (22J 0712575 / 6852152)	Beta 280008
4120 ± 220	charcoal	Sample collected in the first excavation	Hannover167

Based on these results, the occupation of the site was situated between approximately 5,000 and 1,600 BP. In Table 6.1, it is possible to observe different time periods for the occupation. A group of four samples, including two shells from the base of the site and a human bone, give the oldest radiocarbon ages ($\sim$ 4,000 BP). Two samples of shell collected at different parts of the site present intermediate results ($\sim$ 3,600 - 4,000 BP). Finally, four samples recovered during the early excavations of the site present the most recent radiocarbon ages ($\sim$ 1,800 - 2,300 BP). This indicates that the archaeological layers excavated in the past are situated above the areas more recently studied and correspond to a more recent period. The set of dates presented in Table 6.1 led the archaeologists to estimate a very long occupational period for Cabeçuda, with conservative calculations of a minimum of 2,000 years without evidence of abandonment.

6.2 The Cabeçuda Burials

The bone samples analysed in the present study correspond to six burials excavated at Sambaqui da Cabeçuda in 2010. Previous excavations have recovered more than 200 inhumations from this site, all of them found in hyperflexed position, which is common for other sambaquis in the region. Nevertheless, the funerary pattern disclosed in the most recent excavation is different (Figure 6.1a and Figure 6.1b). All the skeletons recovered were found extended, with hands resting on the pelvis and legs possibly tied. Below I give a summary of these inhumations (see Figure 6.1):

- **Burial 1:** This is a primary burial of an adult of undetermined sex. The presence of a dark sediment containing charcoal, suggesting a large combustion structure (hearth), is reported below and around the individual. The hearth was situated on an area containing a large amount of fish bone. Around the skeleton, the presence of dyestuff, lithic material, gastropods, fish otoliths, and closed bivalve shells was documented. Moreover, perforated shells were found around the neck, suggesting a collar.

- **Burial 3:** This is a primary burial of an adult of undetermined sex. The individual was deposited on a combustion area characterized by dark sediment and a large quantity of charcoal. Similar to the burial 1 context, this hearth was above an area containing a high concentration of fish bone. There were many lithic artifacts near this individual as well as two other skeletons.

- **Burial 5:** This burial was found near burial 1. It is a primary burial of a male adult. Underneath the individual there was a combustion area with dark sediment and many pieces of charcoal.

- **Burial 6:** This inhumation was found involved in sandy sediment, with a few shells and many charcoal fragments. Remnants of a hearth were found near the feet and a large fragment of charcoal was found next to the femur.

- **Burial 7:** Primary burial of a child of undetermined sex. This inhumation was accompanied by ritual paraphernalia, including one or two collars (numerous perforated gastropod shells of different species). The whole burial presented a reddish color and next to the feet there was a high concentration of ochre and the vestiges of a hearth. There was a high concentration of charcoal next to the right arm.

- **Burial 13:** Primary burial of a young individual of undetermined sex (possibly female). Closed bivalve shells were found next to the waistline.

It is important to emphasize that the assumption of contemporaneity would be extremely questionable in the case of secondary burials and, therefore, these are not indicated for MRE studies. As previously mentioned, the presence of charcoal associated with the burials of Cabeçuda can be explained by the importance of fire in the funerary ritual of sambaqui societies. Gaspar (2000) states that the burning of wood gives visibility to the funerary ritual and, given the proximity between some sites, the smoke could be seen from other sambaquis. Layers of fish bone and shells associated with the burials, in turn, seem to be the remnants of a funeral feast.

6.3 Analyses

Six bone fragments were analysed in the present study. Besides the radiocarbon analyses, the stable isotopes of carbon and nitrogen were measured for a dietary study of the Cabeçuda builders following the procedures described in Figure 6.3.

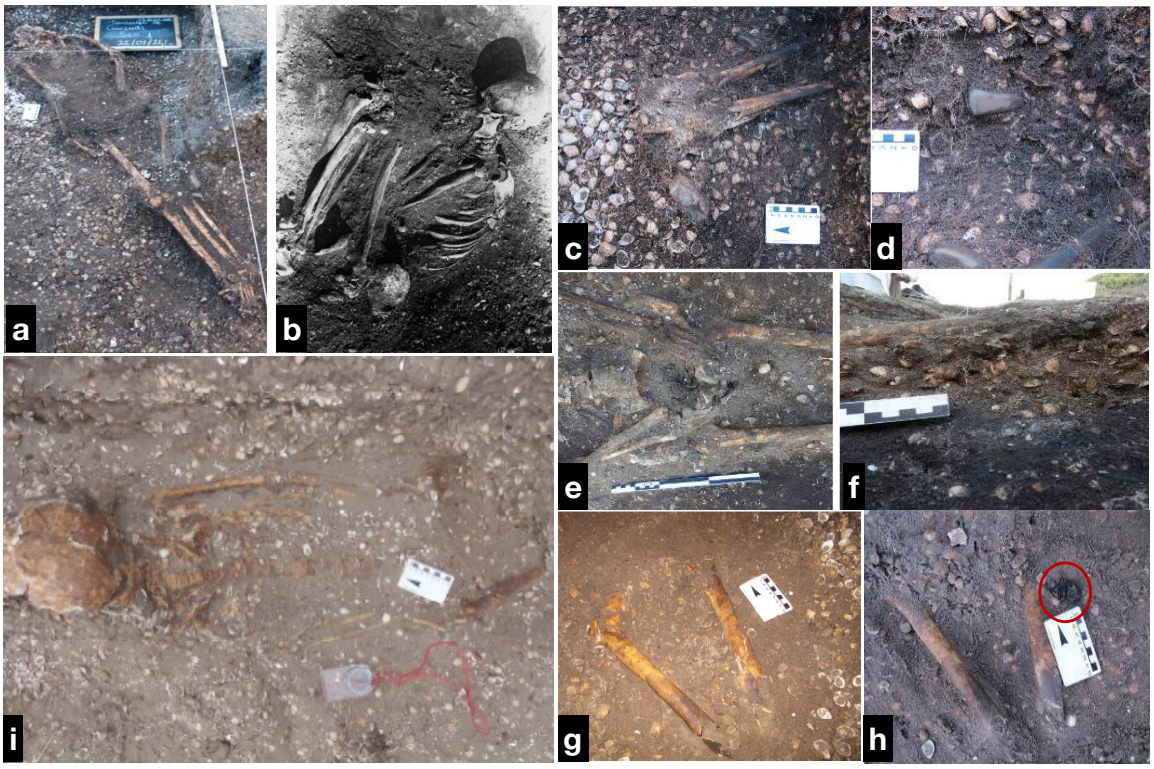


Figure 6.1. a: Burial 1. b: Burial found in the early excavations of the site. Compare the body positions. c: Burial 3. d: Lithic material found next to burial 3. e: Burial 5 showing the individual with hands resting on the pelvis. f: The stratigraphy of burial 5 showing a hearth and shell layer under the body. g: Burial 6. h: Large fragment of charcoal found next to burial 6. i: Burial 13. (Photos: Scheel-Ybert, R.).

Results are presented in Table 5.7. These samples were pre-treated following the protocol described in subsection 4.1.1. However, the bone derived from burial 3 underwent a slightly different pretreatment, without the ultrafiltration step. This was done after the normal procedure failed to yield enough collagen. Unfortunately, the sample derived from burial 7 did not yield enough collagen for measurement and the available material was exhausted. As mentioned in chapter 2, this poor preservation of archaeological bone is a common problem in Brazil. The country is situated in a tropical and humid zone where the acidic conditions of the soil contribute to the degradation of archaeological material. Organic matter (i.e., seeds, charcoal, wood), in turn, tend to be degraded by the enhanced biochemical activity in the soils as a consequence of the alternation of dry and wet seasons. Never-

theless, in this context, sambaquis tend to be less affected due to the protection offered by their carbonate matrix (Prous, 1991). The bone fragments analysed in this research present collagen C/N atomic weight ratios within the acceptable range of 2.9 - 3.5, which indicates the absence of exogenous carbon contamination (van Klinken, 1999). Radiocarbon ages fall within the range 3,500 - 4,000 BP, in agreement with previous results for other samples derived from the same excavation. Stable isotopes results indicate a diet heavily based on marine resources with mean values of δ^{13}C = -10.56 $\pm$ 1.41 ‰ and δ^{15}N = 18.42 $\pm$ 0.49 ‰ for the five individuals (cf. Figure 1.16). Below I give a brief discussion of the diet of sambaqui builders. When not indicated otherwise, information in the next section has been extracted from Prous (1991).

Table 6.2: Results for the bone samples analysed in the present study.

Site	Material	Identification	Sample	Burial	OxA Code	^{14}C age ± 1σ (^{14}C yr)	$\delta^{13}C_{VPDB}$ (‰)	$\delta^{15}N_{AIR}$ (‰)	C:N
Cabeçuda	Bone	Human (Pelvis)	43,230	1	35,552	3762 ± 28	-10.5	18.7	3.2
Cabeçuda	Bone	Human (Femur)	43,231	3	X-2722-37	3761 ± 31	-9.5	18.5	3.3
Cabeçuda	Bone	Human (Torax)	43,232	5	35,553	3768 ± 29	-9.8	17.7	3.2
Cabeçuda	Bone	Human	43,233	6	35,554	3930 ± 31	-10.5	19.2	3.2
Cabeçuda	Bone	Human	43,234	7	—	—	—	—	—
Cabeçuda	Bone	Human (Torax)	43,235	13	36,750	3539 ± 27	-12.5	18	3.5

6.4 The Diet of Sambaqui Populations

In sambaquis, remains such as fish otoliths, mollusc shells, and animal bones may constitute evidence of past subsistence and diet. Tools for the grinding of vegetables are commonly found in the archaeological contexts, but plant remains are rarely recovered due to the poor preservation conditions as discussed in the previous paragraphs (Lima, 2000; Scheel-Ybert, 2001; Scheel-Ybert et al., 2003). This leads to an underestimation of the relative contribution of plants to the subsistence strategy and diet of these coastal populations. In some sites, bones of terrestrial fauna are equally scarce or even absent, corroborating the hypothesis that they

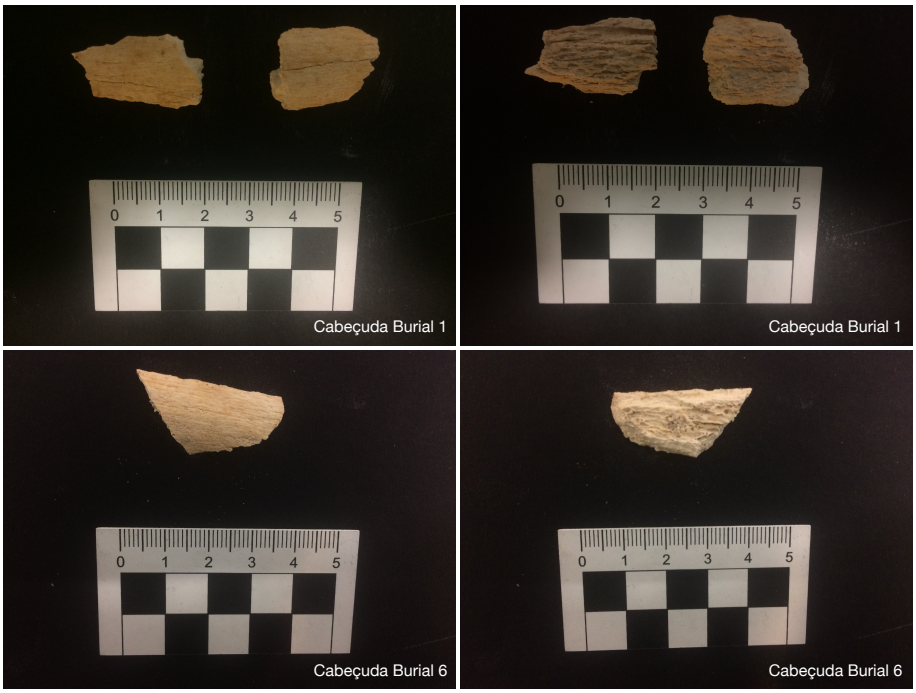


Figure 6.2. Some of the bone fragments analysed in this research.

probably played a secondary role in the diet of the sambaqui people (Lima, 2000) or at least in the site formation process. On the other hand, although the remains of fish are less noticeable than mollusc shells, the former had a major role in the subsistence system of these coastal societies (e.g., Figuti, 1993; Lima, 2000; Gaspar, 2000). In fact, cases of absent fish remains are extremely rare and even large sharks can be found in the sedimentary record of some sambaquis, suggesting a widespread traditional knowledge linked to coastal and marine ecosystems (Gaspar, 2000; Lopes et al., 2016). Moreover, numerous and diverse fishing tools found at some sites indicate that fishing was a central activity in the subsistence of these prehistoric populations (e.g., Gaspar, 2000; Guimarães, 2013). Even though shellfish was not the basis of the diet, it is undeniably the most abundant remains, and are represented by a variety of taxa (de Souza et al., 2011). The species analysed in the present study, *Anomalocardia brasiliana* (Linnaeus, 1767), is dominant in many sites, possibly for being abundant and relatively easy to collect (see

Colonese et al., 2017). Closed valves and complete fish skeletons have been explained as the leftovers of abundant meals during mortuary rituals.[1] Despite the low nutrition values, crustaceans may have been a substantial dietary complement, with remains of crab being documented in many sites (e.g., Figuti, 2008). In this discussion, it is important to bear in mind that not all the faunal remains found in these sites represent the diet of coastal populations but, in any case, it is possible to conclude that the sambaqui societies were strongly dependent on the aquatic environment as a source of food (e.g., Figuti, 1993; Bastos, 2014; Colonese et al., 2014).

For the specific case of Cabeçuda, the fish species most commonly found in the funerary deposits are the whitemouth croaker (*Micropogonias furnieri*) and catfish (*Genidens sp.*), two estuarine specimens widely distributed along the coast of Brazil (Klokler, 2016a). Based on the faunal remains deposited in the site, Klokler (2016b) concludes that activities such as the hunting, processing and deposition of birds and mammals did not occur on a daily basis. Nevertheless, the author presents the possibility of these activities happening at a nearby site or location. Although the archaeological context does not show evidence for a large consumption of marine mammals, Klokler (2016a) hypothesizes that these animals largely contributed to the diet of Cabeçuda builders, similar to groups in Terra Nova (Canada), Ushuaia (Argentina) and California (USA). The author argues that, given the funerary function of the site, the remains found in Cabeçuda do not represent the daily diet but rather the remnants of special meals. Nevertheless, remains of marine mammals that probably died after stranding on the shore, such as whales, dolphins and seals, have been reported in several sites and interpreted as opportunistic sources of food (de Castilho, 2008). Moreover, stable isotopes data for

[1] Some mollusc shells found in sambaquis present signs of heating, which could be a way of opening the valves. Closed valves have also been explained as being a result of an intact shell ligament closing the valves after death. A third explanation for closed shells refers to their use as construction material.

fish found in sambaquis are scarce. However, previous studies have found that taxa widely abundant in sambaquis, such as catfish, may have bone stable nitrogen isotope values around +15‰ (Colonese et al., 2014). If an average dietary fractionation of +4‰ is considered between diet and consumer tissue for nitrogen isotope values, then the regular consumption of many commonly found fish in sambaquis would justify the high nitrogen isotope values of human bone collagen without necessarily implying a large dependence on marine mammals. Regarding carbohydrates consumption, the common occurrence of hypoplasias of tooth enamel in the population of Cabeçuda indicates a low carbohydrate diet, which is corroborated by the absence of caries and starch residues in the dental analyses of individuals from this site (Souza, 2018, and references therein).

6.4.1 Modelling Human Diet at Cabeçuda

The stable isotopes results found in this thesis are in agreement with other studies in sambaquis such as Colonese et al. (2014) and Bastos (2014), who observed marine based diets in coastal populations. Klokler (2016a) mentions previous isotopic research for Cabeçuda pointing to the same conclusion, but does not give a reference for the data, which is probably unpublished. In this thesis, the relative contribution of different food sources to human diet at Cabeçuda was calculated using a Bayesian mixing model in FRUITS 2.1.1 (Fernandes et al., 2014). In order to simplify the model, only the most important components of the diet (i.e., fish, terrestrial mammals and C3 plants), based on the archaeological evidence and the discussion in the previous paragraphs, were included in the model input.[2]

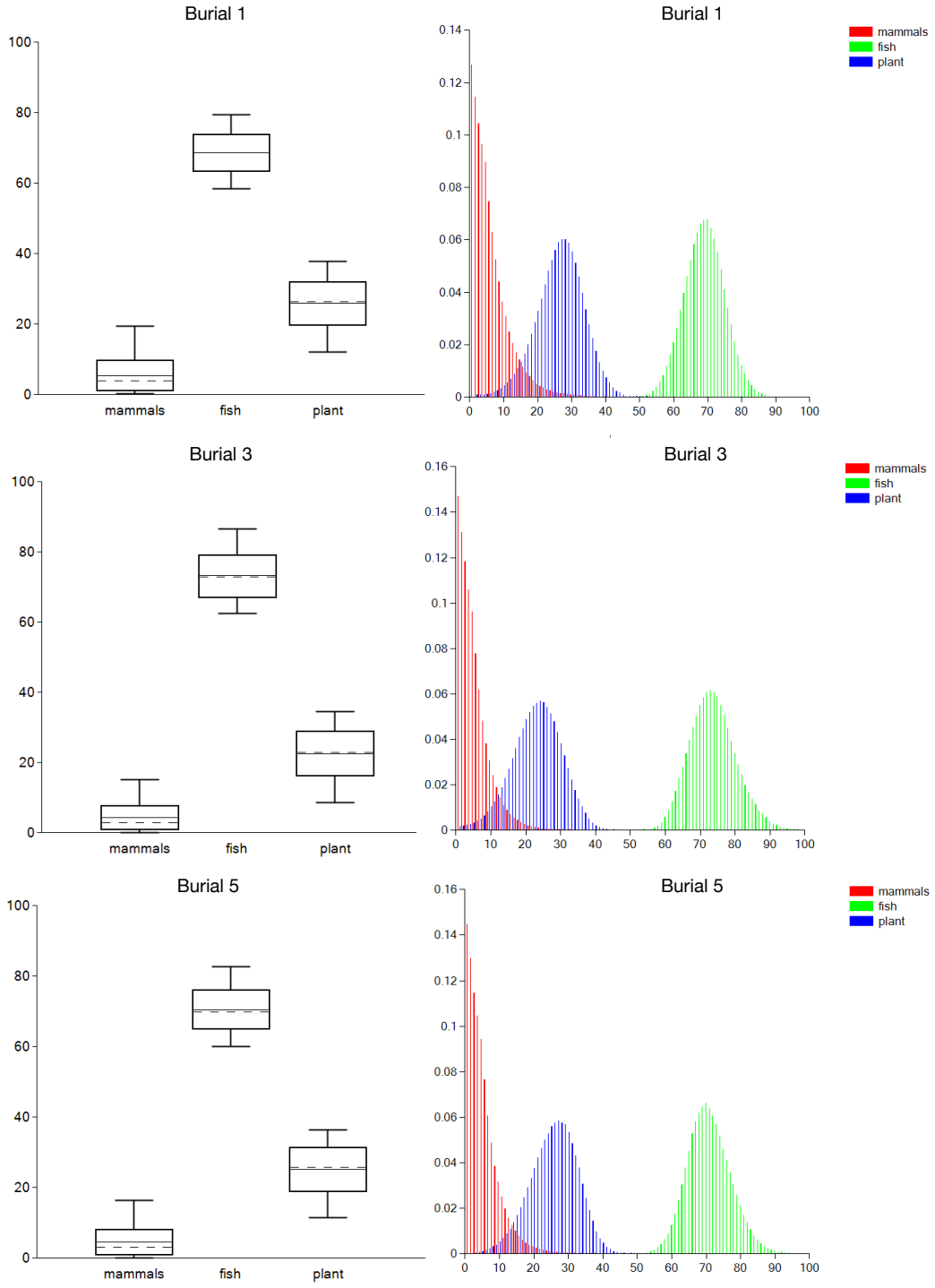
The $\delta^{13}\mathrm{C_{col}}$ and $\delta^{15}\mathrm{N_{col}}$ values of 17 fish specimens from Southern Brazil, reported in Colonese et al. (2014), were averaged to yield -11.4 $\pm$ 1.4‰ and +13.5

[2]Although there is evidence that sambaqui populations consumed maize (Boyadjian et al., 2016), C4 plants do not significantly influence human isotopic composition.

$\pm$ 2.0‰, respectively. These samples consisted of marine and estuarine species derived from both modern and archaeological contexts. Colonese et al. (2014) also report isotopic data for 14 archaeological samples of herbivorous and omnivorous specimens from the Atlantic Forest. An average of these results yielded the terrestrial mammal values ($\delta^{13}C_{col}$ = -22 $\pm$ 1.2‰, $\delta^{15}N_{col}$ = +8.4 $\pm$ 1.7‰) used in this thesis. Finally, the plant isotopic data used in the model (δ^{13}C = -29.2 $\pm$ 3.0‰ and δ^{15}N = +1.1 $\pm$ 2.0‰) were obtained from Galetti et al. (2016), who analysed 48 samples [modern fruits (n = 30); roots (n = 5) and palm-heart (n = 13)] from the Southeastern Atlantic Forest. Modern samples had their isotopic values corrected for the Suess Effect using a value of +2‰ (Hellevang and Aagaard, 2015).

The isotopic values reported in the previous paragraph refer to the bulk of each food source and offsets need to be applied for the derivation of the isotopic signature of the protein, carbohydrate and lipids fractions. Following Fernandes et al. (2015) and Fernandes (2016), the offsets employed in the model were -2‰ ($\Delta^{13}C_{protein-collagen}$), -8‰ ($\Delta^{13}C_{lipids-collagen}$) and +2‰ ($\Delta^{15}N_{protein-collagen}$) for terrestrial mammals, -1‰ ($\Delta^{13}C_{protein-collagen}$), -7‰ ($\Delta^{13}C_{lipids-collagen}$) and +2‰ ($\Delta^{15}N_{protein-collagen}$) for fish and -2‰ ($\Delta^{13}C_{bulk-protein}$) and +0.5‰ ($\Delta^{13}C_{bulk-lipids}$) and $\Delta^{15}N_{protein} = \Delta^{15}N_{bulk}$ for plants. An uncertainty of 1‰ was applied to all of these offsets. While the nitrogen content of collagen is assumed to be exclusively derived from proteins, carbon can be obtained from carbohydrates or lipids via the de novo synthesis of non-essential amino acids (Jim et al., 2006; Fernandes et al., 2012; Webb et al., 2017). Hence, I have assumed that protein and energy (lipids and carbohydrates) contribute with 74 $\pm$ 4% and 26% of carbon to bulk collagen, respectively (Fernandes et al., 2012). The Bayesian analysis of the isotopic data of the individuals of Cabeçuda (Fernandes, 2016) was performed with a model using Δ^{13}C and Δ^{15}N diet-to-collagen offsets of +5 $\pm$ 0.5‰ (Fernandes et al., 2012).

The model assumes a range of protein intake of >5% and <45% of the total calories (Fernandes et al., 2014).



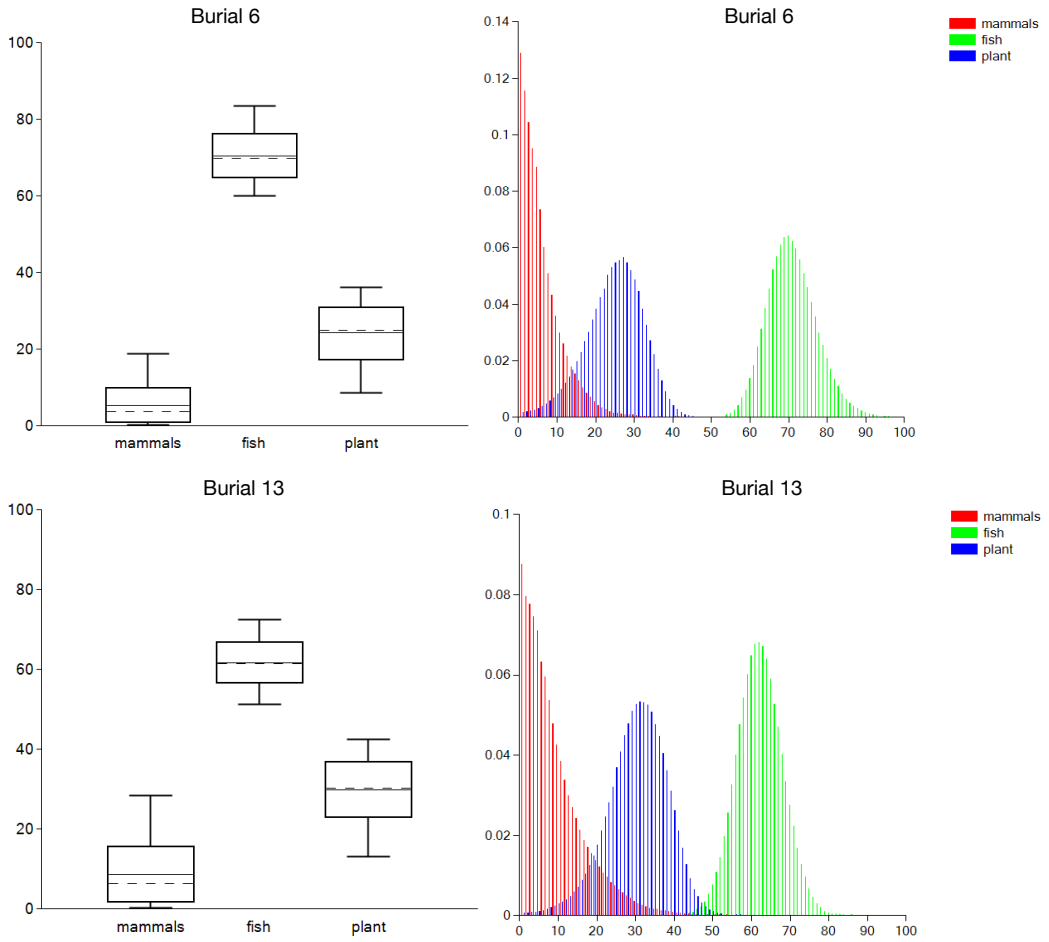


Figure 6.3. Diet model output (credible intervals on the left and probability distributions on the right) for the different burials of Cabeçuda. The y axis represents the relative caloric contribution of distinct food source to diet.

The model output for the caloric contribution to diet shows that the results are consistent among the sample set, indicating a marine based diet, as expected. Figure 6.3 indicates that fish and plant were the two main food groups consumed by the humans of Cabeçuda, which is in agreement with archaeozoological data obtained from the archaeological deposit (Klokler, 2016a). As Scheel-Ybert (2001) pointed out, several studies present evidence that fishing was a very important activity for the builders of the sambaquis (Figuti, 1993; Lima, 2000; Villagran et al., 2011; Colonese et al., 2014; Bastos et al., 2015), who complemented their diet with plants and terrestrial mammal resources. In addition to the contribution of

each food source to the total diet, the model outputs their percentage contribution to the carbon present in the collagen. For fish, the contributions are as follows: burial 1 = 79 ± 4%, burial 3 = 82 ± 4%, burial 5 = 81 ± 4%, burial 6 = 80 ± 4% and burial 13 = 74 ± 4%. This information can be used for the calibration of the ^{14}C ages obtained from these human remains (see Pezo-Lanfranco et al., 2018).

6.5 The Calibration of Cabeçuda ^{14}C Ages

A highly marine diet bears important consequences to the calibration of radiocarbon ages obtained from human remains. In this context, the possibility of a significant consumption of migratory species (e.g., whales and seals) would add complexity to this discussion. Indeed, these animals may carry a completely different isotopic signal than that of the estuary, in which case the MRE offsets calculated in the previous section would not apply to the humans. Nevertheless, in the specific case of Cabeçuda, both the archaeological context and the stable isotopes values point to a diet based on the lagoon resources and, thus, the $\triangle$R value calculated in this thesis can be applied for the correct calibration of the ^{14}C ages obtained from the inhumations.

Based on the contributions of each of the most significant food sources to the diet of the Cabeçuda builders, as estimated by Bayesian modelling in the previous section, the bone samples studied in this thesis were calibrated with mixed calibration curves and the $\triangle$R derived in the previous chapter (Figure 5.26). This practice accounts for the different percentages of marine carbon in each individual, allowing for the correct MRE adjustment of the ^{14}C ages. For the purpose of comparison, Figure 6.4 also presents the calibration of the human ^{14}C ages with the atmospheric curve SHCal13, a procedure commonly adopted when diet is not assessed. As expected, calibration with SHCal13 yields dates that are rather older

than the ones obtained from the use of the mixed curve. Indeed, calibration with mixed curves accounts for the marine component of the sample and compensates for apparent ages that would be too old. Moreover, the probability distributions for the ages calibrated with the atmospheric curve display the oscillations characteristic of the atmospheric curve and absent in the marine one. For reservoirs affected by the mixture of marine waters and freshwater carrying a more terrestrial radiocarbon signal, the approach of using a mixed curve should provide the right balance of high-frequency components for the calibration of radiocarbon ages. Using a phase model for the Cabeçuda bones it is possible to estimate an occupation period between approximately 4200 and 3500 cal BP (Figure 6.5). However, it is important to emphasize that this may not be representative for the whole site since Cabeçuda is much larger than the studied burials.

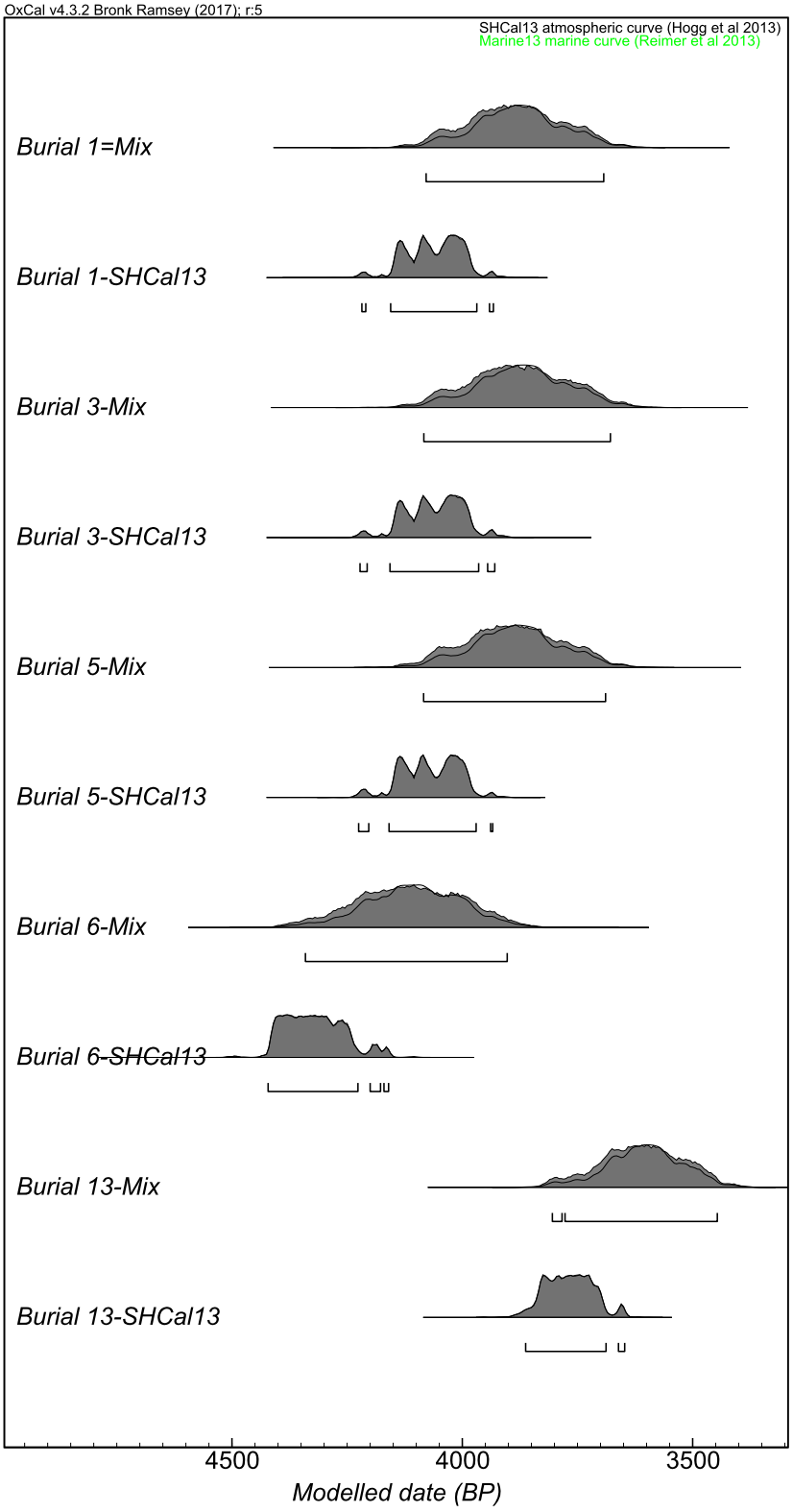


Figure 6.4. Comparison between the calibration of the ages obtained from the humans of Cabeçuda using a mixed curve and SHCal13.

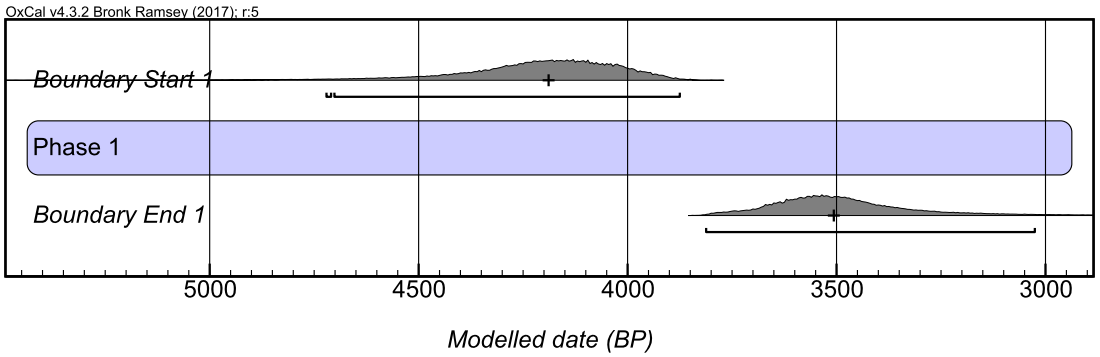


Figure 6.5. Boundaries of a phase model for the Cabeçuda bones.

6.6 Conclusions

The δ^{13}C and δ^{15}N values obtained from the bones of 5 humans from Cabeçuda point to a diet that is heavily dependent on marine resources. Bayesian modelling performed with the FRUITS software reveals the high consumption of fish, with contributions to the total caloric diet exceeding 70% in all of the individuals. This result is consistent with the archaeological evidence found in Cabeçuda and with other studies performed in different sambaquis. Indeed, despite the low number of individuals analysed in this thesis, the results are consistent among the sample set and my findings corroborate the hypothesis of a society that was largely dependent on the sea for their subsistence, eventually recurring to the terrestrial realm to complement their diet. The calibration of the ^{14}C ages obtained from the humans with mixed curves, based on the proportion of marine carbon in the diet, yields results that are significantly different from those obtained by the traditional approach for human bone (i.e., calibration with atmospheric curves). This demonstrates the importance of evaluating archaeological human diets, especially in coastal sites, prior to radiocarbon dating analyses in human bone.

Chapter 7

A Theoretical Approach to Assess the MRE

Introduction

This chapter builds upon the MRE and calibration discussions of previous chapters and presents a theoretical approach to quantify the MRE.[1] Here I address the long-standing issue in radiocarbon research of using a global curve for the calibration of marine radiocarbon ages. By exploring the output of a model for the temporal evolution of the MRE, I discuss a new method that in future could replace the current marine calibration approach. Given that the topic was previously discussed in the background chapter of this thesis, I begin with a very short summary. Next, I describe my methodology and introduce a tool to perform the analyses proposed here. Finally, I test the method and give a thorough discussion on its possibilities and limitations. I finish this chapter with some conclusions on the future of marine radiocarbon calibration.

[1] This chapter is largely based on a recently published paper (DOI: 10.1016/j.quascirev.2019.02.013). The design of the research was my own work and I led the writing of both the code and the manuscript, with input from the other authors.

7.1 Motivation

As previously discussed, radiocarbon calibration curves have been constructed with datasets obtained from different carbon reservoirs (e.g., Stuiver et al., 1986; Stuiver and Braziunas, 1993, 1998; Reimer et al., 2004, 2009, 2013) and software such as OxCal (Bronk Ramsey, 2009) and CALIB (Stuiver et al., 2019) use these curves for the calibration of radiocarbon ages employing Bayesian methods. Although terrestrial calibration accounts for the interhemispheric offset (Lerman et al., 1970; McCormac et al., 2002; Hogg et al., 2011; Rodgers et al., 2011) by using distinct curves for the Southern and Northern Hemispheres (Hogg et al., 2013; Reimer et al., 2013, respectively), a global curve (Marine13 for the mixed layer of the global ocean) has been used for the heterogeneous marine reservoir (Reimer et al., 2013). Marine radiocarbon calibration currently relies on the worldwide quantification of $\triangle$R values. However, the available data are extremely limited and patchy, compromising the accuracy of this method. Moreover, the quantification of $\triangle$R values involves significant uncertainty and variability, meaning that a large number of samples from the same locality need to be analysed for the achievement of a reliable value. Furthermore, $\triangle$R is time dependent (e.g., Kennett et al., 1997; Bondevik et al., 2006; Soares and Dias, 2006; Ortlieb et al., 2011) and a timeseries of these values is needed for calibration in different time scales. Therefore, an alternative approach to the current calibration practice would be the use of regional marine calibration curves for the ocean (Deo et al., 2004; Bondevik et al., 2006).

7.2 Methodology

Marine models have been used as tools for the study of the underlying dynamics of different systems. This includes worldwide investigations of the MRE (e.g., Butzin et al., 2005; Ritz et al., 2008; Singarayer et al., 2008). Recently, Butzin et al. (2017) generated a continuous record of MRA[2] for the whole radiocarbon time scale (50 - 0 ka BP). The authors applied a 3-D large scale ocean circulation model forced with wind stress, surface air temperature and freshwater flux fields derived from previous climate simulations. Their model accounts for factors such as wind speed and atmospheric pCO_2 to calculate air-sea carbon exchange and uses the IntCal13 atmospheric calibration curve as the input to generate local marine Δ^{14}C values. MRA are then derived from the atmospheric and local marine Δ^{14}C values.

In order to account for MRA variations due to climate variability, Butzin et al. (2017) considered three scenarios with specific boundary conditions. The PD (Present Day) scenario for the Holocene and interstadials is used from 11.5 to 0 kcal BP while the glacial scenarios GS (Glacial Scenario) and CS (Climate Scenario) for the Last Glacial Maximum are used for the period 50 – 11.5 kcal BP. While in the GS scenario, the Meridional Overturning Circulation (MOC) (see Figure 1.6 in this thesis) is weakened by approximately 30% compared to PD, this reduction is about 60% in the CS scenario. Although the model simulates radiocarbon as Δ^{14}C, it only outputs the MRA values. Therefore, from equation 1 in Butzin et al. (2017) and following their notation, it is possible to obtain the local marine Δ^{14}C values:

$$\Delta^{14}C_{\mathrm{mar}} = \left[\frac{(0.001\Delta^{14}C_{\mathrm{atm}} + 1)}{e^{\lambda MRA}} - 1\right]1000 \tag{7.1}$$

[2]Marine Reservoir Age, equivalent to the R offset defined in Chapter 1.

where $\Delta^{14}\mathrm{C}_{\mathrm{atm}}$ is the atmospheric Δ^{14}C value and λ(1/8033 yr) is the conventional decay constant of radiocarbon. One can obtain the conventional radiocarbon ages as:

$$CRA = -8033\left[\ln\left(\frac{\Delta^{14}C_{\mathrm{mar}}}{1000}+1\right)+\lambda'(y-1950)\right] \tag{7.2}$$

where y is the calendar year and λ' = 1/8267 yr. Ideally, it should be possible to extract $\Delta^{14}\mathrm{C}_{\mathrm{mar}}$ and CRA directly from the model but, in this particular case, the model outputs MRA and the equations above need to be applied. In this discussion, my rationale derives from the fact that, for calibration purposes or comparisons with empirical data, one only needs time slices from the model output. Therefore, I have developed a tool, available via a REST API freely downloadable at https://github.com/eduqq/local_curves, for the extraction of CRA time slices from the Butzin et al. (2017) model output. The user can choose geographic coordinates for their study area and retrieve information on how the CRA varied in that particular location for the past 50,000 years. Effectively, this pulls out local calibration curves from the output of the model. The steps performed by the script are described below.

Given that the model does not output the uncertainty associated with MRA, as a preliminary approach I have assumed the uncertainties in Marine13 are a first approximation of this uncertainty. The Marine13 and IntCal13 data files available at http://intcal.qub.ac.uk/blurb.html and the MRA model output from Butzin et al. (2017) (temporal resolution = 50 yr, 0-100 m or 200-300 m depth) available at https://doi.pangaea.de/10.1594/PANGAEA.876733 are the data needed to run the code. In order to match the temporal resolutions of the MRA model output (50 yr) and Marine13 [50,000-25,000 cal BP (20 yr); 25,000-10,500 cal BP (10 yr); 10,500 – 0 cal BP (5 yr)], I have performed a simple linear interpolation. Nevertheless, this step is only necessary in the case where the model being used does not output

at higher resolutions. For the removal of high frequency ^{14}C variations (wiggles), inherited from the use of IntCal13, a low-pass filter (centred moving average, triangular window, width = 21) is applied to the $\Delta^{14}\mathrm{C}_{\mathrm{mar}}$ and CRA timeseries. The complete methodology is summarized in the flowchart in Figure 7.1.

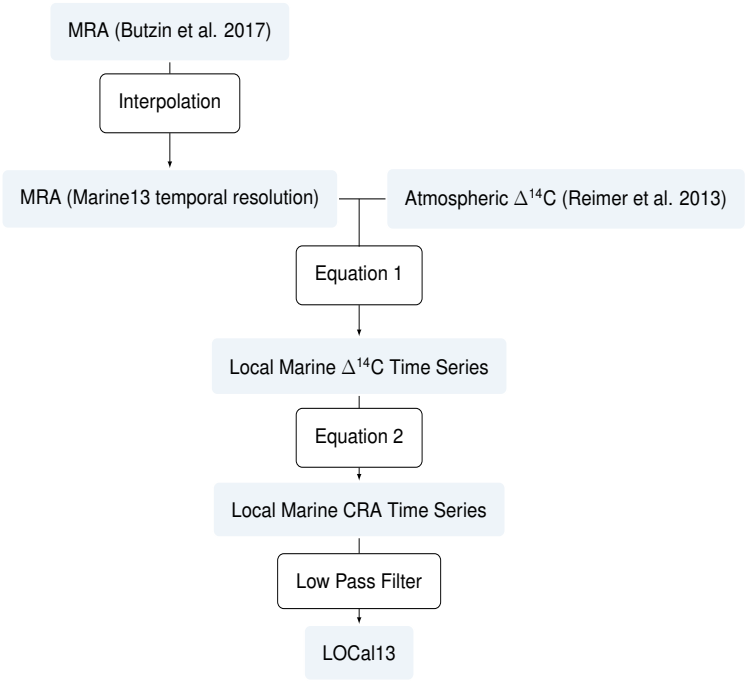


Figure 7.1. Flowchart illustrating the methodology employed for the curves construction.

7.3 Results and Discussion

Results from Butzin et al. (2017) show a pattern of higher MRA at high latitudes, in agreement with experimental data (see Figure 1.7 in this thesis). Figure 7.2 shows that their MRA values at 0 cal BP vary from approximately 300 to 450 ^{14}C yr in low latitudes and increase towards the poles, where they reach values up to approximately 1500 ^{14}C yr. Nevertheless, the model underestimates high empirical MRA values in upwelling regions on the west coasts of North and South America (e.g., Ingram and Southon, 1996; Ortlieb et al., 2011), and on the Argentinian coast, due

to the presence of ^{14}C-depleted limestone in the local geology (Gómez et al., 2008) (Figure 7.3).

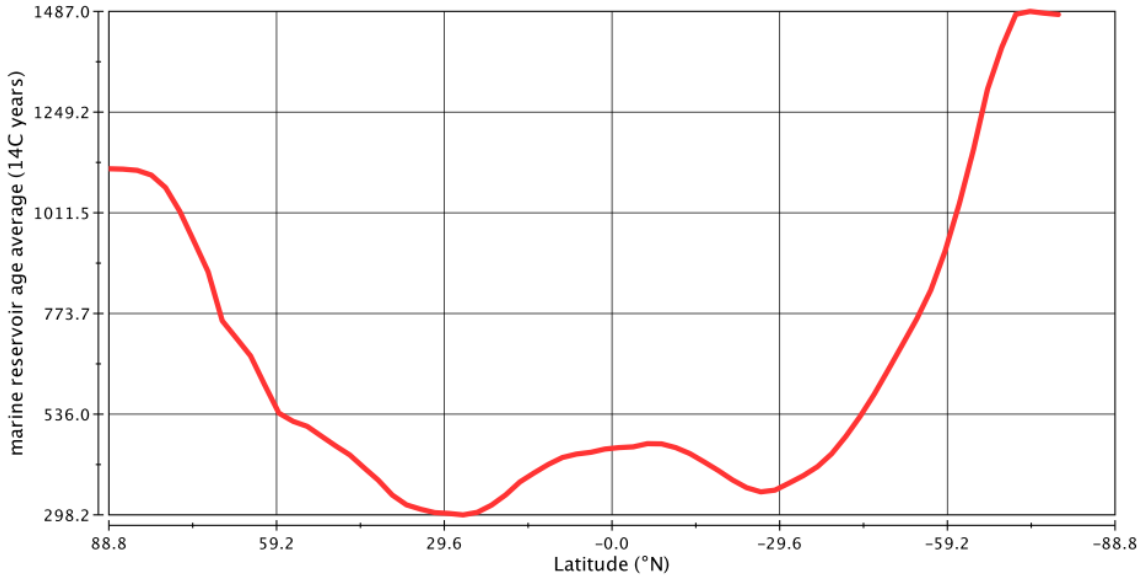


Figure 7.2. MRA plotted against latitude. The figure shows the average over the longitudes available in the model output for 0 cal BP (cf. Figure 1.8. Data from Butzin et al. (2017).

The most recent time slice of Butzin et al. (2017) data (0 cal BP) was compared to experimental observations held in the marine reservoir database (Reimer and Reimer, 2001). Figure 7.3 reveals locations where the agreement between the local calibration curves (herein named LOCal13, Local Ocean Calibration) and empirical data can be assessed. The lack of experimental ΔR data is evident for many regions of the globe, where the accurate calibration of marine radiocarbon ages is currently hindered. For some of these locations, the use of local curves could provide reasonable estimates for the MRE and thus represent a unique source of information. In the Southern Ocean, the few ΔR values available are in agreement with the model and, in open ocean areas of the Pacific, the differences between modelled and experimental data are minimal. This supports the idea of using local curves for the calibration of the radiocarbon time scale in these ocean regions.

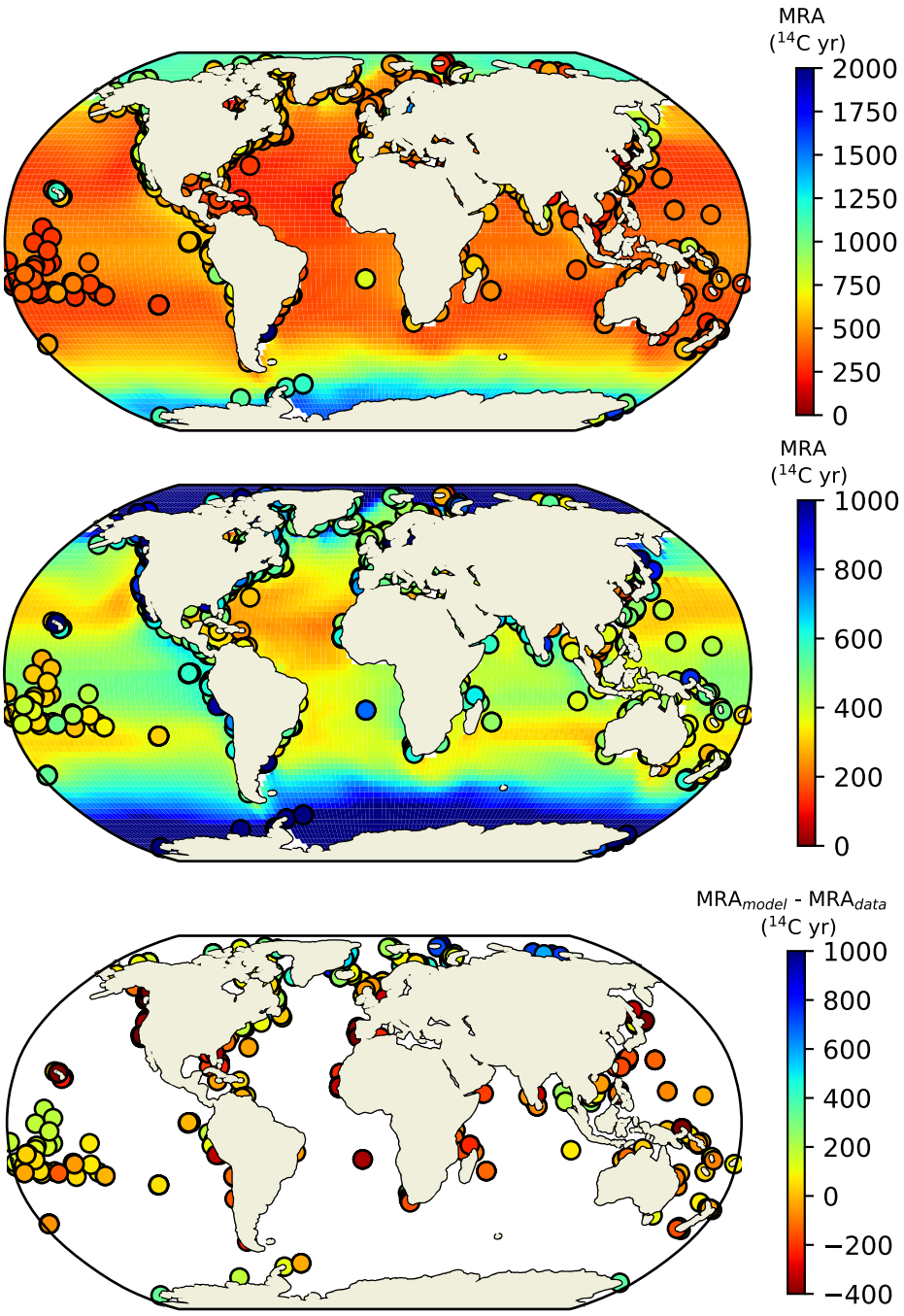


Figure 7.3. MRA (0 cal BP, 0 – 100 m depth) derived from the model described in Butzin et al. (2017) plotted together with experimental MRA data (pre-bomb samples from depths shallower than 75 m) from the marine reservoir database (Reimer and Reimer, 2001). The reduced colour scale in the second plot allows for the observation of small variations in the MRA. The third panel shows the difference between Butzin et al. (2017) model output and experimental data held and the marine reservoir database. References for the experimental data are available at the marine reservoir database.

For accurate calibration, local marine curves should take into account variations in atmospheric ^{14}C and the ^{14}C distribution within the complex ocean reservoir. For this reason, an ideal model for the MRE would consider factors such as ocean circulation and coastal dynamics. For a temporal evaluation of LOCal13, MRA reconstructions based on experimental data derived from records such as U/Th dated corals, tephra isochrones and paired archaeological samples can be used. Unfortunately, these comparisons between modelled and empirical data are extremely temporally and geographically limited due to the lack of experimental data. Figure 7.4 shows a comparison of the Marine13 and LOCal13 datasets with experimental data derived from coral records collected at two open ocean locations in the Pacific Ocean. In these locations, both curves agree reasonably well with the data. Therefore, given that radiocarbon ages from these locations in the time range considered would yield similar calibrated age ranges with LOCal13 or Marine13, the use of either curve should be valid.

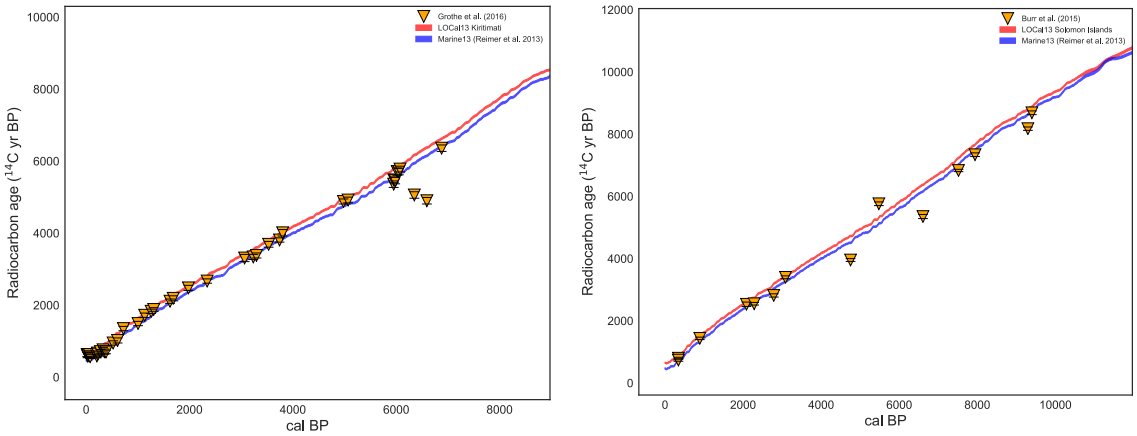


Figure 7.4. Comparison of LOCal13 and Marine13 for Kiritimati (Grothe et al., 2016) and Solomon Islands (Burr et al. 2015), two open ocean locations in the Pacific Ocean.

The MRA incorporated in local curves at low latitudes is remarkably lower than the offsets in high latitude curves (see Figure 7.2). This can be easily observed in Figure 7.5, where LOCal13 - Tropical is close to Marine13 and LOCal13 - Polar lies far above the other two, as a consequence of its higher MRA. As Reimer

et al. (2013) point out, Marine13 was constructed based on tropical and subtropical records and is unable to account for the much larger MRA observed near the poles.

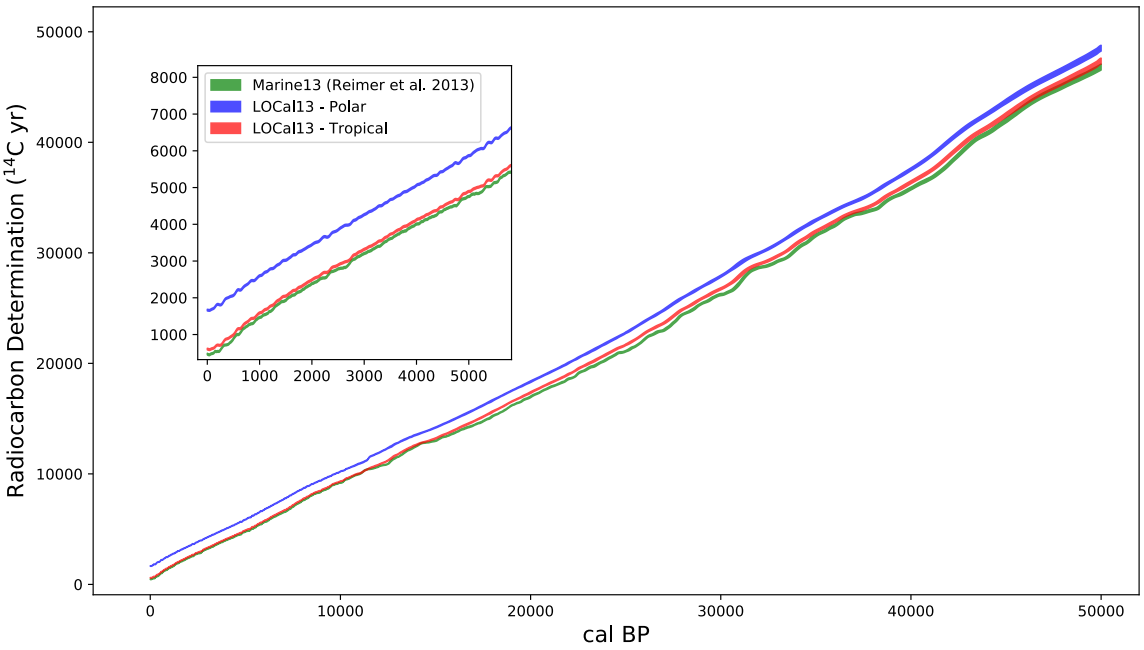


Figure 7.5. Local calibration curves for a tropical (latitude = $1.25°$N; longitude =0) and a polar (latitude = $68.75°$S; longitude = $45°$W) region plotted together with the global curve Marine13. The global curve strongly reflects the tropical and subtropical origin of the records used in its construction.

For the assessment of LOCal13 at a region near Antarctica (latitude = $68.75°$S; longitude = $45°$W), this curve was employed for the calibration of hypothetical radiocarbon ages in different time periods (5, 8, 15 and 30 kBP). Calibration was also performed with Marine13 and a ΔR value of 881 ± 115 ^{14}C yr (Berkman and Forman, 1996; Bjoerck et al., 1991; Peck and Brey, 1996), obtained from pre-bomb values held in the marine reservoir database (Figure 7.6).

Figure 7.6 shows that the use of both curves results in a similar interval for the calibrated age distribution of the most recent age, being slightly larger using Marine13. The discrepancy is more pronounced for older ages due to the increased modelled MRE magnitude in the past. It is evident that the use of Marine13 for the

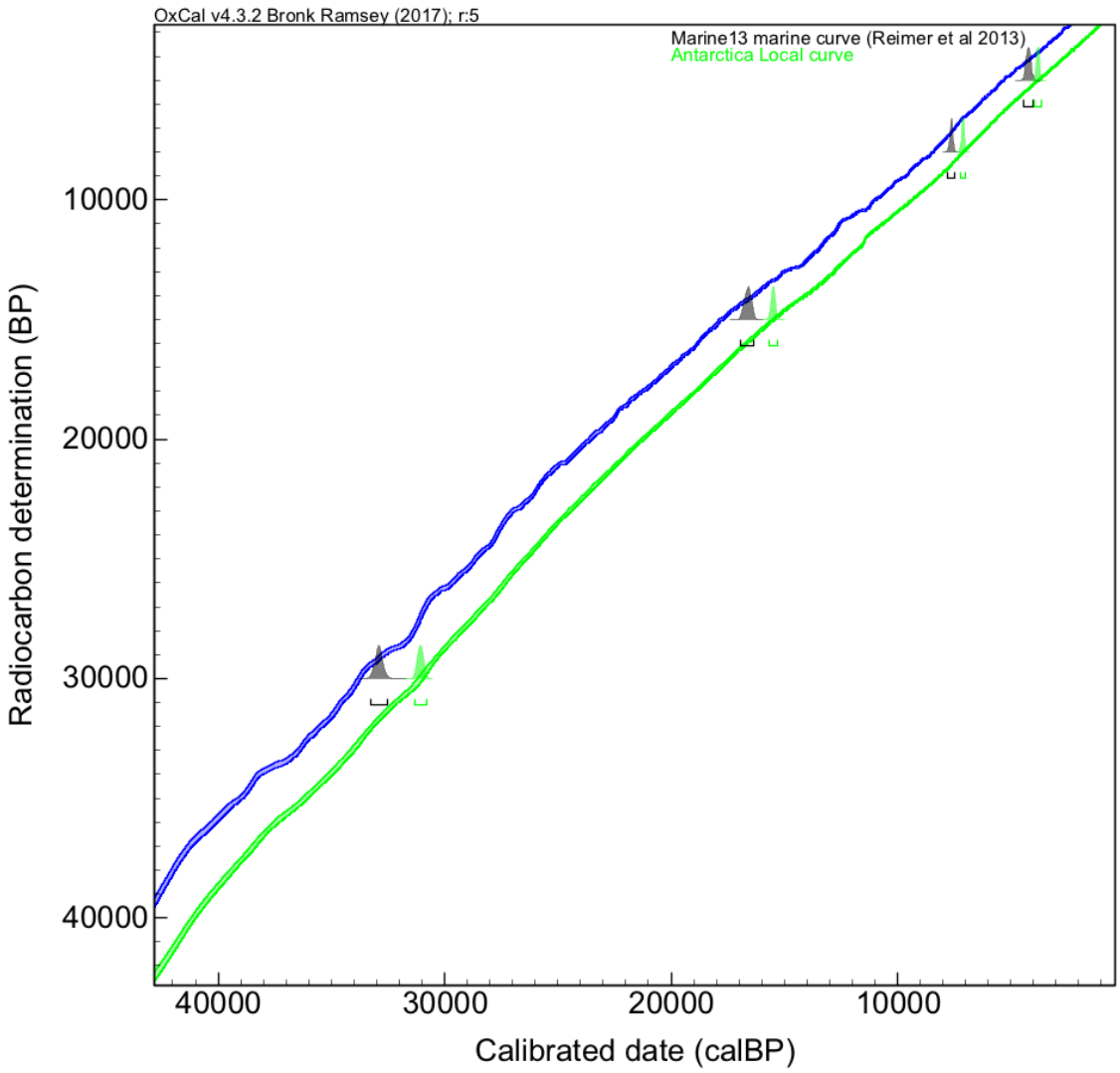


Figure 7.6. Comparison of LOCal13 and Marine13 for the calibration of hypothetical radiocarbon ages (5, 8, 15 and 30 kBP) from a location near the South Pole.

calibration of radiocarbon ages in the Southern Ocean is not appropriate. Even by using the ΔR value available for the region, this procedure inherits all the errors involved in the calculation of ΔR values (e.g., selection of samples, pre-treatments, measurement and calculation uncertainties). In locations where many experimental values are available, such as the East coast of the United States, there is large ΔR variability. For $36.25°$N, $75°$W the 10 closest points available in the database (Thomas et al., 2008; Rick et al., 2012) range from -109 to 144 ^{14}C yr with a

weighted mean of 27 and standard deviation of 108 ^{14}C yr. Using this value to calibrate different radiocarbon ages from this region, a comparison can be made with the correspondent local curve. Figure 7.7 shows a set of hypothetical radiocarbon ages (1, 5, 8, 15 and 30 ka BP) calibrated with both curves. Figure 7.8 shows the same comparison for the East coast of Africa ($1.25°$S, $45°$W) using a weighted mean (148 $\pm$ 82 ^{14}C yr) derived from 6 $\triangle$R values ranging from 50 to 310 ^{14}C yr (Southon et al., 2002). For the Holocene both approaches yield similar results, while for the late Pleistocene, LOCal13 curves give slightly younger dates. This indicates a higher MRE in agreement with the model output for the Late Pleistocene (Figure 7.9).

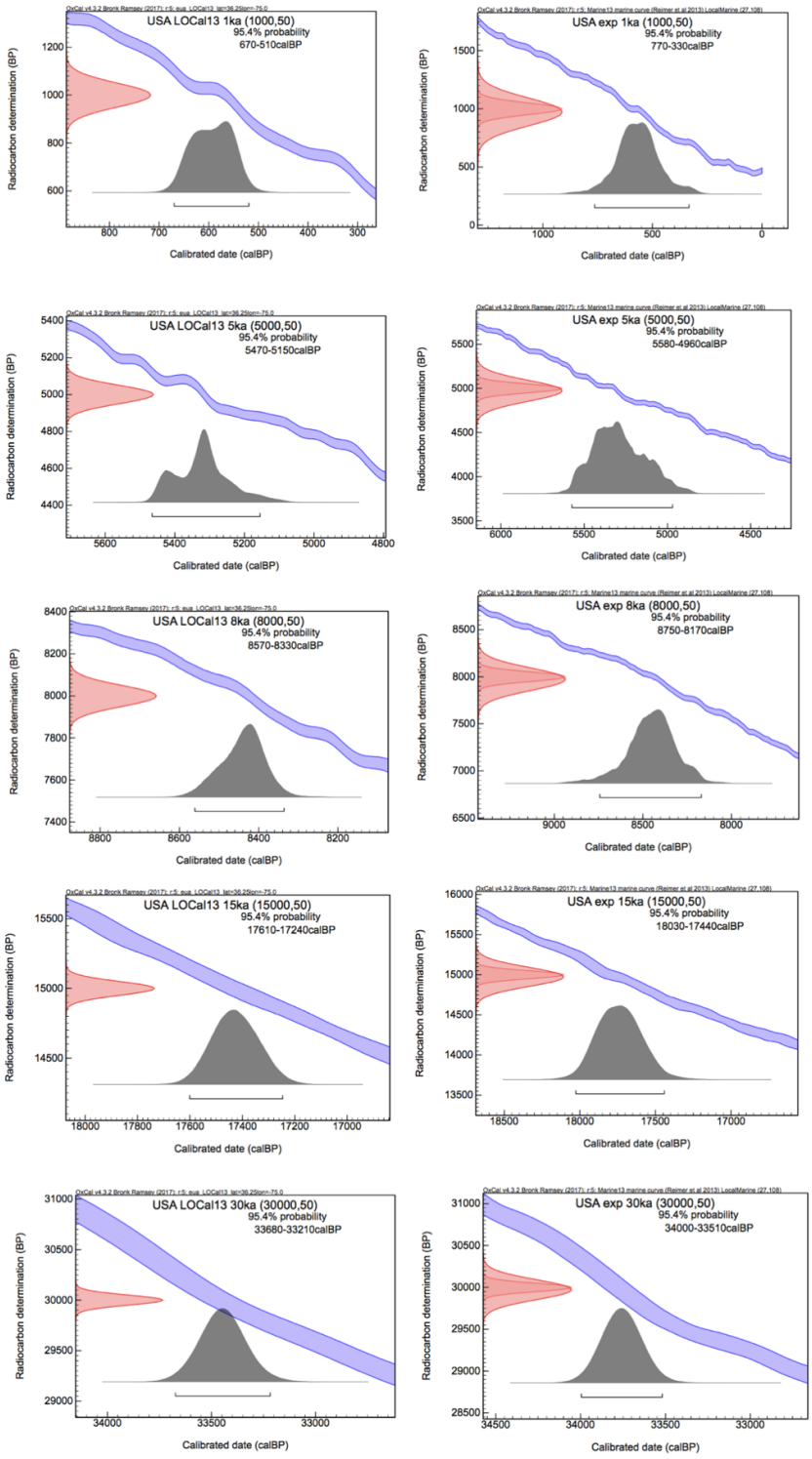


Figure 7.7. Comparison of calibrated ages for hypothetical radiocarbon ages with Marine13 and available ΔR vs LOCal13 curve for latitude = $36.25°$N and longitude $75°$W.

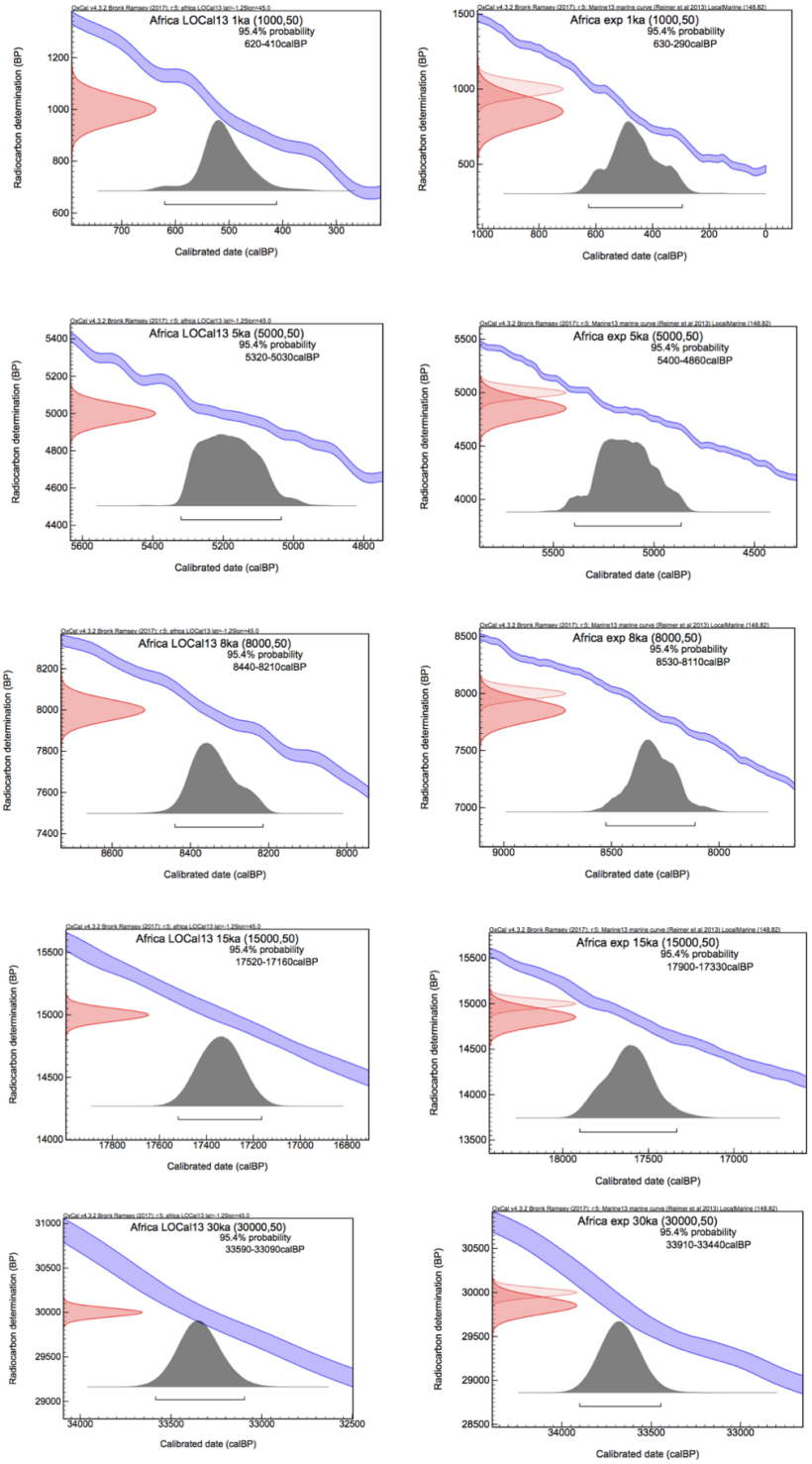


Figure 7.8. Comparison of calibrated ages for hypothetical radiocarbon ages with Marine13 and available ΔR vs the LOCal13 curve for latitude = $1.25°$S and longitude = $45°$E.

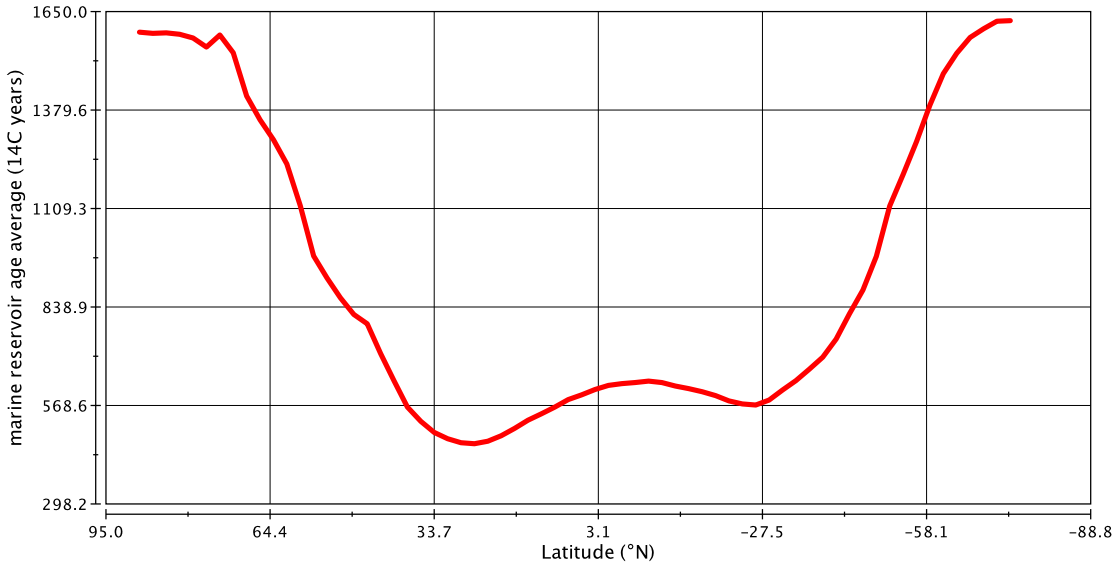


Figure 7.9. MRA plotted against latitude. The figure shows the average over the longitudes available in the model output for 15ka cal BP.

Although MRA models have the potential to overcome the uncertainties associated with the geographic and temporal representability of a $\triangle$R value, they do not always incorporate carbon cycle and ocean circulation changes. This is indeed a limiting factor for the model employed here. Butzin et al. (2017) considers only two circulation modes (glacial and close to modern) for the past 50,000 yr and, by using the IntCal13 atmospheric radiocarbon signal to derive marine values, assumes that the ocean responded passively to atmospheric radiocarbon forcing. It is also important to consider that ocean model tendencies and biases may also have influenced their simulations (see e.g., Toggweiler et al., 1989; Matsumoto et al., 2004). Moreover, it is possible to notice an anomalous behaviour in the output of the MRA by Butzin et al. (2017) in high latitudes (Figure 7.10). This happens at 11.5 cal kBP, where Butzin et al. (2017) switched from the glacial circulation state (GS/CS) to the Holocene state (PD), which raises further concerns about the reliability of these scenarios. Overall, the approach described here is not yet ready for the calibration of radiocarbon ages in coastal regions, but may be useful for com-

parison reasons in the open ocean. The increasing amount of experimental data reconstructing marine reservoir ages (e.g., Zhao and Keigwin, 2018) means more possibilities for the comparison of local and global curves. Even simple statistical calculations such as computing the standard deviation between experimental points and the curves can be a quantitative method to choose which curve better describes the empirical data for a given region and timescale. Hitherto, the limited availability of MRE data has prevented the definition of such a metric.

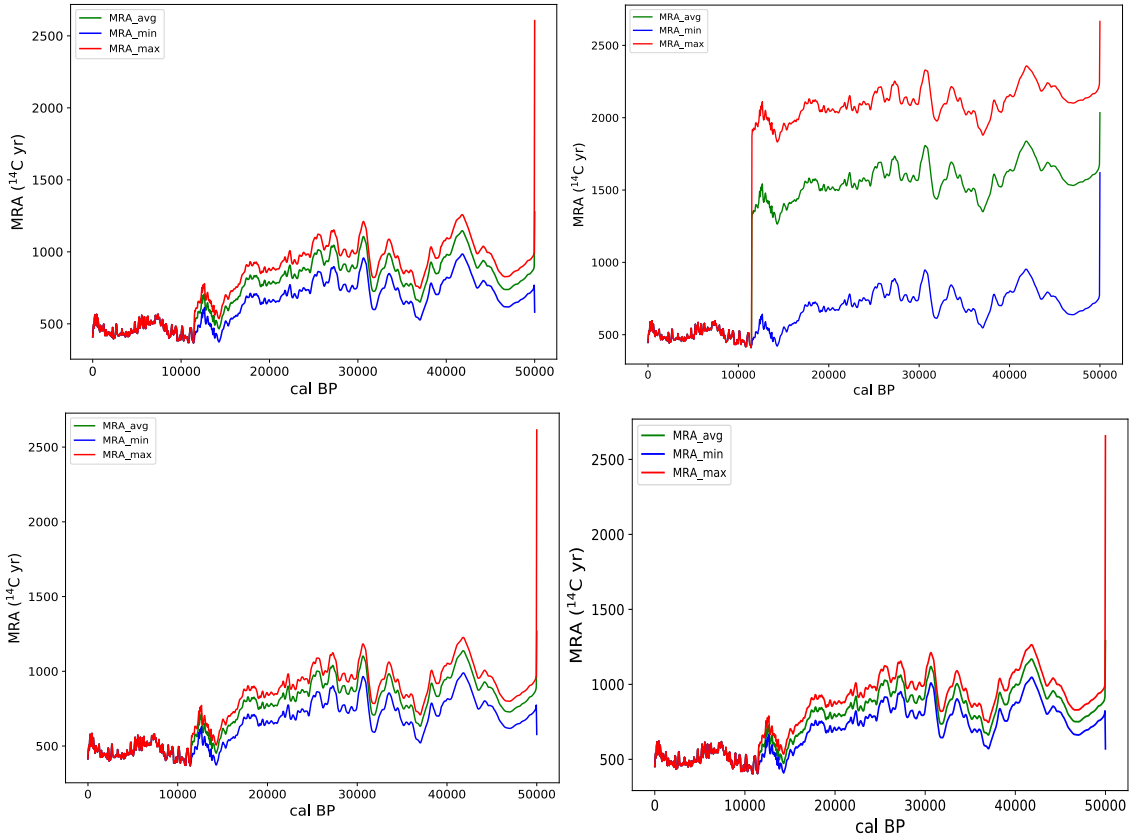


Figure 7.10. The three scenarios output by Butzin et al. (2017) for low latitudes (latitude=1.25°N, longitude = 20°W; latitude = 6.25°S, longitude = 80°E; latitude = 21.25°S, longitude = 150°W) and a high latitude (latitude = 68.25°N; longitude = 5°E) region. MRA_min corresponds to scenario PD, MRA_max can be either GS or CS depending on location and MRA_avg is the average of the three scenarios. For high latitudes, there is an artificial discontinuity at around 11 kcal BP.

7.4 Conclusions

The method presented in this thesis retrieves time slices of CRA from the output of a MRA model. Current models present significant limitations, meaning that this approach is not ready for general application. For instance, near estuaries or in upwelling locations LOCal13 may not be able to pick up these features. In these locations, Marine13 will remain a better option (provided that the local ΔR corrections are used). Nevertheless, the method might be the only option for the calibration of ages obtained from open ocean settings where ΔR values are not available. A great advantage of the approach presented here is that it can be easily updated whenever a new generation of calibration curves arises. With the future development of more accurate and better resolved MRE models, the methodology described here would become a widely applicable approach for the construction of regional marine calibration curves, filling a long-standing gap in radiocarbon research. It is important to highlight that this is not a calibration method *per se*, but rather a way of accounting for the MRE spatiotemporal variation in the calibration process. In fact, calibration with LOCal13 still essentially means calibration with the existing curves from which the local curve is derived. Nevertheless, the method presented here would represent a step forward from the current practice of using local marine corrections and a global curve. Given that the box diffusion model used in Marine13 does not take into account circulation and carbon changes either, it is valid to try and use the Butzin et al. (2017) model. It has a higher spatial resolution than the modelled component of Marine13, which allows higher reservoir ages to be resolved at high latitudes. I argue that this approach is independent of Butzin et al. (2017) work and can be used for any model. In the future, if we can feed enough information into a model so it takes into account changes in the carbon cycle and ocean circulation and presents high spatial resolution to constrain

what is happening in terms of MRE in the boundaries, then in the long run no $\triangle$R or global curves should be needed. Nevertheless, it is important to acknowledge that model biases can affect this method and that paleo observations are critical for assessing the accuracy of the models themselves. For the future, a user-friendly interface for the API described here or the possibility of running the API directly from calibration programs would make the data from models more accessible to users of radiocarbon data.

Chapter 8

Conclusions and Perspectives

This research has involved the examination of empirical and theoretical aspects of the ^{14}C Marine Reservoir Effect, as well as their implications for archaeology. Given the importance of knowing the origin of the carbon present in a sample, the MRE is at the heart of the radiocarbon dating tool. I therefore argue that this work contributes not only to unravel some of the mechanisms involved in the MRE at specific locations and time periods but also to the methodology of assessing the effect and accounting for it in marine radiocarbon calibration. To illustrate the importance of the MRE for archaeology, this research provides the means to properly calibrate ^{14}C ages for an archaeological site in Southern Brazil.

For this research I have employed a two-pronged approach (chapter 5) for the derivation of the $\triangle R$ values. My results for the known-age pre-bomb sample approach disclose a pattern of relatively low MRE corrections on the coast of Brazil (from -100 to 100 ^{14}C yr) and identify regions (i.e., the southeast and northeast coasts) that should be further studied due to the presence of local processes directly affecting the ^{14}C signal of the coastal waters (upwelling and limestone geology, respectively, yielding $\triangle R$ values up to 462 $\pm$ 30 ^{14}C yr). By using the paired sample approach, on the other hand, I have derived a fairly negative signal ($\triangle R$)

for the Late Holocene shell mound Sambaqui da Cabeçuda, in the Laguna region, Southern Brazil. Cabeçuda is a massive shell mound deemed to be a cemetery and undoubtedly a key site in Brazilian pre-history.

Acknowledging that human bone is an important material for archaeological research, often radiocarbon dated for chronometric investigations, this work assessed to what extent bone is affected by the MRE. I employed stable isotopes of C and N to evaluate the diet of 5 individuals from Cabeçuda. As it is the case for other shell mounds in the region, I have found that these people were mostly consuming marine resources from the region, meaning that the proportion of marine carbon in their bone collagen is significant (up to 80%). In this case, the impact of the MRE on their ^{14}C ages is very high and I have used a mixed curve for the calibration of these ages.

Finally, after exposing all the obstacles involved in the study of the MRE, in this work I have also discussed local calibration curves for the marine environment, which, in the future, could be an alternative to the use of $\triangle R$ to compensate for the MRE. This has been previously proposed but never investigated in depth, so the discussion presented in this thesis represents a step further for marine radiocarbon calibration. Here it is important to highlight the promising results obtained in open ocean regions, where LOCal13 curves seem to calibrate the radiocarbon timescale reasonably well, in agreement with the few experimental data available.

It is important to emphasize that a proper contextualization is at the forefront of MRE research. For this reason, this work has included a methodology that maximizes the accuracy of the results obtained. Regarding the known-age approach, I advise that, whenever possible, future studies should prioritise samples collected during large and well-documented scientific expeditions. To complement this information, stable isotopes of carbon and oxygen could be used to track the source of aquatic carbonate, but bearing in mind that their results may only serve as a

first approximation. Concerning the paired sample approach using archaeological material, I advocate the use of accessory techniques such as anthracology and X-ray diffraction in order to reduce the chances of analysing carbon that is not co-eval. Notably, this work has showed that, even when all precautions are taken, the production of spurious results is still a possibility. This is when Bayesian modelling is extremely useful. For this research I have employed a variety of OxCal models, taking into account prior information regarding the samples, to calculate $\triangle$R in the most accurate way that I possibly could with the results I had at hand. The use of interdisciplinary analyses such as stable isotopes, radiocarbon, anthracology, X-ray diffraction and Bayesian modelling for the study of a topic of archaeological interest turns this thesis into a work of real archaeological science.

Data generated in this work is useful for the calibration of marine radiocarbon simulations for the Southwestern Atlantic Ocean and invaluable for a proper chronometric investigation of the occupation of the Brazilian littoral. The $\triangle$R values derived here are, in fact, useful for any study (i.e., archaeological, environmental, climatic) employing radiocarbon analyses for marine material in Brazil. Moreover, I argue that my methodology is applicable to the study of the MRE in other regions of the world and that my analyses for Cabeçuda could be extended to other shell mounds in Brazil. Finally, the local curves generated in this thesis are now available for the radiocarbon community for testing and comparisons with the available data.

Brazilian archaeology is a relatively young discipline whose scientific aspects are still developing. All things considered, it seems reasonable to hope that this thesis represents my -small- contribution to providing the necessary means for more scientific investigations to be performed on the coast.

8.1 Future Perspectives

Although the known-age samples used in this thesis have yielded great insights into the MRE geographic variability over the Brazilian coast, the temporal component of this variability remains poorly known. By using Late Holocene and pre-bomb samples, it is impossible to avoid temporal gaps in the dataset. Nevertheless, analysing longer records such as long lived corals and foraminifera from varved sediment constitute my future plans for this research. Unfortunately, the local curves described in this thesis are not adequate for application in most coastal regions, where they would be more relevant for archaeology. In this limitation, the spatial resolution of current MRE models and the lack of experimental data to test the model play a major role. That is not to say, however, that the discussion is not valid. On the contrary, I have presented ideas that in future could replace the current paradigm of using $\triangle$R values and global curves for marine radiocarbon calibration. Indeed, I intend to adapt the API and make it more user friendly in the future.

Samples from other sambaquis, mostly in the states of Paraná and São Paulo, have been sampled for this DPhil research. Due to funding and time constraints this material could not be included and should be analysed in due course for MRE studies following the methodology described for the samples from Cabeçuda in this thesis. My plan is to have a clear panorama of the Late Holocene MRE in as many locations as possible. More pre-bomb shells are also available and should be analysed soon in order to increase the amount of data on the coast and reveal possible patterns of MRE variability that could not be resolved with the limited sample set used for the present work. This thesis focused on the geographic variability of the MRE. In the future, I want to analyse long lived corals to look at the temporal variability of the MRE at specific locations along the coast. I want to correlate the

MRE recorded in these proxies with other climate archives in the studied regions such as speleothems and foraminifera.

On a more methodological note, the future perspectives of this work involve the sampling of mollusc shells along salinity gradients (river, estuary and open ocean) for the investigation of stable isotopes (C and O) and radiocarbon compositions. This will allow for a better understanding of how the isotopic ratios of these organisms respond to the environment in different parts of the Brazilian coast. Moreover, the relationship between the δ^{13}C, δ^{18}O and ^{14}C signatures within the shell will be further investigated. A study comparing the isotopic composition of shell and flesh in bivalves that inhabit the Brazilian coastline and are commonly found in sambaquis is also expected. This will be important to investigate whether the isotopic signal derived from the shell is suitable for diet studies in the case of humans that were eating the flesh of these animals. I also want to radiocarbon date shells from the wet collections of natural history museums with the aim of investigating any possible interference in the radiocarbon ages and possibly for the development of protocols to remove this contamination.

Appendices

Appendix A

Science at Sea: European and American Voyages of Scientific Exploration

Introduction

Many of the pre-bomb samples used in this research were collected in Brazil as part of American and European scientific expeditions. Taking advantage of 18th century technological improvements that made navigation safer, these 19th century government-sponsored large-scale voyages were mostly dedicated to the investigation of the ocean. After the Enlightenment period, interest in science joined the more traditional commercial and political motivations for these journeys. Their legacy is still relevant today and their discoveries remain valid as a source of material for this research. Indeed, due to resources such as onboard diaries, sketches and publications, samples derived from expeditions are very well documented, which is an essential requirement for MRE studies. Although this thesis cannot do justice to a thorough description of these journeys of exploration and their out-

comes for modern science, my intention in this chapter is to present a very short historical background to the expeditions that provided the samples I use now, more than a century later.

A.1 Expeditions of Exploration and Discovery

– **The Rattlesnake Expedition:** In December of 1846, the frigate HMS Rattlesnake departed from Plymouth, England, on a journey that would last until 1850. Although hydrography was the leading motivation for the expedition, natural history was also a major aspect.[1] Onboard, among other scientists, was Thomas H. Huxley, the eminent British naturalist, on his maiden voyage. The crew arrived in Rio de Janeiro on the 23^{J}anuary 1847 and stayed there until the 2 February 1847. John MacGillivray, who was the official naturalist of the expedition, describes the activities carried out by the team while in Rio de Janeiro, including dredging in the Guanabara Bay (MacGillivray, 1852). Thomas Huxley's grandson published his grandfather's diary for the trip (Huxley, 1935).

– **The Herald Expedition:** The voyage of the HMS Herald was intended to be a surveying expedition of the Southwest Pacific. The crew left Plymouth on the 9 June 1852 and on the 25 September 1852, the HMS Herald arrived in Rio de Janeiro, staying there for about one month.[2] Onboard this ship was John MacGillivray who, at this point, had made a name for himself after boarding the HMS Rattlesnake. During their trip, the crew made nautical, meteorological and astronomical observations. Moreover, the expedition brought various collections of natural history to Europe. A narrative of this voyage is given by David (1995).

[1] This is exemplified by the fact that many people onboard the HMS Rattlesnake had their own shell collection during the voyage (Goodman, 2005).

[2] The same ship called at Rio de Janeiro during a previous expedition in 1845 (Seemann, 1853).

– **Novara Expedition**: The SMS Novara was a frigate of the Austrian Navy. In 1857, it started a large-scale scientific expedition around the world, reaching the Guanabara Bay on the 5 August 1857. Onboard, there was a commission formed by a botanist, a zoologist, an artist, and a flower-gardener, responsible for the investigation of natural phenomena and the collection of rare specimens and natural history objects. During the whole journey, most of the specimens were collected by hand at the sea shore, no dredge was used due to lack of time. The crew stayed in Rio de Janeiro for about 26 days and von Scherzer (1861) describes their experience at the city.

– **The Thayer Expedition:**[3] This voyage of scientific exploration was led by Louis Agassiz, who had a team of 12 assistants and volunteers. Among the crew, there were a conchologist, two geologists, an ornithologist, a preparator and an artist. Uniquely, among the expeditions mentioned in this chapter, the Thayer Expedition had the specific objective of studying the natural history of Brazil. Indeed, the expedition started in 1865 and lasted for 19 months, exploring many different regions in the country. In 1868, Agassiz and his wife, Elizabeth, published a very rich narrative of their journey, describing the local fauna and flora, as well as the societies of the places they visited (Agassiz and Agassiz, 1868).

– **The Challenger Expedition:** The purpose of this journey was primarily a scientific exploration of the oceans, making e.g., soundings, astronomical and magnetic measurements.[4] The voyage of the HMS Challenger is considered one of the greatest expeditions of all time, comparable to that of the HMS Beagle. Departing from Portsmouth, England, in December of 1872, it lasted almost four years. The HMS Challenger arrived at the Fernando de Noronha island on the 1

[3]The expedition was named after Nathaniel Thayer, a Boston financier who funded the cruise.

[4]Indeed, early 19th century scientific knowledge of the sea was limited to its surface and the voyage of the HMS Challenger (1872) is considered to mark the foundation of oceanography as a scientific discipline.

September 1873, leaving on 3 September. The crew arrived in the state of Bahia, where they remained for 10 days, on 14 September. An account of this voyage is given by Swire (1938). A more recent narrative can be found in Corfield (2003).

Information about some of the research expeditions relevant to this thesis can be found only in books which today are rare and not readily accessible, being scattered in different libraries and written in various languages (e.g., von Martens, 1867). My intention is to include fuller accounts of these expeditions as part of future research on this topic. For now, it is important to acknowledge the potential of such voyages for the quantification of the MRE in different parts of the world ocean, along their routes. As an example, Figure A.1 shows the route of the HMS Challenger.

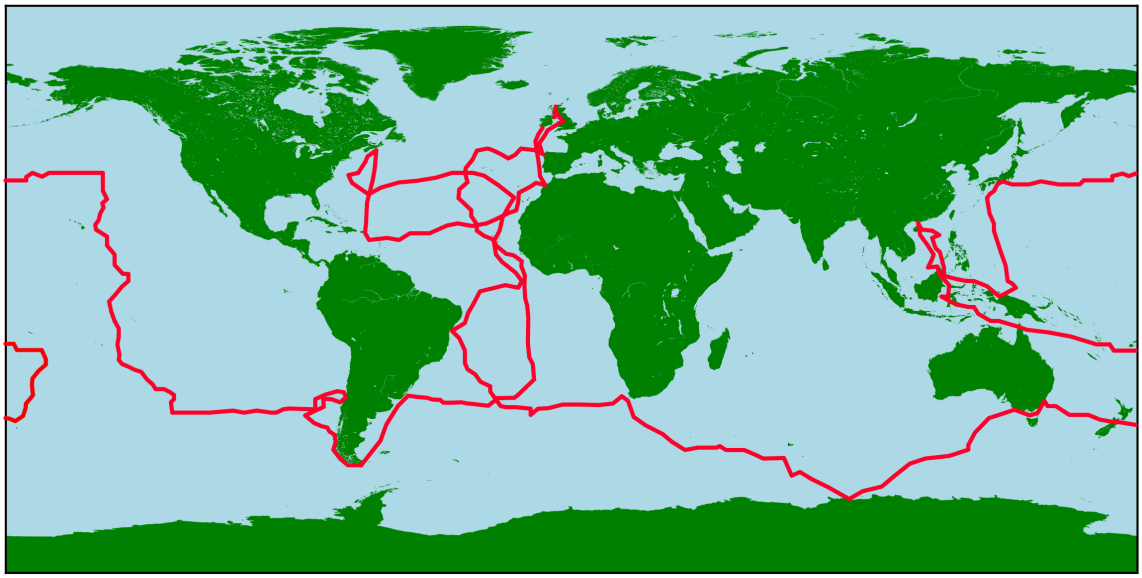
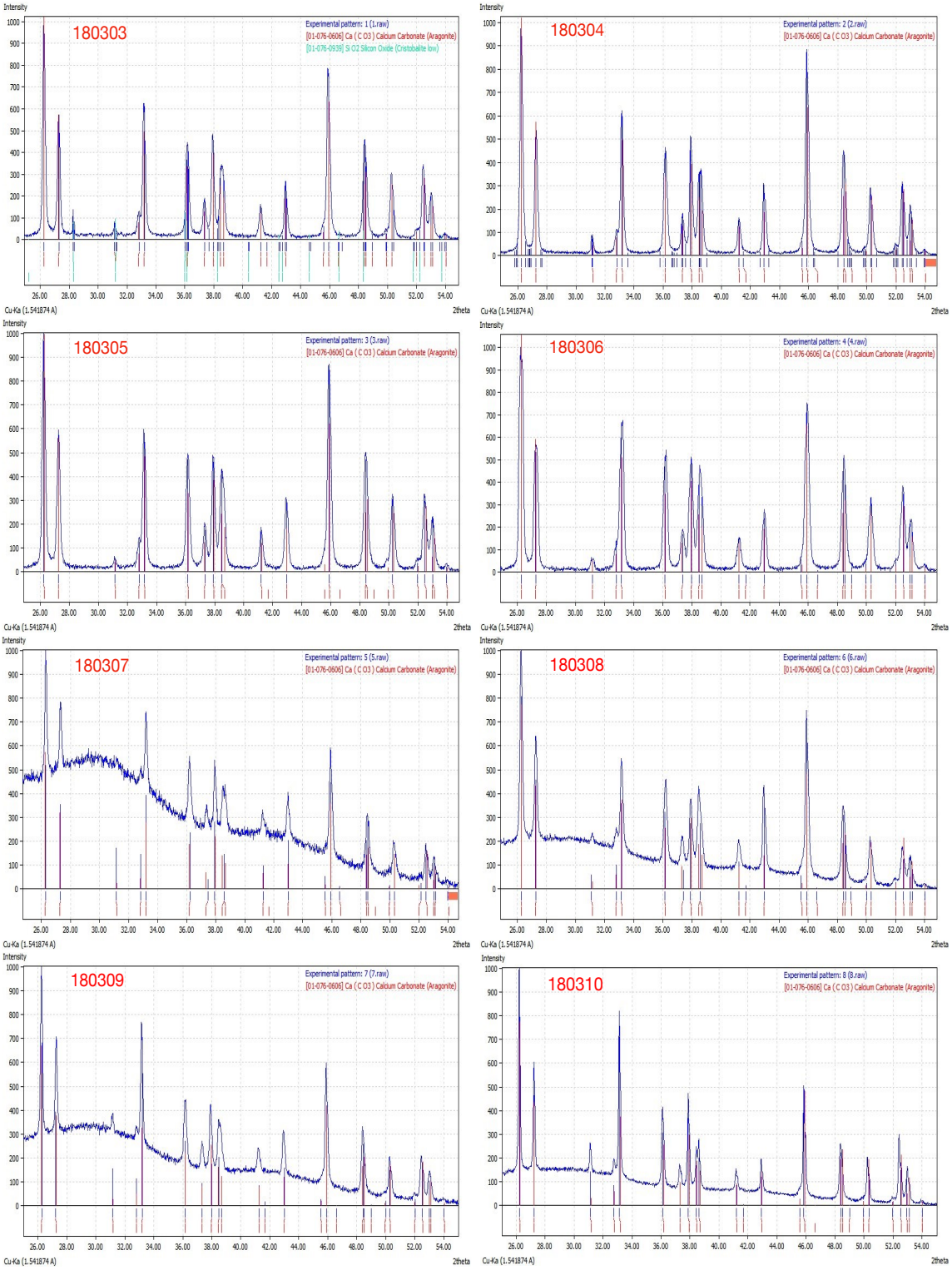
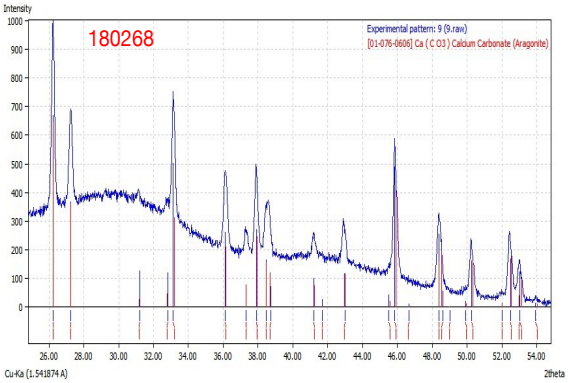


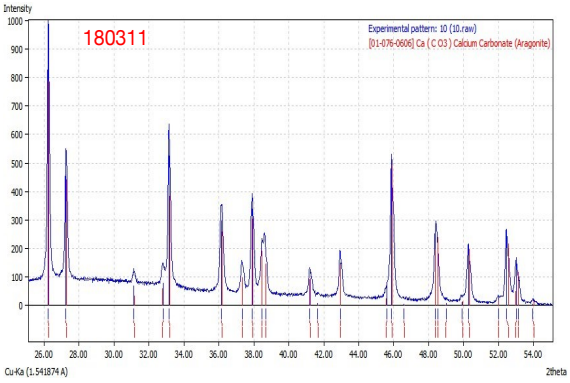
Figure A.1. The route of HMS Challenger. This expedition created possibilities for MRE studies in different parts of the ocean.

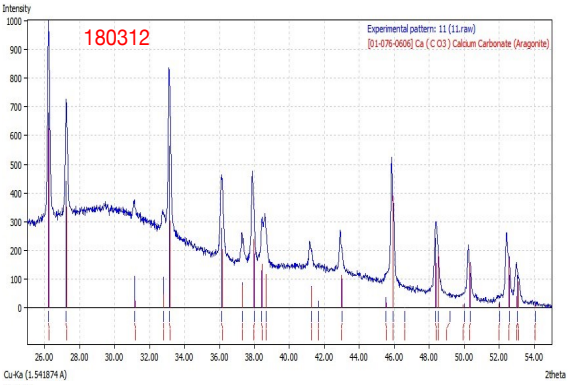
Appendix B

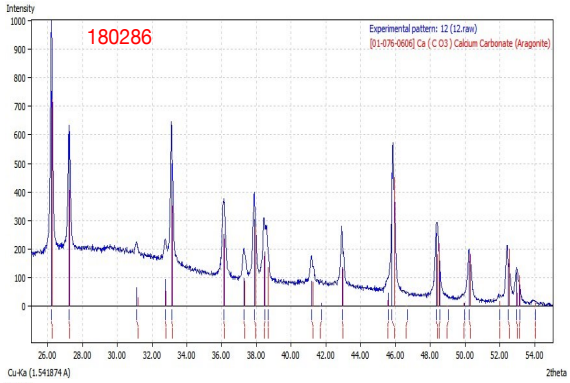
X-Ray Diffractograms

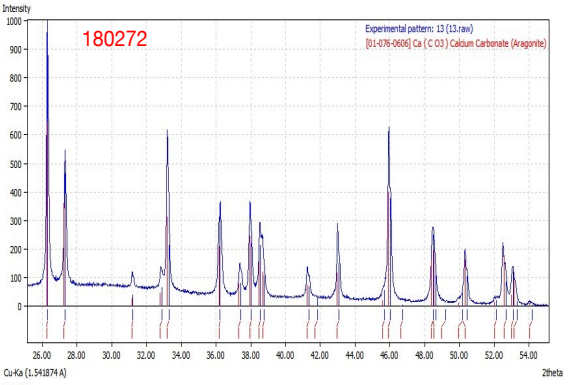

180303
Experimental pattern: 1 (1.raw)
[01-076-0606] Ca (C O3) Calcium Carbonate (Aragonite)
[01-076-0939] Si O2 Silicon Oxide (Cristobalite low)
180304
Experimental pattern: 2 (2.raw)
[01-076-0606] Ca (C O3) Calcium Carbonate (Aragonite)
180305
Experimental pattern: 3 (3.raw)
[01-076-0606] Ca (C O3) Calcium Carbonate (Aragonite)
180306
Experimental pattern: 4 (4.raw)
[01-076-0606] Ca (C O3) Calcium Carbonate (Aragonite)
180307
Experimental pattern: 5 (5.raw)
[01-076-0606] Ca (C O3) Calcium Carbonate (Aragonite)
180308
Experimental pattern: 6 (6.raw)
[01-076-0606] Ca (C O3) Calcium Carbonate (Aragonite)
180309
Experimental pattern: 7 (7.raw)
[01-076-0606] Ca (C O3) Calcium Carbonate (Aragonite)
180310
Experimental pattern: 8 (8.raw)
[01-076-0606] Ca (C O3) Calcium Carbonate (Aragonite)
Intensity
Cu-Ka (1.541874 A)
2theta

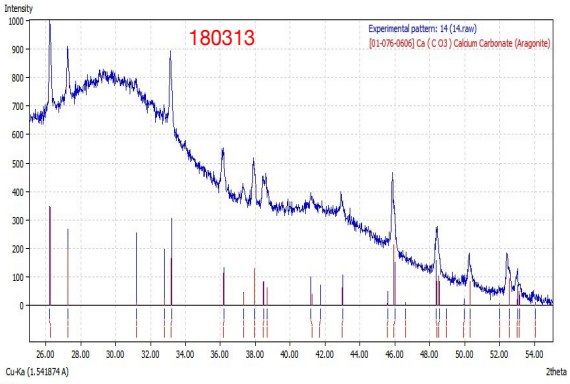

180268
Experimental pattern: 9 (9.raw)
[01-076-0606] Ca (C O3) Calcium Carbonate (Aragonite)
Intensity
Cu-Ka (1.541874 A)
2theta

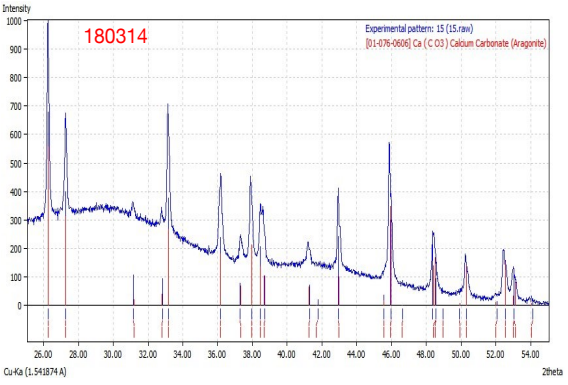

180311
Experimental pattern: 10 (10.raw)
[01-076-0606] Ca (C O3) Calcium Carbonate (Aragonite)
Intensity
Cu-Ka (1.541874 A)
2theta

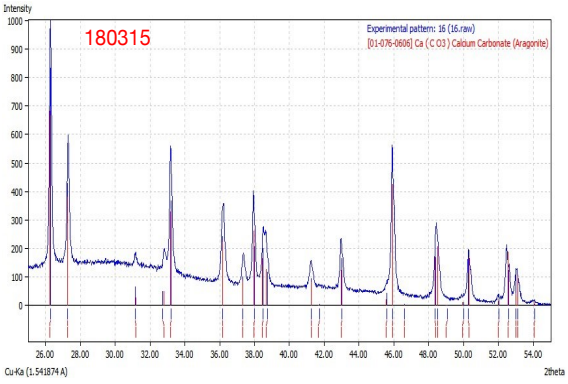

180312
Experimental pattern: 11 (11.raw)
[01-076-0606] Ca (C O3) Calcium Carbonate (Aragonite)
Intensity
Cu-Ka (1.541874 A)
2theta

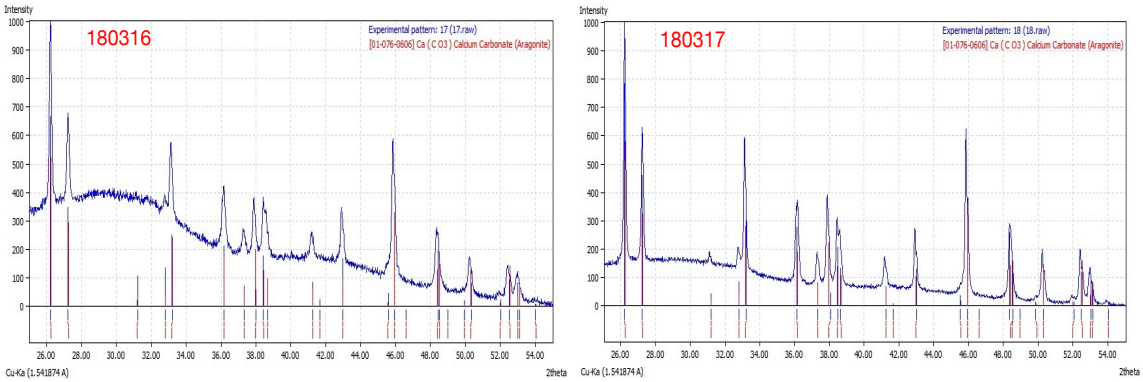

180286
Experimental pattern: 12 (12.raw)
[01-076-0606] Ca (C O3) Calcium Carbonate (Aragonite)
Intensity
Cu-Ka (1.541874 A)
2theta


180272
Experimental pattern: 13 (13.raw)
[01-076-0606] Ca (C O3) Calcium Carbonate (Aragonite)
Intensity
Cu-Ka (1.541874 A)
2theta


180313
Experimental pattern: 14 (14.raw)
[01-076-0606] Ca (C O3) Calcium Carbonate (Aragonite)
Intensity
Cu-Ka (1.541874 A)
2theta


180314
Experimental pattern: 15 (15.raw)
[01-076-0606] Ca (C O3) Calcium Carbonate (Aragonite)
Intensity
Cu-Ka (1.541874 A)
2theta


180315
Experimental pattern: 16 (16.raw)
[01-076-0606] Ca (C O3) Calcium Carbonate (Aragonite)
Intensity
Cu-Ka (1.541874 A)
2theta


Intensity
180316
Experimental pattern: 17 (17.raw)
[01-076-0606] Ca (C O3) Calcium Carbonate (Aragonite)
Cu-Ka (1.541874 A)
2theta
Intensity
180317
Experimental pattern: 18 (18.raw)
[01-076-0606] Ca (C O3) Calcium Carbonate (Aragonite)
Cu-Ka (1.541874 A)
2theta

Appendix C

OxCal Code

C.1 Independent △R

```
Plot()
{
Outlier_Model("General",T(5),U(0,4),"t");
Curve("ShCal13","ShCal13.14c");
Curve("Marine13","Marine13.14c");
Phase()
{
Sequence()
{
Boundary("Start 1");
Phase("1")
{
Curve("=ShCal13");
R_Date("180200", 3868, 50)
{
Outlier(0.05);
};
Curve("=Marine13");
Delta_R("DRCabecuda1",U(-500,500));
R_Date("180303", 3725,30)
{
Outlier(0.05);
};
R_Date("180304", 3750,35)
{
Outlier(0.05);
};
R_Date("180305", 3705,35)
{
Outlier(0.05);
};
};
Boundary("End 1");
};
Sequence()
{
Boundary("Start 3");
Phase("3")
{
Curve("=ShCal13");
R_Date("180201", 3859, 50)
{
Outlier(0.05);
};
Curve("=Marine13");
Delta_R("DRCabecuda3",U(-500,500));
R_Date("180306", 3740,35)
{
Outlier(0.05);
};
R_Date("180307", 3735,30);
{
Outlier(0.05);
};
};
Boundary("End 3");
};
Sequence()
{
Boundary("Start 5");
Phase("5")
{
```

```
Curve("=ShCal13");
R_Date("180202", 4229, 54)
{
Outlier(0.05);
};
Curve("=Marine13");
Delta_R("DRCabecuda5",U(-500,500));
R_Date("180309", 3795,35)
{
Outlier(0.05);
};
R_Date("180310", 3835,30)
{
Outlier(0.05);
};
R_Date("180268", 3675,25);
{
Outlier(0.05);
};
};
Boundary("End 5");
};
Sequence()
{
Boundary("Start 6");
Phase("6")
{
Curve("=ShCal13");
R_Date("180203", 3647, 52)
{
Outlier(0.05);
};
Curve("=Marine13");
Delta_R("DRCabecuda6",U(-500,500));
R_Date("180311", 4035,40)
{
Outlier(0.05);
};
R_Date("180312", 3805,35)
{
Outlier(0.05);
};
};
Boundary("End 6");
};
Sequence()
{
Boundary("Start 7");
Phase("7")
{
Curve("=ShCal13");
R_Date("180253", 3760, 35)
{ Outlier(0.05);
};
Curve("=Marine13");
Delta_R("DRCabecuda7",U(-500,500));
R_Date("180272", 3995,35)
{
Outlier(0.05);
};
R_Date("180313", 3935,35)
{
Outlier(0.05);
};
R_Date("180314", 3985,30)
{
Outlier(0.05);
};
};
Boundary("End 7");
};
Sequence()
{
Boundary("Start 13");
Phase("13")
{
Curve("=ShCal13");
R_Date("180204", 3865, 50)
{
Outlier(0.05);
};
Curve("=Marine13");
Delta_R("DRCabecuda13",U(-500,500));
R_Date("180315", 4085,35)
{
Outlier(0.05);
};
R_Date("180316", 3925,35)
{
Outlier(0.05);
};
R_Date("180317", 4060,30)
{
Outlier(0.05);
};
};
Boundary("End 13");
};
};
};
```

C.2 Common △R (Different Phases)

```
Plot()
{
Outlier_Model("General",T(5),U(0,4),"t");
Curve("ShCal13","ShCal13.14c");
Curve("Marine13","Marine13.14c");
Delta_R("DRCabecuda",U(-500,500));
Phase()
{
Sequence()
{
Boundary("Start 1");
Phase("1")
{
Curve("=ShCal13");
R_Date("180200", 3868, 50)
{
Outlier(0.05);
};
Curve("=Marine13");
Delta_R("=DRCabecuda");
R_Date("180303", 3725,30)
{
Outlier(0.05);
};
R_Date("180304", 3750,35)
{
Outlier(0.05);
};
R_Date("180305", 3705,35)
{
Outlier(0.05);
};
};
Boundary("End 1");
};
Sequence()
{
Boundary("Start 3");
Phase("3")
{
Curve("=ShCal13");
R_Date("180201", 3859, 50)
{
Outlier(0.05);
};
Curve("=Marine13");
Delta_R("=DRCabecuda");
R_Date("180306", 3740,35)
{
Outlier(0.05);
};
R_Date("180307", 3735,30);
{
Outlier(0.05);
};
};
Boundary("End 3");
};
Sequence()
{
Boundary("Start 5");
Phase("5")
{
Curve("=ShCal13");
R_Date("180202", 4229, 54)
{
Outlier(0.05);
};
Curve("=Marine13");
Delta_R("=DRCabecuda");
R_Date("180309", 3795,35)
{
Outlier(0.05);
};
R_Date("180310", 3835,30)
{
Outlier(0.05);
};
R_Date("180268", 3675,25);
{
Outlier(0.05);
};
};
Boundary("End 5");
};
Sequence()
{
Boundary("Start 6");
Phase("6")
{
Curve("=ShCal13");
R_Date("180203", 3647, 52)
{
Outlier(0.05);
};
Curve("=Marine13");
Delta_R("=DRCabecuda");
R_Date("180311", 4035,40)
{
Outlier(0.05);
};
R_Date("180312", 3805,35)
{
Outlier(0.05);
};
};
Boundary("End 6");
};
Sequence()
{
Boundary("Start 7");
Phase("7")
```

```
{
Curve("=ShCal13");
R_Date("180253", 3760, 35)
{
Outlier(0.05);
};
Curve("=Marine13");
Delta_R("=DRCabecuda");
R_Date("180272", 3995,35)
{
Outlier(0.05);
};
R_Date("180313", 3935,35)
{
Outlier(0.05);
};
R_Date("180314", 3985,30)
{
Outlier(0.05);
};
};
Boundary("End 7");
};
Sequence()
{
Boundary("Start 13");
Phase("13")
{
Curve("=ShCal13");
R_Date("180204", 3865, 50)
{
Outlier(0.05);
};
Curve("=Marine13");
Delta_R("=DRCabecuda");
R_Date("180315", 4085,35)
{
Outlier(0.05);
};
R_Date("180316", 3925,35)
{
Outlier(0.05);
};
R_Date("180317", 4060,30)
{
Outlier(0.05);
};
};
Boundary("End 13");
};
};
};
```

C.3 Single Phase △R

```
Plot()
{
Outlier_Model("General",T(5),U(0,4),"t");
Curve("ShCal13","ShCal13.14c");
Curve("Marine13","Marine13.14c");
Delta_R("DRCabecuda",U(-500,500));
Sequence()
{
Boundary("Start 1");
Phase("1")
{
Curve("=ShCal13");
R_Date("180200", 3868, 50)
{
Outlier(0.05);
};
R_Date("180201", 3859, 50)
{
Outlier(0.05);
};
R_Date("180202", 4229, 54)
{
Outlier(0.05);
};
R_Date("180203", 3647, 52)
{
Outlier(0.05);
};
R_Date("180204", 3865, 50)
{
Outlier(0.05);
};
R_Date("180253", 3760, 35)
{
Outlier(0.05);
};
Curve("=Marine13");
Delta_R("=DRCabecuda");
R_Date("180303", 3725,30)
{
Outlier(0.05);
};
R_Date("180304", 3750,35)
{
```

```
Outlier(0.05);
};
R_Date("180305", 3705,35)
{
Outlier(0.05);
};
R_Date("180306", 3740,35)
{
Outlier(0.05);
};
R_Date("180307", 3735,30)
{
Outlier(0.05);
};
R_Date("180309", 3795,35)
{
Outlier(0.05);
};
R_Date("180310", 3835,30)
{
Outlier(0.05);
};
R_Date("180268", 3675,25)
{
Outlier(0.05);
};
R_Date("180311", 4035,40)
{
Outlier(0.05);
};
R_Date("180312", 3805,35)
{
Outlier(0.05);
};
R_Date("180272", 3995,35)
{
Outlier(0.05);
};
R_Date("180313", 3935,35)
{
Outlier(0.05);
};
R_Date("180314", 3985,30)
{
Outlier(0.05);
};
R_Date("180315", 4085,35)
{
Outlier(0.05);
};
R_Date("180316", 3925,35)
{
Outlier(0.05);
};
R_Date("180317", 4060,30)
{
Outlier(0.05);
};
};
Boundary("End 1");
};
};
```

C.4 Single Phase R

```
Plot()
{
Outlier_Model("General",T(5),U(0,4),"t");
Curve("ShCal13","ShCal13.14c");
Delta_R("RCabecuda",U(-500,500));
Sequence()
{
Boundary("Start 1");
Phase("1")
{
Curve("=ShCal13");
R_Date("180200", 3868, 50)
{
Outlier(0.05);
};
R_Date("180201", 3859, 50)
{
Outlier(0.05);
};
R_Date("180202", 4229, 54)
{
Outlier(0.05);
};
R_Date("180203", 3647, 52)
{
Outlier(0.05);
};
R_Date("180204", 3865, 50)
{
Outlier(0.05);
};
R_Date("180253", 3760, 35)
{
Outlier(0.05);
```

```
};
Delta_R("=RCabecuda");
R_Date("180303", 3725,30)
{
Outlier(0.05);
};
R_Date("180304", 3750,35)
{
Outlier(0.05);
};
R_Date("180305", 3705,35)
{
Outlier(0.05);
};
R_Date("180306", 3740,35)
{
Outlier(0.05);
};
R_Date("180307", 3735,30)
{
Outlier(0.05);
};
R_Date("180309", 3795,35)
{
Outlier(0.05);
};
R_Date("180310", 3835,30)
{
Outlier(0.05);
};
R_Date("180268", 3675,25)
{
Outlier(0.05);
};
R_Date("180311", 4035,40)
{
Outlier(0.05);
};
R_Date("180312", 3805,35)
{
Outlier(0.05);
};
R_Date("180272", 3995,35)
{
Outlier(0.05);
};
R_Date("180313", 3935,35)
{
Outlier(0.05);
};
R_Date("180314", 3985,30)
{
Outlier(0.05);
};
R_Date("180315", 4085,35)
{
Outlier(0.05);
};
R_Date("180316", 3925,35)
{
Outlier(0.05);
};
R_Date("180317", 4060,30)
{
Outlier(0.05);
};
};
Boundary("End 1");
};
};
```

C.5 Burials Multiplot

```
Plot()
{
Curve("SHCal13","SHCal13.14c");
Curve("Marine13","Marine13.14c");
Delta_R("LocalMarine",-102,74);
Mix_Curve("Mixed1","SHCal13","LocalMarine",79,4);
R_Date("Burial 1-Mix", 3762, 28);
Curve("=SHCal13");
R_Date("Burial 1-SHCal13", 3762, 28);
Mix_Curve("Mixed3","SHCal13","LocalMarine",82,4);
R_Date("Burial 3-Mix", 3761, 31);
Curve("=SHCal13");
R_Date("Burial 3-SHCal13", 3761, 31);
Mix_Curve("Mixed5","SHCal13","LocalMarine",81,4);
R_Date("Burial 5-Mix", 3768, 29);
Curve("=SHCal13");
R_Date("Burial 5-SHCal13", 3768, 29);
Mix_Curve("Mixed6","SHCal13","LocalMarine",80,4);
R_Date("Burial 6-Mix", 3930, 31);
Curve("=SHCal13");
R_Date("Burial 6-SHCal13", 3930, 31);
Mix_Curve("Mixed13","SHCal13","LocalMarine",74,4);
R_Date("Burial 13-Mix", 3539, 27);
Curve("=SHCal13");
R_Date("Burial 13-SHCal13", 3539, 27);
};
```

C.6 Burials Phase Model

```
Plot()
{
Sequence()
{
Boundary("Start 1");
Phase("1")
{
Curve("SHCal13","SHCal13.14c");
Curve("Marine13","Marine13.14c");
Delta_R("LocalMarine",-102,74);
Mix_Curve("Mixed1","SHCal13","LocalMarine",79,4);
R_Date("Burial 1-Mix", 3762, 28);
Mix_Curve("Mixed3","SHCal13","LocalMarine",82,4);
R_Date("Burial 3-Mix", 3761, 31);
Mix_Curve("Mixed5","SHCal13","LocalMarine",81,4);
R_Date("Burial 5-Mix", 3768, 29);
Mix_Curve("Mixed6","SHCal13","LocalMarine",80,4);
R_Date("Burial 6-Mix", 3930, 31);
Mix_Curve("Mixed13","SHCal13","LocalMarine",74,4);
R_Date("Burial 13-Mix", 3539, 27);
};
Boundary("End 1");
};
};
```

Appendix D

Species habitat

Table D.1: Habitat preferences for some of the mollusc species analysed in this research. The species in the table are commonly found in sambaquis along the Brazilian coast and, therefore, are the most important ones for archaeological studies in these sites. Some names may vary due to nomenclature changes.

Species	Habitat
Amiantis purpuratus (Lamarck, 1818)	sandy bottom at low depths
Anomalocardia brasiliana (Gmelin, 1791)	muddy beaches inside bays or estuaries or in the intertidal region, up to 5 m deep
Atrina seminuda (d'Orbigny, 1846)	muddy and sandy beaches, from 0.3 to 2 m deep
Brachidontes solisianus (d'Orbigny, 1846)	hard substrates in the intertidal zone and on corals, from 0.3 to 2 m deep
Crassostrea rhizophorae (Guilding, 1828)	hard substrates, rocks and roots in the intertidal zone, up to 50 m deep
Divaricella quadrisulcata (d'Orbigny, 1842)	sandy substrates, up to 100 m deep
Donax hilairea Guerin, 1832	sandy beaches in the intertidal zone
Dosinia concentrica (Born, 1778)	sandy bottom, up to 60 m deep
Iphigenia brasiliana (Lamarck, 1818)	muddy or sandy beaches in the intertidal zone or in estuaries
Macoma constricta (Bruguière, 1792)	muddy or sandy beaches in the intertidal zone or in estuaries
Macrocallista maculata (Linnaeus, 1758)	sandy bottoms, up to 100 m deep
Mactra isabelleana d'Orbigny, 1846	sandy bottoms, up to 25 m deep
Mactrellona alata (Spengler, 1802)	sandy or muddy bottoms, up to 20 m deep
Ostrea cristata Born, 1778	hard substrates or calcareous algae, from 35 to 75 m deep
Ostrea equestris Say, 1834	rocks in the intertidal region
Ostrea puelchana d'Orbigny, 1841	rocky or calcareous bottom, from 1 to 100 m deep
Phacoides pectinatus (Gmelin, 1791)	sandy or muddy substrates
Pinctada imbricata Röding, 1798	rocks, corals and roots in shallow waters
Pitar circinatus (Born, 1778)	sandy bottoms in shallow waters
Semele proficua (Pulteney, 1799)	sandy or muddy substrates in the intertidal zone, up to 75 m deep
Tagelus plebeius (Lightfoot, 1786)	sandy or muddy bottoms, close to river mouths, up to 10 m deep
Tellina angulosa Gmelin, 1791	sandy bottoms in the intertidal zone, up to 10 m deep
Tivela mactroides (Born, 1778)	sandy bottoms in shallow waters
Cerithium atratum (Born, 1778)	sandy, muddy or rocky substrates in the intertidal zone, up to 80 m deep
Neritina virginea (Linnaeus, 1758)	muddy bottoms of brackish waters
Olivancillaria urceus (Röding, 1798)	sandy bottoms in the intertidal zone, up to 30 m deep
Olivella formicacorsii Klappenbach, 1962	sandy substrates in shallow waters
Stramonita haemastoma (Linnaeus, 1758)	rocky substrates in the intertidal zone

Bibliography

Faria, L. (1959). O problema da proteção aos sambaquis. *Arquivos do Museu Nacional*, pages 95–138.

Abbott, R. (1974). *American Seashells; The Marine Molluska of the Atlantic and Pacific Coasts of North America*. Van Nostrand Reinhold, New York.

Aerts-Bijma, A., Meijer, H., and van der Plicht, J. (1997). AMS sample handling in Groningen. *Nuclear Instruments and Methods in Physics Research Section B: Beam Interactions with Materials and Atoms*, 123(1-4):221–225.

Agassiz, L. and Agassiz, E. (1868). *A Journey in Brazil*. Ticknor and Fields, Boston.

Aitken, M. (1990). *Science-based dating in archaeology*. Pearson Education.

Albero, M. C., Angiolini, F. E., and Piana, E. (1986). Discordant ages related to reservoir effect of associated archaeologic remains from the tunel site, beagle channel, Argentine Republic. *Radiocarbon*, 28(2):748–753.

Als-Nielsen, J. and McMorrow, D. (2011). *Elements of Modern X-ray Physics*. Jon Wiley & Sons, 2 edition.

Álvarez, M., Briz Godino, I., Balbo, A., and Madella, M. (2011). Shell middens as archives of past environments, human dispersal and specialized resource management. *Quaternary International*, 239:1–7.

Alves, E., Macario, K., Ascough, P., and Bronk Ramsey, C. (2018). The Worldwide Marine Radiocarbon Reservoir Effect: Definitions, Mechanisms, and Prospects. *Reviews of Geophysics*, 56:1–28.

Alves, E., Macario, K., Souza, R., Aguilera, O., Goulart, A., Scheel-Ybert, R., Bachelet, C., Carvalho, C., Oliveira, F., and Douka, K. (2015a). Marine Reservoir Corrections on the Southeastern Coast of Brazil: Paired Samples from the Saquarema Shellmound. *Radiocarbon*, 57(4):517–525.

Alves, E., Macario, K., Souza, R., Pimenta, A., Douka, K., Oliveira, F., Chanca, I., and Angulo, R. (2015b). Radiocarbon Reservoir corrections on the Brazilian coast from pre-bomb marine shells. *Quaternary Geochronology*, 29:30–35.

Amador, E. (1997). *Baía de Guanabara e ecossistemas periféricos: homem e natureza*. Edição do Autor, Rio de Janeiro.

Ambrose, S. H. (1986). Stable carbon and nitrogen isotope analysis of human and animal diet in Africa. *Journal of Human Evolution*, 15(8):707–731.

Ambrose, S. H. (1991). Effects of diet, climate and physiology on nitrogen isotope abundances in terrestrial foodwebs. *Journal of Archaeological Science*, 18:293–317.

Anderson, A. (1991). The Chronology of Colonization in New Zealand. *Antiquity*, 65(249):767–795.

Anderson, E. and Libby, W. (1951). World-Wide Distribution of Natural Radiocarbon. *Physical Review*, 81(1):64–69.

Anderson, E. C., Libby, W. F., Weinhouse, S., Reid, A. F., Kirshenbaum, A. D., and Grosse, A. V. (1947). Natural radiocarbon from cosmic radiation. *Physical Review*, 72(10):931–936.

Angulo, R., Reimer, P., Souza, M., Scheel-Ybert, R., Tenório, M., Disaró, S., and Gaspar, M. (2007). A Tentative Determination of Upwelling Influence on the Paleo-Surficial Marine Water Reservoir Effect in Southeastern Brazil. *Radiocarbon*, 49(3):1255–1259.

Angulo, R. J., de Souza, M. C., Reimer, P. J., and Sasaoka, S. K. (2005). Reservoir effect of the southern and southeastern Brazilian coast. *Radiocarbon*, 47:67–73.

Angulo, R. J., Giannini, P. C. F., Suguio, K., and Pessenda, L. C. R. (1999). Relative sea-level changes in the last 5500 years in southern Brazil (Laguna – Imbituba region, Santa Catarina State) based on vermetid ^{14}C ages. *Marine Geology*, 159:323–339.

Angulo, R. J., Lessa, G. C., and de Souza, M. (2006). A critical review of mid- to late-Holocene sea-level fluctuations on the eastern Brazilian coastline. *Quaternary Science Reviews*, 25:486–506.

Araguas-Araguas, L., Froehlich, K., and Rozanski, K. (2000). Deuterium and oxygen-18 isotope composition of precipitation and atmoshperic moisture. *Hydrological Processes*, 14:1341–1355.

Arneborg, J., Heinemeier, J., Lynnerup, N., Nielsen, H., Rud, N., and Sveinbjornsdottir, A. (1999). Change of Diet of the Greenland Vikings Determined From Stable Carbon Analysis and ^{14}C Dating of their Bones. *Radiocarbon*, 41(2):157–168.

Arnold, J. R. and Libby, W. F. (1949). Age Determinations by Radiocarbon Content : Checks with Samples of Known Age. *Science*, 110:678–680.

Ascough, P., Cook, G., and Dugmore, A. (2005a). Methodological approaches to determining the marine radiocarbon reservoir effect. *Progress in Physical . . .* , 29(4):532–547.

Ascough, P., Cook, G., Dugmore, A., Barber, J., Higney, E., and Scott, E. M. (2004). Holocene Variations in the Scottish Marine Radiocarbon Reservoir Effect. *Radiocarbon*, 46(2):611–620.

Ascough, P., Cook, G., Dugmore, A., Scott, E., and Freeman, S. (2005b). Influence of mollusc species on marine ΔR determinations. *Radiocarbon*, 47(3):433–440.

Austin, W., Bard, E., Hunt, J., Kroon, D., and Peacock, J. (1995). The ^{14}C Age of the Icelandic Vedde Ash: Implications for Younger Dryas Marine Reservoir Age Corrections. *Radiocarbon*, 37(1):53–62.

Bailey, G., Hardy, K., and Camara, A. (2013). Shell energy: an introduction. In Bailey, G., Hardy, K., and Camara, A., editors, *Shell Energy - Mollusc Shells as Coastal Resources*, pages 1–6. Oxbow Books, Oxford.

Bailey, G. and Parkington, J., editors (1988). *The archaeology of prehistoric coastlines*. Cambridge University Press, Cambridge.

Bailey, G. N. (1975). The Role of Molluscs in Coastal Economies : The Results of Midden Analysis in Australia. *Journal of Archaeological Science*, 2:45–62.

Bailey, G. N. (1978). Shell middens as indicators of postglacial economies: a territorial perspective. In Mellars, P., editor, *The Early Postglacial Settlement of Northern Europe*, pages 37–63. Duckworth, London.

Bar-Yosef Mayer, D. E., Leng, M. J., Aldridge, D. C., Arrowsmith, C., Gümüş, B. A., and Sloane, H. J. (2012). Modern and early-middle Holocene shells of the freshwater mollusc Unio, from Çatalhöyük in the Konya Basin, Turkey: Preliminary palaeoclimatic implications from molluscan isotope data. *Journal of Archaeological Science*, 39:76–83.

Bard, E. (1988). Correction of accelerator mass spectrometry ^{14}C ages measured in planktonic foraminifera: paleoceanographic implications. *Paleoceanography*, 3(6):635–645.

Bard, E., Arnold, M., Hamelin, B., Tisnerat-Laborde, N., and Cabioch, G. (1998). Radiocarbon calibration by means of mass spectrometric ^{230}Th/^{234}U and ^{14}C ages of corals: an updated database including samples from Barbados, Mururoa and Tahiti. *Radiocarbon*, 40:1085–1092.

Bard, E., Labeyrie, L., Arnold, M., Labracherie, M., Pichon, J. J., Duprat, J., and Duplessy, J. C. (1989). AMS-^{14}C ages measured in deep sea cores from the Southern Ocean: Implications for sedimentation rates during isotope stage 2. *Quaternary Research*, 31(2):309–317.

Barletta, M., Lima, A. R. A., Dantas, D. V., Oliveira, I. M., Neto, J. R., Fernandes, C. A. F., Farias, E. G. G., Filho, J. L. R., and Costa, M. F. (2017). How Can Accurate Landing Stats Help in

Designing Better Fisheries and Environmental Management for Western Atlantic Estuaries? In *Coastal Wetlands: Alteration and Remediation*, pages 631–703. Springer.

Bastos, M. (2014). *Dos Sambaquis do Sul do Brasil à Diáspora Africana: Estudos de Geoquímica Isotópica de Séries Esqueléticas Humanas Escavadas de Sítio Arqueológicos Brasileiros*. PhD thesis, Universidade de Brasília.

Bastos, M. Q., de Souza, S. M., Santos, R. V., Lima, B. A., Santos, R. V., and Rodrigues-Carvalho, C. (2011). Human mobility on the Brazilian coast: An analysis of strontium isotopes in archaeological human remains from Forte Marechal Luz Sambaqui. *Anais da Academia Brasileira de Ciencias*, 83(2):731–743.

Bastos, M. Q., Santos, R. V., Tykot, R. H., Mendonça de Souza, S. M., Rodrigues-Carvalho, C., and Lessa, A. (2015). Isotopic evidences regarding migration at the archeological site of Praia da Tapera: New data to an old matter. *Journal of Archaeological Science: Reports*, 4:588–595.

Beavan, N. R. and Sparks, R. J. (1998). Factors influencing ^{14}C ages of the pacific rat Rattus exulans. *Radiocarbon*, 40(2):601–613.

Beavan-Athfield, N. R., McFadgen, B. G., and Sparks, R. J. (2001). Environmental influences on dietary carbon and ^{14}C ages in modern rats and other species. *Radiocarbon*, 43(1):7–14.

Bennett, C., Beukens, R., Clover, M., Gove, H., Liebert, R., Litherland, A., Purser, K., and Sondheim, W. (1977). Radiocarbon Dating Using Electrostatic Accelerators: Negative Ions Provide the Key. *Science*, 198.

Berger, R., Taylor, R. E., and Libby, W. F. (1966). Radiocarbon Content of Marine Shells from the California and Mexican West Coast. *Science (New York, N.Y.)*, 153(3738):864–6.

Berkman, P. A. and Forman, S. L. (1996). Pre-bomb radiocarbon and the reservoir correction for calcareous marine species in the Southern Ocean. *Geophysical Research Letters*, 23(4):363–366.

Bethe, H. A., Korff, S. A., and Placzek, G. (1940). On the interpretation of neutron measurements in cosmic radiation. *Physical Review*, 57(7):573–587.

Beukens, R. P. (1990). High-precision intercomparison at IsoTrace. *Radiocarbon*, 32(3):335–339.

Bisbal, G. A. (1995). The Southeast South American shelf large marine ecosystem. Evolution and components. *Marine Policy*, 19(1):21–38.

Bjoerck, S., Hjort, C., Ingolfsson, O., and Skog, G. (1991). Radiocarbon dates from the Antarctic Peninsula region-problems and potential. In Lowe, J. J., editor, *Radiocarbon Dating: Recent Applications and Future Potential, Quaternary Proceedings*. Quaternary Research Association, Cambridge.

Blau, M., Deevey, E. S., and Gross, M. S. (1953). Yale natural radiocarbon measurements, I. Pyramid Valley, New Zealand, and its problems. *Science*, 118:1–6.

Blockley, S. and Housley, R. (2009). Calibration commentary. *Radiocarbon*, 51(1):287–290.

Boehs, G. and Magalhães, A. R. M. (2004). Simbiontes associados com Anomalocardia brasiliana (Gmelin) (Mollusca, Bivalvia, Veneridae) na Ilha de Santa Catarina e região continental adjacente, Santa Catarina, Brasil.

Bolin, B. and Fung, I. (1992). Report: The carbon cycle revisited. *Modeling the Earth system*, pages 151–164.

Bondevik, S., Mangerud, J., Birks, H., Gulliksen, S., and Reimer, P. (2006). Changes in North Atlantic Radiocarvon Reservoir Ages During the Allerod and Younger Dryas. *Science*, 312:1514–1517.

Boyadjian, C. and Eggers, S. (2014). Micro-Remains Trapped in Dental Calculus Reveal Plants Consumed by Brazilian Shell-Mound Builders. In Roksandic, M., Souza, S., Eggers, S., Burchell, M., and Klokler, D., editors, *The Cultural Dynamics of Shell-Matrix Sites*, pages 279–288. University of New Mexico Press, Albuquerque.

Boyadjian, C., Eggers, S., Reinhard, K., and Scheel-Ybert, R. (2016). Dieta no Sambaqui de Jabuticabeira-II (SC): Consumo de Plantas Revelado por Microvestígios Provenientes de Cálculo Dentário. *Cadernos do Lepaarq*, XIII(25).

Braje, T., Erlandson, J., and Rick, T. (2014). Factors influencing the formation of large shell mounds in California's Santa Barbara Channel Region. In Roksandic, M., Souza, S., Eggers, S., Burchell, M., and Klokler, D., editors, *The Cultural Dynamics of Shell-Matrix Sites*, pages 1–10. University of New Mexico Press, Albuquerque.

Brock, F., Higham, T., Ditchfield, P., and Ramsey, C. B. (2010). Current Pretreatment Methods for AMS Radiocarbon Dating at the Oxford Radiocarbon Accelerator Unit (ORAU). *Radiocarbon*, 52(1):103–112.

Broecker, W. (1991). The Great Ocean Conveyor. *Oceanography*, 4(2):79–89.

Broecker, W. and Barker, S. (2007). A 190‰ drop in atmosphere's $\Delta^{14}C$ during the "Mystery Interval" (17.5 to 14.5 kyr). *Earth and Planetary Science Letters*, 256(1-2):90–99.

Broecker, W., Gerard, R., Ewing, M., and Heezen, B. (1960). Natural Radiocarbon in the Atlantic Ocean. *Journal of Geophysical Research*, 65(9).

Broecker, W. S., Peng, T. H., Ostlund, G., and Stuiver, M. (1985a). The distribution of bomb radiocarbon in the ocean. *Journal of Geophysical Research*, 90(C4):14331.

Broecker, W. S., Peteet, D. M., and Rind, D. (1985b). Does the ocean-atmosphere system have more than one stable mode of operation? *Nature*, 315:21–26.

Bronk Ramsey, C. (1995). Radiocarbon Calibration and Analysis of Stratigraphy: the OxCal Program. *Radiocarbon*, 37(2):425–430.

Bronk Ramsey, C. (2001). Development of the radiocarbon calibration program. *Radiocarbon*, 43(2):355–363.

Bronk Ramsey, C. (2009). Bayesian Analysis of Radiocarbon Dates. *Radiocarbon*, 51:337–360.

Bronk Ramsey, C. (2013). Recent and Planned Developments of the Program OxCal. *Radiocarbon*, 55(3–4):720–730.

Bronk Ramsey, C., Buck, C. E., Manning, S. W., Reimer, P., and Plicht, H. V. D. (2015). Developments in radiocarbon calibration for archaeology. *Antiquity*, 80(310):783–798.

Bronk Ramsey, C. and Hedges, R. (1997). Hybrid ion sources: Radiocarbon measurements from microgram to milligram. *Nuclear Instruments and Methods in Physics Research Section B: Beam Interactions with Materials and Atoms*, 123(1-4):539–545.

Bronk Ramsey, C., Higham, T., and Leach, P. (2004). Towards high-precision AMS: Progress and Limitations. 46(1):17–24.

Brown, T. A., Nelson, D. E., Vogel, J. S., and Southon, J. R. (1988). Improved collagen extraction by modified Longin method. *Radiocarbon*, 30(2):171–177.

Bruhns, K. (1994). *Ancient South America*. Cambridge University Press.

Bruns, M., Levin, I., Munnich, K. ., Hubberten, H. H., and Fillipakis, S. (1980). Regional Sources of Volcanic Carbon Dioxide and their Influence on ^{14}C Content of Present-Day Plant Material. *Radiocarbon*, 22(2):532–536.

Burchell, M., Hallmann, N., Schone, B., Cannon, A., and Schwarcz, H. (2014). Biogeochemical Signatures of Marine and Estuarine Bivalves: Implications for Interpreting Seasonality at Shell-Midden Sites Using High-Resolution Stable Isotope Sclerochronology. In Roksandic, M., Souza, S., Eggers, S., Burchell, M., and Klokler, D., editors, *The Cultural Dynamics of Shell-Matrix Sites*, pages 241–249. University of New Mexico Press, Albuquerque.

Burman, J. and Schmitz, B. (2005). Proxy Periwinkle (Littorina littorea) intrashell δ^{18}O and δ^{13}C records from the mid- Holocene Limfjord region, Denmark: a new high-resolution palaeoenvironmental proxy approach. *The Holocene*, 15(4):567–575.

Butzin, M., Köhler, P., and Lohmann, G. (2017). Marine radiocarbon reservoir age simulations for the past 50,000 years. *Geophysical Research Letters*, 44(16):8473–8480.

Butzin, M., Prange, M., and Lohmann, G. (2005). Radiocarbon simulations for the glacial ocean: The effects of wind stress, Southern Ocean sea ice and Heinrich events. *Earth and Planetary Science Letters*, 235(1-2):45–61.

Byrne, C., Dotte-Sarout, E., and Winton, V. (2013). Charcoals as indicators of ancient tree and fuel strategies: An application of anthracology in the Australian Midwest. *Australian Archaeology*, 77:94–106.

Calado, L., da Silveira, I. C., Gangopadhyay, A., and de Castro, B. M. (2010). Eddy-induced upwelling off Cape São Tomé (22°S, Brazil). *Continental Shelf Research*, 30(10-11):1181–1188.

Calvin, M. and Benson, A. (1948). The Path of Carbon in Photosynthesis. *Science*, 107:476–480.

Carvalho, C., Macario, K., Oliveira, M. D., Oliveira, F., Chanca, I., Alves, E., Souza, R., Aguilera, O., and Douka, K. (2015). Potential Use of Archaeological Snail Shells for the Calculation of Local Marine Reservoir Effect. *Radiocarbon*, 57(3):459–467.

Castagnoli, G. and Lal, D. (1980). Solar modulation effects in terrestrial production of carbon-14. *Radiocarbon*, 22(2):133–158.

Castelao, R. M. and Barth, J. A. (2006). Upwelling around Cabo Frio, Brazil: The importance of wind stress curl. *Geophysical Research Letters*, 33(3):2–5.

Castro Faria, L. (1952). Pesquisas de Antropologia Física no Brasil. *Boletim do Museu Nacional - Série Antropologia*, 13:1–106.

Castro Faria, L. (1955). Le problème des sambaquis du Brésil: recentes excavations du gisement de Cabeçuda (Laguna, Santa Catarina). In *Anais do XXXI Congresso Internacional de Americanistas*, pages 569–577.

Ceci, L. (1984). Shell midden deposits as coastal resources. *World Archaeology*, 16(1):62–74.

Chappell, J. and Polach, H. (1972). Some Effects of Partial Recrystallisation on ^{14}C Dating Late Pleistocene Corals and Molluscs. *Quaternary Research*, 252.

Chauvaud, L., Lorrain, A., Dunbar, R. B., Paulet, Y. M., Thouzeau, G., Jean, F., Guarini, J. M., and Mucciarone, D. (2005). Shell of the Great Scallop Pecten maximus as a high-frequency archive of paleoenvironmental changes. *Geochemistry, Geophysics, Geosystems*, 6(8):1–15.

Chelton, D. B., Schlax, M. G., Witter, D. L., and Richman, J. G. (1990). Geosat altimeter observations of the surface circulation of the Southern Ocean. *Journal of Geophysical Research*, 95(C10):17877–17903.

Cheney, R. E., Marsh, J. G., and Beckley, B. D. (1983). Global mesoscale variability from collinear tracks of SEASAT altimeter data. *Journal of Geophysical Research*, 88(C7):4343–4354.

Chiessi, C. M., Ulrich, S., Mulitza, S., Pätzold, J., and Wefer, G. (2007). Signature of the Brazil-Malvinas Confluence (Argentine Basin) in the isotopic composition of planktonic foraminifera from surface sediments. *Marine Micropaleontology*, 64(1-2):52–66.

Chisholm, B., Nelson, D. E., and Schwarcz, H. P. (1982). Stable-carbon isotope ratios as a measure of marine versus terestrial protein in ancient diets. *Science*, 216:11131–1132.

Claassen, C. (1991). Normative Thinking and Shell-Bearing Sites. *Archaeological Method and Theory*, 3:249–298.

Claassen, C. (2013). Invertebrates on San Salvador Island, Bahamas: the use of shellfish as bait. In Bailey, G., Hardy, K., and Camara, A., editors, *Shell Energy - Mollusc Shells as Coastal Resources*, pages 59–67. Oxbow Books, Oxford.

Clarke, E. T. and Korff, S. A. (1941). The Radiosonde: The Stratosphere Laboratory. *J. Frank. Inst.*, 232(4):339–355.

Clayton, R. N. (1961). Oxygen isotope fractionation between calcium carbonate and water. *The Journal of Chemical Physics*, 34(3):724–726.

Clilverd, M., Clarke, E., Clark, T., Rishbeth, H., and Ulich, T. (2004). . . . and a reply. *Astronomy & Geophysics*, 45:2.7.

Clilverd, M., Clarke, E., Rishbeth, H., Clarck, T., and Ulich, T. (2003). Solar activity levels in 2100. *Astronomy & Geophysics*, 44:5.20–5.22.

Collins, M. J., Hiller, J., Smith, C. I., Roberts, J. P., Prigodich, R. V., Wess, T. J., and Millard, A. R. (2002). The Survival of Organic Matter in Bone: A Review. *Archaeometry*, 3(44):383–394.

Colonese, A. C., Collins, M., Lucquin, A., Eustace, M., Hancock, Y., Ponzoni, R. D. A. R., Mora, A., Smith, C., DeBlasis, P., Figuti, L., Wesolowski, V., Plens, C. R., Eggers, S., De Farias, D. S. E., Gledhill, A., and Craig, O. E. (2014). Long-term resilience of late Holocene coastal subsistence system in southeastern South America. *PLoS ONE*, 9(4):1–13.

Colonese, C., Netto, S., Francisco, A., Deblasis, P., Villagran, X. S., Ponzoni, R., Hancock, Y., Hausmann, N., Farias, D., Prendergast, A., Schöne, B. R., Francisco, W. C., and Fonseca, P. C. G. (2017). Shell sclerochronology and stable isotopes of the bivalve Anomalocardia flexuosa (Linnaeus , 1767) from southern Brazil : Implications for environmental and archaeological studies. *Palaeogeography, Palaeoclimatology, Palaeoecology*, 484:7–21.

Commendador, A. (2014). Radiocarbon Dating Human Skeletal Material on Rapa Nui: Evaluating the Effect of Uncertainty in Marine-Derived Carbon. *Radiocarbon*, 56(1):277–294.

Cook, G. T., Ascough, P. L., Bonsall, C., Hamilton, W. D., Russell, N., Sayle, K. L., Scott, E. M., and Bownes, J. M. (2015). Best practice methodology for ^{14}C calibration of marine and mixed terrestrial/marine samples. *Quaternary Geochronology*, 27:164–171.

Cook, G. T., Scott, E. M., and Harkness, D. D. (2009). *Chapter 4 Radiocarbon as a Tracer in the Global Carbon Cycle*, volume 16.

Coplen, T. B. (1994). Reporting of stable hydrogen, carbon, and oxygen isotopic abundances (Technical Report). *Pure and Applied Chemistry*, 66(2):273–276.

Corfield, R. (2003). *The silent landscape: the scientific voyage of HMS Challenger*. Joseph Henry Press.

Costa Santos, S., Brandini, N., Cotovicz Jr, L., Costa, L., Abril, G., and Knoppers, B. (2015). Evaluation of the trophic state of Guanabara Bay, SE-Brazil, wih the TRIX and O'Boyle Indices. In *XIII International Estuarine Biogeochemistry Symposium*, Bordeaux.

Cotovicz Junior, L. (2016). *Concentrations and atmospheric exchanges of carbon dioxide (CO_2) and methane (CH_4) in a tropical eutrophic estuary (Guanabara Bay, RJ, Brazil)*. PhD thesis, Université de Bordeaux.

Craig, H. (1953). The geochemistry of the stable carbon isotopes. *Geochimica et Cosmochimica Acta*, 3:53–92.

Craig, H. (1954). Carbon 13 in Plants and the Relationships between Carbon 13 and Carbon 14 Variations in Nature. *The Journal of Geology*, 62(2):115–149.

Craig, H. (1957). The Natural Distribution of Radiocarbon and the Exchange Time of Carbon Dioxide Between Atmosphere and Sea. *Tellus A*, 9(I):1–17.

Craig, H. (1965). The measurement of oxygen isotope palaeotemperatures. In Tongiori, E., editor, *Stable Isotopes in Oceanographic Studies and Paleotemperatures*, pages 161–182. Consiglio Nazionale delle Ricerche Laboratorio di Geologia Nucleare, Pisa.

Culleton, B. J., Kennett, D. J., Ingram, B. L., Erlandson, J. M., and Southon, J. R. (2006). Intrashell radiocarbon variability in marine mollusks. *Radiocarbon*, 48(3):387–400.

Damon, P. E., Lerman, J. C., and Long, A. (1978). Temporal Fluctuations of Atmospheric ^{14}C: Causal Factors and Implications. *Annual Review of Earth and Planetary Sciences*, 6(1):457–494.

Dansgaard, W. (1964). Stable isotopes in precipitation. *Tellus*, 16(4):436–468.

David, A. (1995). *The Voyage of HMS Herald to Australia and the South-west Pacific, 1852-1861 Under the Command of Captain Henry Mangles Denham*. Melbourne University Press.

de Castilho, P. V. (2008). Utilization of cetaceans in shell mounds from the southern coast of Brazil. *Quaternary International*, 180(1):107–114.

De Niro, M. and Epstein, S. (1978). Influence of diet on the distribution of carbon isotopes in animals. *Geochimica et Cosmochimica Acta*, 42:495–506.

de Souza, R., Lima, T., and da Silva, E. (2011). *Conchas Marinhas de Sambaquis do Brasil*. Technical Books.

de Vries, H. (1958). Variation in concentration of radiocarbon with time and location on earth. *Proceedings of the Koninklijke Nederlandse Akademie Van Weten- schappen Series B-Palaeontology Geology Physics Chemistry Anthropology*, B61:94–102.

DeBlasis, P., Fish, S. K., Gaspar, M. D., and Fish, P. R. (1998). Some references for the discussion of complexity among the sambaqui moundbuilders from the southern shores of Brazil. *Revista de Arqueologia Americana*, (15):75–105.

DeBlasis, P., Kneip, A., Scheel-Ybert, R., Giannini, P. C., and Gaspar, M. D. (2007). Sambaquis e Paisagem - Dinâmica natural e arqueologia regional no litoral do sul do Brasil. *Arqueología Suramericana*, 3(1):29–61.

Dee, M. and Bronk Ramsey, C. (2000). Refinement of graphite target production at ORAU. *Nuclear Instruments and Methods in Physics Research Section B: Beam Interactions with Materials and Atoms*, 172:449–453.

Deevey, E. S., Gross, M. S., Hutchinson, G. E., and Kraybill, H. L. (1954). The natural ^{14}C contents of materials from hard-water lakes. *Geology*, 40:285–288.

Deforce, K., Boeren, I., Adriaenssens, S., Bastiaens, J., De Keersmaeker, L., Haneca, K., Tys, D., and Vandekerkhove, K. (2013). Selective woodland exploitation for charcoal production. A detailed analysis of charcoal kiln remains (ca. 1300-1900 AD) from Zoersel (northern Belgium). *Journal of Archaeological Science*, 40(1):681–689.

Dehling, H. and van der Plicht, J. (1993). Statistical Problems in Calibrating Radiocarbon Dates. *Radiocarbon*, 35(1):239–244.

del Giorgio, P. A. and Duarte, C. M. (2002). Respiration in the open ocean. *Nature*, 420(6914):379–384.

DeNiro, M. J. and Epstein, S. (1981). Influence of diet on the distribution of nitrogen isotopes in animals. *Geochimica et Cosmochimica Acta*, 45:341–351.

Deo, J. N., Stone, J. O., and Stein, J. K. (2004). Building Confidence in Shell : Variations in the Marine Radiocarbon Reservoir Correction for the Northwest Coast over the past 3 , 000 Years. *American Antiquity*, 69(4):771–786.

Detienne, P. and Jacquet, P. (1983). *Atlas d'identification des bois de l'Amazonie et des regions voisines*. Centre Technique Forestier Tropical, France.

Dettman, D., Reische, A., and Lohmann, K. (1999). Controls on the stable isotope composition of seasonal growth bands in aragonitic fresh-water bivalves (unionidae). *Geochimica et Cosmochimica Acta*, 63(7/8):1049–1057.

Donahue, D. J., Jull, A. J. T., and Toolin, L. J. (1990). Radiocarbon measurements at the University of Arizona AMS facility. *Nuclear Inst. and Methods in Physics Research, B*, 52(3-4):224–228.

Doney, S. C., Fabry, V. J., Feely, R. A., and Kleypas, J. A. (2009). Ocean Acidification: The Other CO_2 Problem. *Annual Review of Marine Science*, 1(1):169–192.

Douka, K., Hedges, R. M., and Higham, T. G. (2010). Improved AMS ^{14}C Dating of Shell Carbonates Using High-Precision X-Ray Diffraction and a Novel Density Separation Protocol (CarDS). *Radiocarbon*, 52(2):735–751.

Dufour, E., Bocherens, H., and Mariotti, A. (1999). Palaeodietary implications of isotopic variability in Eurasian lacustrine fish. *Journal of Archaeological Science*, 26(6):617–627.

Dye, T. (1994). Apparent ages of marine shells: implications for archaeological dating in Hawai'i. *Radiocarbon*, 36(1):51–57.

Eastoe, C. J., Fish, S., Fish, P., Dulce Gaspar, M., and Long, A. (2002). Reservoir corrections for marine samples from the South Atlantic Coast, Santa Catarina state, Brazil. *Radiocarbon*, 44:145–148.

Emery-Barbier, A. and Thiébault, S. (2005). Preliminary conclusions on the Late Glacial vegetation in south-west Anatolia (Turkey): The complementary nature of palynological and anthracological approaches. *Journal of Archaeological Science*, 32(8):1232–1251.

Emilsson, I. (1961). The shelf and coastal waters off southern Brazil *. *Boletim do Instituto Oceanográfico*, 11(2):101–112.

Emperaire, J. and Laming-Emperaire, A. (1956). Les sambaquis de la côte méridionale du Brésil (campagnes de fouilles 1954-1956). *Journal de la Société des Américanistes (nouvelle série)*, 45:5–164.

Enmar, R., Stein, M., Bar-Matthews, M., Sass, E., Katz, A., and Lazar, B. (2000). Diagenesis in live corals from the Gulf of Aqaba. I. The effect on paleo-oceanography tracers. *Geochimica et Cosmochimica Acta*, 64(18):3123–3132.

Epstein, S., Buchsbaum, H., Lowenstam, H., and Urey, H. (1953). Revised Carbonate-Water Isotopic Temperature Scale. *Bulletin of the Geological Society of America*, 64:1315–1326.

Epstein, S., Buchsbaum, R., Lowenstam, H., and Urey, H. (1951). Carbonate-Water Isotopic Temperature Scale. *Bulletin of the Geological Society of America*, 62(April):417–426.

Epstein, S. and Mayeda, T. (1953). Variation of O^{18} content of waters from natural sources. *Geochimica et Cosmochimica Acta*, 4:213–224.

Eriksson, G. (2013). Stable Isotope Analysis of Humans. In Stutz, L. N. and Tarlow, S., editors, *The Oxford Handbook of the Archaeology of Death and Burial*. Oxford University Press.

Erlandson, J. (1988). The Role of Shellfish in Prehistoric Economies: A Protein Perspective. *American Antiquity*, 53(1):102–109.

Erlandson, J. O. N. M., Kennett, D. J., Ingram, B. L., Guthrie, D. A., Morris, D. O. N. P., Tveskov, M. A. T., West, G. J., and Walker, P. L. (1996). An Archaeological and Paleontological Chronology for Daisy Cave (CA-SMI-261), San Miguel Island, California. *Radiocarbon*, 38(2):355–373.

Ervynck, A. (2014). Dating Human Remains from the Historical Period in Belgium: Diet Changes and the Impact of Marine and Freshwater Reservoir Effects. *Radiocarbon*, 56(2):779–788.

Euba, I., Allué, E., and Burjachs, F. (2016). Wood uses at El Mirador Cave (Atapuerca, Burgos) based on anthracology and dendrology. *Quaternary International*, 414:285–293.

Facorellis, Y. (1998). Apparent ^{14}C ages of marine mollusk shells from a Greek Island : Calculation of the marine reservoir effect in the Aegean Sea. *Radiocarbon*, 40(2):963–973.

Facorellis, Y. and Vardala-Theodorou, E. (2015). Sea surface radiocarbon reservoir age changes in the aegean sea from about 11,200 BP to present. *Radiocarbon*, 57(3):493–505.

Fairbanks, R. G., Mortlock, R. A., Chiu, T. C., Cao, L., Kaplan, A., Guilderson, T. P., Fairbanks, T. W., Bloom, A. L., Grootes, P. M., and Nadeau, M. J. (2005). Radiocarbon calibration curve spanning 0 to 50,000 years BP based on paired $^{230}Th/^{234}U/^{238}U$ and ^{14}C dates on pristine corals. *Quaternary Science Reviews*, 24:1781–1796.

Falkowski, P., Scholes, R., Boyle, E., Canadell, J., Canfield, D., Elser, J., Gruber, N., Hibbard, K., Hogberg, P., Linder, S., Mackenzie, F., Moore III, B., Pedersen, T., Rosenthal, Y., Seitzinger, S., Smetacek, V., and Steffen, W. (2000). The Global Carbon Cycle: A Test of Our Knowledge of Earth as a System. *Science*, 290(5490):291–296.

Fallon, S. J., Fifield, L. K., and Chappell, J. M. (2010). The next chapter in radiocarbon dating at the Australian National University: Status report on the single stage AMS. *Nuclear Instruments and Methods in Physics Research, Section B: Beam Interactions with Materials and Atoms*, 268(7-8):898–901.

Feigl, F. (1958). *Spot Tests in Inorganic Analysis*. Elsevier, Amsterdam.

Fenger, T., Surge, D., Schöne, B., and Milner, N. (2007). Sclerochronology and geochemical variation in limpet shells (Patella vulgata): A new archive to reconstruct coastal sea surface temperature. *Geochemistry, Geophysics, Geosystems*, 8(7).

Ferigolo, J. (1987). *Paleopatologia comparada de vertebrados: "Homem de Lagoa Santa", "Homem do Sambaqui Cabeçuda" e Mamíferos Pleistocênicos*. PhD thesis, UFRGS.

Fernandes, R. (2016). A Simple(r) Model to Predict the Source of Dietary Carbon in Individual Consumers. *Archaeometry*, 58(3):500–512.

Fernandes, R., Grootes, P., Nadeau, M. J., and Nehlich, O. (2015). Quantitative diet reconstruction of a Neolithic population using a Bayesian mixing model (FRUITS): The case study of Ostorf (Germany). *American Journal of Physical Anthropology*, 158(2):325–340.

Fernandes, R., Millard, A. R., Brabec, M., Nadeau, M. J., and Grootes, P. (2014). Food reconstruction using isotopic transferred signals (FRUITS): A bayesian model for diet reconstruction. *PLoS ONE*, 9(2):1–9.

Fernandes, R., Nadeau, M. J., and Grootes, P. M. (2012). Macronutrient-based model for dietary carbon routing in bone collagen and bioapatite. *Archaeological and Anthropological Sciences*, 4(4):291–301.

Fifield, L. K. (1999). Accelerator mass spectrometry and its applications. *Reports on Progress in Physics*, 62:1223–1274.

Figuti, L. (1993). O Homem Pré-Histórico, o Molusco e o Sambaqui: Considerações Sobre a Subsistência dos Povos Sambaquieiros. *Rev. do Museu de Arqueologia e Etnologia*, 3:67–80.

Figuti, L. (2008). A Recipe for a Sambaqui: Considerations on Brazilian Shell Mound Composition and Building. *Early human impact on megamolluscs*, (January 2005):67–80.

Figuti, L. and Plens, C. (2014). The Riverine Sambaqui: Zooarchaeological Studies of Inland Brazilian Shell Mounds. In Roksandic, M., Souza, S., Eggers, S., Burchell, M., and Klokler, D., editors, *The Cultural Dynamics of Shell-Matrix Sites*, pages 213–222. University of New Mexico Press, Albuquerque.

Fish, P., Fish, S., DeBlasis, P., and Gaspar, M. (2013). Monumental Shell Mounds as Persistent Places in Southern Brazil. In Thompson, V. and Waggoner Jr, J., editors, *The Archaeology and Historical Ecology of Small Scale Economies*, pages 120–140. University of Florida Press, Gainesville.

Fonseca, G. and Netto, S. A. (2006). Shallow Sublittoral Benthic Communities of The Laguna Estuarine System, South Brazil. *Brazilian Journal of Oceanography*, 54(1):41–54.

Forman, S. L. and Polyak, L. (1997). Radiocarbon content of pre-bomb marine mollusks and variations in the ^{14}C reservoir age for coastal areas of the Barents and Kara seas Russia. *Geophysical Research Letters*, 24(8):885–888.

Fornari, M., Giannini, P., and Nascimento Junior, D. (2012). Facies associations and controls on the evolution from a coastal bay to a lagoon system, Santa Catarina Coast, Brazil. *Marine Geology*, 323-325:56–68.

Friederich, G. E., Ledesma, J., Ulloa, O., and Chavez, F. P. (2008). Air-sea carbon dioxide fluxes in the coastal southeastern tropical Pacific. *Progress in Oceanography*, 79(2-4):156–166.

Friedman, G. (1959). Identification of carbonate minerals by staining methods. *Journal of Sedimentary Petrology*, 29(1):87–97.

Fry, B. (2006). *Stable Isotope Ecology*. Springer, New York.

Galetti, M., Rodarte, R. R., Neves, C. L., Moreira, M., and Costa-Pereira, R. (2016). Trophic niche differentiation in rodents and marsupials revealed by stable isotopes. *PLoS ONE*, 11(4):1–15.

Galli, I., Bartalini, S., Ballerini, R., Barucci, M., Cancio, P., De Pas, M., Giusfredi, G., Mazzotti, D., Akikusa, N., and De Natale, P. (2016). Spectroscopic detection of radiocarbon dioxide at parts-per-quadrillion sensitivity. *Optica*, 3(4):385.

Galli, I., Bartalini, S., Borri, S., Cancio, P., Mazzotti, D., De Natale, P., and Giusfredi, G. (2011). Molecular gas sensing below parts per trillion: Radiocarbon-dioxide optical detection. *Physical Review Letters*, 107(27):1–4.

Galli, I., Bartalini, S., Cancio, P., De Natale, P., Mazzotti, D., Giusfredi, G., Fedi, M. E., Mandò, P. A., and Mando, P. A. (2013). Optical detection of radiocarbon dioxide: First results and AMS intercomparison. *Radiocarbon*, 55(2-3):213–223.

Garzoli, S. and Garrafo, Z. (1989). Transports, frontal motions and eddies at the Brazil-Malvinas Currents Confluence. *Deep Sea Research*, 36(5):681–703.

Garzoli, S. L. and Giulivi, C. (1994). What forces the variability of the southwestern Atlantic boundary currents? *Deep-Sea Research Part I*, 41(10):1527–1550.

Gaspar, M. (1998). Considerations of the sambaquis of the Brazilian coast. *Antiquity*, 72(1998):592–615.

Gaspar, M. (2000). *Sambaqui: arqueologia do litoral brasileiro*. Jorge Zahar Editor, Rio de Janeiro.

Gaspar, M., DeBlasis, P., Fish, S., and Fish, P. (2008). Sambaqui (Shell Mound) Societies of Coastal Brazil. In Silverman, H. and Isbell, W., editors, *Handbook of South American Archaeology*, pages 319–335. Springer.

Gaspar, M., Klokler, D., and DeBlasis, P. (2014). Were Sambaqui People Buried in Trash? Archaeology, Physical Anthropology, and the Evolution of the Interpretation of Brazilian Shell Mounds. In Roksandic, M., Souza, S., Eggers, S., Burchell, M., and Klokler, D., editors, *The Cultural Dynamics of Shell-Matrix Sites*, pages 91–100. University of New Mexico Press, Albuquerque.

Gaspar, M. D. (2004). Cultura: Comunicação, arte, oralidade na pré-história do Brasil. *Rev. do Museu de Arqueologia e Etnologia*, 14:153–168.

Gat, J. R. (1996). Oxygen and Hydrogen Isotopes in the Hydrologic Cycle. *Annual Review of Earth and Planetary Sciences*, 24(1):225–262.

Gaudinski, J. B., Trumbore, S. E., Davidson, E. A., and Zheng, S. (2000). Soil carbon cycling in a temperate forest: Radiocarbon-based estimates of residence times, sequestration rates and partitioning of fluxes. *Biogeochemistry*, 51:33–69.

Gavin, D. G. (2001). Estimation of inbuilt age in radiocarbon ages of soil charcoal for fire history studies. *Radiocarbon*, 43(1):27–44.

Geiger, H. and Müller, W. (1929). Technische Bemerkungen zum Elektronenzählorohr. *Physikalische Zeitschrift*.

Giannini, P. C., Villagran, X. S., Fornari, M., Nascimento Jr, D. R., Menezes, P., Tanaka, A. P., Assunçao, D., De Blasis, P., and Amaral, P. (2010). Interações entre evolução sedimentar e ocupação humana pré-histórica na costa centro-sul de Santa Catarina, Brasil. *Boletim do Museu Paraense Emílio Goeldi. Série Ciências Humanas*, 5(1):105–128.

Gillespie, R. (1984). *Radiocarbon User's Handbook*.

Gillespie, R. and Hedges, R. (1984). Accelerator mass spectrometry. *Nuclear Instruments and Methods in Physics Research B*, 5:294–296.

Gillikin, D. P., De Ridder, F., Ulens, H., Elskens, M., Keppens, E., Baeyens, W., and Dehairs, F. (2005). Assessing the reproducibility and reliability of estuarine bivalve shells (Saxidomus giganteus) for sea surface temperature reconstruction: Implications for paleoclimate studies. *Palaeogeography, Palaeoclimatology, Palaeoecology*, 228:70–85.

Gillikin, D. P., Lorrain, A., Bouillon, S., Willenz, P., and Dehairs, F. (2006). Stable carbon isotopic composition of Mytilus edulis shells: relation to metabolism, salinity, $\delta^{13}C_{DIC}$ and phytoplankton. *Organic Geochemistry*, 37:1371–1382.

Gillikin, D. P., Lorrain, A., Meng, L., and Dehairs, F. (2007). A large metabolic carbon contribution to the $\delta^{13}C$ record in marine aragonitic bivalve shells. *Geochimica et Cosmochimica Acta*, 71(12):2936–2946.

Godwin, H. (1951). Comments on radiocarbon dating for samples from the British Isles. *American Journal of Science*, 249:301–307.

Godwin, H. (1962). Half-Life of Radiocarbon.

Goewert, A., Surge, D., Carpenter, S. J., and Downing, J. (2007). Oxygen and carbon isotope ratios of Lampsilis cardium (Unionidae) from two streams in agricultural watersheds of Iowa, USA. *Palaeogeography, Palaeoclimatology, Palaeoecology*, 252(3-4):637–648.

Goh, K. and Molloy, B. (1972). Reliability of radiocarbon dates from buried charcoals. In *Proceedings of the 8th International Conference on Radiocarbon Dating*, Wellington. The Royal Society of New Zealand.

Gómez, E. A., Borel, C. M., Aguirre, M. L., and Martínez, D. E. (2008). Radiocarbon reservoir ages and hardwater effect for the northeastern coastal waters of Argentina. *Radiocarbon*, 50(1):119–129.

Gonçalves, T. (2010). *Anatomia do lenho e do carvão de espécies arbóreas do cerrado no estado de São Paulo, Brasil*. Msc dissertation, Universidade Estadual Paulista Júlio de Mesquita Filho.

Gonzalez, M. and Amenomori, S. (2003). Osteologia e utilização de dentes de tubarão branco, Carcharodon carcharias (Linnaeus, 1758)(Elasmobranchii, Lamnidae) em sambaquis do estado de São Paulo. *Rev. do Museu de Arqueologia e Etnologia*, 13:25–37.

Goodman, J. (2005). Losing it in New Guinea: The voyage of HMS Rattlesnake. *Endeavour*, 29(2):60–65.

Gordon, A. L. (1981). South Atlantic thermocline ventilation. *Deep Sea Research*, 28A(11):1239–1264.

Gordon, A. L. (1989). Brazil-Malvinas Confluence-1984. *Deep-Sea Research*, 36(3).

Gordon, A. L. and Greengrove, C. L. (1986). Geostrophic circulation of the Brazil-Falkland confluence. *Deep Sea Research Part A, Oceanographic Research Papers*, 33(5):573–585.

Gordon, J. E. and Harkness, D. D. (1992). Magnitude and geographic variation of the radiocarbon content in antarctic marine life: implications for reservoir corrections in radiocarbon dating. *Quaternary Science Reviews*, 11:697–708.

Gosse, J. C. and Phillips, F. M. (2001). Terrestrial in situ cosmogenic nuclides: Theory and application.

Grossman, E. L. and Ku, T.-L. (1986). Oxygen and carbon isotope fractionation in biogenic aragonite: Temperature effects. *Chemical Geology: Isotope Geoscience section*, 59:59–74.

Grothe, P., Cobb, K., Bush, S., Cheng, H., Santos, G., Southon, J., Lawrence Edwards, R., Deocampo, D., and Sayani, H. (2016). A comparison of U/Th and rapid screen 14C dates from Line Island fossil corals. *Geochemistry, Geophysics, Geosystems*, 17:833–845.

Gruber, N., Keeling, C., Bacastow, R., Guenther, P., Lueker, T., Wahlen, M., Meijer, H., Mook, W., and Stocker, T. (1999). Spatiotemporal patterns of carbon-13 in the global surface oceans and the oceanic Suess effect. *Global Biogeochemical Cycles*, 13(2):307–335.

Guerra, A. T. (1950). Contribuição ao estudo da geomorfologia e do quaternário do litoral de Laguna (Santa Catarina). *Revista Brasileira de Geografia*, 12(4):535–564.

Guimarães, M. B. (2013). Fishing strategies among prehistoric populations at Saquarema Lagoonal Complex, Rio de Janeiro, Brazil. *Anais da Academia Brasileira de Ciencias*, 85(1):415–429.

Hadden, C. S., Loftis, K. M., and Cherkinsky, A. (2018). Carbon Isotopes (δ^{13}C and Δ^{14}C) in Shell Carbonate, Conchiolin, and Soft Tissues in Eastern Oyster (Crassostrea Virginica). *Radiocarbon*, pages 1–13.

Hajdas, I., Bonani, G., Thut, J., Leone, G., Pfenninger, R., and Maden, C. (2004). A report on sample preparation at the ETH/PSI AMS facility in Zurich. *Nuclear Instruments and Methods in Physics Research, Section B: Beam Interactions with Materials and Atoms*, 223-224(SPEC. ISS.):267–271.

Hales, B., Takahashi, T., and Bandstra, L. (2005). Atmospheric CO_2 uptake by a coastal upwelling system. *Global Biogeochemical Cycles*, 19(1):1–11.

Hall, B. L., Henderson, G. M., Baroni, C., and Kellogg, T. B. (2010). Constant Holocene Southern-Ocean ^{14}C reservoir ages and ice-shelf flow rates. *Earth and Planetary Science Letters*, 296(1-2):115–123.

Hamell, G. R. (1992). The Iroquois and the World's Rim : Speculations on Color, Culture, and Contact. *American Indian Quaterly*, 16(4):451–469.

Harding, J. M., Spero, H. J., Mann, R., Herbert, G. S., and Sliko, J. L. (2010). Reconstructing early 17th century estuarine drought conditions from Jamestown oysters. *Proceedings of the National Academy of Sciences*, 107(23):10549–10554.

Harkness, D. (1983). The extent of natural ^{14}C deficiency in the coastal environment of the United Kingdom. *Pact*, 8.

Hatch, M. and Slack, C. (1970). Photosynthetic CO_2-fixation pathways. *Annual Review of Plant Physiology*, 21(July 1969):141–162.

Hedges, R. E. and Reynard, L. M. (2007). Nitrogen isotopes and the trophic level of humans in archaeology. *Journal of Archaeological Science*, 34:1240–1251.

Hedges, R. E. M. (1992). Sample Treatment Strategies in Radiocarbon Dating. In Taylor, R., Long, A., and Kra, R., editors, *Radiocarbon After Four Decades*, chapter 12, page 610. LLC.

Hellevang, H. and Aagaard, P. (2015). Constraints on natural global atmospheric CO_2 fluxes from 1860 to 2010 using a simplified explicit forward model. *Scientific Reports*, 5(June):1–12.

Herndl, G. J. and Reinthaler, T. (2013). Microbial control of the dark end of the biological pump. *Nature Geoscience*, 6(9):718–724.

Hesshaimer, V., Heimann, M., and Levin, I. (1994). Radiocarbon evidence for a smaller oceanic carbon dioxide sink than previously believed. *Letters to Nature*, 370:201–203.

Hoefs, J. (1997). *Stable Isotope Geochemistry*. Springer, New York.

Hogg, A., Hua, Q., Blackwell, P., Niu, M., Buck, C., Guilderson, T., Heaton, T., Palmer, J., Reimer, P., Reimer, R., Turney, C., and Zimmerman, S. (2013). SHCal13 Southern Hemisphere Calibration, 0–50,000 Years cal BP. *Radiocarbon*, 55(4):1889–1903.

Hogg, A., Palmer, J., Boswijk, G., and Turney, C. (2011). High-Precision Radiocarbon Measurements of Tree-Ring Dated Wood from New Zealand: 195 BC-AD 995. *Radiocarbon*, 53(3):529–542.

Hua, Q., Barbetti, M., and Rakowski, A. Z. (2013). Atmospheric radiocarbon for the period 1950-2010. *Radiocarbon*, 55(4):2059–2072.

Hua, Q., Jacobsen, G., Zoppi, U., Lawson, E., Williams, A., Smith, A., and McGann, M. (2001). Progress in Radiocarbon Target Preparation at the Antares AMS Centre. *Radiocarbon*, (October).

Hughen, K., Baillie, M., and Bard, E. (2004). Marine04 marine radiocarbon age calibration, 0-26 cal kyr BP.

Hughen, K., Southon, J., Lehman, S., Bertrand, C., and Turnbull, J. (2006). Marine-derived ^{14}C calibration and activity record for the past 50,000 years updated from the Cariaco Basin. *Quaternary Science Reviews*, 25(23-24):3216–3227.

Hut, G. (1987). Consultant's group meeting on stable isotope reference samples for geochemical and hydrological investigations. Technical report, IAEA, Vienna.

Huxley, T. (1935). *T.H. Huxley's Diary of the Voyage of HMS Rattlesnake*. Chatto and Windus.

Huyer, A. (1983). Coastal upwelling in the California current system. *Progress in Oceanography*, 12(3):259–284.

IBGE (2011). *Atlas geográfico das zonas costeiras e oceânicas do Brasil*. Instituto Brasileiro de Geografia e Estatística - IBGE, Rio de Janeiro.

Ikeda, Y., Miranda, L. B., and Rock, N. J. (1974). Observations on stages of upwelling in the region of Cabo Frio (Brazil) as conducted by continuous surface temperature and salinity measurements. *Boletim do Instituto Oceanográfico, São Paulo*, 23:33–46.

Ingram, B. and Southon, J. (1996). Reservoir ages in eastern Pacific coastal and estuarine waters. *Radiocarbon*, 38(3):573–582.

Jahne, B. and Haussecker, H. (1998). Air-Water Gas Exchange. *Annu. Rev. Fluid Mech.*, 30:443–468.

JICA (1994). The study on recuperation of the Guanabara Bay ecosystem.

Jim, S., Jones, V., Ambrose, S. H., and Evershed, R. P. (2006). Quantifying dietary macronutrient sources of carbon for bone collagen biosynthesis using natural abundance stable carbon isotope analysis. *British Journal of Nutrition*, 95(06):1055.

Jong, A. D. and Mook, W. (1982). An anomalous Suess effect above Europe. *Nature*.

Keith, M. L., Anderson, G. M., and Eichler, R. (1964). Carbon and oxygen isotopic composition of mollusk shells from marine and fresh-water environments. *Geochimica et Cosmochimica Acta*, 28:1757–1786.

Kennett, D., Ingram, B., Erlandson, J., and Walker, P. (1997). Evidence for Temporal Fluctuations in Marine Radiocarbon Reservoir Ages in the Santa Barbara Channel, Southern California. *Journal of Archaeological Science*, 24:1051–1059.

Killingley, J. S. and Berger, W. H. (1979). Stable isotopes in a mollusk shell: Detection of upwelling events. *Science*, 205:186–188.

Kim, S.-T. and O'Neil, J. R. (1997). Equilibrium and nonequilibrium oxygen isotope effects in synthetic carbonates. *Geochimica et Cosmochimica Acta*, 61(16):3461–3475.

Kirby, M. X., Soniat, T. M., and Spero, H. J. (1998). Stable Isotope Sclerochronology of Pleistocene and Recent Oyster Shells (Crassostrea virginica). *Palaios*, 13(6):560–569.

Kjerfve, B. (1994). Coastal Lagoons. In Kjerfve, B., editor, *Coastal Lagoon Processes*. Elsevier.

Kjerfve, B., Ribeiro, C., Dias, G., Filippo, A., and Quaresma, V. (1997). Oceanographic characteristics of an impacted coastal bay: Baía de Guanabara, Rio de Janeiro, Brazil. *Continental Shelf Research*, 17(13):1609–1643.

Klein, J., Lerman, J. C., Damion, P. E., and Ralph, E. K. (1982). Calibration of radiocarbon dates: tables based on the consensus data of the Workshop on Calibrating the Radiocarbon Time Scale. *Radiocarbon*, 24(2):103–150.

Klinken, G. J. V. and Mook, W. G. (1990). Preparative high-performance liquid chromatographic separation of individual amino acids derived from fossil bone collagen. *Radiocarbon*, 32(2):155–164.

Klokler, D. (2014a). A Ritually Constructed Shell Mound: Feasting at the Jabuticabeira II Site. In Roksandic, M., Souza, S., Eggers, S., Burchell, M., and Klokler, D., editors, *The Cultural Dynamics of Shell-Matrix Sites*, pages 151–162. University of New Mexico Press, Albuquerque.

Klokler, D. (2014b). Adornos em concha do sítio cabeçuda. *Revista de Arqueologia*, 27(2):150–169.

Klokler, D. (2016a). A fauna do sambaqui cabeçuda: 65 anos depois. In *III Encuentro Latinoamericano de Zooarqueologia (ELAZ)*.

Klokler, D. (2016b). Animal para toda obra: fauna ritual em sambaquis. *Habitus*, 14(1):21–34.

Klokler, D. M. (2008). *Food for Body and Soul: Mortuary Ritual in Shell Mounds (Laguna-Brazil)*. PhD thesis, The University of Arizona.

Klokler, D. M. (2012). Consumo ritual, consumo no ritual: festins funerários e sambaquis. *Habitus*, 10(1):83–104.

Kneip, A. (2004). *O povo da lagoa: Uso do SIG para modelamento e simulação na área arqueológica do Camacho*. PhD thesis, Universidade de São Paulo.

Korff, S. (1939). Recent Studies at High Elevations. *Reviews of Modern Physics*, 11.

Korff, S. and Clarke, E. (1942). The Production of Neutrons and Protons by the Cosmic Radiation at 14,125 Feet. *Physical Review*, 61(1941).

Korff, S. and Hamermesh, B. (1946). The Energy Distribution and Number of Cosmic-Ray Neutrons in the Free Atmosphere. *Physical Review*, 69(5-6).

Korff, S. A. and Mendell, R. B. (1980). Variations in Radiocarbon Production in the Earth's Atmosphere. *Radiocarbon*, 22(2):159–165.

Krantz, D. E., Williams, D. F., and Jones, D. S. (1987). Ecological and paleoenvironmental information using stable isotope profiles from living and fossil molluscs.

Krueger, H. W. and Sullivan, C. H. (1984). Models for Carbon Isotope Fractionation Between Diet and Bone. In Turnlund, J. and Johnson, P., editors, *Stable Isotopes in Nutrition*, pages 205–220. American Chemical Society Symposium Series, Washington DC.

Kulp, J. L., Tryon, L. E., Eckelman, W. R., and Snell, W. A. (1952). Lamont Natural Radiocarbon Measurements, II. *Science*, 116.

Lal, D. (1988). In Situ- Produced Cosmogenic Isotopes In Terrestrial Rocks. *Annual Review of Earth and Planetary Sciences*, 16:355–388.

Lal, D. and Jull, a. J. T. (2001). In-situ cosmogenic C-14: Production and examples of its unique applications in studies of terrestrial and extraterrestrial processes. *Radiocarbon*, 43(2B):731–742.

Lal, D. and Peters, B. (1967). Cosmic ray produced radioactivity on the Earth. *Kosmische Strahlung II/Cosmic Rays II*, pages 551–612.

Larson, L. (1980). *Aboriginal Subsistence Technology on the Southeastern Coastal Plain During the Late Prehistoric Period*. University of Florida Press, Gainesville.

Lee-Thorp, J. A. (2008). On isotopes and old bones. *Archaeometry*, 50(6):925–950.

LeGrande, A. N. and Schmidt, G. A. (2006). Global gridded data set of the oxygen isotopic composition in seawater. *Geophysical Research Letters*, 33(12):1–5.

Leng, M. J. and Lewis, J. P. (2016). Oxygen isotopes in Molluscan shell : Applications in environmental archaeology. *Environmental Archaeology*, 21(3):295–306.

Leonel, R., Magalhães, A., and Lunetta, J. (1983). Sobrevivência de Anomalocardia brasiliana (Gmelin, 1791)(Mollusca: Bivalvia), em diferentes salinidades.". *Boletim de Fisiologia Animal*, 7:63–72.

Lerman, J., Mook, W., and Vogel, J. (1970). C14 in tree rings from different localities. *... and Absolute Chronology. Proceedings, XII Nobel ...*.

Lessa, A. (2011). Daily Risks: A Biocultural Approach to Acute Trauma in Pre-colonial Coastal Populations from Brazil. *International Journal of Osteoarchaeology*, 21:159–172.

Lessa, A. and Medeiros, J. (2001). Reflexões preliminares sobre a questão da violência em populações construtoras de sambaquis: análise dos sítios Cabeçuda (SC) e Arapuan (RJ). *Revista do Museu de Arqueologia e Etnologia*, 11:77–93.

Levin, I. and Hesshaimer, V. (2000). Radiocarbon – a Unique Tracer of Global Carbon Cycle Dynamics. *Radiocarbon*, 42(1):69–80.

Levin, I., Kromer, B., Wagenbach, D., and Münnich, K. O. (1987). Carbon isotope measurement of atmospheric CO_2 at a coastal station in Antarctica. *Tellus*, 39B:89–95.

Levin, I., Schuchard, J., Kromer, B., and Münnich, K. (1989). The Continental European Suess Effect. *Radiocarbon*, 31(3):431–440.

Libby, W. (1954). Radiocarbon Dating. *American Scientist*, 44(1):98–112.

Libby, W., Anderson, E., and Arnold, J. (1949). Age determination by radiocarbon content: worldwide assay of natural radiocarbon. *Science*, 109:227–228.

Libby, W. F. (1934). Radioactivity of Neodymium and Samarium. *Physical Review*, 46(196).

Libby, W. F. (1946). Atmospheric helium three and radiocarbon from cosmic radiation. *Physical Review*, 69:671–672.

Lima, T., Macario, K., Anjos, R., Gomes, P., Coimbra, M., and Elmore, D. (2002). The antiquity of the prehistoric settlements of the central-south Brazilian coast. *Radiocarbon*, 44:733–738.

Lima, T., Mello, E., and Silva, R. (1986). Analysis of Molluscan Remains from the Ilha de Santana Site, Macaé, Brazil. *Journal of Field Archaeology*, 13:83–97.

Lima, T. A. (2000). Em busca dos frutos do mar: os pescadores-coletores do litoral centro-sul do Brasil. *REVISTA USP*, (44):270–327.

Lima, T. A., Macario, K. D., Anjos, R. M., Gomes, P. R. S., Coimbra, M. M., and Elmore, D. (2004). The earliest shellmounds of the central-south Brazilian coast. *Nuclear Instruments and Methods in Physics Research, Section B: Beam Interactions with Materials and Atoms*, 223-224:691–694.

Lingenfelter, R. E. (1963). Production of Carbon 14 by Cosmic-Ray Neutrons. *Review of Geophysics*, 1(1):35–55.

Little, E. (1993). Radiocarbon Age Calibration at Archaeological Sites of Coastal Massachusetts and Vicinity. *Journal of Archaeological Science*, 20:457–471.

Longin, R. (1971). New method of collagen extraction for radiocarbon dating. *Nature*, 230(5291):241–2.

Lopes, M. S., Bertucci, T. C. P., Rapagnã, L., Tubino, R. D. A., Monteiro-Neto, C., Tomas, A. R. G., Tenório, M. C., Lima, T., Souza, R., Carrillo-Briceño, J. D., Haimovici, M., Macario, K., Carvalho, C., and Socorro, O. A. (2016). The path towards endangered species: Prehistoric fisheries in southeastern Brazil. *PLoS ONE*, 11(6):1–36.

Lorrain, A., Paulet, Y. M., Chauvaud, L., Dunbar, R., Mucciarone, D., and Fontugne, M. (2004). δ^{13}C variation in scallop shells: Increasing metabolic carbon contribution with body size? *Geochimica et Cosmochimica Acta*, 68(17):3509–3519.

Lougheed, B. C., Filipsson, H. L., and Snowball, I. (2013). Large spatial variations in coastal ^{14}C reservoir age - A case study from the Baltic Sea. *Climate of the Past*, 9(3):1015–1028.

Ludemann, T., Michiels, H. G., and Nölken, W. (2004). Spatial patterns of past wood exploitation, natural wood supply and growth conditions: Indications of natural tree species distribution by anthracological studies of charcoal-burning remains. *European Journal of Forest Research*, 123(4):283–292.

Lumpkin, R. and Garzoli, S. (2011). Interannual to decadal changes in the western South Atlantic's surface circulation. *Journal of Geophysical Research: Oceans*, 116(1):1–10.

Macario, K. D., Alves, E. Q., Belém, A. L., Aguilera, O., Bertucci, T., Tenório, M. C., Oliveira, F. M., Chanca, I. S., Carvalho, C., Souza, R., Scheel-Ybert, R., Nascimento, G. S., Dias, F., and Caon, J. (2018). The marine reservoir effect on the coast of rio de janeiro: Deriving $\triangle$R values from fish otoliths and mollusk shells. *Radiocarbon*, 60(4):1151–1168.

Macario, K. D., Alves, E. Q., Chanca, I. S., Oliveira, F. M., Carvalho, C., Souza, R., Aguilera, O., Tenório, M. C., Rapagnã, L. C., Douka, K., et al. (2016). The usiminas shellmound on the cabo frio island: marine reservoir effect in an upwelling region on the coast of brazil. *Quaternary Geochronology*, 35:36–42.

Macario, K. D., Souza, R. C. C. L., Aguilera, O. A., Carvalho, C., Oliveira, F. M., Alves, E. Q., Chanca, I. S., Silva, E. P., Douka, K., Decco, J., Trindade, D. C., Marques, A. N., Anjos, R. M., and Pamplona, F. C. (2015). Marine reservoir effect on the Southeastern coast of Brazil: results from the Tarioba shellmound paired samples. *Journal of environmental radioactivity*, 143:14–9.

Macario, K. D., Souza, R. C. C. L., Trindade, D. C., Decco, J., Lima, T. A., Aguilera, O. A., Marques, A. N., Alves, E. Q., Oliveira, F. M., Chanca, I. S., Carvalho, C., Anjos, R. M., Pamplona, F. C., and Silva, E. P. (2014). Chronological Model of a Brazilian Holocene Shellmound (Sambaqui da Tarioba, Rio de Janeiro, Brazil). *Radiocarbon*, 56(2):489–499.

Macario, K. D., Tenório, M. C., Alves, E. Q., Oliveira, F. M., Chanca, I. S., Netto, B., Carvalho, C., Souza, R., Aguilera, O., and Guimarães, R. B. (2017). Terrestrial Mollusks as Chronological Records in Brazilian Shellmounds. *Radiocarbon*, 59(05):1561–1577.

MacGillivray, J. (1852). *Narrative of the Voyage of HMS Rattlesnake*. T. & W. Boone, London.

Mainieri, C. and Chimelo, J. (1989). *Fichas de características das madeiras brasileiras*. São Paulo, second. edition.

Mangerud, J. (1972). Radiocarbon dating of marine shells including a discussion of the apparent age of recent shells from Norway. *Boreas*, 1(l):143–172.

Masarik, J. and Beer, J. (1999). Simulation of particle fluxes and cosmogenic nuclide production in the earth atmosphere. *Journal of Geophysical Research*, 104(10):12099–12111.

Masuda, K., Nagaya, K., Miyahara, H., Muraki, Y., and Nakamura, T. (2009). Cosmogenic Radiocarbon and the Solar Activity. *J. Phys. Soc. Jpn.*, 78:1–6.

Matano, R. P., Palma, E. D., and Piola, A. R. (2010). The influence of the Brazil and Malvinas Currents on the Southwestern Atlantic Shelf circulation. *Ocean Science*, 6(4):983–995.

Matsumoto, K., Sarmiento, J. L., Key, R. M., Aumont, O., Bullister, J. L., Caldeira, K., Campin, J., Doney, S. C., Drange, H., Dutay, J., Follows, M., Gao, Y., Gnanadesikan, A., Gruber, N., Ishida, A., Joos, F., Lindsay, K., Maier-Reimer, E., Marshall, J., Matear, R., Monfray, P., Mouchet, A.,

Najjar, R., Plattner, G., Schlitzer, R., Slater, R., Swati, P., Totterdell, I., Weirig, M., Yamanaka, Y., Yool, A., and Orr, J. (2004). Evaluation of ocean carbon cycle models with data-based metrics. *Geophysical Research Letters*, 31:13–16.

Matsuura, Y. (1996). A probable cause of recruitment failure of the Brazilian sardine Sardinella aurita population during the 1974/75 spawning season. *South African Journal of Marine Science*, 17:29–35.

Mayr, L. M., Tenenbaum, D. R., Villac, M. C., Paranhos, R., Nogueira, C. R., Bonecker, S. L. C., and Bonecker, A. C. T. (1989). Hydrobiological characterization of Guanabara Bay. *Coastlines of Brazil*, (January):124–138.

McConnaughey, T., Burdett, J., Whelan, J., and Paull, C. (1997). Carbon isotopes in biological carbonates: Respiration and photosynthesis. *Geochimica et Cosmochimica Acta*, 61(3):611–622.

McConnaughey, T. A. and Gillikin, D. P. (2008). Carbon isotopes in mollusk shell carbonates. *Geo-Marine Letters*, 28:287–299.

McCormac, F. G., Hogg, A. G., Higham, F. G., Baillie, G. L., Palmer, J. G., Xiong, L., Pilcher, J. R., Brown, D., and Hoper, T. (1998). Variations of Radiocarbon in Tree Rings: Southern Hemisphere Offset Preliminary Results. *Radiocarbon*, 40(3):1153–1159.

McCormac, F. G., Reimer, P. J., Hogg, A. G., Higham, T. F. G., Baillie, M. G. L., Palmer, J., and Stuiver, M. (2002). Calibration of the radiocarbon time scale for the southern hemisphere: AD 1850–950. *Radiocarbon*, 44(3):641–651.

McCrea, J. M. (1950). On the isotopic chemistry of carbonates and a paleotemperature scale. *The Journal of Chemical Physics*, 18(6):849–857.

McElroy, M. B. (1983). Marine biological controls on atmospheric CO_2 and climate. *Nature*, 302(3):328–329.

McFadgen, B. (1982). Dating New Zealand archaeology by radiocarbon. *New Zealand Journal of Science*, 25:379–392.

McGregor, H. V. and Gagan, M. K. (2003). Diagenesis and geochemistry of Porites corals from Papua New Guinea: Implications for paleoclimate reconstruction. *Geochimica et Cosmochimica Acta*, 67(12):2147–2156.

McManamon, F. (1984). Cultural Resources Management Study. In *Chapters in the Archaeology of Cape Cod*. Division of Cultural Resources, North Atlantic Regional Office, National Parks Service, U.S. Department of Interior, Boston.

McNichol, A. P., Schneider, R. J., Von Reden, K. F., Gagnon, A. R., Elder, K. L., Key, R. M., and Quay, P. D. (2000). Ten years after - The WOCE AMS radiocarbon program. *Nuclear Instruments and Methods in Physics Research, Section B: Beam Interactions with Materials and Atoms*, 172(1-4):479–484.

Meehan, B. (1982). *Shell Bed to Shell Midden*. Australian Institute of Aboriginal Studies, Canberra.

Mello e Alvim, M. and Gomes, J. (1989). Análise e interpretação das condições patológicas – órbita crivosa, osteoporose puntiforme e hiperosteose esponjosa – em crânios humanos provenientes de sítio arqueológico – sambaqui de Cabeçuda, Laguna, SC, Brasil. *Revista de Pré-História*, 7:127–145.

Mello e Alvim, M. and Mendonça de Souza, S. (1990). Relações biológicas entre populações indígenas atuais e pré-históricas do Brasil. *Clio*, 1(6):69–79.

Mello e Alvim, M. and Seyferth, G. (1971a). Estudo morfológico do úmero na população do Sambaqui de Cabeçuda (Laguna, Santa Catarina). In *O Homem Antigo na América*, pages 25–28. São Paulo.

Mello e Alvim, M. and Seyferth, G. (1971b). O fêmur na população do sambaqui de Cabeçuda (Laguna, Estado de Santa Catarina, Brasil) – Estudo morfológico e comparativo. *Boletim do Museu Nacional - Série Antropologia*, 24:1–14.

Mendonça de Souza, S. (1995). Estresse, doença e adaptabilidade. In *Congresso da Sociedade de Arqueologia Brasileira*.

Merlivat, L. and Memery, L. (1983). Gas exchange across an air-water interface: Experimental results and modeling of bubble contribution to transfer. *Journal of Geophysical Research*, 88:707–724.

Metcalfe, C. and Chalk, L. (1950). *Anatomy of the dicotyledons, vol. 2*. The Clarendon Press, Oxford, London.

Milheira, R., Macario, K., Chanca, I., and Alves, E. (2017). Archaeological Earthen Mound Complex in the Patos Lagoon, Southern Brazil: Chronological Model and Freshwater Influence. *Radiocarbon*, 59(1):195–214.

Mills, G. A. and Urey, H. C. (1940). The Kinetics of Isotopic Exchange between Carbon Dioxide, Bicarbonate Ion, Carbonate Ion and Water. *Journal of the American Chemical Society*, 62:1019–1026.

Minagawa, M. and Wada, E. (1984). Stepwise enrichment of ^{15}N along food chains: Further evidence and the relation between δ^{15}N and animal age. *Geochimica et Cosmochimica Acta*, 48(5):1135–1140.

Molnár, M., Janovics, R., and Major, I. (2013). Status Report of the New AMS ^{14}C Sample Preparation Lab of the Hertelendi Laboratory of Environmental Studies (Debrecen, Hungary). *Radiocarbon*, 55(2):665–676.

Montgomery, C. and Montgomery, D. (1939). The Intensity of Neutrons of Thermal Energy in the Atmosphere at Sea Level. *Physical Review*, 56:10–12.

Monti, D., Frenkiel, L., and Moueza, M. (1991). Demography And Growth of Anomalocardia Brasiliana (Gmelin) (Bivalvia: Veneridade) in a Mangrove, in Guadeloupe (French West Indies). *Journal of Molluscan Studies*, 57:249–257.

Mook, W., Bommerson, J., and Staverman, W. (1974). Carbon isotope fractionation between dissolved bicarbonate and gaseous carbon dioxide. *Earth and Planetary Science Letters*, 22:169–176.

Mook, W. G. and Vogel, J. C. (1968). Isotopic equilibrium between shells and their environment. *Science*, 159(3817):874–875.

Moskal-del Hoyo, M. (2013). Mid-Holocene forests from Eastern Hungary: New anthracological data. *Review of Palaeobotany and Palynology*, 193:70–81.

Mueller, K. and Muzikar, P. (2002). Correcting for Contamination in AMS ^{14}C Dating. 44(2):591–595.

Muller, R. A. (1977). Radioisotope dating with a cyclotron. *Science*, 196(4289):489–494.

Muzikar, P., Elmore, D., and Granger, D. E. (2003). Accelerator mass spectrometry in geologic research. *Bulletin of the Geological Society of America*, 115(6):643–654.

Nadal De Masi, M. (2001). Pescadores coletores da costa sul do Brasil. *Pesquisas. Antropologia*, 57:1–136.

Nadal De Masi, M. (2009). Aplicações de Isótopos Estáveis de $^{18}/^{16}$O, $^{13}/^{12}$C e $^{15}/^{14}$N em Estudos de Sazonalidade, Mobilidade e Dieta de Populações Pré-Históricas no Sul do Brasil. *Revista de Arqueologia*, 22(2):55–76.

Naito, Y. I., Chikaraishi, Y., Ohkouchi, N., Mukai, H., Shibata, Y., Honch, N. V., Dodo, Y., Ishida, H., Amano, T., Ono, H., and Yoneda, M. (2010). Dietary reconstruction of the Okhotsk culture of Hokkaido, Japan, based on nitrogen composition of amino acids: implications for correction of ^{14}C marine reservoir effects on human bones. *Radiocarbon*, 52(2):671–681.

Nelson, D., Korteling, R., and Stott, W. (1977). Carbon-14 : Direct Detection at Natural Concentrations. *Science*, 198:507–508.

Neves, W. (1982). Variação métrica nos construtores de sambaquis do sul do Brasil: primeira aproximação multivariada. *Revista de Pré-História*, 4:83–108.

Nier, A. O. and Gulbransen, E. A. (1939). Variations in the Relative Abundance of the Carbon Isotopes. *Journ. Am. Chem. Soc.*, 61:697.

O'Connor, S., Ulm, S., Fallon, S. J., Barham, A., and Loch, I. (2010). Pre-bomb marine reservoir variability in the Kimberley region, Western Australia. *Radiocarbon*, 52(2-3):1158–1165.

Oeschger, H., Siegenthaler, U., Schotterer, U., and Gugelmann, A. (1975). A box diffusion model to study the carbon dioxide exchange in nature. *Tellus*, 27(2):168–192.

Okumura, M. and Eggers, S. (2014). Cultural Formation Processes of the Bioarchaeological Record of a Brazilian Shellmound. In Roksandic, M., Souza, S., Eggers, S., Burchell, M., and Klokler, D., editors, *The Cultural Dynamics of Shell-Matrix Sites*, pages 103–112. University of New Mexico Press, Albuquerque.

Okumura, M. M. M. (2007). *Diversidade morfológica craniana, micro-evolução e ocupação pré-histórica da costa brasileira*. PhD thesis, Instituto de Biociências da Universidade de São Paulo.

Okumura, M. M. M., Boyadjian, C. H. C., and Eggers, S. (2006). Análise da Exostose do Meato Auditivo Externo como um Marcador de Atividade Aquática em Restos Esqueletais Humanos da Costa e do Interior do Brasil. *Revista do Museu de Arqueologia e Etnologia*, 15-16:181–197.

O'Leary, M. H. (1981). Carbon isotope fractionation in plants. *Phytochemistry*, 20(4):553–567.

O'Leary, M. H. (1988). Carbon isotopes in photosynthesis: fractionation technique may reveal new aspects of carbon dynamics in plants. *BioScience*, 38:328–336.

Oliveira, M. S. C. and Horn Filho, N. O. (2001). De Guaratuba a Babitonga: uma contribuição geológico-evolutiva ao estudo da espacialidade dos sambaquianos no litoral norte catarinense. *Revista do Museu de Arqueologia e Etnologia*, 11:55–75.

Olsen, J., Ascough, P., Lougheed, B. C., and Rasmussen, P. (2017). Radiocarbon Dating in Estuarine Environments. In Weckström, K., Saunders, K., Gell, P., and Skilbeck, C., editors, *Applications of Paleoenvironmental Techniques in Estuarine Studies*, volume 20, pages 141–170. Springer, Dordrecht.

Olson, D. B., Podestá, G. P., Evans, R. H., and Brown, O. B. (1988). Temporal variations in the separation of Brazil and Malvinas Currents. *Deep Sea Research Part A, Oceanographic Research Papers*, 35(12):1971–1990.

Olsson, I. (1970). Radiocarbon Variations and Absolute Chronology - Review.

Olsson, I. (1996). ^{14}C dates and the reservoir effect. In van der Plicht, J. and Punning, J., editors, *Internation Workshop on Isotope-Geochemical Research in the Baltic Region*, pages 5–23, Groningen. Centre for Isotope Research Groningen.

Olsson, I. U. (1983). Dating non-terrestrial materials. In Hackens, T., Mook, W., and Walterbolk, H., editors, *Proceedings of ^{14}C and archaeology (PACT8)*, pages 277–294, Groningen. PACT publication.

Onat, A. (1985). The Multifunctional Use of Shellfish Remains: From Garbage to Community Engineering. *Northwest Anthropological Research Notes*, 19:201–207.

Ortlieb, L., Vargas, G., and Saliège, J. F. (2011). Marine radiocarbon reservoir effect along the northern Chile-southern Peru coast (14-24S) throughout the Holocene. *Quaternary Research*, 75(1):91–103.

Owen, R., Kennedy, H., and Richardson, C. (2002). Experimental investigation into partitioning of stable isotopes between scallop (Pecten maximus) shell calcite and sea water. *Palaeogeography, Palaeoclimatology, Palaeoecology*, 185:163–174.

Pandow, M., MacKay, C., and Wolfgang, R. (1960). The reaction of atomic carbon with oxygen: Significance for the natural radio-carbon cycle. *Journal of Inorganic and Nuclear . . .*, 14:153–158.

Parmalee, P. and Klippel, W. (1974). Freshwater Mussels as a Prehistoric Food Resource. *American Antiquity*, 39(3):421–434.

Passariello, I. and Rubino, M. (2016). Radiocarbon Sample Preparation at the CIRCE AMS Laboratory in Caserta, Italy. *Radiocarbon*, 49(2007).

Pearson, G. and Stuiver, M. (1993). High-precision bidecadal calibration of the radiocarbon time scale, 500-2500 BC. *Radiocarbon*, 35(1):25–33.

Pearson, G. W. (1987). How to cope with calibration. *Antiquity*, 61:98–103.

Peck, L. and Brey, T. (1996). Bomb signals in old Antarctic brachiopods. *Nature*, 380(6571):207–208.

Petchey, F., Anderson, A., Hogg, A., and Zondervan, A. (2008). The marine reservoir effect in the southern ocean: An evaluation of extant and new $\triangle$R values and their application to archaeological chronologies. *Journal of the Royal Society of New Zealand*, 38(4):243–262.

Petchey, F. and Clark, G. (2011). Tongatapu hardwater: Investigation into the ^{14}C marine reservoir offset in lagoon, reef and open ocean environments of a limestone island. *Quaternary Geochronology*, 6(6):539–549.

Petchey, F., Ulm, S., David, B., Mcniven, I., Asmussen, B., Tomkins, H., Richards, T., Rowe, C., Leavesley, M., Mandui, H., and Stanisic, J. (2012). ^{14}C marine reservoir variability in herbivores and deposit-feeding gastropods from an open coastline, Papua New Guinea. *Radiocarbon*, 54(3-4):967–978.

Petchey, F., Ulm, S., David, B., McNiven, I. J., Asmussen, B., Tomkins, H., Dolby, N., Aplin, K., Richards, T., Rowe, C., Leavesley, M., and Mandui, H. (2013). High-resolution radiocarbon dating of marine materials in archaeological contexts: Radiocarbon marine reservoir variability between Anadara, Gafrarium, Batissa, Polymesoda spp. and Echinoidea at Caution Bay, Southern Coastal Papua New Guinea. *Archaeological and Anthropological Sciences*, 5:69–80.

Peterson, R. (1992). The boundary currents in the western Argentine Basin. *Deep-Sea Research*, 39(3/4):623–644.

Peterson, R. and Stramma, L. (1991). Upper-level circulation in the South Atlantic Ocean. *Progress in Oceanography*, 26:1–73.

Pezo-Lanfranco, L., Eggers, S., Petronilho, C., Toso, A., da Rocha Bandeira, D., Von Tersch, M., dos Santos, A. M. P., Ramos da Costa, B., Meyer, R., and Colonese, A. C. (2018). Middle Holocene plant cultivation on the Atlantic Forest coast of Brazil? *Royal Society Open Science*, 5:180432.

Piola, A. and Matano, R. (2001). Brazil and Falklands (Malvinas) Current. In Steele, J., Thorpe, S. A., and Turekian, K., editors, *Encyclopedia of Ocean Sciences: Ocean Currents*, pages 35–43. 2nd edition.

Post, W., Peng, T., Emanuel, W., King, A., Dale, V., and DeAngelis, D. (1990). The global carbon cycle.

Povinec, P. P., Litherland, A. E., and von Reden, K. F. (2009). Developments in radiocarbon technologies: from the libby counter to compound-specific AMS analyses. *Radiocarbon*, 51(1):45–78.

Prates, A., Gonçalves, M., and Rosa, M. (2010). *Panorama da Conservação dos Ecossistemas Costeiros e Marinhos no Brasil*. MMA/SBF/GBA, Brasilia.

Price, P. (1989). Heavy-particle radioactivity (A> 4). *Annual Review of Nuclear and Particle Science*, 39:19–42.

Prous, A. (1991). *Arqueologia Brasileira*. Editora Universidade de Brasilia, Brasilia.

Prous, A. (2006). *O Brasil antes dos brasileiros - A pré-história do nosso país*. Zahar, Rio de Janeiro.

Rakowski, A., Kuc, T., Nakamura, T., and Pazdur, A. (2005). Radiocarbon concentration in urban area. *Geochronometria*, 24:63–68.

Rauth, J. (1962). O sambaqui de Saquarema S.10. *Curitiba: Boletim da Universidade do Paraná, Conselho de Pesquisas*.

Raven, J. A. and Falkowski, P. G. (1999). Oceanic sinks for atmospheric CO_2. *Plant, Cell and Environment*, 22(6):741–755.

Record, S. and Hess, R. (1943). *Timbers of the New World*. Yale University Press, New Haven.

Reid, R. P. and Macintyre, I. G. (1998). Carbonate Recrystallization in Shallow Marine Environments: a Widespread Diagenetic Process Forming Micritized Grains. *Journal of Sedimentary Research*, 68(5):928–946.

Reimer, P., Baillie, M., Bard, E., Bayliss, A., Beck, J., Blackwell, P., Bronk Ramsey, C., Buck, C., Burr, G., Edwards, R., Friedrich, M., Grootes, P., Guilderson, T., Hajdas, I., Heaton, T., Hogg, A., Hughen, K., Kaiser, K., Kromer, B., McCormac, F., Manning, S., Reimer, R., Richards, D., Southon, J., Talamo, S., Turney, C., van der Plicht, J., and Weyhenmeyer, C. (2009). IntCal09 and Marine09 radiocarbon age calibration curves, 0-50,000 years cal BP. *Radiocarbon*, 51(4):1111–1150.

Reimer, P., Bard, E., and Bayliss, A Beck, JW Blackwell, PG Bronk Ramsey, C Buck, CE Cheng, H Edwards, RL Friedrich, M Grootes, PM Guilderson, TP Haflidason, H Hajdas, I Hatté, C Heaton, T Hoffman, DL Hogg, AG Hughen, KA Kaiser, KF Kromer, B Manning, SW Niu, M Reimer, RW Richards,, J. (2013). IntCal13 and Marine13 radiocarbon age calibration curves 0-50,000 years cal BP. *Radiocarbon*, 55(4):1869–1887.

Reimer, P. J., Baillie, M. G. L., Bard, E., Bayliss, A., Beck, J. W., Bertrand, C. J. H., Blackwell, P. G., Buck, C. E., Burr, G. S., Cutler, K. B., Damon, P. E., Edwards, R. L., Fairbanks, R. G., Friedrich, M., Guilderson, T. P., Hogg, A. G., Hughen, K. A., Kromer, B., McCormac, G., Manning, S., Bronk Ramsey, C., Reimer, R., Remmele, S., Southon, J., Stuiver, M., Talamo, S., Taylor, F., van der Plicht, J., and Weyhenmeyer, C. (2004). IntCal04 Terrestrial Radiocarbon Age Calibration 0-26 cal kyr BP. *Radiocarbon*, 46(3):1029–1058.

Reimer, P. J. and Reimer, R. W. (2001). A marine reservoir correction database and on-line interface. *Radiocarbon*, 43(2A):461–463.

Reimer, R. W. and Reimer, P. J. (2016). An Online Application for $\triangle$R Calculation. *Radiocarbon*, 13(July):1–5.

Reynolds, G., Harrison, F., and Salvini, G. (1950). Liquid Scintillation Counters. *Physical Review*, 78:1950.

Rick, T. C., Henkes, G. A., Lowery, D. L., Colman, S. M., and Culleton, B. J. (2012). Marine radiocarbon reservoir corrections ($\triangle$R) for Chesapeake Bay and the Middle Atlantic Coast of North America. *Quaternary Research*, 77(1):205–210.

Rieth, T. M., Hunt, T. L., Lipo, C., and Wilmshurst, J. M. (2011). The 13th century polynesian colonization of Hawai'i Island. *Journal of Archaeological Science*, 38(10):2740–2749.

Rios, E. (1994). *Seashells of Brazil*. Editora Fundação Universidade do Rio Grande, Rio Grande.

Riser, G. (1987). The Quave Ceramic Collection: Mississippian Presence on the North Shore of Lake Pontchartrain. In *Paper read at the Annual Meeting of the Louisiana Archaeological Society*.

Ritz, S. P., Stocker, T. F., and M??ller, S. A. (2008). Modeling the effect of abrupt ocean circulation change on marine reservoir age. *Earth and Planetary Science Letters*, 268(1-2):202–211.

Rodgers, K. B., Mikaloff-Fletcher, S. E., Bianchi, D., Beaulieu, C., Galbraith, E. D., Gnanadesikan, A., Hogg, a. G., Iudicone, D., Lintner, B. R., Naegler, T., Reimer, P. J., Sarmiento, J. L., and Slater, R. D. (2011). Interhemispheric gradient of atmospheric radiocarbon reveals natural variability of Southern Ocean winds. *Clim. Past*, 7:1123–1138.

Rodrigues, A., Borges-Azevedo, C., Costa, R., and Henry-Silva, G. (2013). Population structure of the bivalve Anomalocardia brasiliana, (Gmelin, 1791) in the semi-arid estuarine region of northeastern Brazil. *Brazilian Journal of Biology*, 73(5):819–833.

Rodrigues, C. (1997). *Perfis dento-patológicos nos remanescentes esqueletais de dois sítios pré-históricos brasileiros: o cemitério de Furna do Estrago, PE e o Sambaqui de Cabeçuda, SC*. PhD thesis, Escola Nacional de Saúde Pública/ Fundação Oswaldo Cruz.

Rodrigues, R. R. and Lorenzzetti, J. A. (2001). A numerical study of the effects of bottom topography and coastline geometry on the Southeast Brazilian coastal upwelling. *Continental Shelf Research*, 21(4):371–394.

Rodrigues-Carvalho, C. and de Souza, S. M. (1998). Uso de adornos labiais pelos construtores do sambaqui de Cabeçuda, Santa Catarina, Brasil: Uma hipótese baseada no perfil dento-patológico. *Revista de Arqueologia*, 11:43–55.

Rodrigues-Carvalho, C., Scheel-Ybert, R., Gaspar, M., Bianchini, G. F., Klokler, D. M., Andrade, M. N., and Borges, D. d. S. (2011). Cabeçuda-II: um conjunto de amoladores-polidores evidenciado em Laguna, SC. *Revista do Museu de Arqueologia e Etnologia*, (21):401–405.

Rohr, J. (1961). Pesquisas paleoetnográficas na Ilha de Santa Catarina e notícias prévias sobre sambaquis da Ilha de São Francisco do Sul. *Pesquisas*, 12:1–18.

Roksandic, M., de Souza, S. M., Eggers, S., Burchell, M., and Klokler, D. (2014). Introduction. In Roksandic, M., de Souza, S. M., Eggers, S., Burchell, M., and Klokler, D., editors, *The Cultural Dynamics of Shell-Matrix Sites*, pages xiii–xv. University of New Mexico Press, Albuquerque.

Rollins, H. B., Sandweiss, D., and Rollins, J. C. (1990). Mollusks and Coastal Archaeology: A Review Mollusks and coastal archaeology; A review. *Geological Society Special Publication*, 4.

Romanek, C. S. and Grossman, E. L. (1989). Stable Isotope Profiles of Tridacna maxima as Environmental Indicators. *PALAIOS*, 4(5):402–413.

Rose, H. and Jones, G. (1984). A new kind of natural radioactivity. *Nature*, 307:245–247.

Russell, N., Cook, G. T., Ascough, P. L., Scott, E. M., and Dugmore, A. J. (2011). Examining the Inherent Variability of ΔR: New Methods of Presenting ΔR Values and Implications for MRE Studies. *Radiocarbon*, 53(2):277–288.

Salles, A., Teixeira, A., Araújo, R., and Alexandre, D. (2005). A Musculoskeletal stress markers on skeletal remains of Cabeçuda shellmound population, Laguna, Santa Catarina, Brazil: a biocultural approach. In *Proceedings of the Paleopathology Meetings in South America*, page 17.

Sallun Filho, W. and Karmann, I. (2007). Geomorphological map of the Serra da Bodoquena karst, west-central Brazil. *Journal of Maps*, 3(1):282–295.

Sarmiento, J. L., Hughes, T. M. C., Stouffer, R. J., and Manabe, S. (1998). Simulated response of the ocean carbon cycle to anthropogenic climate warming. *Nature*, 393(6682):245–249.

Saunders, N. J. (1999). Biographies of brilliance: Pearls , transformations of matter and being, c. AD 1492. *World Archaeology*, 31(2):243–257.

Scheel-Ybert, R. (1999). Paleoambiente e paleoetnologia de populações sambaquieiras do sudeste do Estado do Rio de Janeiro. *Revista do Museu de Arqueologia e Etnologia*, 9:43–59.

Scheel-Ybert, R. (2000). Vegetation stability in the Southeastern Brazilian coastal area from 5500 to 1400 ^{14}C yr BP deduced from charcoal analysis. *Review of Palaeobotany and Palynology*, 110:111–138.

Scheel-Ybert, R. (2001). Man and Vegetation in Southeastern Brazil During the Late Holocene. *Journal of Archaeological Science*, 28:471–480.

Scheel-Ybert, R. (2011). Sambaqui de Cabeçuda (Laguna, SC) - 1 Relatório de Pesquisa de Campo. Technical report, Museu Nacional/UFRJ, Rio de Janeiro.

Scheel-Ybert, R. (2012). Sambaqui de Cabeçuda (Laguna, SC) - 2 Relatório de Pesquisa de Campo. Technical report, Museu Nacional/UFRJ, Rio de Janeiro.

Scheel-Ybert, R. (2013). Preliminary Data on Nonwood Plant Remains at Sambaquis from the Southern and Southeastern Brazilian Coast: Considerations on Diet, Ritual, and Site Particularities. *Cuadernos del Instituo Nacional de Antropologia y Pensamento Latinoamericano - Series Especiales*, 1(1).

Scheel-Ybert, R. (2014). Landscape and Use of Plants by Southern and Southeastern Brazilian Shell-Mound Builders. In Roksandic, M., Souza, S., Eggers, S., Burchell, M., and Klokler, D., editors, *The Cultural Dynamics of Shell-Matrix Sites*, pages 289–300. University of New Mexico Press, Albuquerque.

Scheel-Ybert, R., Afonso, M. C., Guimarães, M. B., Gaspar, M. D., and Ybert, J.-P. (2009). Considerações sobre o papel dos sambaquis como indicadores do nível do mar. *Quaternary and Environmental Geosciences*, 01:03–09.

Scheel-Ybert, R. and Dias, O. F. (2007). Corondó: palaeoenvironmental reconstruction and palaeoethnobotanical considerations in a probable locus of early plant cultivation (south-eastern Brazil). *Environmental Archaeology*, 12(2):129–138.

Scheel-Ybert, R., Eggers, S., Wesolowski, V., Petronilho, C., Boyadjian, C., DeBlasis, P., Barbosa-Guimarães, M., and Gaspar, M. (2003). Novas perspectivas na reconstituição do modo de vida dos sambaquieiros: uma abordagem multidisciplinar. *Revista Arqueologia*, 16:109–137.

Schiffer, M. B. (1986). Radiocarbon dating and the "old wood" problem: The case of the Hohokam chronology. *Journal of Archaeological Science*, 13(1):13–30.

Schleicher, M., Grootes, P., Nadeau, M., and Schoon, A. (1998). The carbonate ^{14}C background and its components at the Leibniz AMS facility. *Radiocarbon*, 40(1):85–93.

Schoeninger, M. J. and DeNiro, M. J. (1984). Nitrogen and carbon isotopic composition of bone collagen from marine and terrestrial animals. *Geochimica et Cosmochimica Acta*, 48(4):625–639.

Schoeninger, M. J., DeNiro, M. J., and Tauber, H. (1983). Stable nitrogen isotope ratios of bone collagen reflect marine and terrestrial components of prehistoric human diet. *Science (New York, N.Y.)*, pages 1381–1383.

Schulting, R. J. (1998). Slighting the sea: stable isotope evidence for the transition to farming in northwestern Europe. *Documenta Praehistorica: Poročilo O Raziskovanju Paleolitika, Neolitika in Eneolitika V Sloveniji*, 25:203–218.

Schuur, E., Trumbore, S. E., Druffel, E., Southon, J., Steinhof, A., Taylor, R., and Turnbull, J. (2016). Radiocarbon and the global carbon cycle. In *Radiocarbon and Climate Change*, pages 1–19. Springer.

Schwalb, A. (2003). Lacustrine ostracodes as stable isotope recorders of late-glacial and Holocene environmental dynamics and climate. *Journal of Paleolimnology*, 29:265–351.

Schwarcz, H. P., Melbye, J., Anne Katzenberg, M., and Knyf, M. (1985). Stable isotopes in human skeletons of Southern Ontario: reconstructing Palaeodiet. *Journal of Archaeological Science*, 12(3):187–206.

Seemann, B. (1853). *Narrative of the Voyage of HMS Herald During the Years 1845-1851, Under the Command of Captain Henry Kellett: Being a Circumnavigation of the Globe, and Three Cruizes to the Arctic Regions in Search of Sir John Franklin*. Reeve and Company, London.

Sepulcre, S., Durand, N., and Bard, E. (2009). Mineralogical determination of reef and periplatform carbonates: Calibration and implications for paleoceanography and radiochronology. *Global and Planetary Change*, 66(1-2):1–9.

Shackleton, N. J. (1974). Attainment of isotopic equilibrium between ocean water and the benthonic foraminifera genus Uvigerina: Isotopic changes in the ocean during the last glacial. *Colloques Internationaux du C.N.R.S.*, 219:203–210.

Siegenthaler, U. and Sarmiento, J. L. (1993). Atmospheric carbon dioxide and the ocean. *Nature*, 365:119–125.

Sierra, C. A., Müller, M., Metzler, H., Manzoni, S., and Trumbore, S. E. (2017). The muddle of ages, turnover, transit, and residence times in the carbon cycle. *Global Change Biology*, 23(5):1763–1773.

Sigman, D. M. and Boyle, E. A. (2000). Glacial/Interglacial Variations In Atmospheric Carbon Dioxide. *Nature*, 407:859–869.

Sikes, E. L., Burgess, S. N., Grandpre, R., and Guilderson, T. P. (2008). Assessing modern deep-water ages in the New Zealand region using deep-water corals. *Deep-Sea Research Part I: Oceanographic Research Papers*, 55(1):38–49.

Sikes, E. L., Cook, M. S., and Guilderson, T. P. (2016). Reduced deep ocean ventilation in the Southern Pacific Ocean during the last glaciation persisted into the deglaciation. *Earth and Planetary Science Letters*, 438:130–138.

Singarayer, J. S., Richards, D. A., Ridgwell, A., Valdes, P. J., Austin, W. E. N., and Beck, J. W. (2008). An oceanic origin for the increase of atmospheric radiocarbon during the Younger Dryas. *Geophysical Research Letters*, 35(14):1–6.

Smith, B. N. and Epstein, S. (1971). Two Categories of $^{13}C/^{12}C$ Ratios for Higher Plants. *Plant Physiology*, 47(3):380–384.

Soares, A. and Dias, J. (2006). Coastal upwelling and radiocarbon: evidence for temporal fluctuations in ocean reservoir effect off Portugal during the Holocene. *Radiocarbon*, 48(1):45–60.

Southon, J., Kashgarian, M., Fontugne, M., Metivier, B., and Yim, W. W.-S. (2002). Marine reservoir corrections for the Indian Ocean and Southeast Asia. *Radiocarbon*, 44(1):167–180.

Southon, J., Noronha, A. L., Cheng, H., Edwards, R. L., and Wang, Y. (2012). A high-resolution record of atmospheric ^{14}C based on Hulu Cave speleothem H82. *Quaternary Science Reviews*, 33:32–41.

Souza, S. (2018). Dentes, Ossos e Suas Formas: Lições Aprendidas Sobre os Construtores de Sambaquis. *Revista Memorare*, 5(1):218–247.

Spadone, A. and Provost, C. (2009). Variations in the Malvinas Current volume transport since October 1992. *Journal of Geophysical Research: Oceans*, 114(2):1–21.

Stein, J. K. (1992). The Analysis of Shell Middens. In Stein, J. K., editor, *Deciphering a Shell Midden*, pages 1–24. Academic Press Limited, San Diego, CA.

Storto, C. (1999). Estudo preliminar das paleopatologias da população do sambaqui Jaboticabeira II, Jaguaruna, SC. *Rev. do Museu de Arqueologia e Etnologia*, 9:61–71.

Strub, P., Mesías, J., Montecino, V., Rutlant, J., and Salinas, S. (1998). Coastal ocean circulation off western South America. In *The sea, Vol 11*, pages 273–314.

Stuiver, M. (1961). Variations in radiocarbon concentration and sunspot activity. *Journal of Geophysical Research*, 66(1):273–276.

Stuiver, M. and Braziunas, T. F. (1993). Modeling Atmospheric ^{14}C Influences and ^{14}C Ages of Marine Samples to 10,000 BC. *Radiocarbon*, 35(1):137–189.

Stuiver, M. and Braziunas, T. F. (1998). Anthropogenic and solar components of hemispheric ^{14}C. *Geophysical Research Letters*, 25(3):329–332.

Stuiver, M., Braziunas, T. F., Becker, B., and Kromer, B. (1991). Climatic, solar, oceanic, and geomagnetic influences on late-glacial and holocene atmospheric $^{14}C/^{12}C$ change. *Quaternary Research*, 35(1):1–24.

Stuiver, M., Braziunas, T. F., Grootes, P. M., and Zielinski, G. A. (1997). Is There Evidence for Solar Forcing of Climate in the GISP2 Oxygen Isotope Record? *Quaternary Research*, 48:259–266.

Stuiver, M., Pearson, G., and Braziunas, T. (1986). Radiocarbon age calibration of marine samples back to 9000 cal yr BP. *Radiocarbon*, 28:980–1021.

Stuiver, M. and Polach, H. A. (1977). Reporting of ^{14}C Data. *Radiocarbon*, 19(3):355–363.

Stuiver, M. and Quay, P. D. (1981). Atmospheric ^{14}C changes resulting from fossil fuel CO_2 release and cosmic ray flux variability. *Earth and Planetary Science Letters*, 53:349–362.

Stuiver, M., Reimer, P., Bard, E., Beck, J., Burr, G., Hughen, K., Kromer, B., McCormac, G., van der Plicht, J., and Spurk, M. (1998a). INTCAL98 radiocarbon age calibration, 24,000-0 cal BP. *Radiocarbon*, 40(3):1041–1083.

Stuiver, M., Reimer, P., and Braziunas, T. (1998b). High-precision radiocarbon age calibrations for terrestrial and marine samples. *Radiocarbon*, 40(3):1127–1151.

Stuiver, M., Reimer, P., and Reimer, R. (2019). CALIB 7.1 [WWW program] at. http:// calib.org. (Accessed 15 February 2019).

Stuiver, M. and Reimer, P. J. (1993). Extended ^{14}C data base and revised CALIB 3.0 ^{14}C age calibration program. *Radiocarbon*, 35(1):215–230.

Stuiver, M. and Robinson, S. W. (1974). University of Washington Geosecs North Atlantic carbon-14 results. *Earth and Planetary Science Letters*, 23:87–90.

Stuiver, M. and Suess, H. (1966). On the relationship between radiocarbon dates and true sample ages. *Radiocarbon*, 8:534–540.

Suess, H. E. (1955). Radiocarbon Concentration in Modern Wood. *Science*, 122:415–417.

Sulerzhitzky, L. (1971). Radiocarbon Dating of Volcanoes *. *Bulletin of Volcanology*, 35(1):85–94.

Surge, D., Lohmann, K. C., and Dettman, D. L. (2001). Controls on isotopic chemistry of the American oyster, Crassostrea virginica: Implications for growth patterns. *Palaeogeography, Palaeoclimatology, Palaeoecology*, 172(3-4):283–296.

Surge, D. M., Lohmann, K. C., and Goodfriend, G. A. (2003). Reconstructing estuarine conditions: Oyster shells as recorders of environmental change, Southwest Florida. *Estuarine, Coastal and Shelf Science*, 57:737–756.

Swire, H. (1938). *The Voyage of the Challenger. A Personal Narrative of the Historic Circumnavigation of the Globe in the Years 1872-1876*. The Golden Cockerel Press.

Tagliabue, A. and Bopp, L. (2008). Towards understanding global variability in ocean carbon-13. *Global Biogeochemical Cycles*, 22(1):1–13.

Takahashi, T., Sutherland, S. C., Sweeney, C., Poisson, A., Metzl, N., Tilbrook, B., Bates, N., Wanninkhof, R., Feely, R. A., Sabine, C., Olafsson, J., and Nojiri, Y. (2002). Global sea-air CO_2 flux based on climatological surface ocean pCO_2, and seasonal biological and temperature effects. *Deep-Sea Research Part II: Topical Studies in Oceanography*, 49:1601–1622.

Takahashi, T., Sutherland, S. C., Wanninkhof, R., Sweeney, C., Feely, R. A., Chipman, D. W., Hales, B., Friederich, G., Chavez, F., Sabine, C., Watson, A., Bakker, D. C., Schuster, U., Metzl, N., Yoshikawa-Inoue, H., Ishii, M., Midorikawa, T., Nojiri, Y., Körtzinger, A., Steinhoff, T., Hoppema, M., Olafsson, J., Arnarson, T. S., Tilbrook, B., Johannessen, T., Olsen, A., Bellerby, R., Wong, C. S., Delille, B., Bates, N. R., and de Baar, H. J. (2009). Climatological mean and decadal change in surface ocean pCO_2, and net sea-air CO_2 flux over the global oceans. *Deep-Sea Research Part II: Topical Studies in Oceanography*, 56(8-10):554–577.

Talley, L. (2013). Closure of the global overturning circulation through the Indian, Pacific, and Southern Oceans: Schematics and transports. *Oceanography*, 26(1):80–97.

Talley, L. D., Pickard, G., Emery, W., and Swift, J. (2011). *Descriptive Physical Oceanography: An Introduction*. Elsevier Science.

Tanaka, N., Monaghan, M., and Rye, D. (1986). Contribution of metabolic carbon to mollusc and barnacle shell carbonate. *Nature*, 320:520–523.

Tans, P. P., De Jong, A. F. M., and Mook, W. G. (1979). Natural atmospheric ^{14}C variation and the Suess effect.

Taylor, N. (1992). The role of the ocean in the global carbon cycle. *Weather*, 47(5):146–151.

Taylor, R. E. (1987). *Radiocarbon Dating: An Archaeological Perspective*.

Taylor, R. E. and Berger, R. (1967). Radiocarbon Content of Marine Shells from the Pacific Coasts of Central and South America. *Science*, 158(1180-1182):157–168.

Teixeira, A. (2004). *Estudo dos marcadores de estresse musculoesquelético, em restos esqueléticos dos habitantes do Sambaqui de Cabeçuda, Laguna, SC. Uma abordagem biocultural.* PhD thesis, ICB/UFRJ.

Thomas, D., Andrus, C., Bishop, G., Blair, E., Blanton, D., Crowe, D., DePratter, C., Dukes, J., Francis Jr., P., Guerrero, D., and Hayes, R. (2008). Native American landscapes of St. Catherines Island, Georgia. *Anthropological papers of the American Museum of Natural History*, (88).

Tobias, S., Weiss, N., and Beer, J. (2004). Long-term prediction of solar activity - a discussion... *Astronomy & Geophysics*, 3:209–216.

Toby, B. H. and Von Dreele, R. B. (2013). GSAS-II: The genesis of a modern open-source all purpose crystallography software package. *Journal of Applied Crystallography*, 46(2):544–549.

Toggweiler, J. R., Dixon, K., and Bryan, K. (1989). Simulations of Radiocarbon in a Coarse-Resolution World Ocean Model. *Journal of Geophysical Research*, 94(C6):8217–8242.

Tucker, M. and Wright, V. (1990). *Carbonate Sedimentology*. Blackwell Science, Oxford, UK.

Tuniz, C., Kutschera, W., Fink, D., Herzog, G., and Bird, J. (1998). *Accelerator mass spectrometry: ultrasensitive analysis for global science*.

Ulm, S. (2002). Marine and estuarine reservoir effects in central Queensland, Australia: Determination of $\triangle$R values. *Geoarchaeology*.

Ulm, S., Petchey, F., and Ross, A. (2009). Marine reservoir corrections for Moreton Bay, Australia. *Archaeology in Oceania*, 44(3):160–168.

Urey, H., Lowenstam, H., Epstein, S., and McKinney, C. (1951). Measurement of Paleotemperatures and Temperatures of the Uper Cretaceous of England, Denmark and the Southeastern United States. *Bulletin of the Geological Society of America*, 62(April):399–416.

Urey, H. C. (1947). The thermodynamic properties of isotopic substances. *J. Chem. Soc.*, pages 562–581.

Urey, H. C. (1948). Oxygen Isotopes in Nature and in the Laboratory. *Science*, 108:489–496.

Valentin, J. (2001). The Cabo Frio Upwelling System, Brazil. In Seeliger, U. and Kjerfve, B., editors, *Coastal Marine Ecosystems of Latin America*, pages 97–105. Springer, Berlin.

Van de Merwe, N. (1982). Carbon Isotopes, Photosynthesis, and Archaeology. *American Scientist*, 70(6):596–606.

van Klinken, G. (1999). Bone collagen quality indicators for paleodietary and radiocarbon measurements. *Journal of Archaeological Sciences*, 26(6):687–695.

Van Klinken, G. J., Bowles, A. D., and Hedges, R. E. M. (1994). Radiocarbon dating of peptides isolated from contaminated fossil bone collagen by collagenase digestion and reversed-phase chromatography. *Geochimica et Cosmochimica Acta*, 58(11):2543–2551.

Vernet, J. (1999). Reconstructing Vegetation and Landscapes in the Mediterranean: the Contribution of Anthracology. In *Environmental Reconstruction in Mediterranean Landscape Archaeology*, pages 25–33.

Villagran, X. S. (2013). O que sabemos dos grupos construtores de sambaquis? Breve revisão da arqueologia da costa sudeste do Brasil, dos primeiros sambaquis até a chegada da cerâmica Jê. *Revista do Museu de Arqueologia e Etnologia*, 23:139–154.

Villagran, X. S. and Giannini, P. C. (2014). Shell mounds as environmental proxies on the southern coast of Brazil. *Holocene*, 24(8):1009–1016.

Villagran, X. S., Klokler, D., Peixoto, S., Deblasis, P., and Giannini, P. C. (2011). Building coastal landscapes: Zooarchaeology and geoarchaeology of Brazilian shell mounds. *Journal of Island and Coastal Archaeology*, 6(2):211–234.

Voelker, A. H., Grootes, P. M., Nadeau, M. J., and Sarnthein, M. (2000). Radiocarbon levels in the iceland sea from 25-53 kyr and their link to the earth's magnetic field intensity. *Radiocarbon*, 42(3):437–452.

Vogel, J., Fuls, A., and Visser, E. (1993). Pretoria calibration curve for short-lived samples, 1930-3350 BC. *Radiocarbon*, 35(1):73–85.

Vogel, J., Southon, J., and Nelson, D. (1987). ^{14}C Background Levels in an Accelerator Mass Spectrometry System. *Radiocarbon*, 29(3):323–333.

Volk, T. and Hoffert, M. I. (1985). Ocean carbon pumps: analysis of relative strengths and efficiencies in ocean-driven atmospheric CO_2 changes. *The Carbon Cycle and Atmospheric CO: Natural Variations Archean to Present*, 32:99–110.

von Martens, E. C. (1867). *Die preussische Expedition nach Ost-Asien: nach amtlichen Quellen. Zoologischer Theil/bearb. von Eduard v. Martens*, volume 2. Verlag der Königlichen geheimen ober-hofbuchdruckerei (R. v. Decker).

von Scherzer, K. R. (1861). *Narrative of the Circumnavigation of the Globe by the Austrian Frigate Novara, in the Years 1857, 1858, & 1859*. Saunders, Otley and Company, London.

Vorobyov, A. A., Seleverstov, D. M., Grachov, V. T., Kondurov, I. A., Nikitin, A. M., Smirnov, N. N., and Zalite, Y. K. (1972). Light nuclei from ^{235}U neutron fission. *Physics Letters B*, 40B(1):102–104.

Wagner, G., Hilbert, K., Bandeira, D., Tenório, M. C., and Okumura, M. M. (2011). Sambaquis (shell mounds) of the Brazilian coast. *Quaternary International*, 239:51–60.

Walker, P. L. and DeNiro, M. J. (1986). Stable nitrogen and carbon isotope ratios in bone collagen as indices of prehistoric dietary dependence on marine and terrestrial resources in Southern California. *American Journal of Physical Anthropology*, 71(1):51–61.

Walter, S. (2000). *Palaeoenvironmental analysis of the Upper Cenomanian and Lower Turonian limestone beds in the Sergipe Basin, northeastern Brazil, based on microfacies analysis, micropalaeontology, and stable isotopes*. PhD thesis, Ruprecht-Karls-Universität, Heidelberg.

Waselkov, G. (1987). Shellfish Gathering and Shell Midden Archaeology. *Advances in Archaeological Method and Theory*, 10(1987):93–210.

Waterbolk, H. T. (1971). Working with Radiocarbon Dates. *Proceedings of the Prehistoric Society*, 37(2):15–33.

Webb, E. C., Lewis, J., Shain, A., Kastrisianaki-Guyton, E., Honch, N. V., Stewart, A., Miller, B., Tarlton, J., and Evershed, R. P. (2017). The influence of varying proportions of terrestrial and marine dietary protein on the stable carbon-isotope compositions of pig tissues from a controlled feeding experiment. *Science and Technology of Archaeological Research*, 3(1):28–44.

Webb, G. E., Price, G. J., Nothdurft, L. D., Deer, L., and Rintoul, L. (2007). Crytic meteoric diagenesis in freshwater bivalves: Implications for radiocarbon dating. *Geology*, 35(9):803–806.

Wefer, G. and Berger, W. H. (1991). Isotope paleontology: growth and composition of extant calcareous species. *Marine Geology*, pages 207–248.

Weska, T. (2010). *Atividade física e comprometimento osteo-articular na série esquelética do Sambaqui de Cabeçuda, SC.* PhD thesis, Museu Nacional/UFRJ.

Wesolowski, V., Ferraz Mendonça de Souza, S. M., Reinhard, K. J., and Ceccantini, G. (2010). Evaluating microfossil content of dental calculus from Brazilian sambaquis. *Journal of Archaeological Science*, 37:1326–1338.

Widmer, R. (1989). Archaeological Research Strategies in the Investigation of Shell-Bearing Sites, a Florida Perspective. In *Annual Meeting of the Society for American Archaeology*, Atlanta.

Williams, R. G. and Follows, M. J. (2011). *Ocean Dynamics and the Carbon Cycle: Principles and Mechanisms*. Cambridge University Press.

Willson, H. R. and Rees, N. W. (2000). Classification of mesoscale features in the Brazil-Falkland Current confluence zone. *Progress in Oceanography*, 45(3-4):415–426.

Wilmshurst, J. M., Hunt, T. L., Lipo, C. P., and Anderson, A. J. (2011). High-precision radiocarbon dating shows recent and rapid initial human colonization of East Polynesia. *Proceedings of the National Academy of Sciences*, 108(5):1815–1820.

Wood, R. E., Douka, K., Boscato, P., Haesaerts, P., Sinitsyn, A., and Higham, T. F. (2012). Testing the ABOx-SC method: Dating known-age charcoals associated with the Campanian Ignimbrite. *Quaternary Geochronology*, 9:16–26.

Woodman, P. (2013). Shell Energy: An Overview. In Bailey, G., Hardy, K., and Camara, A., editors, *Shell Energy - Mollusc Shells as Coastal Resources*, pages 299–307. Oxbow Books, Oxford.

Xu, X., Trumbore, S. E., Zheng, S., Southon, J. R., McDuffee, K. E., Luttgen, M., and Liu, J. C. (2007). Modifying a sealed tube zinc reduction method for preparation of AMS graphite targets: Reducing background and attaining high precision. *Nuclear Instruments and Methods in Physics Research, Section B: Beam Interactions with Materials and Atoms*, 259:320–329.

Zare, R. N. (2012). Analytical chemistry: Ultrasensitive radiocarbon detection. *Nature*, 482:312–313.

Zeebe, R. and Wolf-Gladrow, D. (2001). *CO_2 in seawater: equilibrium, kinetics, isotopes*. Elsevier, Amsterdam.

Zhao, N. and Keigwin, L. D. (2018). An atmospheric chronology for the glacial-deglacial. *Nature Communications*, 9(3077).

Zito, R., Donahue, J., Davis, S. N., Bentley, H. W., and Fritz, P. (1980). Possible subsurface productions of carbon-14. *Geophysical Research Letters*, 7(4):235–238.